Low dose ionizing radiation induces morphological and immunological modulation of immune cells

Niedrig dosierte ionisierende Strahlung bewirkt bei Zellen des Immunsystems morphologische und immunologische Veränderungen

TECHNISCHE UNIVERSITÄT DARMSTADT

Dem Fachbereich Biologie der Technischen Universität Darmstadt

zur Erlangung des akademischen Grades

eines Doctor rerum naturalium

genehmigte Dissertation von

Dipl.-Biol. Patrick Voos (geb. Becker)

aus Karlsruhe

1. Referent: Prof. Dr. Gerhard O. Thiel

2. Referent: Prof. Dr. Bodo Laube

Tag der Einreichung: 03.05.2017

Tag der mündlichen Prüfung: 14.07.2017

Darmstadt 2017

D17

Experience is what you get when you didn't get what you wanted.

Randy Pausch, US-amerikanischer Informatiker (1960-2008)

I Table of contents

II Summary

In the present thesis I examine the effect of ionizing radiation on normal and leukemic immune cells. Stimulation of freshly isolated peripheral blood lymphocytes (PBLs) by mitogens like phytohemagglutinin (PHA-L) or by a specific T-cell activator that crosslinks different clusters of differentiation (CD) causes an immune activation. The latter is associated with a strong increase in the cell diameter. In addition the electrophysiological properties and the ion channel composition of the plasma membrane of PBLs are altered. In the present thesis I show that a similar increase in cell diameter occurs in response to irradiation of immune cells with low doses of X-ray. This indicates that ionizing radiation (IR) triggers a signaling cascade, which results in an immunomodulation or activation of PBLs. This irradiation phenomena was studied here in more detail with Jurkat cells, a T-cell progenitor cell line derived from a patient with acute T-cell leukemia, a specific type of acute lymphatic leukemia (ALL).

The data show that IR elicits in these cells a dose dependent increase in cell diameter. The latter is similar to the increase in the cell diameter of PBLs after immune stimulation. The IR induced increase in cell diameter originates from two different sources: one is the IR dependent arrest of the cell cycle in G2, the second one is associated with an immune activation. The second component can also be triggered by external application of hydrogen peroxide (H_2O_2), a reactive oxygen species (ROS), and inhibited by immunosuppressant drugs like cyclosporine A. The morphological changes in irradiated Jurkat cells are associated with changes in the electrical properties including an upregulation of a calcium dependent potassium channel. Furthermore the expression of the interleukin-2-receptor alpha chain (CD25), which is expressed in activated and regulatory T-cells, was found. Adhesion assays and single molecule microscopy furthermore show that IR also triggers cell-cell and cell-surface adhesion, a process that is mediated by upregulation and clustering of integrin-β-1 due to IR. All these cellular responses to IR are similar to those found in T-cells after immune activation.

The finding that ionizing radiation elicits an increase in cell size in immune cells, enhanced expression of adhesion molecules and altered ion channel composition in the plasma membrane leads to the hypothesis that IR presumably effects an immunological activation or modulation of these cells. This immunomodulation could explain why low dose IR can be beneficial in the treatment of patients suffering from e.g. chronic inflammation and autoimmune diseases like rheumatoid arthritis. Furthermore the finding that integrin-β-1 mediated adhesion is increased in Jurkat cells after IR could be of importance for the clinical treatment of leukemia patients. Here treatment is often a combination of chemotherapy and radiotherapy. On the background of the present data it is possible that radiation treatment could have previously unknown negative side effects. A rise in cell size, an increased adhesion to endothelial tissue as well as changes in the ion channel composition could lead to massive adhesion and transmigration of acute lymphoblastic leukemia (ALL) cells after radiotherapy. Drugs, which suppress specific integrin-β-1 mediated adhesion might reduce such negative side effects.

III Zusammenfassung

In dieser Arbeit wurden die Auswirkungen von ionisierender Strahlung (IR) auf native und leukämische Zellen des Immunsystems untersucht. Stimulation von frisch isolierten peripheren Blutlymphozyten (PBL) durch Mitogene wie Phytohämagglutinin (PHA-L) oder durch einen spezifischen Aktivator, welcher verschiedene Differenzierungsmarker quervernetzt, führt zu einer immunologischen Aktivierung von ruhenden T-Zellen. Eine solche Aktivierung führt zu einer starken Vergrößerung des Zelldurchmessers von ruhenden Lymphozyten und einer damit einhergehenden Veränderung der elektrophysiologischen Eigenschaften und der Zusammensetzung der verschiedenen Ionenkanäle in der Plasmamembran. In der vorliegenden Arbeit zeige ich, dass eine vergleichbare Vergrößerung dieser Zellen nach Bestrahlung mit niedrigen Dosen von Röntgenstrahlung eintritt. Diese Beobachtung weist auf eine durch ionisierende Strahlung ausgelöste Signalkaskade hin, welche in der Aktivierung oder Modulation des immunologischen Status von Lymphozyten resultiert. Dieses, durch ionisierende Strahlung ausgelöste, Phänomen wurde in der vorliegenden Arbeit im Detail anhand von Jurkat-Zellen untersucht. Diese sind immortalisierte T-Zell-Vorläuferzellen, welche von einem Patienten mit akuter lymphatischer Leukämie (ALL) gewonnen wurden.

Die in dieser Arbeit vorgestellten Ergebnisse zeigen, dass ionisierende Strahlung in Jurkat-Zellen eine dosisabhängige Vergrößerung des Zelldurchmessers bewirkt. Diese Vergrößerung ist in Ausmaß und zeitlichem Ablauf mit der durch Immunstimulation ausgelösten Vergrößerung von frisch isolierten peripheren Blutlymphozyten vergleichbar. Die Vergrößerung des Zelldurchmessers beruht auf zwei unabhängigen Vorgängen: der Erste ist ein durch ionisierende Strahlung hervorgerufener Arrest in der G2 Zellzyklusphase, der Zweite ist mit einer Immunantwort verbunden. Der mit einer Immunantwort verbundene Vergrößerungsvorgang, lässt sich ebenfalls durch eine extrazelluläre Zugabe von Wasserstoffperoxid auslösen und durch das immunsupressiv wirkende Zyklosporin A unterbinden. Die morphologischen Veränderungen der Jurkat-Zellen sind darüber hinaus mit einer Veränderung der elektrophysiologischen Eigenschaften einschließlich der Hochregulation eines kalziumabhängigen Kaliumkanals verbunden. Des Weiteren konnte gezeigt werden, dass die Polypeptid-α-Kette des Interleukin-2-Rezeptors nach Bestrahlung exprimiert wird. Diese ist ein Marker für aktivierte T-Zellen und T-regulatorische Zellen. Adhäsionsexperimente und Einzelmolekülmikroskopie zeigen darüber hinaus, dass ionisierende Strahlung eine verstärkte Zell-Zell- und Zell-Oberflächenadhäsion durch die Hochregulation und verstärkte Zusammenlagerung von Integrin-β-1 bewirkt. Alle durch ionisierende Strahlung hervorgerufenen genannten zellulären Effekte haben große Ähnlichkeit zu den durch Stimulation hervorgerufenen Effekten in peripheren Blutlymphozyten.

Die Erkenntnis, dass ionisierende Strahlung in Zellen des Immunsystems eine Zelldurchmesservergrößerung, eine erhöhte Expression von Adhäsionsmolekülen und eine veränderte Ionenkanalzusammensetzung in der Plasmamembran bewirkt, führt zu der Annahme, dass ionisierende Strahlung eine Modulation des immunologischen Status dieser

Zellen bewirken kann. Diese immunologische Modulation könnte erklären, warum die Strahlentherapie von Patienten mit chronischen Entzündungen oder Autoimmunerkrankungen wie beispielweise rheumatoider Arthritis mit niedrig dosierter ionisierender Strahlung zu einer Linderung der Krankheitssymptome und Beschwerden führt. Darüber hinaus könnte die Erkenntnis, dass die Integrin-β-1 vermittelte Adhäsion von Immunzellen nach Bestrahlung zunimmt, von klinischer Relevanz für die Behandlung von Leukämiepatienten sein, da die Behandlung dieser Krankheit oft eine Kombination von Chemotherapie und Strahlentherapie beinhaltet. Diese Strahlentherapie könnte jedoch noch weitere unbekannte negative Nebeneffekte haben. Anhand der in dieser Arbeit präsentierten Ergebnisse ist anzunehmen, dass diese Strahlentherapie zu einer Vergrößerung, Adhäsion und Transmigration durch Endothele sowie Veränderungen der elektrophysiologischen Eigenschaften der leukämischen Zellen bewirken kann. Dies könnte in einer massiven Adhäsion und Einwanderung der leukämischen Zellen resultieren. Medikamente, welche die Integrin-β-1 vermittelte Adhäsion unterbinden, könnten diese negativen Nebeneffekte vermindern.

1 Chapter 1: General introduction

Ionizing radiation (IR) is commonly used in medical diagnostics and tumor therapy. An additional field of application is radio surgery in which ionizing radiation substitutes the surgery blade; this new method of surgery finds increasing application in recent years. But the use of IR also bears a lot of negative side effects. In particular high-energy photon irradiation often triggers secondary cancers or cell invasiveness (Tucker et al. 1991; Curtis et al. 1992; Walter et al. 1998; Brodin et al. 2011).

Until today, the general paradigm is that all irradiation effects, including the negative side effects, can be traced back to DNA damage. More recent studies however also report an increasing number of extra-nuclear targets of ionizing irradiation. These include for example the plasma membrane, kinases, phosphatases and other proteins, mitochondria and ion channels (Haimovitz-Friedman et al. 1994; Leach et al. 2001; Szumiel 2008; Roth et al. 2015). An interaction of IR with these extra-nuclear targets often results in a generation of reactive oxygen species (ROS). This can elicit Ca^{2+} mediated signaling cascades with a variety of downstream reactions (Todd and Mikkelsen 1994; Gibhardt et al. 2015).

We recently discovered in this context that an irradiation of lung carcinoma cells (A549) with low doses of X-ray triggered a transient elevation of radical oxygen species (ROS) including H_2O_2. It could be shown that this increase in ROS was not restricted to the nucleus but was spreading throughout the cytosol. Further studies showed that this cytosolic ROS triggers an elevation in the concentration of free cytosolic Ca^{2+} in the cytosol ($[Ca^{2+}]_{cyt}$) and with this signal transduction cascades. As result of the increase in $[Ca^{2+}]_{cyt}$, Ca^{2+} dependent potassium channels are activated which in turn results in a hyperpolarization of the plasma membrane voltage (Roth et al. 2015; Gibhardt et al. 2015). Since Ca^{2+} signaling cascades are involved in a variety of cellular processes (Berridge 1995; Berridge et al. 2003; Clapham 2007; Feske 2007), it is reasonable to assume that IR could trigger in the same manner different cellular functions like altered protein expression, differentiation or induction of specific cell responses like activation.

Especially cells of the immune system are interesting in this context. It is well established that Ca^{2+} signaling cascades and ROS are playing crucial roles in the immune activation of T-cells. After the contact with an antigen presenting cell, T-cells respond with a rise in $[Ca^{2+}]_{cyt}$ and ROS which then triggers a signaling cascade resulting in morphological changes, altered protein expression and changes in the phosphorylation status of key proteins like the nuclear factor of activated T-cells (NFAT) or the activation of NF-κB (Cruse and Lewis 2003; Macian 2005; Murphy 2012). Also gene regulation and the expression of protein e.g. ion channels is altered in this manner. At the end of these activation processes the cells are immunological active (Panyi et al. 2004; Čemerski and Shaw 2006; Feske 2007; Smith-Garvin et al. 2009; Simeoni and Bogeski 2015).

1.1 Basics in radiation physics and chemistry

1.1.1 X-ray

X-radiation is a form of electromagnetic radiation that is also called Roentgen-rays after Wilhelm Roentgen, who discovered this kind of radiation in 1895. X-rays can be generated by accelerating electrons and their subsequent collision with matter. X-ray tubes contain a cathode, which emit electrons into a vacuum. The electrons are accelerated from the cathode to an anode, which collects the electrons. By applying a high voltage between cathode and anode the electrons get accelerated and an electron beam is produced. At the anode the electrons collide with a metal – mostly copper or tungsten. Only about 1 % of the total deposed energy is emitted as radiation; the vast portion is converted to heat. The electromagnetic radiation is composed of so-called "Bremsstrahlung" and characteristic X-rays with different wavelengths. The interaction with matter can be classified in three different types: photoelectric effect (PE), Compton effect (C) and pair production at energies higher than 10 MeV. The PE is the dominant process at energies lower than 500 keV.

1.1.2 LET and RBE

The linear energy transfer (LET) is a scale to characterize the density of the applied ionization energy. The LET is defined as the energy loss divided by the length of the track of the primary charged particle like alpha particles. A general rule is that high LET radiation corresponds to a larger relative biological effectiveness (RBE) in comparison to low LET (Hollaender 1954). The RBE is a value without dimension and is determined as the ratio between the energy dose of the reference divided by the energy dose of the radiation of interest for obtaining the same biological effect (Failla and Henshaw 1931).

1.1.3 Alpha particles

Alpha particles are identical to a helium nucleus and consist of two protons and two neutrons. They are spontaneously produced in alpha decay processes of heavy ions. Alpha particles have a kinetic energy of 5 MeV and are heavy enough to penetrate matter but only in a low depth. Alpha particles can be stopped by several centimeters of air and only a few millimeters of water. Because of their two positive charged protons the interaction with other atoms results in a high ionization density and high linear energy transfer (LET). This leads to a high relative biological effectiveness (RBE). The dose depends on the sum of the particles that hit the target; the dimension of the amount of particles is the fluency.

$$D = 1.602\ x\ 10^{-9}\ x\ LET\ x\ F\ x\ \frac{1}{p} \text{ (eqn 1)}$$

Equation 1: D is the Dose [Gy], LET the linear energy transfer [keV/µm], F the fluency [1/cm^2], d the density [g/cm^3].

In particle irradiation of cells not every cell is hit. The distribution of particles can be described by an equation (eqn 2) according to Hall (Hall and Giaccia 2005)

$$P_\lambda\,(n) = \frac{\lambda^n}{n!}\,e^{-\lambda}, \lambda = AF \text{ (eqn 2)}$$

Equation 2: P is the probability of n impacts, A is the cell surface, F is the fluency, λ is the average number of particle impacts per cell and n is the number of impacts.

Equation 2 allows an estimation of the consequences of particle irradiation of cells and biological material. For this estimation it is important to know how many particles actually hit their target, pass through a cell and deposit their dose.

In the medical field of so-called radon balneotherapy the alpha particle emitting gas radon (^{222}Rn) is used to treat patients with inflammatory diseases like Morbus-Bechterew, spondylarthrosis, osteochondrosis or eczemas (Zdrojewicz and Strzelczyk 2006). The mechanism of the curative effect of radon remains unclear until now. A direct interaction of alpha particles with DNA cannot be the main explanation since alpha particles penetrate only over a very small distance into tissues. Because of the high relative biological effectiveness of alpha particles (RBE = 20) a direct hit of a nucleus should cause cell death. Apart from such direct effects also indirect effects are observed. For the aforementioned reasons DNA damage observed after alpha particle exposure cannot be explained by a direct traversal of α-particles through a nucleus but must result from indirect effects (Nagasawa et al. 1991; Deshpande et al. 1996). An elevated ROS level in the cell cytosol in response to alpha particle exposure seems to be a good explanation for such extra-nuclear effects. It was recently shown that a scenario of indirect effects would not cause cell death (Shao et al. 2004).

1.1.4 Radiation of the cell nucleus results in DNA damage

DNA damage can occur in different ways; either by direct hits of bases or by hits of the DNA backbone. Also indirect radiation effects, which are caused by radicals that arise in every aqueous solution like the hydrated envelope of the DNA can cause DNA damage. According to Azzam and co-workers (Azzam et al. 2012), ⅓ of all DNA damages are induced by direct impact on the DNA whereas ⅔ of all damages are due to indirect effects. DNA damages can be divided into different classes of severity: DNA double strand breaks are the most severe damages that can lead to loss of information without repair. Single strand breaks and single base damages in contrast are less severe and they can be repaired very efficient with low error rates.

1.1.5 Extra-nuclear targets and the generation of ROS & RNS

It has been mentioned before that the general paradigm still is that all irradiation effects can be traced back to DNA damage. For this reason DNA damage for many years has been the main focus of radiation biology. The damage in other compartments of cells was considered neglectable. Recent studies however report an increasing number of extra-nuclear targets of ionizing irradiation (Haimovitz-Friedman et al. 1994; Leach et al. 2001; Szumiel 2008; Roth et al. 2015). As a result these targets are now also coming into the focus of research.

Especially in the case of heavy ions and alpha particle radiation it is known that non-homogenous scattering of the main radiolytic species results in the production of radicals along their tracks. These free radicals have a very short lifetime in the range of microseconds to a few milliseconds. In spite of the short lifetime they can interfere with matter and especially inside of cells they can trigger red-ox-reactions resulting in secondary radicals like reactive oxygen species (ROS) or reactive nitrogen species (RNS). The latter are produced from the reaction of nitric oxide (NO) and superoxide (O_2^-). The highly active RNS peroxynitric ($ONOO^-$) is formed and can interact with biological targets and components of the cell. Furthermore the reaction of peroxynitric with other molecules like carbon dioxide or nitrogen dioxide leads to the generation of additional RNS and ROS species. An elevated radical level with ROS and RNS generation can hereby persist in cells for minutes or even hours (Narayanan et al. 1997; Mikkelsen and Wardman 2003). Also mitochondria can amplify ROS in a calcium dependent manner (Leach et al. 2001).

One of these longer lasting molecules, which still has the property of reactive oxygen species, is hydrogen peroxide (H_2O_2). H_2O_2 acts by oxidation of proteins and can develop spontaneously when free oxygen radicals react with water molecules or when this reaction is catalyzed by the enzyme superoxide-dismutase (SOD). Hydrogen peroxide and other ROS have a special role in biological systems since they can function at low concentrations as second messengers for example in lymphocyte activation. High intracellular concentrations of H_2O_2 induce apoptosis and leads to DNA damage, but low concentrations seem to enhance cell proliferation (Liu et al. 2002; Reth 2002; Nakagawa et al. 2004; Williams and Kwon 2004; Simeoni and Bogeski 2015). Also RNS elicits considerable interest in recent years. The relative stable RNS nitric oxide (NO) is a second messenger with broad biological functions, including vascular and muscle relaxation and anti-microbial activity. In many cells NO synthase (NOS) is expressed, an enzyme that synthesizes NO from L-arginine. NOS is expressed in a variety of immunological important cell types including macrophages, leukocytes and endothelial cells. There is evidence that NO is regulating T-cell proliferation; at low amounts it induces proliferation whereas a NO burst inhibits T-cell expansion (Liew 1995; Matoba and Shimokawa 2003; Mikkelsen and Wardman 2003; Rödel et al. 2007).

1.2 Ion channels

Ion channels are proteins that facilitate the passive flux of ions across biological membranes which are otherwise impermeable for charged particles. The ion flux through ion channels is selective and tightly regulated in many different ways. The stochastic opening and closing of ion channels is known as gating (Hille 2001). The gating of ion channels and as a result their activity can be regulated by physical factors (voltage, mechanical stretching) or chemical modifications like phosphorylation and calcium binding. With these properties ion channels play a crucial role in many physiological processes. These include not only neuronal excitation and muscle contraction but also the control of the cell cycle, gene expression, secretion or

apoptosis. In recent years also the role of channels, here in particular of K^+ channels, in the regulation of cell differentiation became evident (Wulff et al. 2004).

1.3 The cell cycle and ion channel regulation

The cell cycle describes the different phases of growth, DNA replication, chromosome separation and cytokinesis resulting in two separated daughter cells. The cell cycle phases are: G0 in which cells are resting, G1 in which cells are growing and checking for errors preparing for the replication, the S (synthesis) phase in which DNA replication occurs, the G2 phase in which cells continue to grow and check for errors that occurred during replication and finally the M phase in which the chromosomes are separated and by a process called cytokinesis two daughter cells are formed. The cyclin-dependent kinase 1 (CDK1) is one of the key players of this cell cycle progression. It is a highly conserved serine/threonine kinase that phosphorylates key proteins like the RNA-polymerase II. This event induces the transition from G2 to S-phase and as a result mitosis and proliferation (Nigg 1995).

In recent years it became evident that also ion channels play important roles in cell cycle control and cell cycle progression. K^+ channels for instance are known to be associated with cell cycle progression in many different cell types, e.g. MCF-7 breast cancer cells (Wonderlin et al. 1995). In the case of breast cancer cells, the Ca^{2+} dependent KCa3.1 is upregulated at the end of G1 and S phase. Blocking of KCa3.1 channels causes a membrane depolarization and a decrease in $[Ca^{2+}]_{cyt}$ that is eventually leading to an inhibition of proliferation (Ouadid-Ahidouch et al. 2004). Felipe and co-workers (Felipe et al. 2006) reviewed the role of K^+ channels and found that different types of K^+ channels play a predominant role at different phases of the cell cycle. The dominant activity of distinct K^+ channels during the cell cycle is shown in Fig. 1-1.

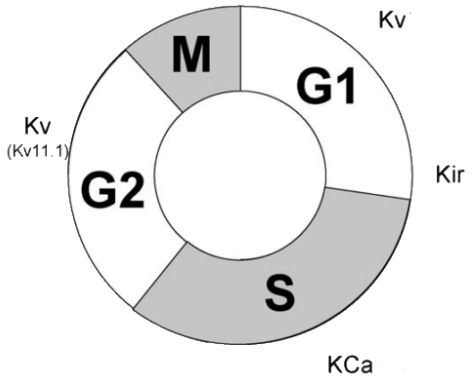

Fig. 1-1: Different potassium channels play important roles at every cell cycle step
Different channel types and subtypes are involved in different phases, but Kv channels for example play an important role in the G1 and the G1/S check points (Modified from Felipe et al. 2006).

In T-cells for instance Kv1.3 is known to be associated with progression from G1 to S phase (Deutsch et al. 1991). Also other cation channels and even Cl^- channels are essential for cell cycle control and progression (Kunzelmann 2005). Because of the important role in the control of proliferation, apoptosis and migration, ion channels are associated with many cancer developments (Kunzelmann 2005; Becchetti 2011; Yang and Brackenbury 2013).

1.4 Volume regulation and apoptosis / proliferation

Cell cycle progression and cell cycle arrest are associated with volume increases and decreases. Large volume changes occur during different steps of the cell cycle (G1/S & M phase) (Yu and Choi 2000; Kunzelmann 2005). When resting cells like T-cells are stimulated, their cell diameter and cytosolic volume increases dramatically reflecting an upregulation of enzymes and other proteins that are essential for the immunological function of the active T-cell (Iritani et al. 2002; Bobak et al. 2011; Andronic et al. 2013). Volume regulation is always correlated with ion channel activity (Fig. 1-2) no matter whether the volume decreases (apoptosis) or increases (proliferation). In this scenario the types of ion channel and the degree in the increase of current are crucial for determining the direction in which a cell differentiates. In this context ion channels can be regarded as molecular switches that determine the fate of cells. In the case of a volume increase following e.g. a cell division or T-cell activation, ion channels have the crucial role of promoting an osmotic swelling of the cells (Sarkadi and Parker 1991; Cahalan et al. 2001; Lang et al. 2006).

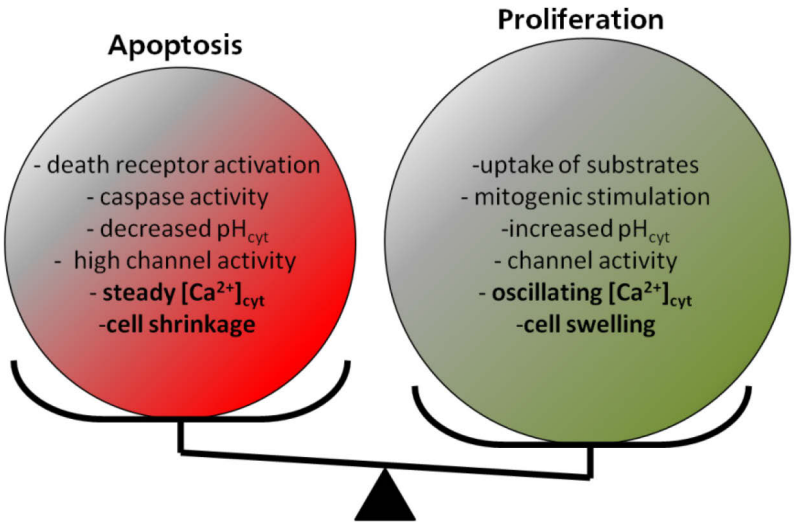

Fig. 1-2: Overview of various factors that differ between apoptosis and proliferation
Ion channels are active under apoptosis as well as during proliferation: here the amplitude of ion channel activity besides other factors determine whether ion channels support apoptosis or proliferation (after Kunzelmann 2005).

For volume regulation and homeostasis the activity of K^+ channels and Cl^- channels is essential. The swelling of cells in hypotonic medium for example is counteracted by the activation of volume-sensitive chloride and various potassium channels. The activation of these ion channels lead to an osmotic water efflux and a restoration of normal cell volume. When the activity of these channels is on the other hand depressed by blockers or regulatory effects like phosphorylation a long lasting swelling can occur (Lang et al. 1998; Andronic et al. 2013).

1.5 Calcium in cells

Calcium is involved as second messenger in almost all physiological processes. In proliferating cells, Ca^{2+} signaling is often organized in oscillatory patterns in which $[Ca^{2+}]_{cyt}$ alternates between elevated levels and the low basal concentration (Eisner and Orchard 1984). In resting

T-cells for instance $[Ca^{2+}]_{cyt}$ is 50-100 nM; it increases transiently to even micromolar concentrations (1-10 µM) during and after activation (Lewis and Cahalan 1995; Clapham 2007). In this signaling processes Ca^{2+} is entering the cell via Ca^{2+} channels and IP_3 receptors in the plasma membrane. In addition Ca^{2+} is released from internal stores like mitochondria and the endosplasmatic reticulum. Stimulus induced oscillations of $[Ca^{2+}]_{cyt}$ are very complex and the dynamic pattern of these signals encode a large spectrum of information. Short $[Ca^{2+}]_{cyt}$ spikes are known to regulate specific functions like changes in metabolism or exocytosis (Berridge et al. 2003) while global and prolonged high $[Ca^{2+}]_{cyt}$ levels can trigger cell death (Panner and Wurster 2006). The dynamics of these oscillations with different amplitudes and durations can be influenced by Ca^{2+} dependent K^+ channels like KCa3.1 and KCa2.2. These potassium channels serve as a feedback of changes in $[Ca^{2+}]_{cyt}$ and respond directly to changes in $[Ca^{2+}]_{cyt}$. In combination with their low voltage dependency and instantaneous activation they are well suited to modulate these oscillations by either supporting or suppressing them (Panner and Wurster 2006). As an additional level of control also phosphatases can increase the activity of KCa2.2 channels by dephosphorylation of the associated Calmodulin (CaM) leading to a higher Ca^{2+} affinity promoting hyperpolarization and increased Ca^{2+} influx. The antagonists of phosphatases are kinases like casein kinase 2 (CK2), which can phosphorylate K^+ channels like KCa2.2 directly or the channel associated CaM. In this way they can inhibit the activity of a channel which leads to a depolarization and decreased Ca^{2+} signaling (Bildl et al. 2004; Panner and Wurster 2006; Allen et al. 2007).

1.6 The immune system and T-cells

The immune system of mammalians consists of two subsystems - the innate and the adaptive immune system. The innate immune system can be described as the evolutionary older system that is also expressed in plant, fungi and insects and provides a non-specific physical or chemical barrier against pathogens and foreign substances. The adaptive immune system on the other hand provides a strong, highly specific immune response and protects not only from pathogens but also fights aberrant, malignant cells (Cruse and Lewis 2003; Murphy 2012).

For the adaptive immune response, peripheral blood lymphocytes (PBLs) are the most important cells (Fig. 1-3). PBLs can be activated by an antigen presenting cell via the major histocompatibility complex (MHC) molecules. This activation is triggering a differentiation of the lymphocytes into proliferative cells with effector functions. These activated T-cells are able to fight immediate infection in the so-called primary response (Moulin 1989).

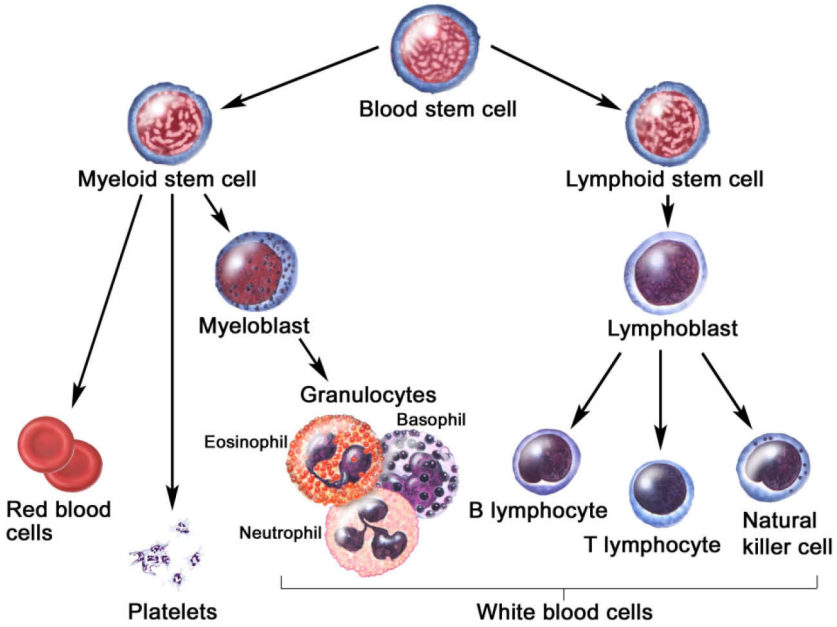

Fig. 1-3: Hematopoietic and stromal cell differentiation

Hematopoietic blood stem cells are able to form all cells in the hematopoietic system, which includes red blood cells, platelets, and the whole lymphatic system (T- and B-lymphocytes). Jurkat cells are so-called "T-cell blast cells" that exhibit most T-cell characteristics but proliferate without external stimulus. Most but not all leukemia cells still can differentiate (from Winslow, 2007).

It is worth mentioning that blood cells and especially individual lymphocytes are, according to the literature, extremely radiosensitive (Boreham et al., 1996). This could be due to the law of Bergonié and Tribondeau (Vogin and Foray 2013). It states that the radio sensitivity of cell is directly proportional to their reproductive activity and inversely proportional to their degree of differentiation. In contrast to these negative effects of ionizing irradiation, low dose radiotherapy is known to be able to cure inflammatory diseases like arthritis (Rödel et al. 2007; Large et al. 2015).

1.7 References

Allen D, Fakler B, Maylie J, et al (2007) Organization and regulation of small conductance Ca2+-activated K+ channel multiprotein complexes. J Neurosci 27:2369–2376.

Andronic J, Bobak N, Bittner S, et al (2013) Identification of two-pore domain potassium channels as potent modulators of osmotic volume regulation in human T lymphocytes. Biochim Biophys Acta - Biomembr 1828:699–707.

Azzam E, Jay-Gerin J-P, Pain D (2012) Ionizing radiation-induced metabolic oxidative stress and prolonged cell injury. Cancer Lett 327:48-60.

Becchetti A (2011) Ion channels and transporters in cancer. 1. Ion channels and cell proliferation in cancer. Am J Physiol Cell Physiol 301:C255–C265.

Berridge MJ (1995) Calcium signalling and cell proliferation. BioEssays 17:491–500.

Berridge MJ, Bootman MD, Roderick HL (2003) Calcium signalling: dynamics, homeostasis and remodelling. Nat Rev Mol Cell Biol 4:517–29.

Bildl W, Strassmaier T, Thurm H, et al (2004) Protein kinase CK2 is coassembled with small conductance Ca(2+)-activated K+ channels and regulates channel gating. Neuron 43:847–858.

Bobak N, Bittner S, Andronic J, et al (2011) Volume regulation of murine T lymphocytes relies on voltage-dependent and two-pore domain potassium channels. Biochim Biophys Acta - Biomembr 1808:2036–2044.

Boreham DR, Gale KL, Maves SR, et al (1996) Radiation-induced apoptosis in human lymphocytes: potential as a biological dosimeter. Heal Phys 71:685–91.

Brodin NP, Munck A, Rosenschöld P, et al (2011) Radiobiological risk estimates of adverse events and secondary cancer for proton and photon radiation therapy of pediatric medulloblastoma. Acta Oncol 50:806–16.

Cahalan MD, Wulff H, Chandy KG (2001) Molecular properties and physiological roles of ion channels in the immune system. J Clin Immunol 21:235–252.

Čemerski S, Shaw A (2006) Immune synapses in T-cell activation. Curr Opin Immunol 18:298–304.

Clapham DE (2007) Calcium Signaling. Cell 131:1047–1058.

Cruse JM, Lewis RE (2003) Atlas of Immunology, 2., Springer Science & Business, New York

Curtis RE, Boice JD, Stovall M, et al (1992) Risk of leukemia after chemotherapy and radiation treatment for breast cancer. N Engl J Med 326:1745–1751.

Deshpande A, Goodwin EH, Bailey SM, et al (1996) Alpha-particle-induced sister chromatid exchange in normal human lung fibroblasts: evidence for an extranuclear target. Radiat Res 145:260–267.

Deutsch C, Price M, Lee S, et al (1991) Characterization of high affinity binding sites for charybdotoxin in human T lymphocytes. Evidence for association with the voltage-gated K+ channel. J Biol Chem 266:3668–74.

Eisner D, Orchard CH (1984) Calcium concentration. J. Physiol. 352:113–128.

Failla G, Henshaw P (1931) the Relative Biological Effectiveness of X-Rays and Gamma Rays. Radiology 17:1–43.

Felipe A, Vicente R, Villalonga N, et al (2006) Potassium channels: new targets in cancer therapy. Cancer Detect Prev 30:375–85.

Feske S (2007) Calcium signalling in lymphocyte activation and disease. Nat Rev Immunol 7:690–702.

Gibhardt CS, Roth B, Schroeder I, et al (2015) X-ray irradiation activates K+ channels via H2O2 signaling. Sci Rep 5:13861.

Haimovitz-Friedman BA, Kan C, Ehleiter D, et al (1994) Ionizing Radiation Acts on Cellular Membranes to Generate Ceramide and Initiate Apoptosis. J. Exp. Med. 180:525-535

Hall EJ, Giaccia AJ (2005) Radiobiology for the Radiologist. Lippincott Williams & Wilkins, Philadelphia, USA

Hille B (2001) Ion Channels of Excitable Membranes. 1., Sinauer associates Inc., Sunderland, USA.

Hollaender A (1954) High Energy Radiation. 1., McGraw-Hill Book Company Inc., New York, USA

Iritani BM, Delrow J, Grandori C, et al (2002) Modulation of T-lymphocyte development, growth and cell size by the Myc antagonist and transcriptional repressor Mad1. EMBO J 21:4820–4830.

Kunzelmann K (2005) Ion channels and cancer. J Membr Biol 205:159–173.

Lang F, Busch GL, Ritter M, et al (1998) Functional Significance of Cell Volume Regulatory Mechanisms. Physiol Rev 78:247–307.

Lang F, Shumilina E, Ritter M, et al (2006) Ion channels and cell volume in regulation of cell proliferation and apoptotic cell death. Contrib Nephrol 152:142–160.

Large M, Hehlgans S, Reichert S, et al (2015) Study of the anti-inflammatory effects of low-dose radiation. Strahlentherapie und Onkol 191:742–749.

Leach JK, Tuyle G Van, Lin P, et al (2001) Ionizing Radiation-induced , Mitochondria-dependent Generation of Reactive Oxygen/Nitrogen. Cancer Research 61:3894–3901.

Lewis RS, Cahalan MD (1995) Potassium and calcium channels in lymphocytes. Annu. Rev. Immunol. 13:623–653.

Liew FY (1995) Regulation of lymphocyte functions by nitric oxide. Curr Opin Immunol 7:396–399.

Liu S-L, Lin X, Shi D-Y, et al (2002) Reactive oxygen species stimulated human hepatoma cell proliferation via cross-talk between PI3-K/PKB and JNK signaling pathways. Arch Biochem Biophys 406:173–182.

Macian F (2005) NFAT proteins: key regulators of T-cell development and function. Nat Rev Immunol 5:472–84.

Matoba T, Shimokawa H (2003) Hydrogen peroxide is an endothelium-derived hyperpolarizing factor in animals and humans. J Pharmacol Sci 92:1–6.

Mikkelsen RB, Wardman P (2003) Biological chemistry of reactive oxygen and nitrogen and radiation-induced signal transduction mechanisms. Oncogene 22:5734–54.

Moulin AM (1989) The Immune System: A Key Concept for the History of Immunology. Hist Philos Life Sci 11:221–236.

Murphy K (2012) Immuno Biology, 8., Garland Science, Taylor & Francis Group, New York, USA

Nagasawa H, Little JB, Inkret WC, et al (1991) Response of X-Ray-Sensitive CHO Mutant Cells (xrs-6c) to Radiation: II. Relationship between Cell Survival and the Induction of Chromosomal Damage with Low Doses of αParticles. Radiation research 126:280–288.

Nakagawa H, Hasumi K, Woo JT, et al (2004) Generation of hydrogen peroxide primarily contributes to the induction of Fe(II)-dependent apoptosis in Jurkat cells by (-)-epigallocatechin gallate. Carcinogenesis 25:1567–1574.

Narayanan PK, Goodwin EH, Lehnert BE (1997) Alpha Particles Initiate Biological Production of Superoxide Anions and Hydrogen Peroxide in Human Cells. Cancer Res 57:3963–3971.

Nigg E (1995) Cyclin-dependent protein kinases: key regulators of the eukaryotic cell cycle. Bioessays 17:471–480.

Ouadid-Ahidouch H, Roudbaraki M, Delcourt P, et al (2004) Functional and molecular identification of intermediate-conductance Ca(2+)-activated K(+) channels in breast cancer cells: association with cell cycle progression. Am J Physiol Cell Physiol 287:C125-34.

Panner A, Wurster RD (2006) T-type calcium channels and tumor proliferation. Cell Calcium 40:253–259.

Panyi G, Varga Z, Gáspár R (2004) Ion channels and lymphocyte activation. Immunol Lett 92:55–66.

Reth M (2002) Hydrogen peroxide as second messenger in lymphocyte activation. Nat Immunol 3:1129–1134.

Rödel F, Keilholz L, Herrmann M, et al (2007) Radiobiological mechanisms in inflammatory diseases of low-dose radiation therapy. Int J Radiat Biol 83:357–366.

Roth B, Gibhardt CS, Becker P, et al (2015) Low-dose photon irradiation alters cell differentiation via activation of hIK channels. Pflugers Arch Eur J Physiol 467:1835–1849.

Sarkadi B, Parker JC (1991) Activation of ion transport pathways by changes in cell volume. Biochim Biophys Acta 1071:407–427.

Shao C, Folkard M, Michael BD, Prise KM (2004) Targeted cytoplasmic irradiation induces bystander responses. Proc Natl Acad Sci USA 101:13495–13500.

Simeoni L, Bogeski I (2015) Redox regulation of T-cell receptor signaling. Biol Chem 396:555–568.

Smith-Garvin JE, Koretzky GA, et al (2009) T cell activation. Annu Rev Immunol 27:591–619.

Szumiel I (2008) Intrinsic radiation sensitivity: cellular signaling is the key. Radiat Res 169:249–58.

Todd DG, Mikkelsen RB (1994) Ionizing radiation induces a transient increase in cytosolic free [Ca2+] in human epithelial tumor cells. Cancer Res 54:5224–5230.

Tucker MA, Jones PHM, Boice JD, et al (1991) Therapeutic Radiation at a Young Age Is Linked to Secondary Thyroid Cancer Therapeutic Radiation at a Young Age Is Linked to Secondary Thyroid Cancer. Cancer Res 51:2885–2888.

Vogin G, Foray N (2013) The law of Bergonié and Tribondeau: A nice formula for a first approximation. Int J Radiat Biol 89:2–8.

Walter AW, Hancock ML, Pui CH, et al (1998) Secondary brain tumors in children treated for acute lymphoblastic leukemia at St Jude Children's Research Hospital. J Clin Oncol 16:3761–3767.

Williams MS, Kwon J (2004) T cell receptor stimulation, reactive oxygen species, and cell signaling. Free Radic Biol Med 37:1144–1151.

Wonderlin WF, Woodfork K, Strobl JS (1995) Changes in membrane potential during the progression of MCF-7 human mammary tumor cells through the cell cycle. J Cell Physiol 165:177–85.

Wulff H, Knaus H-G, Pennington M, et al (2004) K+ channel expression during B cell differentiation: implications for immunomodulation and autoimmunity. J Immunol 173:776–86.

Yang M, Brackenbury WJ (2013) Membrane potential and cancer progression. Front Physiol 4:1–10.

Yu SP, Choi DW (2000) Ions, cell volume, and apoptosis. Proc Natl Acad Sci USA 97:9360–9362.

Zdrojewicz Z, Strzelczyk J (2006) Radon Treatment Controversy. Dose-Response 4(2):106-118.

2 Chapter 2: Ionizing radiation causes an increase in the cell diameter of immune cells reflecting immunological activation or modulation processes

2.1 Abstract

When resting T-cells are activated by specific immune stimulation or by mitogens, a Ca^{2+} mediated signaling cascade is eliciting a variety of changes in protein expression, altered phosphorylation patterns and regulation of transcription factors. At the end of these processes T-cells are immunological active and the cell diameter of these cells is increased. In the present study a similar increase in cell diameter was observed after irradiating freshly isolated peripheral blood lymphocytes (PBLs) with different doses of X-ray. This led to the assumption that ionizing radiation (IR) is capable of triggering a signaling cascade similar to that of immune stimulation. To study this in more detail, Jurkat cells, a T-cell progenitor cell line that is commonly used in immunological studies, were used. A dose dependent increase in cell diameter after irradiation with X-ray was found. This IR stimulated increase in cell diameter can be dissected in two components. One component can be assigned to a dose dependent arrest of cells in the G2 cell cycle phase. The second component seems to reflect an immunological activation or immunomodulation process, which can be attenuated by the immune suppressor cyclosporine A. This immunological activation, which is presumable mediated by SRC kinases , is associated with typical immune reactions like an upregulation of the activation specific interleukin 2 receptor alpha chain (CD25).

2.2 Introduction

Cells of the immune system use a variety of receptors to communicate and interact with their environment. When a signal from the environment is received by plasma membrane receptors, it is transmitted to intracellular signaling pathways involving proteins like kinases, phosphatases and transcription factors (Negulescu et al. 1994; Cruse and Lewis 2003; Smith-Garvin et al. 2009). These proteins interact with each other in a variety of ways leading to biochemical signal transduction and amplification. Signaling cascades that are associated with immune responses generally trigger a specific cell response like proliferation and differentiation. Many of the signal transduction cascades end in the nucleus where they alter gene expression and the consent synthesis of proteins. The subsequent expression of cytokines, chemokines and cell-adhesion molecules are especially important in the context of an activation (Cruse and Lewis 2003; Murphy 2012).

Resting T-cells exhibit a defined cell diameter that is consistently ~ 7 µm. Upon activation in response to immune stimulation via the T-cell receptor (TCR) pathway or after treatment with mitogens like phytohemagglutinin (PHA-L), the cell diameter increases rapidly (Cuschieri and Mughal 1985; Iritani et al. 2002; Loris et al. 1998). This increase in cell diameter is necessary because resting T-cells, which are not proliferating, have little or almost no cytoplasm and their organelles are reduced to a minimum.

Upon activation T-cells can differentiate and become proliferative blast cells, which are active in immune reactions. They increase their metabolic capacities to proliferate and secrete chemokines and cytokines which are needed for immune response (Abbas and Lichtman 2003; Cruse and Lewis 2003).

The enzymes that are most commonly associated with receptor activation and signal transduction are protein kinases. Especially tyrosine kinases of the SRC family like Lck, Syk, Zap-70 and Fyn play key roles in T-cell activation, including the phosphorylation of the immunoreceptor tyrosine-based activation motif (ITAM) (Cruse and Lewis 2003). The phosphorylation of ITAM in turn leads to an inositol 1,4,5-trisphosphate (IP_3) induced calcium signaling via the activation of phospholipase C (PLC) enzymes (Essen et al. 1997; Wange 2000). IP_3 binding to the IP_3 receptor results finally in a Ca^{2+} influx trough the IP_3 receptor itself and calcium release from internal stores as well as NF-κB activation (Lin and Wang 2004). This influx through the IP_3 receptor and Ca^{2+} channels is mandatory because the internal stores are, like all organelles in resting lymphocytes, relatively small (Feske 2007; Akimzhanov and Boehning 2012). This Ca^{2+} signaling is the essential step in the activation of a T-cell and leads to an elevation of the cytosolic Ca^{2+} concentration $[Ca^{2+}]_{cyt}$. An elevated Ca^{2+} level is, amongst others, sensed by calmodulin (CaM), which in turn is activating the serine/threonine phosphatase calcineurin. This signaling scenario is reviewed in recent publications (Kumar et al. 2007; Smith-Garvin et al. 2009; Akimzhanov and Boehning 2012; Murphy 2012). Finally a Ca^{2+} dependent transcriptional response and the upregulation of cytokines, chemokines and cell-adhesion molecules by transcription factors like NFAT and NF-κB is induced. Both NFAT and NF-κB play important roles in the immune response of lymphocytes (Cruse and Lewis 2003; Murphy 2012).

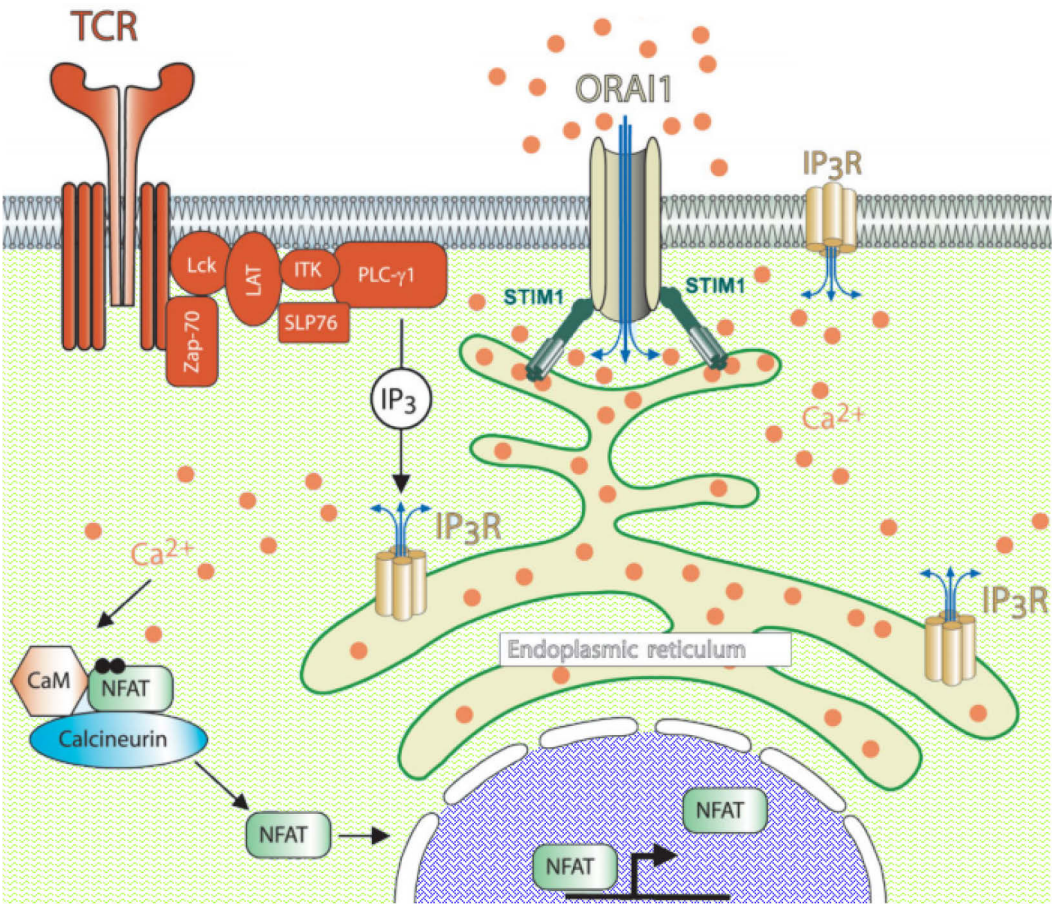

Fig. 2-1: Schematic diagram showing the Ca^{2+}-dependent activation NFAT pathway in T-cells
Activation of T-cells via the T-cell receptor (TCR) is activating a variety of signaling molecules such as kinases and transcription factor as well as second messengers like IP_3 and Ca^{2+}. At the end of an activation T-cells exhibit an altered gene expression shown here by the translocation of NFAT (nucl. factor of activated T-cells) to the nucleus (blue) (modified from Akimzhanov and Boehning 2012).

Calcineurin regulates the activity and localization of NFAT (nuclear factor of activated T-cells), one of the most important transcription factor in activated T-cells. Cyclosporine A is an immune suppressant which is inhibiting calcineurin by forming a complex with cyclophilin. This decreases the production of inflammatory cytokines by T-lymphocytes and the increase in cell diameter (Krönke et al. 1984; Matsuda and Koyasu 2000). Amongst others, SRC kinases also activate CK2 (casein kinase 2). The phosphorylated CK2 in turn activates the transcription factor NF-κB, which plays an important role in the regulation of the immune response. Furthermore CK2 phosphorylates CaM; this phosphorylation is leading to a reduced Ca^{2+} affinity of CaM and a modulation of the immune response (Allende and Allende 1995; Donella-Deana et al. 2003; Roskoski 2005). The antagonist of CK2 action is the protein phosphatase 2 (PP2A) that dephosphorylates CaM (Allen et al. 2007). In about 50 % of all cancer variants SRC kinases are highly active and are thought of being responsible for increased survival, angiogenesis, proliferation and enhanced invasiveness of cancer cells. SRC kinases are therefore important drug targets – “Desantinib” for instance is a SRC kinase inhibitor that is used in cancer treatment (Bristol-Myers Squibb GmbH & Co. KGaA). Other inhibitors like the so-called PP2 inhibitor are used in therapy against special types of acute lymphoid leukemia.

2.3 Materials & Methods

2.3.1 Chemicals and antibodies

All chemicals were purchased from Sigma-Aldrich GmbH (Taufkirchen, Germany), Biochrom AG (Merck KGaA, Darmstadt, Germany), AppliChem GmbH (Darmstadt, Germany), Merck KGaA (Darmstadt, Germany), Bio-Rad Laboratories GmbH (Muinch, Germany), VWR (Darmstadt, Germany), Qiagen (Hilden, Germany), Thermo Fisher Scientific (Walham, USA) or Invitrogen (Karlsruhe, Germany) if not specified further. Hoechst Staining was purchased from Sigma-Aldrich GmbH (Taufkirchen, Germany) and the plasma membrane stain CellMask OrangeTM from Life technologies (Carlsbad, USA). The T-cell activator "ImmunoCult™ Human CD3/CD28/CD2" was purchased from Stemcell Technologies (Vancouver, Kanada). The CDK1 inhibitor RO3306 ((5Z)-5-(6-Quinolinylmethylene)-2-[(2-thienylmethyl)amino)-4(5H)-thiazolone) was purchased from Axon Medchem (Groningen, Netherlands) and Sigma-Aldrich GmbH (Taufkirchen, Germany). For CDK1 inhibition RO3306 was applied in an end concentration of 3 µM directly in cell culture medium. Phytohaemagglutinin (PHA-L) was purchased from Biochrom (Berlin, Germany). The Kinase inhibitor TBB (tetrabromobenzotriazole) was purchased from MCE MedChemExpress (New York, USA) respectively from Tocris Bioscience (Bristol, UK). Cyclosporine A was purchased from Sigma-Aldrich (Taufkirchen, Germany).

2.3.2 Cell lines and isolation protocol for PBL

2.3.2.1 Jurkat cells

Jurkat cells are a cell line established in 1976 from the peripheral blood of a 14-year-old boy with acute T-cell leukemia, a specific type of acute lymphatic leukemia (ALL). The Jurkat cell line is also called JM and grows singly or in small clumps as round, non-adherent suspension cells. The optimal split ratio is about 1:2-1:3 every 2 to 4 days at a maximum cell count of 1×10^6 per ml. The doubling time is 25-35 hours. For cell culture 37° C, 5 % CO_2 and RPMI 1640 medium with stable glutamine and 2.0 g/l $NaHCO_3$ + 2 mM L-glutamine, 10 % heat inactivated fetal calf serum (FCS) (Sigma-Aldrich, Germany) and 1 % mixture of penicillin/streptomycin was used. The Jurkat cell line (ACC 282) was purchased from the Leibniz-Institut DSMZ (Deutsche Sammlung von Mikroorganismen und Zellkulturen GmbH) and their immunological status is $CD2^+$, $CD3^+$, $CD5^+$, $CD6^+$, $CD7^+$, $CD8^-$, $CD13^-$, $CD19^-$, TCR α/β^+, TCR γ/δ^- ($^+$ stands for expression, $^-$ stands for no expression).

2.3.2.2 PBL isolation protocol

Peripheral blood lymphocytes (PBLs) were isolated from buffy coats by using a biocoll-hypaque gradient. In brief, 15 ml of blood samples from healthy donors were diluted 1:1 with PBS (-/-) and layered on top of 15 ml biocoll-hypaque gradient. After a centrifugation step of 40 min at 1200 rpm and room temperature (RT), 3-6 ml blood plasma was taken from the upper phase and heat inactivated for PBMC-Medium creation.

1-3 ml of peripheral blood monocytes (PBMC) including PBLs were taken from interphase (see Fig. 2-2) and diluted with PBS. When contaminated with red blood cells (RBC) was visible, RBC were lysed with RBC lysis buffer containing in mM (150 NH_4Cl, 10 $KHCO_3$, 0.1 EDTA).

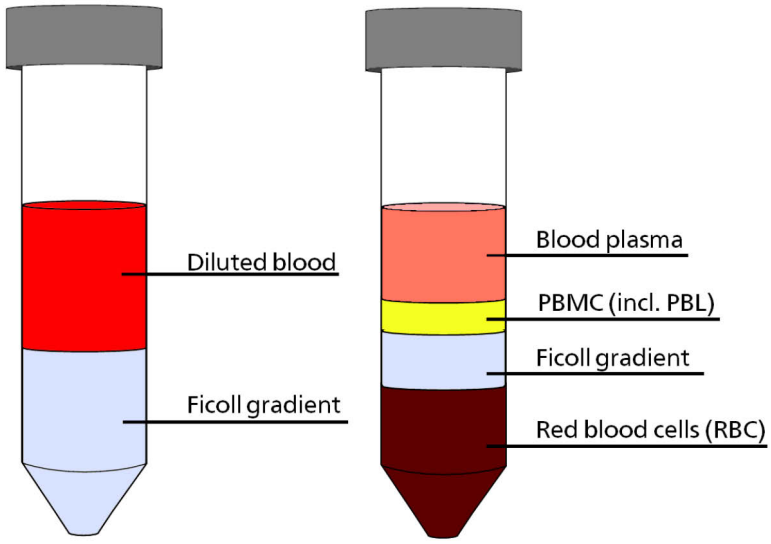

Fig. 2-2: Schematic view of blood sample before (left) and after (right) centrifugation
For separation of PBMC (including PBLs) from the blood plasma and from red blood cells, a ficoll gradient was used. After centrifugation (right) plasma, red blood cells and PBMC are separated and PBMC can be taken from the interphase (yellow).

After lyses of RBC the pellet was centrifuged (1300 rpm for 10 min) and washed with PBS (-/-) twice. The pellet was resuspended in PBMC medium (RPMI 1640 with 3 % heat inactivated autologous serum and 1 % penicillin/streptomycin) and incubated 1 hour at 37° C (separation step). After incubation all non-adherent cells (= PBLs) were collected and counted. After a last centrifugation step (1200 rpm for 10 min) cells were resuspended in PBL medium (RPMI 1640 with 20 % heat inactivated FCS, 1 % HEPES and 1 % penicillin/streptomycin) and stored at 37° C and 5 % CO_2.

2.3.3 Measurement of cell diameter

Cell diameters were determined with “EVE automatic cell counter” (NanoEnTek, Seoul, South Korea) a counting slide based automatic cell counter. For cell diameter studies a suitable protocol for Jurkat cells was established and all measurements were validated and if necessary corrected by hand using a personal computer based software. Viability was estimated by using trypan blue staining which only stains dead cells that have disintegrated plasma membranes.

2.3.4 Confocal laser scanning microscopy & organelle staining

Confocal laser scanning microscopy was performed on a Leica TCS SP or SP5 II (Leica Microsystems, Mannheim, Germany) equipped with a 63 x 1.2 water correction collar objective or 63 x 1.4 oil UV objective (HCX PL APO lambda blue).

Microscopy coverslips were cleaned using technical acetone followed by cleaning in a plasma furnace (Zepto-B) from Diener electronic (Ebhausen, Germany). The external buffer used for microcopy contained in mM (140 NaCl, 4 KCl, 1 $MgCl_2$, 5 Mannitol, 10 HEPES, 2 $CaCl_2$, pH 7.4).

When plasma membrane was stained, CellMask Orange™ from Thermo Fisher Scientific (Walham, USA) was used at a concentration of 0.5 µg/ml. Cells were incubated for 10-15 min in CellMask Orange™ and imaged. When nucleus was stained, Hoechst staining stock (200 µg/ml) was diluted 1:50 in external microscopy buffer or PBS and cells were stained for 10 minutes at 37° C. After this incubation time cells were washed twice and resuspended in microscopy buffer or PBS.

2.3.5 Cell irradiation

Cells were exposed in cell culture flasks to X-ray irradiation with a voltage of 90 kV and 33.7 mA using an Isovolt 160 Titan E X-ray source (GE Sensing & Inspection Technologies, Alzenau, Germany). Doses were delivered at a source to probe distance of 30 cm. Cell culture flasks were placed on a 2 mm aluminum slide and the doses rates were controlled by a dosimeter (DIADOS T11003). Different doses were achieved by varying the irradiation time.

For the alpha particle irradiation the alpha particle source Americium-241 with a radiation energy of 5.49 MeV was used. Due to the short range of alpha particles the Jurkat cells could not be irradiated inside a cell culture flask but mylar foil had to be used for irradiation. For this irradiation a custom-built stainless steel clamping ring was used as shown in Fig. 2-3.

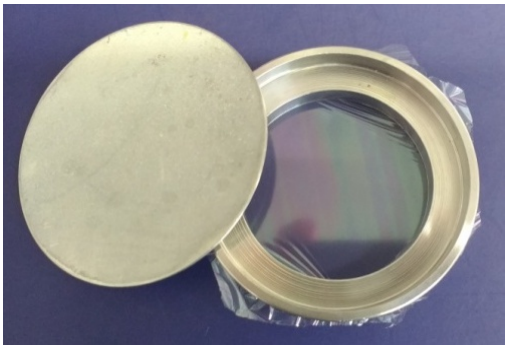

Fig. 2-3: A custom-built steel ring with mylar foil was used for irradiation of cells with α-particles
The combination of mylar foil that was clamped in between a sterilized, reusable steel ring system with lid served as a vessel for irradiation of Jurkat cells.

The stainless steel rings with clamped mylar foil could be autoclaved or sterilized by using 70 % ethanol a lid furthermore is preventing air-borne contamination during irradiation. A total volume of 5-7 ml cell suspension could be pipetted in each ring system. Together with a custom-built frame (Fig. 2-4) the steel rings with mylar foil were placed on the Americium-241 source to obtain a definite source-to-probe distance of a few millimeters.

Fig. 2-4: Custom-built frame for alpha particle irradiation
The mylar foil steel ring system (Fig. 2-3) was placed together with the custom-built steel frame on top of the alpha particle emitter to maintain a defined source to probe distance.

After irradiation cells were removed from the steel rings and pipetted in cell culture flask for further cultivation.

2.3.6 ROS treatment

Cells were directly in the cell culture medium treated for 10 min with different H_2O_2 concentrations. After the incubation time cells were spun down and washed with PBS. Finally cells were resuspended in fresh medium.

2.3.7 Cell cycle analysis by flow cytometry

Flow cytometric measurements were performed on propidium iodide (PI)-stained nuclei using a freshly prepared PI stock (0.5 mg/ml PI, 38 mM sodium citrate, pH 7), a RNaseA stock (RNaseA 5 mg/ml, 10 mM TrisHCl, 15 mM NaCl, pH 7), a BioRad S3 Cell Sorter (Hercules, USA) and the FlowJo 10 software for analysis (FlowJo LLC). Jurkat cells were cultivated for 48 hours after different doses of IR at 37° C and 5 % CO_2 in 25 cm^2 cell culture flasks. For fixation, cells were washed three times with PBS-EDTA. Cells were then fixed drop wise in 10 ml ice cold ethanol (96 %) under continuous vortexing; at this point cells could be stored overnight at 4° C. Cells were first stained by adding staining solution (4 % PI stock, 5 % RNaseA stock, 1 % FCS and PBS) and then incubated for at least 30 min at RT or overnight at 4° C in dark. Samples were passed through 40 µm filters and analyzed by flow cytometry. The percentages of cells in subG1, G1, S and G2/M phases were determined by single-parameter histograms of DNA content. Apoptotic cells were distinguished from normal cells by their fractional DNA content, as revealed by a subG1 peak of DNA content in the histogram.

2.3.8 Western blotting

For western blot experiments cell numbers were quantified with the “Eve Cell Counter” and the volumes of the corresponding cell suspensions were adjusted to obtain constant protein masses per ml cell lysate. Cells were centrifuged and resuspended in immuno precipitation (IP) buffer (8.7 % glycerin, 62.5 mM Tris-HCl, 2 % bromophenol-blue, 2 % β-mercaptoethanol) and incubated at 99° C for 10 minutes. After incubation cells were lysed 3 min at RT by

ultrasonication. Lysis was followed by a centrifugation step at 4° C and 12000 g for 10 min. Proteins were collected from supernatant and stored at -20° C. 15 % SDS-page gels were custom-made and polymerized with TEMED (tetramethylethylenediamine) and APS (ammonium persulfate). The cell lysates were added and gel ran for 40 minutes at 230 Volts. The transfer was performed as semi-dry-electrophoretic-transfer at 0.2 Ampere for 55 minutes. The blot buffer contained 48 mM Tris-HCl and 39 mM Glycin (pH 9.0). As transfer membrane a 0.45 µm PVDF (polyvinylidene difluoride) membrane was used. Immuno staining was performed by the alkaline phosphatase method after blocking of the membrane with skimmed milk powder for 1 hour at RT (or overnight at 4° C). The primary antibody was specific for the protein that should be detected, the secondary antibody was conjugated with the alkaline phosphatase. For detection of alkaline phosphatase activity 0.7 % NBT (nitro blue tetrazolium) and the chromogenic substrate BCIP (5-Bromo-4-chloro-3-indolyl phosphate) (0.3 %) was used. For size estimation of the observed bands the "PageRuler Prestained Protein Ladder" from Thermo Fisher Scientific (Walham, USA) was used. For immuno blot against CD25 a monoclonal IgG1 antibody against IL-2R alpha (CD25) from Thermo Scientific (Walham, USA) was used.

2.3.9 Statistical analysis

Data are expressed as means ± standard deviations (SD) of at least three different experiments; number of biological replicates (n) or independent experiments (N) are denoted. Significance was estimated by using the Student's t-test. A value of probability (p) < 0.05 was considered as significant (*), a $p \leq 0.01$ is specified as ** and a high significant difference of $p \leq 0.001$ was specified as ***.

2.4 Results

2.4.1 PBLs exhibit an increase in cell diameter after stimulation and X-ray treatment

It is well established that the cell diameter of peripheral blood lymphocytes (PBLs) increases in response to immune activation via the T-cell receptor (TCR) pathway or after treatment with mitogens like phytohemagglutinin (PHA-L), a plant lectin (Loris et al. 1998; Iritani et al. 2002). Fig. 2-5 shows representative confocal laser scanning microscope images of control PBLs and PBLs treated for 48 hours with 7.2 µg/ml PHA-L; the diameter of the latter is on average apparently larger than that of the control PBLs.

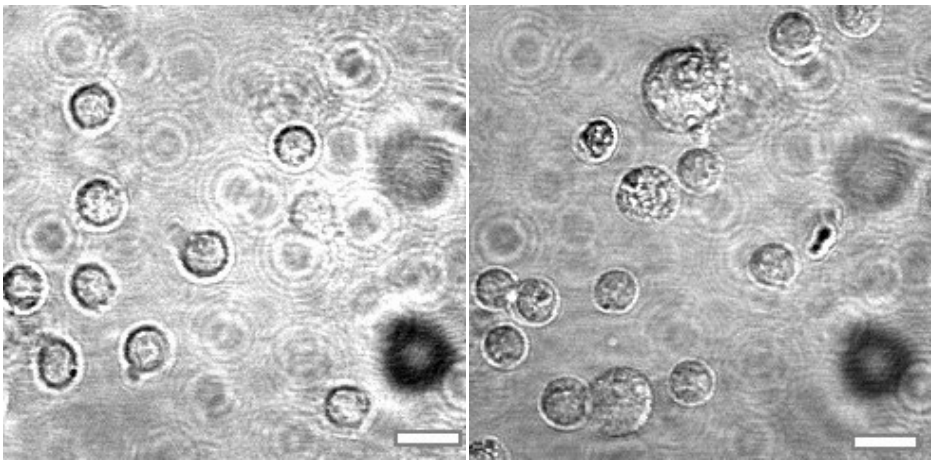

Fig. 2-5: PHA-L treatment induces an increased cell diameter in peripheral blood lymphocytes
Left picture shows PBLs isolated from buffy coat of healthy donor, right picture shows PBLs from the same donor treated with 7.2 µg/ml PHA-L for 48 hours (scale bars = 10 µm).

To study this apparent increase in cell diameter more in detail we measured and plotted the cell diameters of a large number PHA-L treated cells (n = 155) and compared them with control cells (n = 129).

Fig. 2-6 shows the diameter of all individual cells (circles) together with a box plot diagram with median (horizontal line), mean value (filled square) and whiskers indicating 5 % and 95 % of all cells.

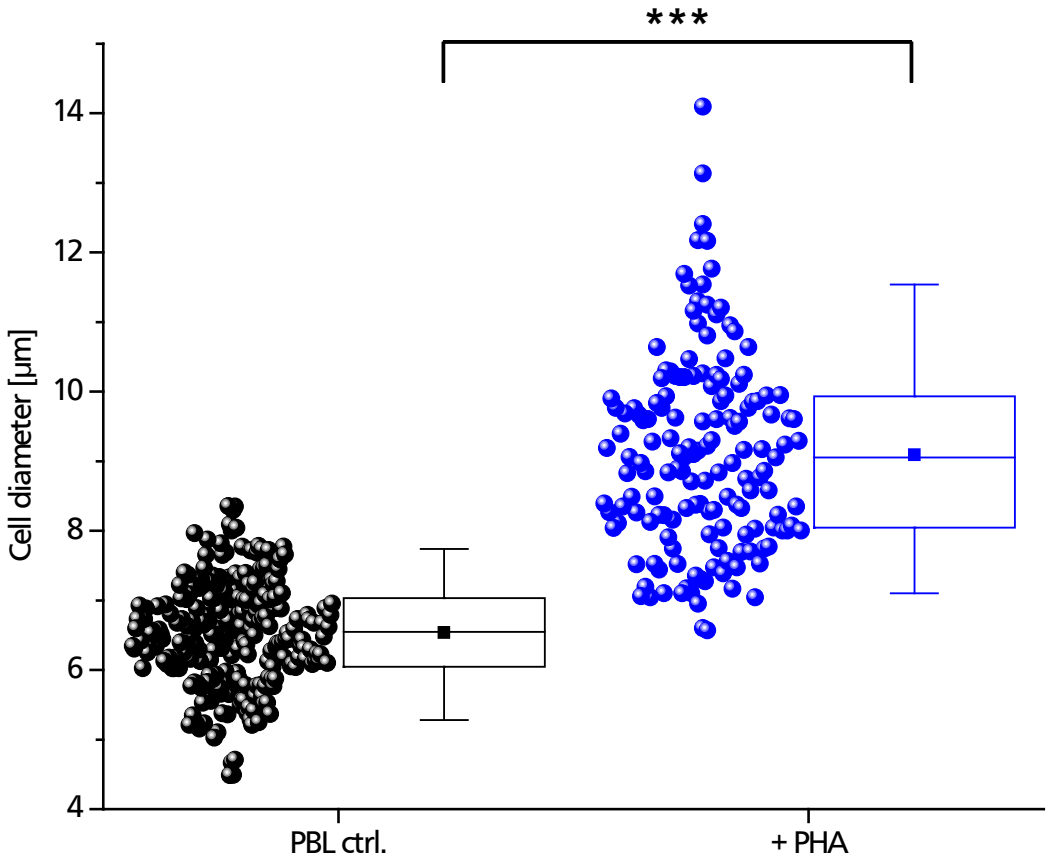

Fig. 2-6 PHA-L stimulation induces a strong increase in the cell diameter of PBLs
Black dots indicate single control PBLs; blue dots represent PHA-L treated PBLs. Corresponding box plots show mean (filled square) and median (line) as well as 25 and 75 % of the data; whiskers indicate 5 and 95 % of all cells. The highly significant difference of $p \leq 0.001$ is indicated by ***.

The average diameter of untreated freshly isolated PBLs is 6.45 ± 0.94 µm. After stimulation with PHA-L the mean diameter increases to 9.1 ± 1.38 µm. This increase is highly significant ($p < 0.0001$). Since the PHA-L induced increase in cell diameter is the consequence of an unspecific stimulation of the lymphocytes involving particularly Ca^{2+} signaling (Grissmer et al. 1992) we asked in the next set of experiments what effect ionizing radiation could have on lymphocytes. It is known that irradiation of tumor cells (A549) with low doses of X-ray triggers a transient elevation of radical oxygen species (ROS) including H_2O_2. This is causing a rise in the concentration of free Ca^{2+} in the cytosol, which in turn is triggering signal transduction cascades (Roth et al. 2015; Gibhardt et al. 2015). We predicted that similar ROS and Ca^{2+} mediated signaling cascades may be triggered in PBLs and that they may cause effects similar to those induced by a stimulation with PHA-L.

To further investigate the effect of both stimuli on the cell size we plotted the diameters of a large number of control cells, PHA treated lymphocytes and irradiated lymphocytes of three different healthy donors in a box plot. For X-ray irradiation we chose doses between 0.5, 2 and 5 Gy; notably the latter triggers a saturating increase in cell diameter. The data in Fig. 2-6 show that PHA-L triggers a homogeneous increase in cell size.

An irradiation of lymphocytes with X-ray on the other hand causes a dose dependent widening in the distribution of cell diameters (Fig. 2-7). Many PBLs exhibit also after irradiation a diameter which is in the range of the untreated controls. But with increasing X-ray dose the mean cell diameter increases clearly.

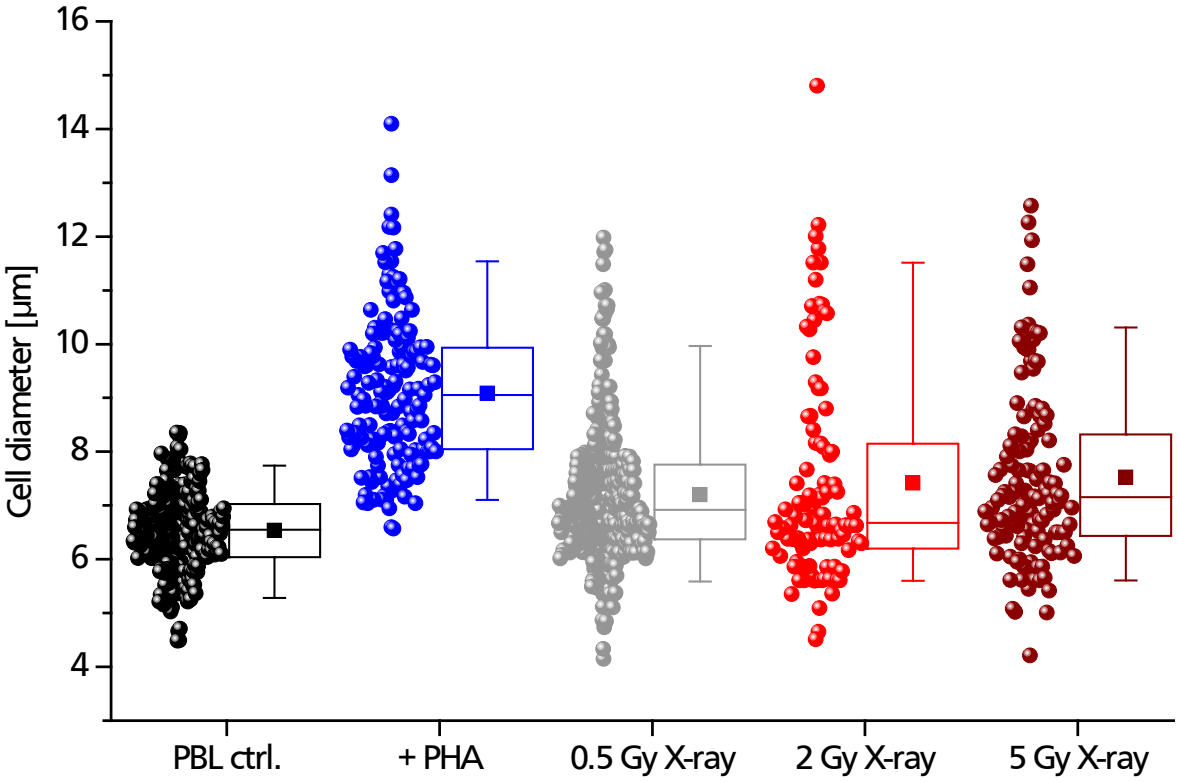

Fig. 2-7 Ionizing radiation elicits a widening in the distribution of PBL cell diameters

PBL populations exhibit cells with clearly increased cell diameter 48 hours after IR (0.5–5 Gy X-ray). The PBLs that show an increased cell diameter are in the size range of PHA stimulated cells (Fig. 2-6). Each circle represents a single PBL, box plots show mean (filled square) and median (line) as well as 25 and 75 % of the data; whiskers indicate 5 and 95 % of all cells.

This IR induced increase in cell diameter can also be seen in the microscopic images presented in Fig. 2-8 which compare control PBLs and PBLs 48 hours after irradiation with 0.5 Gy X-ray.

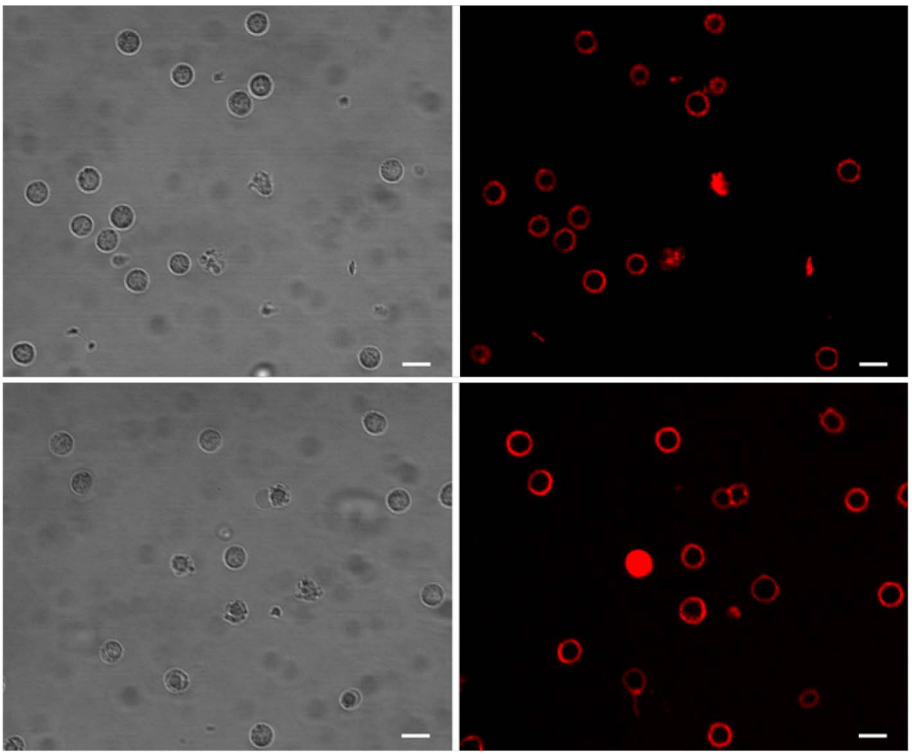

Fig. 2-8: Comparison of ctrl. PBLs (top row) and PBLs 48 h after 0.5 Gy X-ray irradiation (bottom row)
Microscopic images of control PBLs in transmitted light image (top left) and confocal laser scanning microscopy image after staining with CellMask Orange™ (top right). Bottom row shows PBL 48 hours after 0.5 Gy X-ray irradiation in transmitted light (left) and after staining with CellMask Orange™ (right) in confocal laser scanning microscopy image (scale bars = 10 µm).

While control PBLs exhibit a well defined mean cell diameter of 6.45 ± 0.94 µm, the mean diameter of PBLs 48 hours after irradiation with 0.5 Gy X-ray is increased to 7.19 ± 1.21 µm. 48 hours after irradiation with 2 and 5 Gy the mean diameter is 7.39 ± 1.95 µm respectively 7.46 ± 1.66 µm.

The results of these experiments suggest that IR triggers in a subpopulation of lymphocytes a signaling which eventually leads to an increase in cell size similar to the increase after stimulation. There are different possible scenarios by which IR could cause such a rise in cell diameter. IR might trigger the same signaling cascade as antigens and mitogens and thus lead to an increase in size due to higher metabolic activity and differentiation. II. irradiation could generate a G2-arrest. The latter could increase the cell diameter because the nucleus occupies almost ~ 55 % of the cell volume (Rosenbluth et al. 2006). III. Finally IR could cause just a swelling due to necrosis or a mitotic catastrophe. The contributions of these possible scenarios of explaining the IR induced change in cell size are now systematically investigated.

2.4.2 Ionizing irradiation stimulates an increase in cell diameter of Jurkat cells

To examine the effect of cell diameter increases due to ionizing irradiation in more detail, we exposed Jurkat cells to 2 Gy X-ray. 48 hours after the treatment the irradiated cells and control cells of the same age were imaged.

The representative microscopic images in Fig. 2-9 show that the control cells are generally smaller than the irradiated cells; control cells have a typical diameter of 10.11 ± 0.4 µm, while irradiated cells are larger (2 Gy: 11.95 ± 0.7 µm, 5 Gy: 12.7 ± 0.4 µm).

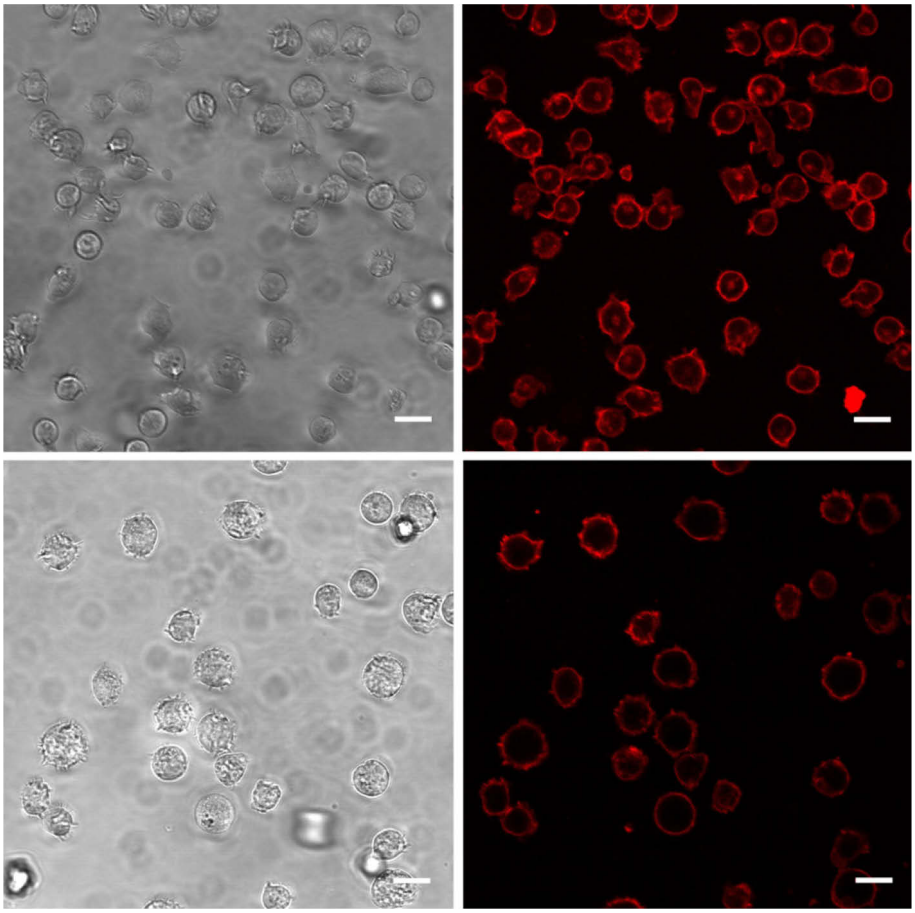

Fig. 2-9: Comparison of control Jurkat cells and Jurkat cells 48 hours after 2 Gy X-ray irradiation
Microscopic images of control Jurkat cells in transmitted light image (top left) and confocal laser scanning microscopy image after staining with CellMask Orange™ (top right). Bottom row shows Jurkat cells 48 hours after 2 Gy X-ray irradiation in transmitted light (bottom left) and confocal laser scanning microscopy image (bottom right) after staining with CellMask Orange™ (scale bars = 20 µm).

This apparent increase in cell diameter can be represented as mean cell diameters of a whole population (Fig. 2-13) or as a box plot diagram (Fig. 2-10) where the diameters of more than 600 individual cells are shown as single data points.

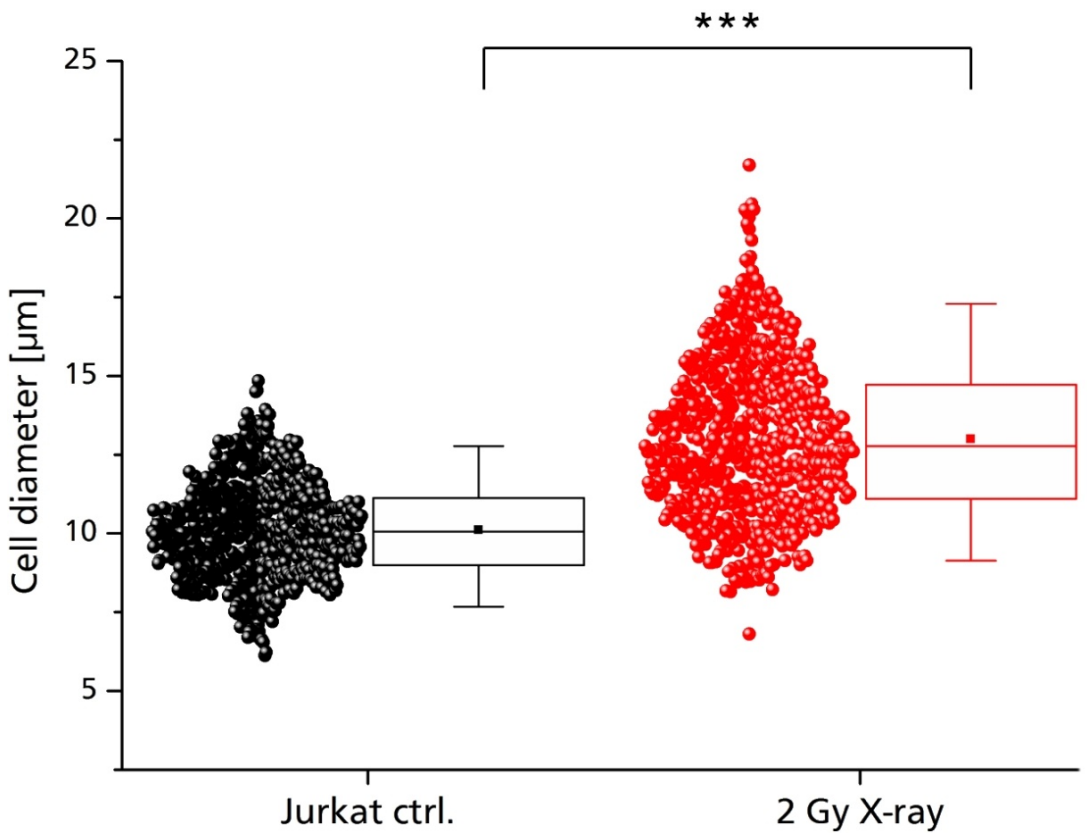

Fig. 2-10: Populations of Jurkat control cells (black) and 48 hours after 2 Gy X-ray irradiation (red)
48 hours after IR the mean cell diameter of Jurkat cells increases significantly and cells with large diameters that can never be found for control cells can be observed. Each circle represents a single Jurkat cell; box plots show mean (filled square) and median (line) as well as 25 and 75 % of the data; whiskers indicate 5 and 95 % of all cells. A high significant difference of $p \leq 0.001$ is indicated by ***.

The data consider more than 600 diameters of control and irradiated cells 48 hours after irradiation. IR apparently causes a strong increase in the mean cell diameter and cell diameter of irradiated cells exceed strongly the diameters that can be found for control cells. The by IR elicited increase in diameter is very similar to that triggered by PHA-L in lymphocytes (Fig. 2-6).

It is possible that Jurkat cells undergo apoptosis, necrosis or experience a mitotic catastrophe after irradiation. The latter would result in disturbed plasma membranes, membrane blebbing and miss-segregated nuclei with micronuclei (Vakifahmetoglu et al. 2008). To test for the occurrence of such morphological changes, the plasma membranes of Jurkat cells were stained with CellMask Orange™ and cell nuclei were stained with Hoechst dye.

The exemplary confocal laser scanning microscope images in Fig. 2-11 and Fig. 2-12 show the results.

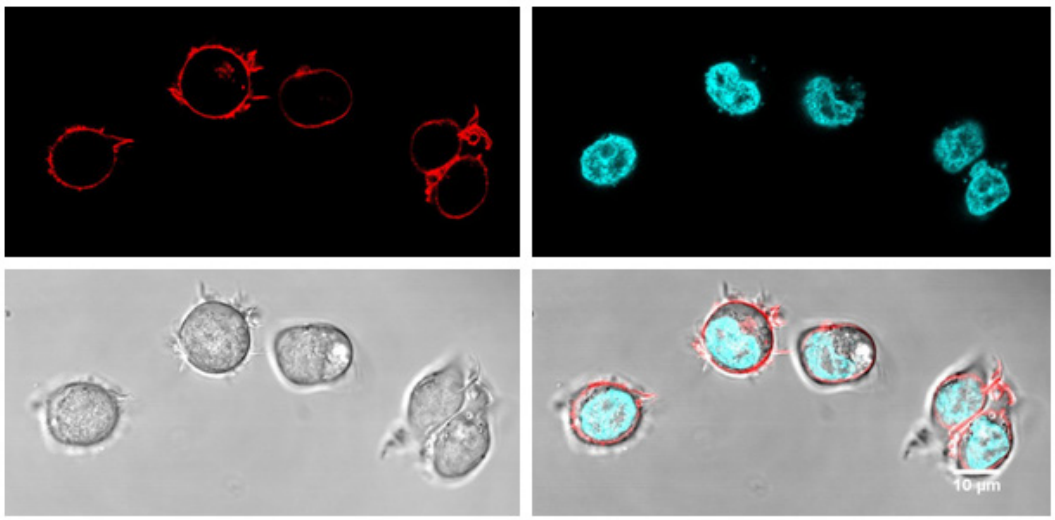

Fig. 2-11: Control Jurkat cells stained with CellMask Orange™ and Hoechst
Exemplary microscopic pictures that show the diversity already in control cells regarding cell nuclei size and appearance. (Top left) fluorescence channel with PM staining; (top right) Hoechst staining; (bottom left) transmitted light image; (bottom right) composite image with all fluorescence channels and transmitted light image (scale bar = 10 µm).

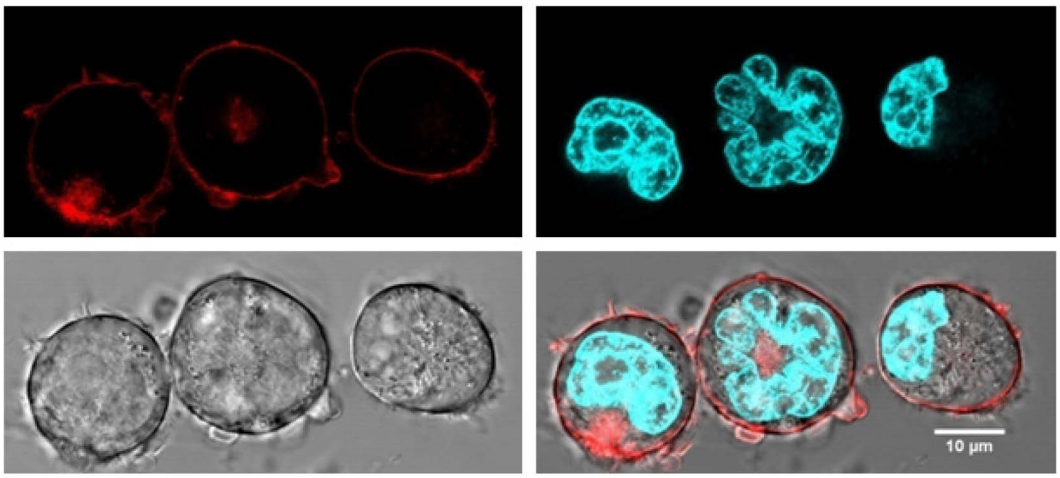

Fig. 2-12: Jurkat cells 48 hours after 2 Gy X-ray irradiation stained with CellMask Orange™ and Hoechst
48 hours after irradiation Jurkat cells are larger but plasma membrane integrity is intact, no blebbing can be observed. (Top left) fluorescence channel with PM staining; (top right) Hoechst staining; (bottom left) transmitted light image; (bottom right) composite image with all fluorescence channels and transmitted light image (scale bar = 10 µm).

Irradiated Jurkat cells appear larger and in many cells also the nucleus looks bigger than in control cells. This can be explained by the induced G2 cell cycle arrest (Chapter 2.3.7). No membrane blebbing, micronuclei or other signs that indicate apoptosis, necrosis or mitotic catastrophe can be found in a mentionable number of cells examined this way.

2.4.3 Viability & proliferation rates of Jurkat cells in response to IR remain high

To make sure that different treatments and / or different doses of ionizing radiation are not lethal for Jurkat cells, also the proliferation rate and the viability of every single cell batch was examined by trypan blue staining. Untreated Jurkat cells exhibit a doubling time of 25-35 hours (DSMZ, Germany). The 48 hour time point after irradiation or treatment is in the range of this doubling time. Not surprisingly, a very high mean proliferation rate of +237 ± 103.5 % and mean viability of 94.6 ± 5.3 % for control cells was evaluated (N = 28) at this time point. The mean proliferation rate of cells irradiated with 2 Gy X-ray was slowed down to +35.1 ± 28.75 % but the cell number still increased and the mean viability rate remained high. With 92.6 ± 4.1 % viability rate the irradiated cells are in the range of that in unirradiated cells (N = 18). This is in agreement with the literature which reports that volume decrease is correlating with apoptosis but volume increase correlates with proliferation and differentiation (Yu and Choi 2000; Lang et al. 2006).

2.4.4 The increase in cell diameter of Jurkat cells after X-ray is dose dependent

To examine the dose dependency of the IR induced increase in cell diameter effect, the same experiments like shown in Fig. 2-10 were repeated over a broad range of X-ray doses between 0.5 and 7 Gy. The mean increase in cell diameter was measured as relative increase (in %) over the diameter of untreated control cells. From the data in Fig. 2-13 it occurs that X-ray treatment generates a dose dependent increase in the diameter (Δcd), which saturates at a maximal increase of 27.3 % for doses ≥ 5 Gy . Higher doses result in an elevated apoptosis in which cells undergo apoptotic shrinking. This results in a lower mean cell diameter increase at higher doses (data not shown). The data can be fitted with a logistic equation (eqn 3) yielding a half maximal effect on the increase in Δcd at 1.11 Gy .

$$y = Vmax * \frac{x^n}{k^n + x^n} \text{ (eqn 3)}$$

Equation 3: Logistic equation

Plotting of the fitted experimental data against the radiation dose results in Fig. 2-13.

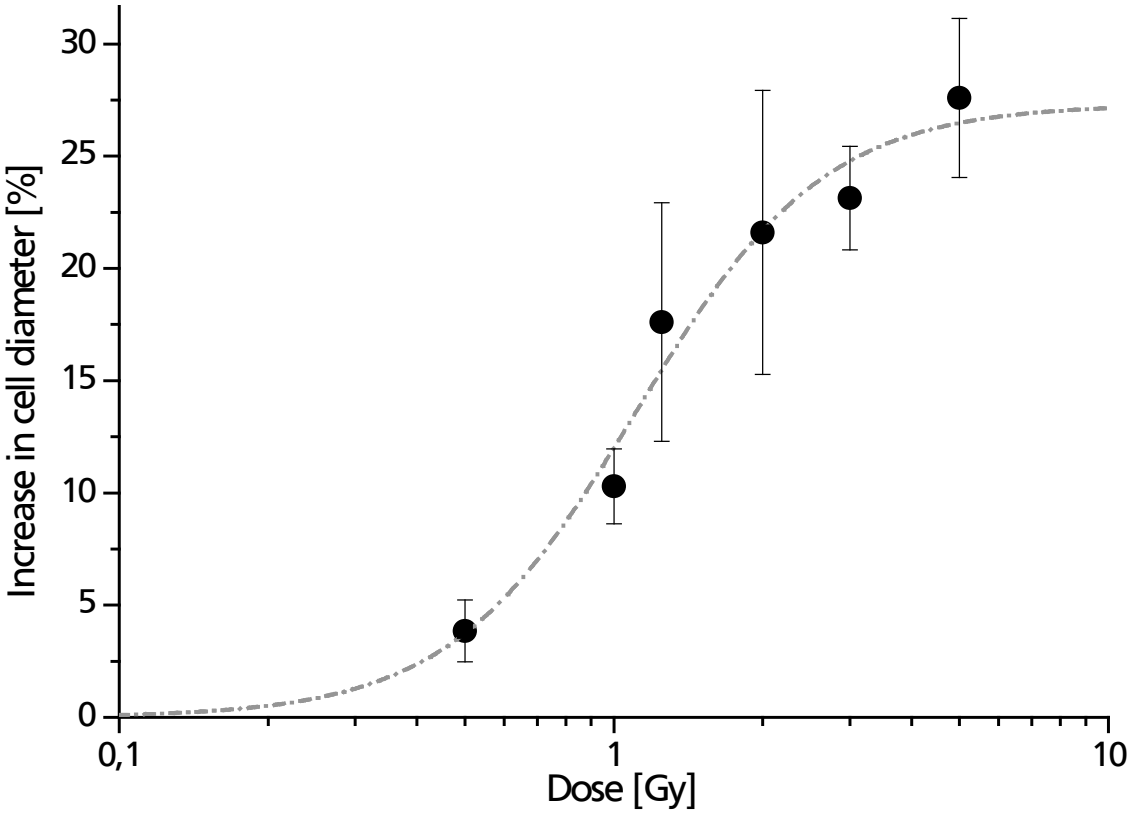

Fig. 2-13: Jurkat cells show a dose dependent increase in the diameter after X-ray irradiation
The mean cell diameter increase in response to X-ray as a function of the dose [Gy] is shown. The observed effect can be described by a logistic function (dashed line). The fit yields a half maximal effect at 1.11 Gy and a maximal effect (Vmax) of 27.3 %. Black circles represent the mean cell diameter of N = 7-15 independent experiments that were evaluated 48 hours after irradiation with "Eve Cell Counter" (see 2.3.3). Error bars indicate the standard deviation.

The mean cell diameter increase of Jurkat cells in response to X-ray exhibits a dose dependency and fitting of the experimental data with a logistic function yields a half maximal effect at 1.11 Gy and a maximal cell diameter increase of 27.3 %.

2.4.5 Cell cycle analysis after X-ray irradiation and cyclosporine A treatment

Cell cycle phase distributions can be examined by propidium iodide (PI) staining of cell nuclei after fixation of cells with ice cold ethanol. PI binds to DNA and the amount of dye bound to the DNA correlates directly with the content of DNA in individual cells. The relative content of DNA indicates in turn the cell cycle phase distribution for populations of cells. Jurkat cells are leukemic cells that proliferate without external stimuli and show a doubling time of 25-35 hours.

When the cell cycle distribution of untreated Jurkat cells is analyzed with a flow cytometer by propidium iodide staining of the nucleus after fixation (Fig. 2-14) we find in N = 17 experiments with each > 40.000 cells the following distribution: most cells were in G1 phase (66.6 ± 5.5 %), 14.6 ± 3.9 % in S phase, 3.2 ± 1.1 % in subG1 (apoptotic cells) and only 15.6 ± 3.9 % appeared to be in G2 phase.

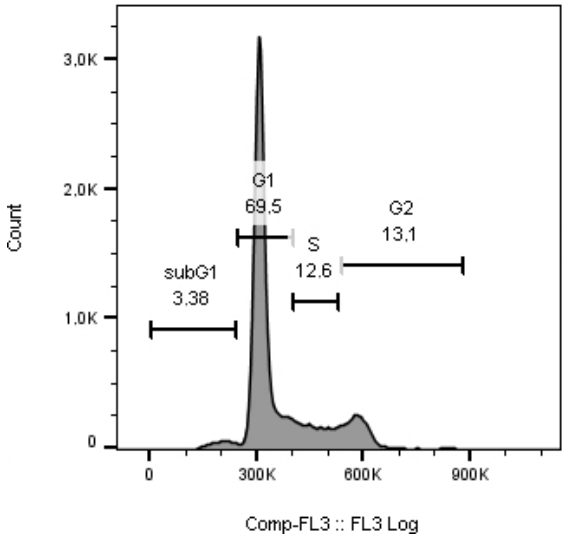

Fig. 2-14: Jurkat control cells exhibit a homogenous cell cycle phase distribution
Jurkat control cells exhibit a distinct G1 phase. The number of cells (count) is plotted as a function of the fluorescence intensity (FL3). Different fluorescence intensity corresponds to different cell cycle phases as it can be seen in this exemplary measurement.

Ionizing irradiation causes in many types of cells an arrest in the G2 phase of the cell cycle. The latter is typically correlated with an increase in the size of the cell nucleus and a decelerated proliferation. When Jurkat cells are irradiated with 1.25 Gy X-ray and the cell cycle distribution is analyzed 48 hours later, the cell cycle distribution is changed dramatically. Fig. 2-15 shows a typical example of cell cycle distribution of > 40.000 stained single cells.

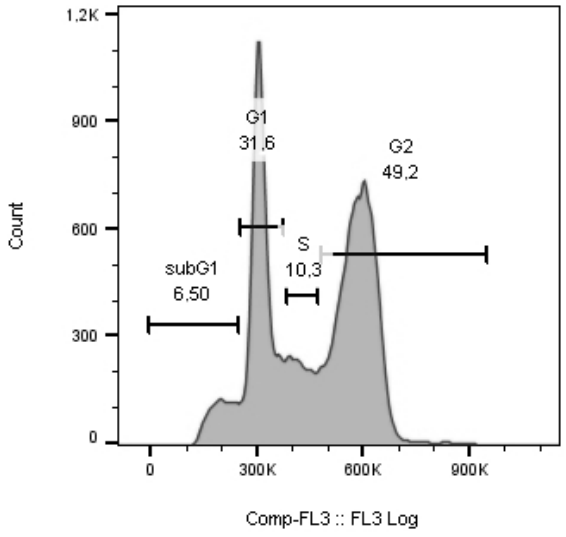

Fig. 2-15: 1.25 Gy X-ray induces a pronounced G2 cell cycle phase arrest
48 hours after IR 43.2 ± 5.2 % of all Jurkat cells are arrested in G2 cell cycle phase. The number of cells (count) is plotted as a function of the fluorescence intensity (FL3).

In N = 7 independent experiments of 1.25 Gy irradiated Jurkat cells, only 36.9 ± 5 % are found in G1 phase. The percentage of cells in G2 phase in contrast increases strongly to 43.2 ± 5.2 %. The apoptotic cells (subG1) remain only a relative small fraction (7.7 ± 1.9 %), while the percentage of cells in S phase is slightly reduced to 11.8 ± 2.4 %. The DNA damages induced by X-ray causes apparently a clear arrest of cells in the G2 phase. This arrest remains active even 48 hours after irradiation. The data also show that the relative high dose of 5 Gy X-ray is not lethal for most cells. Only 17.9 ± 0.1 % of the cells are in subG1 and apoptotic but a strong G2 phase arrest is induced, 76.3 ± 0.6 % of all cells are found to be in G2. Increasing the dose to 10 Gy X-ray clearly augments the rate of apoptosis; now 33.6 ± 3 % of the cells are in subG1 this is consistent with the lower mean cell diameter increase at doses > 5 Gy (Fig. 2-13). At the same time the portion of cells in G2 phase arrest decreases to 59.1 ± 2.1 %. When we examined the distribution of cells in G2 as a function of the X-ray dose (Fig. 2-16) we found that the latter parameter had a dose dependency that correlates to the increase in cell size (see Fig. 2-13).

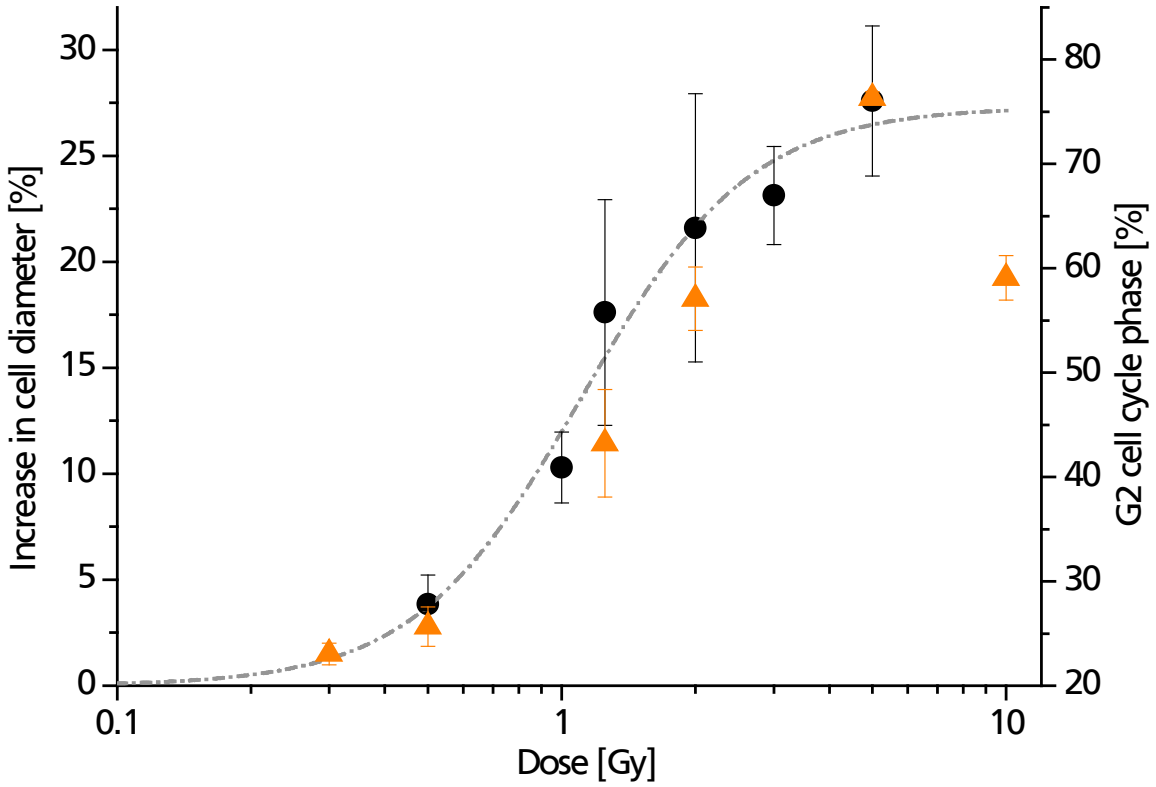

Fig. 2-16: G2 cell cycle phase distribution and increase of cell diameter as a function of X-ray dose
The mean cell diameter increase (left y-axis) in response to X-ray as a function of the dose [Gy] is shown and described by a logistic function (dashed line). Additionally the G2 cell cycle phase portion (right y-axis) as a function of the dose is shown. Orange triangles represent the mean G2 cell cycle phase portions for different doses of X-ray, error bars indicate the standard deviation. (For each dose N = 3-7)

To test if the two parameters are indeed causally related I treated Jurkat cells with the CDK1 inhibitor RO3306 ((5Z)-5-(6-Quinolinylmethylene)-2-[(2-thienylmethyl)amino)-4(5H)-thiazolone), which causes an efficient G2 arrest at concentrations of 3 µM. Challenging Jurkat cells with 3 µM RO3306 shifted 71 ± 2.1 % of all gated PI stained cells into the G2 phase; a value that is similar to the G2 arrest induced by 5 Gy X-ray.

Fig. 2-17 shows a typical example of cell cycle phase distribution of ~ 30.000 gated Jurkat cells after treatment with 3 µM RO3306.

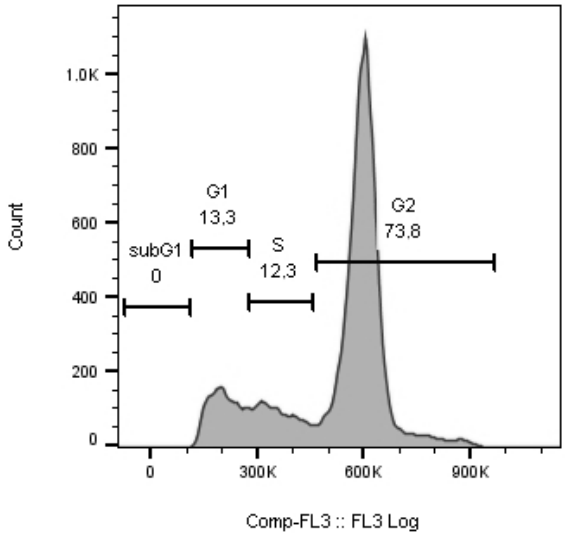

Fig. 2-17: Treatment of unirradiated Jurkat cells with 3 µM RO3306 results in a clear G2 phase arrest
48 hours after treatment of unirradiated cells with RO3306 cells show a clear shift G2 phase while subG1 level and hence apoptosis is low. The number of cells (count) is plotted as a function of the fluorescence intensity (FL3).

The complementary measurements of the cell diameter of unirradiated, RO3306 treated cells show that the CDK1 inhibitor caused only an 11.3 ± 4 % increase in cell diameter. A treatment with 5 Gy X-ray resulted on the one hand in a similar accumulation of cells in the G2 phase (76.3 ± 6 %) but on the other hand in a much stronger increase in diameter (27 ± 5 %). Fig. 2-18 shows the relative distributions of cell diameters after IR or RO3306 treatment.

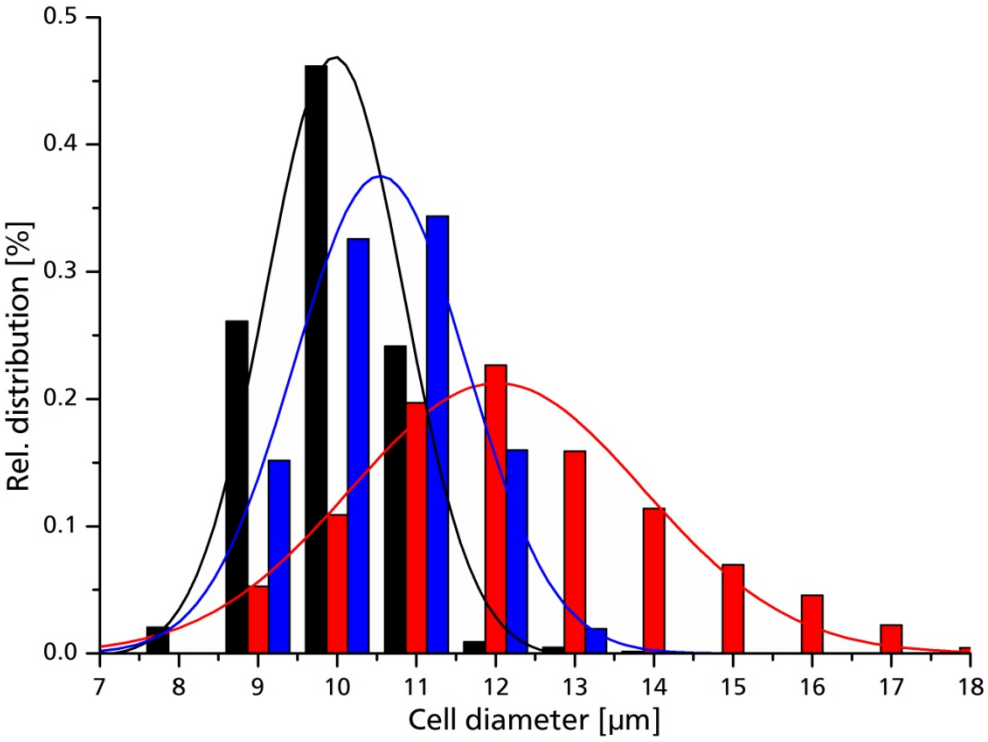

Fig. 2-18: Histogram of the relative distribution of cell diameters after different stimuli
The mean cell diameter distributions of three biological replicates of a representative experiment were Jurkat cell diameter were measured 48 hours after 2 Gy X-ray or 3 µM RO3306 treatment. A Gaussian fit was performed; 2 Gy X-ray apparently yields cell diameters that are not reached by

RO3306 treatment (G2 arrest). Mean values respectively width of Gaussian fits are for ctrl.: 9.97 ± 0.02 µm resp. 0.87 ± 0.03 µm; for RO3306 treatment: 10.54 ± 0.03 µm resp. 1.09 ± 0.03 µm; and for 2 Gy X-ray irradiation: 12.01 ± 0.12 µm resp. 1.85 ± 0.12 µm.

The results of these experiments show that ionizing irradiation causes a G2 arrest in Jurkat cells but the G2 arrest associated increase in cell diameter is not sufficient to explain the entire size increase after irradiation.

To test if the increase in cell diameter, that is cell cycle independent, is associated with an immune activation, I treated 2 Gy X-ray irradiated Jurkat cells with the immune suppressor Cyclosporine A (1 µM). I assumed, that this treatment should abolish any immune responses of the cells without affecting the IR induced cell cycle arrest in G2. The results of these experiments show that cyclosporine A is not influencing the radiation induced cell cycle phase arrest (Fig. 2-19).

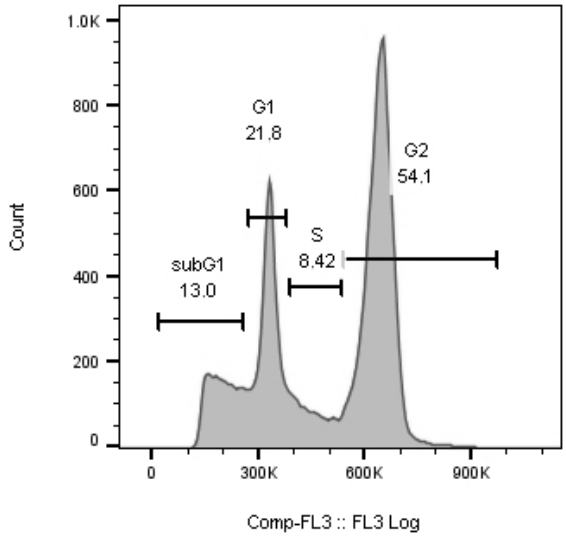

Fig. 2-19: Cyclosporine A treatment does not affect the IR induced cell cycle phase arrest
1 µM Cyclosporine A is not changing the portion of Jurkat cells that are 48 hours after 2 Gy X-ray treatment in held in G2 cell cycle phase. The number of cells (count) is plotted as a function of the fluorescence intensity (FL3Lin).

The cyclosporine A treatment did not influence the IR induced G2 arrest, but nevertheless decreases the effect of X-ray stress on the cell diameter. While the control cells increase by 21.6 ± 6 %, the cyclosporine treated cells, which are not able to undergo an immune response including NFAT, only increase by 12.2 ± 4 %. Notably this value is similar to the increase in size induced by the CDK1-Inhibitor alone, e.g. a treatment, which shifts cells into G2. Taken together the data show that an X-ray triggered increase in the diameter of Jurkat cells can be decomposed into two components: One component of about ~ 50 % of the increase in cell diameter could be caused by the increase in the nucleus during G2. The remaining increase in cell diameter are probably related to X-ray triggered immune activation or modulation in Jurkat cells.

The immune-suppressive effect of cyclosporine A can also be demonstrated by adding the inhibitor in a low concentration of 100 nM directly to the cell culture medium of freshly isolated PBLs.

These cells from three different healthy donors were then stimulated by a specific T-cell activator antibody mix that crosslinks CD2, CD3 and CD28 (Fig. 2-20). Clearly cyclosporine A is suppressing the activation process including the increase in cell diameter of PBLs. While control-PBLs exhibit a mean cell diameter of 6.74 ± 0.7 µm, T-cell activator treated PBLs show a 24.5 % increased mean cell diameter of 8.39 ± 2.1 µm. When T-cell activator stimulated PBLs are at the same time additionally treated with cyclosporine A, the mean cell diameter is only increasing by 7 % to a mean cell diameter of 7.21 ± 1.2 µm. These data support the strong immune-suppressive effect of cyclosporine A.

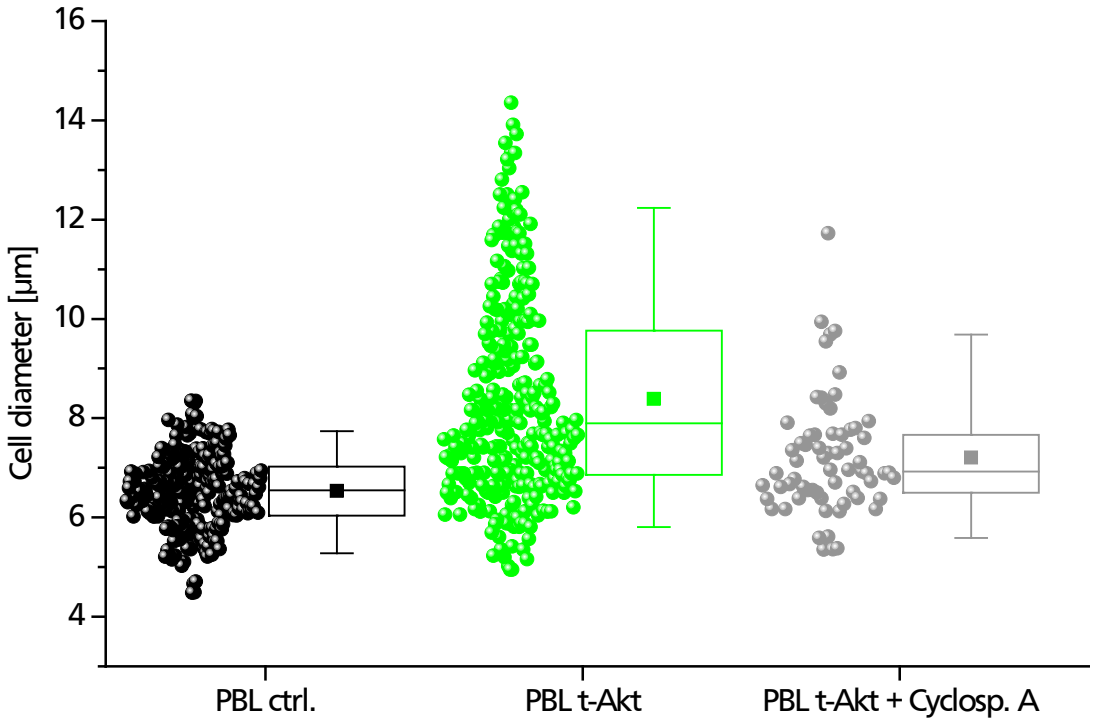

Fig. 2-20: The increase in cell diameter of PBLs after activation can be diminished by cyclosporine A
Control PBLs (black) and PBLs 48 hours after stimulation with the T-cell activator alone (green) or together with cyclosporine A (grey) the mean cell diameter was evaluated by confocal microscopy. Each circle represents a single PBL; box plots show mean (filled square) and median (line) as well as 25 and 75 % of the data; whiskers indicate 5 and 95 % of all cells.

2.4.6 Hydrogen peroxide triggers an increase in cell diameter of Jurkat cells

During irradiation of cells, reactive oxygen species (ROS) like H_2O_2 are generated directly inside the cytoplasm of cells as well as in the external solution. ROS can lead to many physiological reactions by their ability to function as second messenger. Furthermore ROS induce reversible oxidations of cysteines that could result in a similar modification like a phosphorylation or in a mimicked TCR stimulation (Reth 2002; Simeoni and Bogeski 2015). To test if a transient elevation of H_2O_2 in cells is able to substitute the irradiation stress, we treated Jurkat cells for 10 min with variable concentrations of H_2O_2 and monitored the cell diameter 48 hours after these treatments. The peroxide molecule is moderately membrane permeable and increases in this way the intracellular ROS concentration as well. Measurements of the cell diameter show that ROS treatment caused indeed a concentration dependent increase in cell diameter. The latter saturated at a maximal increase of about 10 % for H_2O_2 concentrations > 200 µM.

The fit of the data with a logistic equation provides a concentration of 49 µM for a half maximal increase in cell diameter. Previous studies have shown that the internal concentration, which is generated inside a cell, is approximately 100-500 times lower than that of the external medium (Gibhardt et al. 2015; Sies 2017). On the basis of these data we assume that the physiological concentration of 0.1-0.5 µM in the cell is generating the half maximal increase in cell diameter. In the next step we tested if this H_2O_2 induced increase in cell diameter is caused by an arrest of cells in the G2 phase. Jurkat cells were therefore treated in a similar manner with different concentrations of H_2O_2 and the distribution of cells in the cell cycle was monitored by flow cytometric analyses. The data in Fig. 2-21 show that H_2O_2 over a wide range of concentrations has only a small impact on the number of cells in G2 that is comparable to 0.3-0.5 Gy X-ray.

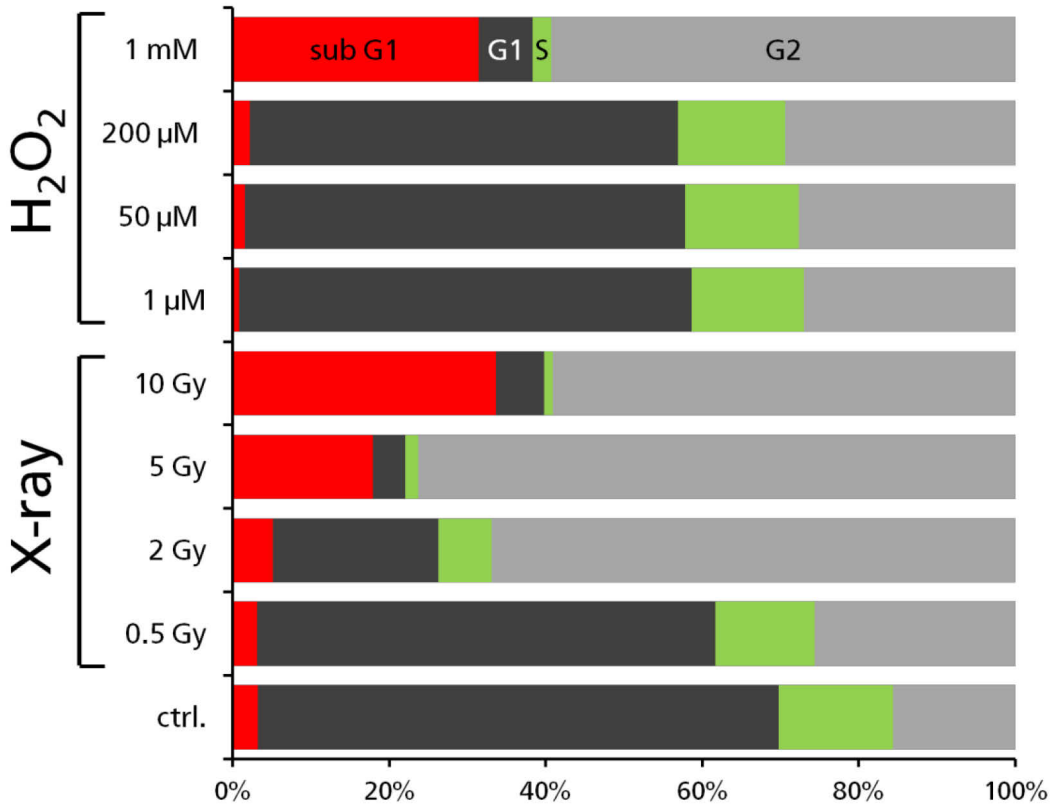

Fig. 2-21: Cell cycle phase distribution 48 hours after IR or treatment with H_2O_2

X-ray is triggering a strong G2 phase arrest already at low doses (> 0.5 Gy) without causing apoptosis (subG1). Only relative high doses of X-ray (≥ 5 Gy) lead to relevant subG1 numbers. H_20_2 in turn is in a wide range of concentrations not effecting a G2 phase arrest of a considerable portion of cells. Only in very high concentrations (1 mM) it leads to a G2 phase arrest but also to high apoptosis rate similar to 10 Gy X-ray. (SubG1 phase = red, G1 phase = black, S phase = green and G2 phase = grey).

The results of these experiments suggest that an increase of H_2O_2 in the cytosol causes an elevation in cell diameter beyond that induced by a G2 arrest (cell cycle dependent). The data hence advocate a role of H_2O_2 as a signaling molecule between radiation stress and increase in cell size. In the analysis above we have concluded that half of the size increase of the Jurkat cells is caused by an arrest in G2 and the remaining half by an effect, which is related to an immune response. The present data suggest that the 10 % increase in cell size, which is evoked by H_2O_2 is mostly due to a hypothetical immune response or immunological modulation.

This finding is in agreement with recent publications that showed data indicating that H_2O_2 is able to trigger signaling pathways similar to specific stimulation of T-cells (Jin et al. 1998; Reth 2002; Sies 2017).

2.4.7 The kinase inhibitors TBB and PP2 reduce the IR induced cell diameter increase

Tyrosine kinases of the SRC family and CK2 are playing a key role in regulation and transduction of various signaling pathways including the phosphorylation of the immunoreceptor tyrosine-based activation motif (ITAM). These kinases are therefore important drug targets (Kumar et al. 2007; Smith-Garvin et al. 2009; Murphy 2012; Nakahata and Morishita 2014). SRC kinases can be inhibited by PP2 (4-amino-5-(4-chlorophenyl)-7-(dimethylethyl)pyrazolo-[3,4-d]pyrimidine) and CK2 can be inhibited by TBB (4,5,6,7-Tetrabromobenzotriazole). Under the assumption, that SRC and CK2 kinases are playing crucial roles in the cell cycle independent cell diameter increase by mediating and amplifying T-cell signaling, I tested if the inhibitors PP2 and TBB are able to reduce the IR triggered cell cycle independent increase in cell diameter. Control experiments show that the inhibitors had no influence on the cell diameter of unirradiated cells. The application of either PP2 (10 µM) or TBB (10 µM) to cells, which were irradiated with 2 Gy X-ray, reduced the radiation triggered increase in cell diameter. While in the absence of inhibitors the cell diameter increases in response to 2 Gy X-ray by 21.6 ± 6.3 % the cell diameter of inhibitor treated cell only increased by 15.7 ± 0.7 % and 12.6 ± 2.5 % in the presence of PP2 or TBB respectively (Fig. 2-22). This remaining increase in cell diameter presumably reflects the cell cycle dependent increase during G2 arrest.

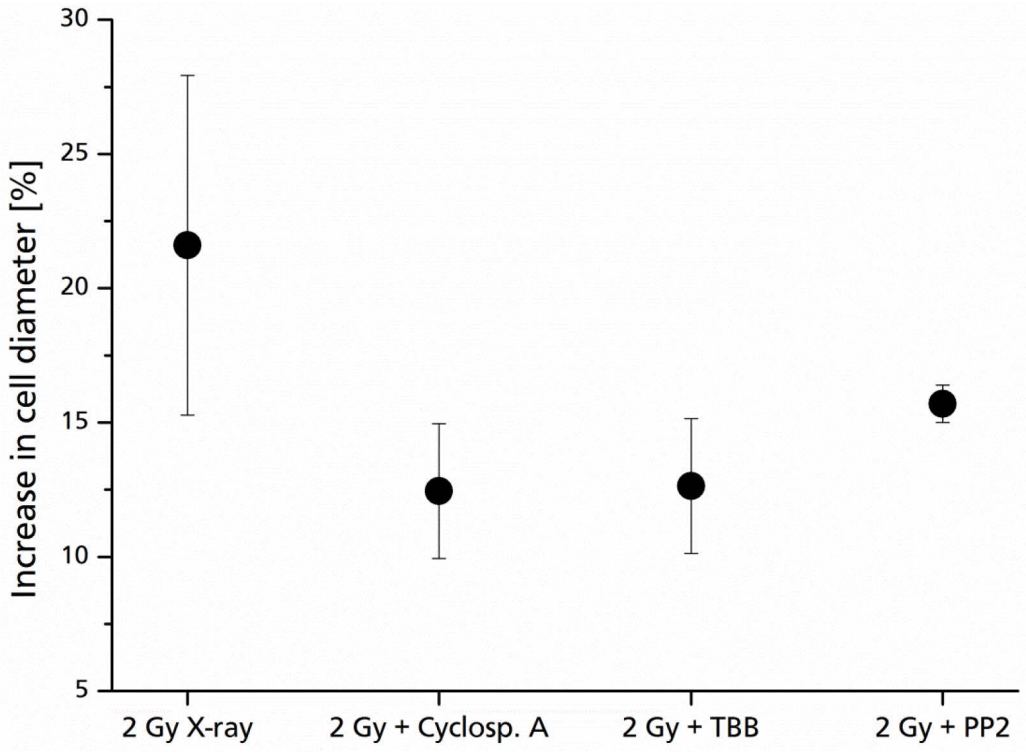

Fig. 2-22: The CK2 inhibitor TBB and the SRC inhibitor PP2 reduce the IR induced cell diameter increase
The increase in cell diameter 48 hours after 2 Gy X-ray is shown without or with simultaneous inhibition of CK2 by the specific inhibitor TBB or the inhibition of SRC kinases by the inhibitor PP2. Error bars indicate standard deviation (N = 3-17).

The reduced increase in cell diameter is presumably due to lower activity of SRC kinases and CK2 in the presence of the inhibitors. It suggests that the cell diameter increase is part of an immunological response of the irradiated immune cells. The increase in cell diameter, that is not blocked by the inhibitors is in the range of the increase of irradiated cells treated with the immunosuppressant cyclosporine A (12.2 ± 4 %). The latter increase in cell diameter, that is not cell cycle dependent, apparently involves the activity of SRC and CK2 kinases. This interpretation must be taken with some caution. There are publications, which report an increase in apoptosis in response of treatment with TBB at concentrations ≥ 25 µM (Ruzzene et al. 2002). To make sure that TBB treatment is at the concentration used in this study not lethal for Jurkat cells, I also measured the proliferation rate and the viability of every single cell batch was examined by trypan blue staining. The mean viability rate of the TBB Jurkat cells was 89.5 ± 9.9 % and in all experiments with 10 µM TBB the Jurkat cells proliferated (+57 ± 37 %). The results of these experiments suggest that the effect of kinase inhibitors on cell size increase is unlikely the result of an unspecific side effect.

2.4.8 Protein immunoblot detection of interleukin-2 receptor alpha chain (CD25)

The integral plasma membrane protein interleukin-2 receptor alpha chain (IL2RA) also called cluster of differentiation 25 (CD25), is widely used to evaluate the immunological activation state of immune cells. Most lymphocytes express the beta chains of the interleukin-2 receptor constitutively yielding a low-affinity receptor (Murphy 2012). After immunological activation of different T- and B-cell subtypes the alpha chain subunits are expressed yielding together with beta and the gamma chain a high specific, high affinity interleukin-2 receptor. One particular interesting T-cell subtype, the so-called T-regulatory (Treg) cells, also express CD25. Treg cells can inhibit and regulate immune responses and are important for treatment of autoimmune and chronic inflammatory diseases (Cruse and Lewis 2003). Western Blot analysis confirms an elevated expression of CD25 after irradiation of immune cells (Jurkat cells) (Fig. 2-23). An antibody against CD25 is expected to label protein bands with a molecular weight of 40 and 55 kDa respectively.

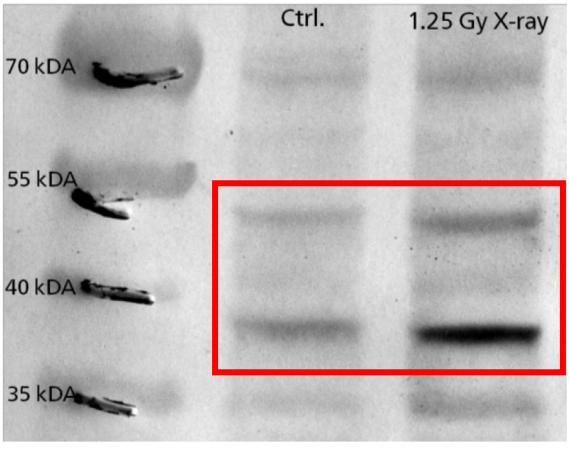

Fig. 2-23: Western blot analysis of CD25 expression by specific immuno staining
Western blot analysis shows that the levels of CD25 is higher in irradiated cells 48 hours after 1.25 Gy X-ray than in unirradiated cells.

The observed bands in the blot run in the range of the expected molecular weight of the interleukin-2 receptor alpha chain (CD25). Band intensities where quantified from the grey values of the images and normalized to the corresponding control bands. The analysis of band intensities of the exemplary western blot shown in Fig. 2-23 yields a factor of 2.74 by which the CD25 protein concentration is 48 hours after 1.25 Gy irradiation increased compared to the control. In N = 6 experiments this observation was consistently reproduced; on average the CD25 concentration is 2.1 ± 0.48 times higher in irradiated Jurkat cells compared to control cells. This increase in protein expression level is highly significant ($p > 0.0001$).

2.4.9 Alpha particle irradiation of Jurkat cells

Alpha particles are used as a therapeutic agent in the so-called balneotherapy where alpha particle emitting gases like radon (^{222}Rn) are employed for treating patients with inflammatory diseases. It has been mentioned in the introduction that the positive effects of this radon treatment must be related to extra-nuclear targets. Here elevated levels of ROS are good candidates for explaining therapeutic effects of Radon in cells and tissues. (Nagasawa et al. 1991; Deshpande et al. 1996; Shao et al. 2004). In analogy to the study with X-ray irradiation I examined in the next set of experiments the effect of alpha particles on Jurkat cells. Irradiation was in these experiments performed like explained in Chapter 1.1.3. Different doses [Gy] of alpha particle irradiation were achieved by varying the exposure time of the cell suspension to an alpha particle source. 48 hours after irradiation, I evaluated the increase in size, the viability and the increase in cell numbers. The data in Fig. 2-25 show that an exposure of Jurkat cells to alpha particles is triggering an increase in cell diameter too. But it is interesting to note that relative high doses of alpha particle irradiation were necessary to induce a clear cell diameter increase and G2 cell cycle arrest in spite of the high RBE of alpha particles. The relevant dose dependency of this treatment was less pronounced than after X-ray treatment. Also the maximal increase in cell diameter was smaller after alpha particle treatment than after X-ray irradiation. The viability of cells remained for all doses < 3 Gy relatively high (> 70 %). Also the proliferation rates were for low doses (0.3 and 0.5 Gy) relative high (> 73 %); for higher doses this parameter decreased (2 Gy: 48 %) or was almost zero (3 Gy: 6 %). The mean viability as well as the mean proliferation rate exhibited relative high standard deviations indicating that the impact of alpha particle irradiation on suspension cells like Jurkat cells is strongly dependent on the distance from the cells to the alpha particle source. Cells which are not precipitated on the mylar foil will not be hit by an alpha particle. An adhesive coating of the mylar foil would have increased the distance from the source to the probe; also coating would have made it difficult to transfer the cells after irradiation back into a cell culture flask for incubation. Fig. 2-24 shows the cell cycle phase distribution after irradiation with different doses of alpha particles. The data indicate that only few cells must have experienced a direct hit since only few cells undergo a G2 arrest or apoptosis (subG1).

This is not in agreement with the data obtained after X-ray irradiation where cells exhibit a strong G2 arrest already at relative low doses (Chapter 2.4.4).

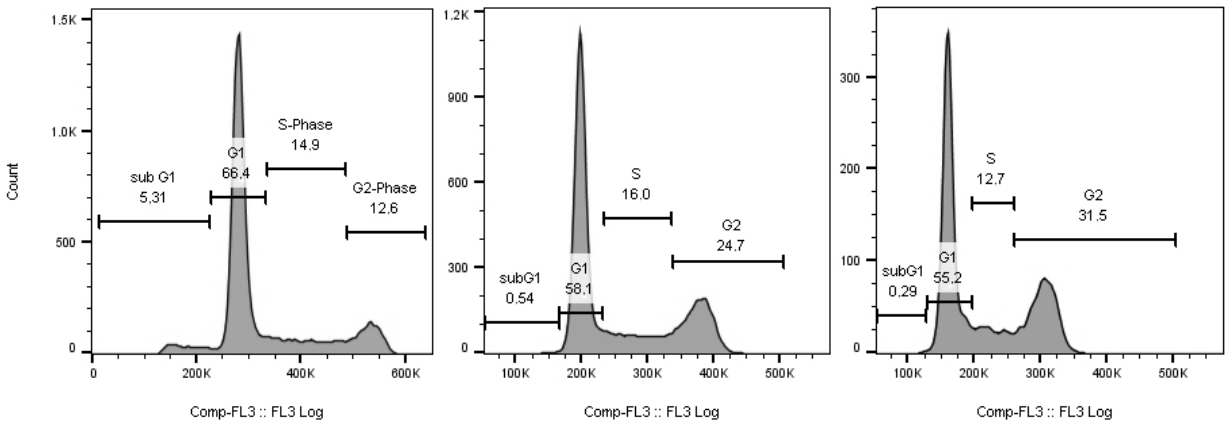

Fig. 2-24: 1-3 Gy alpha particle irradiation yields only small increases in the G2 cell cycle phase fraction

48 hours after cells were exposed to, from left to right, 1, 2 or 3 Gy alpha particle irradiation the cell cycle phase distribution was analyzed by PI staining. The distinct G2 cell cycle phase arrest known from X-ray (Chapter 2.4.4) cannot be observed after alpha particle irradiation. The number of cells (count) is plotted as a function of the fluorescence intensity (FL3).

The mean cell diameter increase after different doses of alpha particles is shown together with the G2 cell cycle phase distribution in Fig. 2-25. Also for the mean cell diameter increase big error bars indicate that the outcome depends strongly on how long the Jurkat cells were left on the mylar foil without agitation or disturbance.

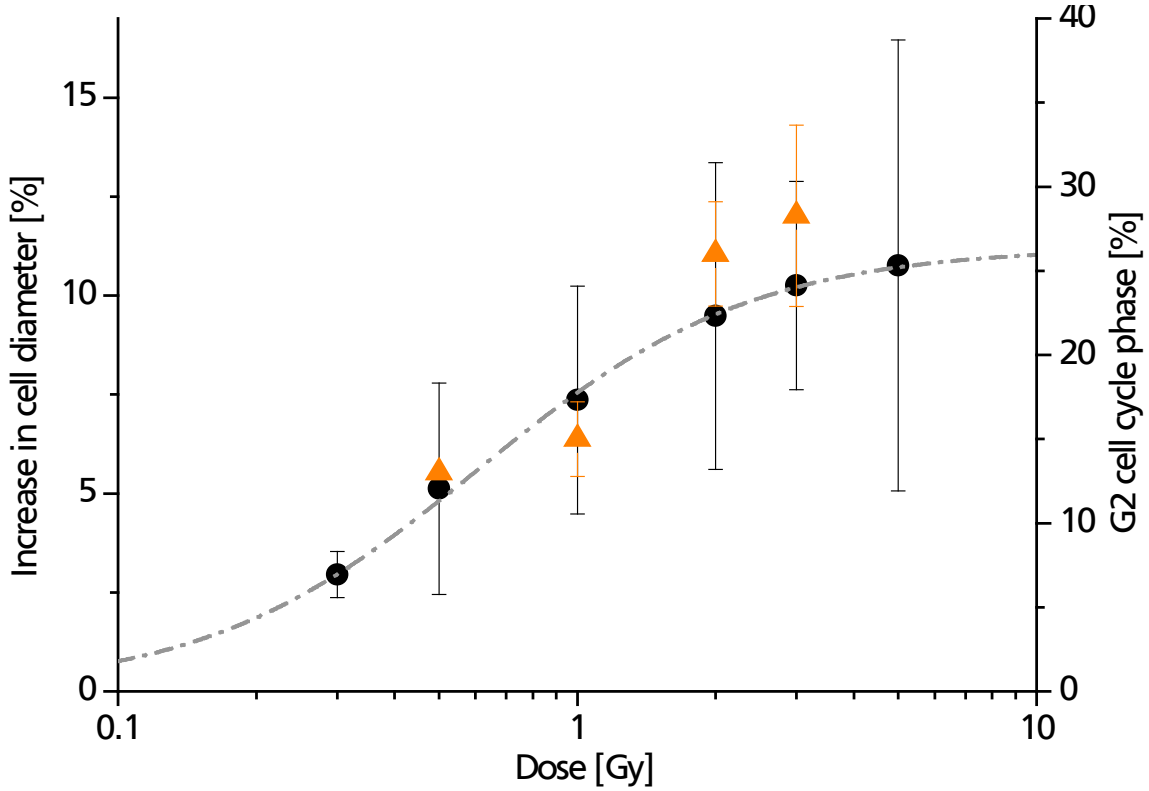

Fig. 2-25: Dose response curve showing increase in cell diameter [%] and G2 cell cycle phase portion [%]

The mean cell diameter increase in response to alpha particles as a function of the dose [Gy] is shown. The observed effect can be described by a logistic function (dashed line) the fit yields a half maximal effect at 1.45 Gy and a maximal effect (Vmax) of 11.2 %. Black circles represent the mean cell diameter of N = 3-12 experiments that were evaluated (see 2.3.3). Additionally the G2 cell cycle phase portion (y-axis) as a function of the dose is shown. Orange triangles represent the mean G2 cell cycle phase portions (for each dose N = 3-5). Error bars indicate the standard deviation.

Since Jurkat cells are suspension cells it is possible that only few cells were precipitated on the mylar foil and experienced a direct hit. This could also explain the high doses that were needed to induce changes in morphology and the cell cycle phase distribution. These relative high doses on the other hand might be capable to induce sufficient radical levels triggering earlier described processes (Chapters 1.1.3, 1.1.5 & 2.3.6)

2.5 Conclusion

Freshly isolated PBLs from healthy donors increased strongly in cell diameter after stimulation with the mitogen PHA-L or specific activation by T-cell activator antibody cocktail. This increase in cell diameter could be diminished by addition of immune suppressant chemicals confirming that the increase is due to an activation. This increase in cell diameter due to an activation is in agreement with the literature and reflects processes leading to cell growth, proliferation and differentiation that are characterized by altered gene expression and signaling pathways including kinases and phosphatases changes in the ion channel composition in the plasma membrane and the expression of, for T-cell function essential, surface proteins and receptors.

Interestingly, exposure of the same PBLs to ionizing radiation (IR) resulted in a similar cell diameter increase raising the question whether IR is able to trigger activation or immuno-modulatory processes. To study this in more detail, Jurkat cells were used in proceeding experiments. We were able to show that the cell diameter increase after exposure to IR is strongly dose dependent and can be described by a logistic function. Doses of X-ray ≤ 5 Gy were not lethal for Jurkat cells, but the proliferation rates were reduced. Flow cytometric cell cycle analyses by propidium iodide staining revealed furthermore that the reduced proliferation is due to a G2 cell cycle phase arrest which exhibits a dose dependency similar to the dose dependency of the increase in cell diameter. Since is it known from the literature that cells undergoing cell cycle arrest in G2 can increase in cell size, I tested if the observed cell diameter increase is simply due to the induced G2 cell cycle phase arrest by addition of a specific CDK1 inhibitor. The results presented in this thesis show that the G2 arrest causes indeed an increase in cell diameter but this increase is only ~ 50 % of the total cell diameter increase after irradiation. The additional increase in cell diameter is due to an immune activation tested by addition of an immuno suppressant drug to irradiated cells. Furthermore we were able to show that externally applied hydrogen peroxide is able to induce cell diameter increase. Since the fraction of cells in G2 is not significantly increased after hydrogen peroxide treatment, this increase in cell diameter is cell cycle phase independent but reflects an immuno-stimulation.

A possible signal transduction pathway after irradiation or hydrogen peroxide treatment could be mediated by SRC and CK2 kinases. SRC and CK2 are well known for playing important roles in immune signaling. In my experiments inhibition of SRC and CK2 led to a diminished cell diameter increase showing that kinase activity is mandatory for IR induced cell diameter increase and that the processes underlying the cell growth are similar to immune activation.

To confirm and underscore these findings I performed immuno blot experiments and was able to show that the interleukin-2 receptor alpha chain (CD25), a marker for activated T-cells, was upregulated due to IR. Interestingly, CD25 is also a marker for Treg cells and expression of CD25 due to IR could indicate a differentiation of the Jurkat T-cell progenitor cells to regulatory T-cells, a circumstance that needs further studies, but could be of significance for explanation of positive effects of IR on autoimmune and chronic inflammatory diseases.

2.6 References

Abbas AK, Lichtman AH (2003) Cellular and Molecular Immunology. 5., Sauders, Philad., USA

Akimzhanov AM, Boehning D (2012) IP3R function in cells of the immune system. Wiley Interdiscip Rev Membr Transp Signal 1:329–339.

Allen D, Fakler B, Maylie J, et al (2007) Organization and regulation of small conductance Ca2+-activated K+ channel multiprotein complexes. J Neurosci 27:2369–2376.

Allende JE, Allende CC (1995) Protein kinase CK2: an enzyme with multiple substrates and a puzzling regulation. FASEB J 9:313–323.

Cruse JM, Lewis RE (2003) Atlas of Immunology. 2., Springer Science & Business, New York, USA

Cuschieri A, Mughal S (1985) Surface morphology of mitogen-activated human lymphocytes and their derivatives in vitro. J Anat 93–104.

Deshpande A, Goodwin EH, Bailey SM, et al (1996) Alpha-particle-induced sister chromatid exchange in normal human lung fibroblasts: evidence for an extranuclear target. Radiat Res 145:260–267.

Donella-Deana A, Cesaro L, Sarno S, et al (2003) Tyrosine phosphorylation of protein kinase CK2 by Src-related tyrosine kinases correlates with increased catalytic activity. Biochem J 372:841–849.

Essen LO, Perisic O, Katan M, et al (1997) Structural mapping of the catalytic mechanism for a mammalian phosphoinositide specific phospholiase C. Biochemistry 36:1704.

Feske S (2007) Calcium signalling in lymphocyte activation and disease. Nat Rev Immunol 7:690–702.

Gibhardt CS, Roth B, Schroeder I, et al (2015) X-ray irradiation activates K+ channels via H2O2 signaling. Sci Rep 5:13861.

Grissmer S, Lewis RS, Cahalan MD (1992) Ca(2+)-activated K+ channels in human leukemic T cells. J Gen Physiol 99:63–84.

Iritani BM, Delrow J, Grandori C, et al (2002) Modulation of T-lymphocyte development, growth and cell size by the Myc antagonist and transcriptional repressor Mad1. EMBO J 21:4820–4830.

Jin YJ, Friedman J, Burakoff SJ (1998) Regulation of tyrosine phosphorylation in isolated T cell membrane by inhibition of protein tyrosine phosphatases. J Immunol 161:1743–50.

Krönke M, Leonard WJ, Depper JM, et al (1984) Cyclosporin A inhibits T-cell growth factor gene expression at the level of mRNA transcription. Proc Natl Acad Sci USA 81:5214–8.

Kumar V, Abbas AK, Aster J (2007) Robbins Basic Pathology. 8., Elsevier,

Amsterdam, Netherlands

Lang F, Shumilina E, Ritter M, et al (2006) Ion channels and cell volume in regulation of cell proliferation and apoptotic cell death. Contrib Nephrol 152:142–160.

Lin X, Wang D (2004) The roles of CARMA1, Bcl10, and MALT1 in antigen receptor signaling. Semin Immunol 16:429–435.

Loris R, Hamelryck T, Bouckaert J, Wyns L (1998) Legume lectin structure. Biochim Biophys Acta - Protein Struct Mol Enzymol 1383:9–36.

Matsuda S, Koyasu S (2000) Mechanisms of action of cyclosporine. Immunopharmacology 47:119–125.

Murphy K (2012) Immuno Biology, 8., Garland Science, Taylor & Francis Group, New York, USA

Nagasawa H, Little JB, Inkret WC, et al (1991) Response of X-Ray-Sensitive CHO Mutant Cells (xrs-6c) to Radiation: II. Relationship between Cell Survival and the Induction of Chromosomal Damage with Low Doses of αParticles. Radiation research 126:280–288.

Nakahata S, Morishita K (2014) PP2A inactivation by ROS accumulation. Blood 124:2163–2165.

Negulescu P a, Shastri N, Cahalan MD (1994) Intracellular calcium dependence of gene expression in single T lymphocytes. Proc Natl Acad Sci USA 91:2873–7.

Reth M (2002) Hydrogen peroxide as second messenger in lymphocyte activation. Nat Immunol 3:1129–1134.

Rosenbluth MJ, Lam WA, Fletcher DA (2006) Force microscopy of nonadherent cells: a comparison of leukemia cell deformability. Biophys J 90:2994–3003.

Roskoski R (2005) Src kinase regulation by phosphorylation and dephosphorylation. Biochem Biophys Res Commun 331:1–14.

Roth B, Gibhardt CS, Becker P, et al (2015) Low-dose photon irradiation alters cell differentiation via activation of hIK channels. Pflugers Arch Eur J Physiol 467:1835–1849.

Ruzzene M, Penzo D, Pinna LA (2002) Protein kinase CK2 inhibitor 4,5,6,7-tetrabromobenzotriazole (TBB) induces apoptosis and caspase-dependent degradation of haematopoietic lineage cell-specific protein 1 (HS1) in Jurkat cells. Biochem J 364:41–7.

Shao C, Folkard M, Michael BD, et al (2004) Targeted cytoplasmic irradiation induces bystander responses. Proc Natl Acad Sci USA 101:13495–13500.

Sies H (2017) Hydrogen peroxide as a central redox signaling molecule in physiological oxidative stress: Oxidative eustress. Redox Biol 11:613–619.

Simeoni L, Bogeski I (2015) Redox regulation of T-cell receptor signaling. Biol Chem 396:555–568.

Smith-Garvin JE, Koretzky GA, Jordan MS (2009) T cell activation. Annu Rev Immunol 27:591–619.

Vakifahmetoglu H, Olsson M, Zhivotovsky B (2008) Death through a tragedy: mitotic catastrophe. Cell Death Differ 15:1153–62.

Wange R (2000) LAT, the Linker for Activation of T Cells: A Bridge Between T Cell-Specific and General Signaling Pathways. Sci STKE 63

Yu SP, Choi DW (2000) Ions, cell volume, and apoptosis. Proc Natl Acad Sci USA 97:9360–9362.

3 Chapter 3: Ionizing radiation induces an increased adhesion of Jurkat cells

3.1 Abstract

Integrin mediated cell-cell and cell-surface adhesion is a key element of immune cell function. An activation of T-cells causes an elevated expression and subsequent clustering of integrins. These clusters in turn mediate cell-cell adhesion and the transmigration of immune cells through endothelia. In the present study a distinct flattening of irradiated Jurkat cells to glass surfaces could be observed 48 hours after irradiation. Comparative 3D confocal laser scanning microscopy images and measurements of the contact angle between cells and their glass support showed that irradiated cells exhibit a much higher propensity of adherence than unirradiated control cells. The same IR stimulated adherence of Jurkat cells was also evident under physiological conditions on endothelial cells. The highest adhesion rates occurred when the endothelial cells were pre-stimulated with TNF-α (tumor necrosis factor α), a factor that stimulates in endothelial cells an elevated expression of cellular adhesion molecules (CAM). The IR induced increased adhesion of Jurkat cells could be inhibited by the RGD peptide (Arg-Gly-Asp) suggesting that the adhesion is mediated by integrin-β-1. This hypothesis was further confirmed by combined immunostaining and single molecule microscopy, which confirms an upregulation and an increased clustering of integrin-β-1 in Jurkat cells after 48 hours after IR exposure. This increased clustering results in a higher biological activity of integrin-β-1 and hence explains the increased adhesion after IR.

3.2 Introduction

Immune cells need to be able to transmigrate from the blood stream through the endothelium of the blood vessel to sites of inflammation. The induction of transmigration depends on the interaction of signaling molecules with plasma membrane receptors. This in turn leads to cytoskeleton reorganization, changes in cell shape and reorganization of cell adhesion molecules (CAM) on the cell surface. CAM facilitate cell-cell and cell-surface adhesions as well as cell-cell interactions. Cellular adhesion molecules are therefore extraordinary important in almost all aspects of leukocyte function (Bevilacqua et al. 1987; Butcher and Picker 1992; Hallmann et al. 1995). CAM are grouped in different subclasses; selectins and integrins are the most important ones for lymphocyte function.

Selectins are glycoproteins and mediate by loose binding the so-called rolling of leukocytes on endothelial cells. Up to now there are three different groups of selectins described. L-selectin expressed in leukocytes, P-selectin expressed in platelets and activated endothelia and E-selectin (ELAM-1) expressed exclusively in activated (inflammatory related) endothelia (Cruse and Lewis 2003). Integrins are heterdimeric glycoproteins and comprised of α- and β-chain subunits. Integrins can cluster together with other transmembrane and intracellular proteins. These clusters can be functional in signal transduction as so-called focal adhesion. The large extracellular domains of β1- and β3-subunits have a specific recognition site,

the RGD sequence (Arg-Gly-Asp) that is found in glycoproteins of the extracellular matrix (Langhans et al. 2016). Because the integrin-mediated cell attachment influences and regulates cell migration, growth, differentiation, and apoptosis, an artificial addition of RGD peptides can be used to probe integrin functions in biological systems (Ruoslahti 1996). Integrin-β-1 in combination with different α-integrins subtypes are known as very late antigens (VLA-1-6). VLA clustering characterizes highly active lymphocytes. VLAs stimulate the attachment of lymphocytes to the endothelium and favor their transmigration trough the endothelium to e.g. inflamed tissues (Cruse and Lewis 2003; Kumar et al. 2007).

3.3 Materials & Methods

3.3.1 Chemicals and antibodies

All chemicals were purchased from Sigma-Aldrich GmbH (Taufkirchen, Germany), Biochrom AG (Merck KGaA, Darmstadt, Germany), AppliChem GmbH (Darmstadt, Germany), Merck KGaA (Darmstadt, Germany), Bio-Rad Laboratories GmbH (Muinch, Germany), VWR (Darmstadt, Germany), Qiagen (Hilden, Germany) or Invitrogen (Karlsruhe, Germany) if not specified further. Hoechst Staining was purchased from Sigma-Aldrich GmbH (Taufkirchen, Germany) and the plasma membrane stain CellMask Orange^{TM} from Life technologies (Carlsbad, USA). The Integrin-β-1 antibody was purchased from Biozol (Eching, Germany). RGD Peptide (GRGDSP) was purchased from ANASPEC INC. (Fremont, CA, USA) and solved in purified water.

3.3.2 Cell culture

Jurkat cells are a cell line established in 1976 from the peripheral blood of a 14-year-old boy with acute T-cell leukemia, a specific type of acute lymphatic leukemia (ALL). The Jurkat cell line is also called JM and grows singly or in small clumps as round, non-adherent suspension cells. The optimal split ratio is about 1:2-1:3 every 2 to 4 days at a maximum cell count of 1 x 10^6 per ml. The doubling time is 25-35 hours. For cell culture 37° C, 5 % CO_2 and RPMI 1640 medium with stable glutamine and 2.0 g/l $NaHCO_3$ + 2 mM L-glutamine, 10 % heat inactivated fetal calf serum (FCS) (Sigma-Aldrich, Germany) and 1 % mixture of penicillin/streptomycin was used. The Jurkat cell line (ACC 282) was purchased from the Leibniz-Institut DSMZ (Deutsche Sammlung von Mikroorganismen und Zellkulturen GmbH) and their immunological status is $CD2^+$, $CD3^+$, $CD5^+$, $CD6^+$, $CD7^+$, $CD8^-$, $CD13^-$, $CD19^-$, TCR α/β^+, TCR γ/δ^- ($^+$ stands for expression, $^-$ stands for no expression). EA.hy926 cells were cultivated in DMEM medium with 10 % FCS and 1 % mixture of penicillin/streptomycin. EA.hy926 cells were detached from cell culture flask for splitting by trypsinization.

3.3.3 Cell irradiation

Cells were exposed in cell culture flasks to X-ray irradiation with a voltage of 90 kV and 33.7 mA using an Isovolt 160 Titan E X-ray source (GE Sensing & Inspection Technologies, Alzenau, Germany). Doses were delivered at a 30 cm source to probe distance with cell culture flasks

placed on a 2 mm aluminum sheet. The doses rates were controlled by a dosimeter (DIADOS T11003). Different doses were achieved by varying the irradiation time.

3.3.4 Physiological adhesion assay

The physiological adhesion assay was carried out at the Universitätsklinikum Frankfurt am Main (Germany) in the workgroup of Prof. Dr. Franz Rödel. The protocol was adopted from Hildebrandt and co-workers (Hildebrandt et al. 2002) using the endothelial cell line EA.hy926 as endothelium. Peripheral blood monocytes (PBMC) or Jurkat cells were added to determine their adhesion rates to the endothelial cells. PBMC served as proof of principle. In contrast to the original protocol (Hildebrandt et al. 2002), not the endothelial cells but the Jurkat cells were irradiated 48 hours before the adhesion experiments were carried out. PBMC were isolated like described in 2.3.2 but no PBMC/PBL separation step was performed. For stimulation of endothelial cells TNF-α (tumor necrosis factor α) was used in a final concentration of 20 ng/ml. After 4 hours of stimulation endothelial cells were washed with PBS and cell culture medium. Adhesion experiments were carried out in 12 well plates using individual wells for different experimental conditions. Three technical replicates (3 wells) were included for each cell type (PBMC, Jurkat ctrl., Jurkat 1.25 Gy X-ray) and condition. PBMC and Jurkat cells were biotinylated using 50 µl biotinhydroxysuccimidester (10 ng/ml in DMF) per 5 ml cell suspension. Cells were incubated 15 min on ice and then washed with PBS to remove excess biotinhydroxysuccimidester. After re-suspending cells in PBL medium (see 2.3.2) cells were counted and 2-3 x 10^5 cells were added per well for the adhesion assay. Adhesion experiments were carried out under different incubation conditions; 4° C or 37° C with (+TNF-α) or without TNF-α pre-stimulation of the endothelia. All plates were incubated under slow agitation for 30 min using a tumbling shaker at ~ 100 rpm. This prevents cells from accumulating in the well centre and resembles physiological condition (modified after Hallmann et al. 1991). Unbound cells were removed by several washing steps using PBS. At the end of the incubation immune cells and endothelial cells were fixed by ice cold methanol (10 min). After fixation cells were washed and blocked with TRIS buffer (0.05 M Tris pH 7.4, 1 % BSA, 0.01 % Tween 20). 500 µl streptavidin-Cy3 conjugate (Dianova, Hamburg, Germany) with a concentration of 1:1500 in TRIS buffer was used to stain biotinylated immune cells (25 min, in dark). After several final washing steps the 12 well plates were dried and adhesion rates were evaluated using an “Operetta High Content Screener” (PerkinElmer, Waltman, USA).

3.3.5 Confocal laser scanning microscopy & staining

Confocal laser scanning microscopy was performed on a Leica TCS SP or SP5 II (Leica Microsystems, Mannheim, Germany) equipped with a 63 x 1.2 water corr (correction ring) objective or 63 x 1.4 oil UV objective (HCX PL APO lambda blue). Microscopy coverslips were cleaned with technical acetone followed by plasma cleaning in a plasma furnace (Zepto-B) from Diener electronic (Ebhausen, Germany). Coverslips were coated with poly-ethylene-glycol (PEG) by adding 50 µl of 0.4 mg/ml PLL(20)-g[3.5]-PEG(2) from SuSoS AG (Dübendorf,

Switzerland) was applied with a spin coater (Spin150 Rev.3.2) from APT GmbH (Bienenbüttel, Germany). The external buffer used for microcopy contained in mM (140 NaCl, 4 KCl, 1 $MgCl_2$, 5 Mannitol, 10 HEPES, 2 $CaCl_2$, pH 7.4). The in single molecule microscopy used STORM buffer contained like described in Babel et al. 2017: 100 mM MEA (beta-mercaptoethylamine, pH 8.5), 140 U catalase and 10 U glucose oxidase. Plasma membrane was stained with CellMask Orange™ (Molecular Probes, Thermo Fisher Scientific, USA) at a concentration of 0.5 µg/ml. For this purpose cells were incubated for 10-15 min with CellMask Orange™ and then imaged.

3.3.6 Single molecule measurements, image acquisition & data analysis

Single molecules measurement, image acquisition and data analysis was performed as described by Babel and co-workers (Babel et al. 2017) using a using a custom-built single molecule microscope, Fiji (Schindelin et al. 2012) and custom written software in MATLAB using the Ripley K function analysis.

3.3.7 Antibody staining

Antibody staining was performed as described by Babel and co-workers (Babel et al. 2017). In brief, a 1:10000 antibody dilution of the integrin anti CD29 Alexa 488 (integrin β1) antibody was used that binds to extracellular integrin domains. Hereby no permeabilization was needed. To analyze single molecules in fixed cells, cells were fixed with 4 % PFA for 1 hour at 4° C and washed three times with PBS. Unspecific binding sites were blocked after fixation for 1 hour with 1 % BSA solution (AppliChem, Darmstadt, Germany) at 37° C and washed with PBS three times. The cells were afterwards incubated for 3 hour at 4° C in the desired antibody solution. Finally, cells were washed three times and imaged using STORM buffer.

3.3.8 Statistical analysis

Data are expressed as means ± standard deviations (SD) of at least three different experiments, number of biological replicates (n) or independent experiments (N) are denoted. Significance was estimated by using the Student's t-test. A $p < 0.05$ was considered as significant (*), $p \leq 0.01$ is specified as ** and a high significant difference of $p \leq 0.001$ was specified as ***.

3.4 Results

3.4.1 3D imaging of Jurkat cells on glass surfaces

To understand the cellular responses of Jurkat cells to irradiation we imaged them 10-15 min after incubation on glass coverslips with a confocal laser scanning microscope (CLSM) 48 hours after exposure to 1.25 Gy X-ray. The plasma membrane of cells was made visible by adding CellMask Orange™ to the external microscopy buffer. This fluorescent dye is intercalating into the plasma membrane and makes it fluorescent. The representative images in Fig. 3-1 and Fig. 3-2 depict control cells and cells irradiated with 1.25 Gy X-ray in the z-axis on glass surface. Scrutiny of the 3D-stacks of CLSM images shows that the control cells are at this time point almost perfect spheres with a small foot with which the cells touch the glass surface. This foot area is clearly larger in irradiated cells which are incubated on the glass surface for the same length of time. The images suggest that the inherent tendency of Jurkat cells to adhere to the glass surface is strongly accelerated after exposure to ionizing irradiation.

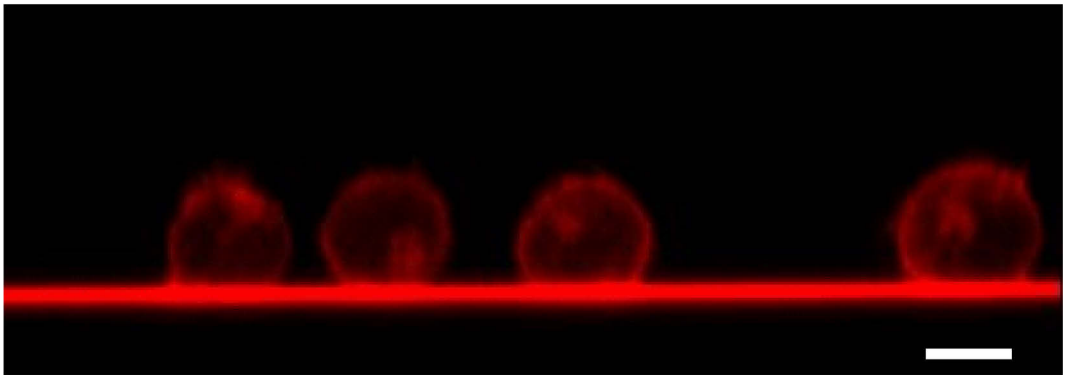

Fig. 3-1: Unirradiated Jurkat cells are almost perfect spheres on glass surfaces
3D-stack of CLSM images showing control Jurkat cells 10 minutes after pipetting the cells on the cover slip. Plasma membranes were stained by addition of CellMask Orange™ (scale bar = 20 µm).

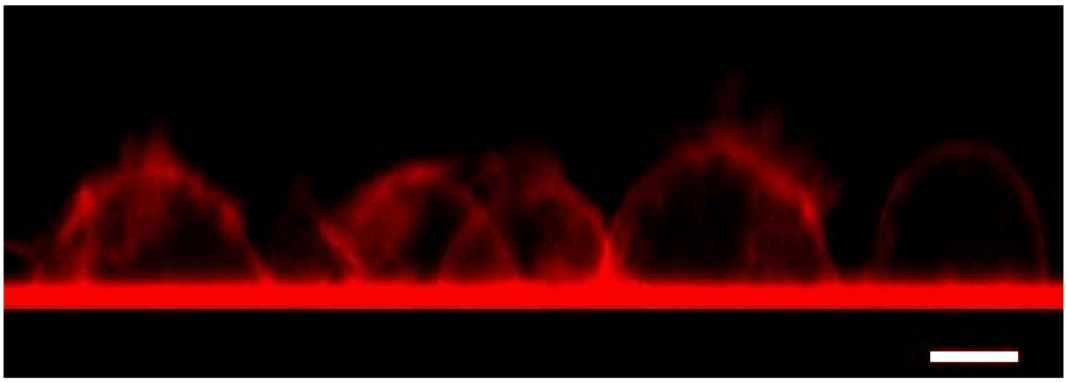

Fig. 3-2: 1.25 Gy X-ray irradiated Jurkat cells (48 h) tend to flatten on glass surfaces
3D-stack of CLSM images showing Jurkat cells 48 hours after irradiation with 1.25 Gy X-ray and 9 minutes after pipetting the cells on the cover slip. The plasma membrane was stained by addition of CellMask Orange™ (scale bar = 20 µm).

To quantify this apparent adhesion of the irradiated cells to glass surfaces we estimated the contact angle between the cells and the glass surfaces (Fig. 3-3).

The contact angle is an established parameter for quantifying the adhesion of spherical particles like Jurkat cells to a surface. The basis for this approach is the Young-Laplace equation.

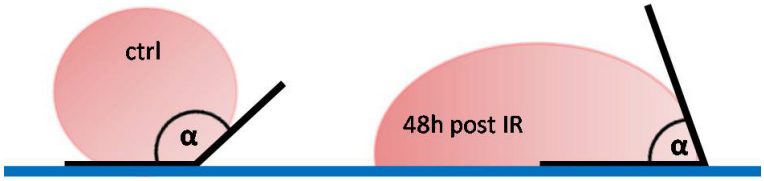

Fig. 3-3: The contact angle was determined according to the Young-Laplace equation
The contact angle (α) between the cells and the surfaces are determined as inner angle between a cell membrane and a cover slip. Basis for this approach is the Young-Laplace equation.

The data in Fig. 3-4 show that an irradiation of cells with 1.25 Gy X-ray triggers a significant decrease in the contact angle from 101.1 ± 17.7° in control cells to 78.3 ± 20.8° in irradiated cells 48 hours after IR. This highly significant decrease in contact angle ($p < 0.001$) is reflecting an irradiation triggered adherence and hence a flattening of Jurkat cells to glass surfaces.

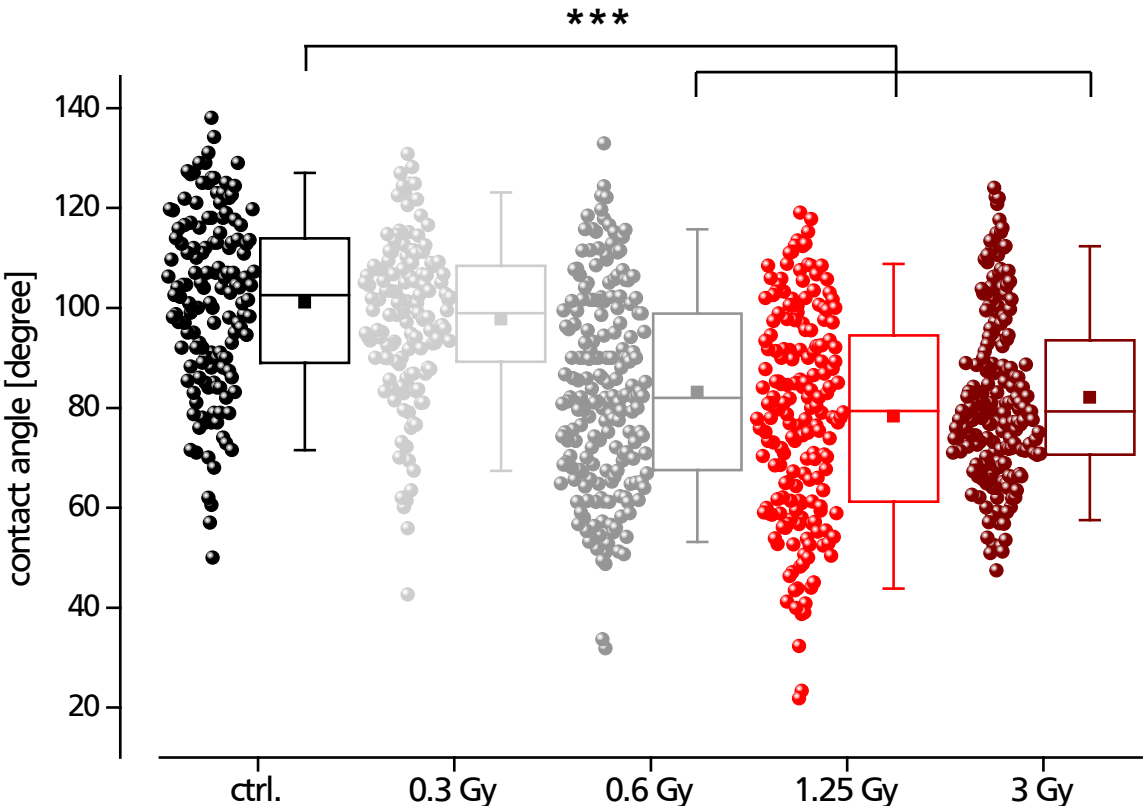

Fig. 3-4: Contact angle of single 3D-scanned Jurkat cells over a wide range of X-ray doses
The mean contact angle of Jurkat cells decreases significantly with increasing dose [Gy] 48 hours after IR ($p < 0.001$). Each circle represents a single Jurkat cell analyzed by 3D-scan; box plots show mean (filled square) and median (line) as well as 25 and 75 % of the data; whiskers indicate 5 and 95 % of all cells. The highly significant difference of $p \leq 0.001$ between control cells and 0.6-3 Gy X-ray irradiated cells is indicated by ***.

To further test whether this effect is indeed the consequence of cell adherence, the same experiments were repeated on glass cover slips which were pretreated by coating with polyethylene glycol (PEG). The increased hydrophilic nature of the PEG surface is expected to prevent cell-cell and cell-surface adhesion. Fig. 3-5 shows a 3D-stack of CLSM images of Jurkat cells irradiated with 1.25 Gy on such a PEG pre-coated cover slip. Even though the cells are

clearly larger after irradiation (Chapter 2), the cells are definitely less flattened to the PEG pre-coated glass surface compared to uncoated cover slips (Fig. 3-2). The results of these experiments show that the flattening of irradiated cells is indeed due to increased cell-surface adhesion. The data illustrate that a PEG coating increases, as expected, the contact angle due to a decreased cell-surface adhesion.

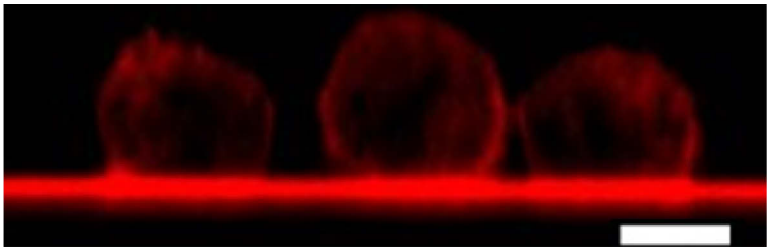

Fig. 3-5: Irradiated Jurkat cells do not flatten on PEG coated glass coverslips
3D-stack of CLSM images showing Jurkat cells 48 hours after irradiation with 1.25 Gy X-ray and 11 min after pipetting the cells on a PEG pre-coated cover slip. The Plasma membrane was stained by addition of CellMask Orange™ (scale bar = 20 µm).

The data in Fig. 3-6 shows that control cells (124.5 ± 12°), as well as irradiated cells (122.1 ± 14.2°) exhibit both on PEG pre-coated cover slips a large contact angle. The mean contact angles of control and irradiated cells are no longer significantly different (p = 0.29).

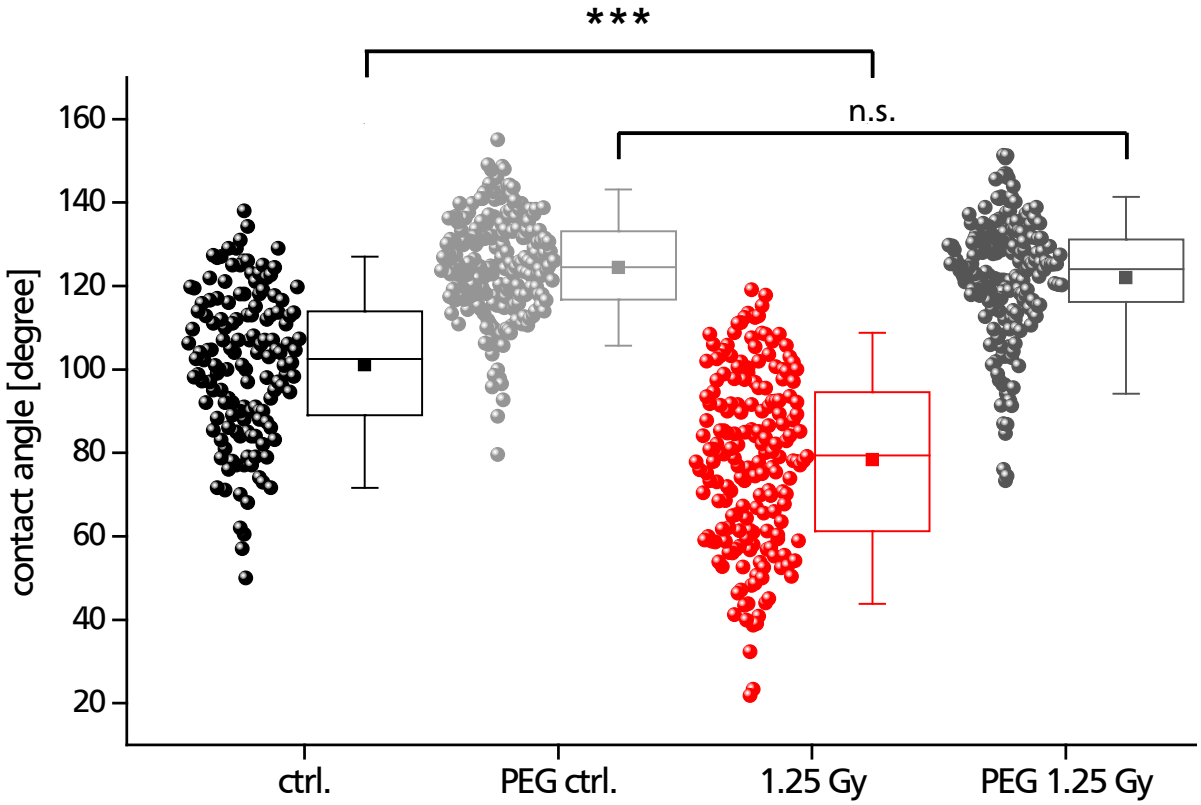

Fig. 3-6: PEG pre-coating of cover slips prevents irradiated cells from adhering
The highly significant irradiation generated decrease in mean contact angle 48 hours past IR (red) compared to unirradiated control cells (black) (data from Fig. 3-4), can be diminished by pre-coating the glass coverslips with PEG. Control cells exhibit on PEG coated cover slips a slightly larger contact angle (light grey) while irradiated Jurkat cells in contrast show a largely increased contact angle (dark grey) compared to uncoated cover slips. The difference between control and irradiated cells is no longer significant (p = 0.29). Each circle represents a single Jurkat cell analyzed by 3D-scanning; box plots show mean (filled square) and median (line) as well as 25 and 75 % of the data; whiskers indicate 5 and 95 % of all cells. A high significant difference of p ≤ 0.001 is indicated by ***; no significant difference (p > 0.5) is indicated by n.s..

The hydrophilic surface of PEG coating prevents an cell-surface adhesion of the irradiated Jurkat cells. The results of these experiments suggest that untreated Jurkat cells have only a low propensity for adhering to glass surfaces. This tendency is strongly accelerated by irradiation of cells with X-ray.

3.4.2 Physiological adhesion assay on endothelial cells,

Induction and maintenance of the immune response of T-cells is mediated by an adhesion of these lymphocytes to various types of cells. To test whether ionizing irradiation is also stimulating cell adhesion of Jurkat cells we performed a conventional physiological adhesion assay on EA.hy926 endothelial cells. Jurkat cells were irradiated again with 1.25 Gy X-ray; unirradiated cells served as control and freshly isolated PBLs as proof of priciple. TNF-α, an established stimulator of endothelial cells was used to induce the surface expression of selectins like E-Selectin (ELAM), an inflammation induced adhesion molecule that is needed for a low affinity binding during rolling of T-cells on the endothelium. Furthermore TNF-α induces the expression of high affinity adhesion molecules of the immunoglobulin superfamily like intercellular adhesion molecules (ICAMs) and vascular cell adhesion molecules (VCAMs) that are binding partner for integrins and needed for adhesion and transmigration of lymphocytes through endothelia (Bevilacqua et al. 1987; Butcher and Picker 1992; Hallmann et al. 1995). The processes of rolling, adhesion and transmigration through endothelia is shown in Fig. 3-7.

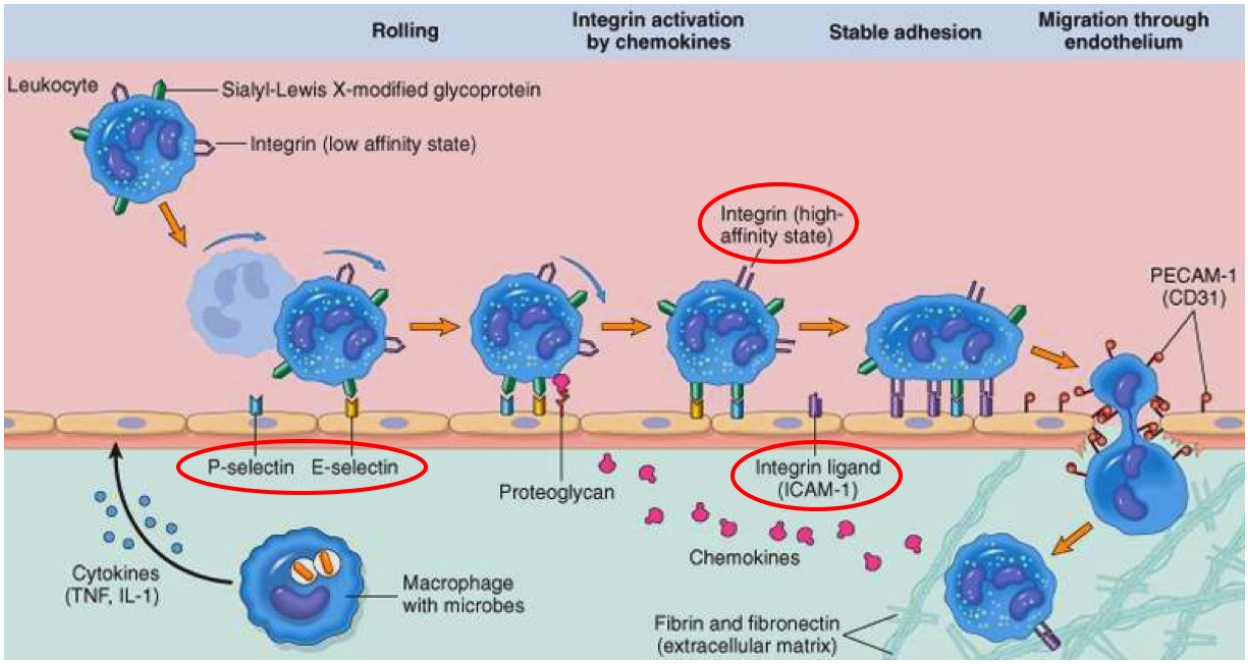

Fig. 3-7: Principles of rolling, adhesion and transmigration of leukocytes on endothelial cells
Inflammation leads to the release of cytokines like TNF-α by macrophages and the expression of cellular adhesion molecules like selectins by endothelial cells. PBLs roll on the endothelial cells via loose binding of selectins. Slow rolling PBLs can get activated by chemokines and activated PBLs express & cluster high affinity integrins that are necessary for tight binding. When integrins bind to e.g. intercellular adhesion molecule-1 (ICAM-1), the PBLs flatten and start to transmigrate via integrin mediated adhesion (modified from Kumar et al. 2007).

The processes underlying rolling, adhesion and transmigration depend on a variety of different signaling events and molecules like cytokines and chemokines. Many different membrane

proteins like selectins for low affinity binding and integrins for high affinity binding are involved (Kumar et al. 2007). Fig. 3-8 shows how the data derived from the different experiment conditions was collected and evaluated using a high content screener (Operetta HCS). Adhesion assays were performed in 12 well plates allowing a sufficient number of biological replicates and different conditions. For each well more than 160 images were taken and software-based analyzed to discriminate between unstained endothelial cells and the Cy3 stained PBMC or Jurkat cells.

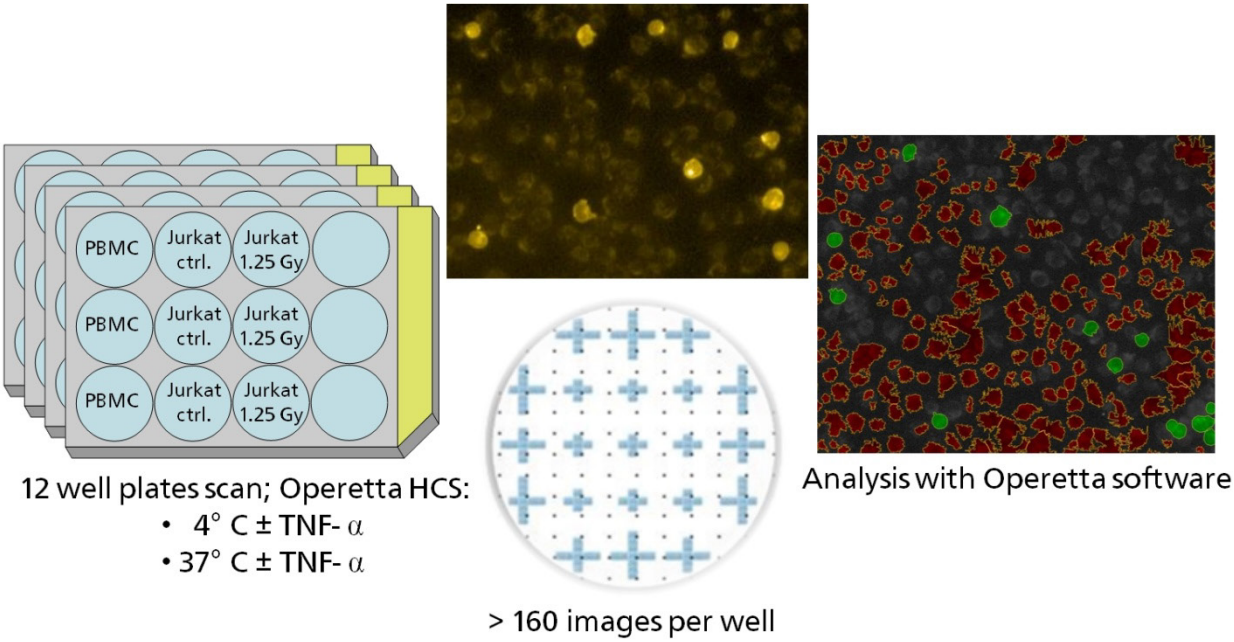

Fig. 3-8: Evaluation of adhesion assay with "Operetta High Content Screener"
12 well plates (left) were scanned using a high content screener- >160 images were taken per well with a defined pattern (bottom). Raw images (top) were software-based analyzed (right). The background highlighted in red was discriminated from adhered, stained cells that were counted automatically (highlighted in green).

PBMC, that were used as a proof of principle, behaved as expected from other studies with highest adhesion rates on TNF-α stimulated endothelial cells and 37° C incubation temperature (Hallmann et al. 1995; Hildebrandt et al. 2002). The data in Fig. 3-9 show for four independent experiments with n = 3 biological replicates for each condition the adhesion rates of unirradiated control cells and irradiated cells. The experimental condition with low temperature (4° C) and without stimulation of the endothelial cells results in the lowest adhesion rates for both irradiated and non irradiated control Jurkat. The later parameter measures the number of adherent cells per incubation well. The adhesion rates for all other conditions were normalized to this condition.

When endothelial cells were stimulated with TNF-α for 4 hours before addition of the Jurkat cells at 4° C incubation temperature, the relative adhesion rates increased but there was no significant difference between control cells and irradiated Jurkat cells. Control cells furthermore behaved at 37° C almost the same as at 4° C and their adhesion rates on unstimulated endothelial cells were low. TNF-α stimulation of endothelial cells only caused a slight increase in adhesion of control cells.

Irradiated Jurkat cells in contrast exhibited clearly elevated adhesion rates. Already in the absence of TNF-α the irradiated Jurkat cells adhered at 37° C more than the respective unirradiated controls. This difference between irradiated and unirradiated cells at 37° C incubation temperature was further amplified by a pre-treatment of the endothelium by TNF-α. On TNF-α stimulated endothelial cells the irradiated cells show on average a significant ($p = 0.0015$), more than 2.5 fold elevated adhesion rate over the control cells.

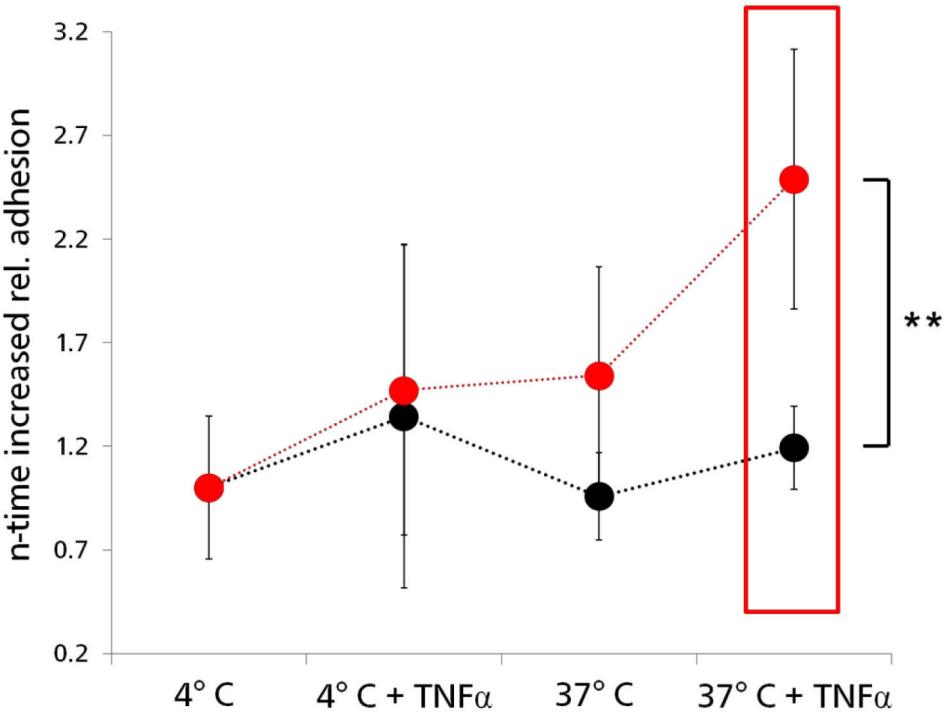

Fig. 3-9: Relative adhesion rates at different incubation conditions
Irradiated Jurkat cells (red) exhibit higher relative adhesion rates than unirradiated control cells (black) on endothelial cells at 37° C. This increased adhesion rate amplifies with TNF-a pre-treatment of the endothelial cells. Plot of means ± standard deviation (SD) (N = 4 independent experiments; n = 3 biological replicates). Significant difference ($p = 0.0015$) is indicated by **.

The stimulating effect of TNF-α pre-treatment on the adhesion of irradiated Jurkat cells on endothelial cells suggests a role of selectins like ELAMs and immunoglobulins like ICAMs and VCAMs in this process. These proteins get upregulated by endothelial cells after TNF-α stimulation and are ligands of integrins, which are presumably employed by the Jurkat cells for adhesion.

We reasoned that if this is the case, adhesion should be inhibited by RGD peptides. These peptides outcompete the binding of integrins to their receptors. To test this hypothesis we repeated the experiments in Fig. 3-10 in the presence of 10 µM RGD peptide.

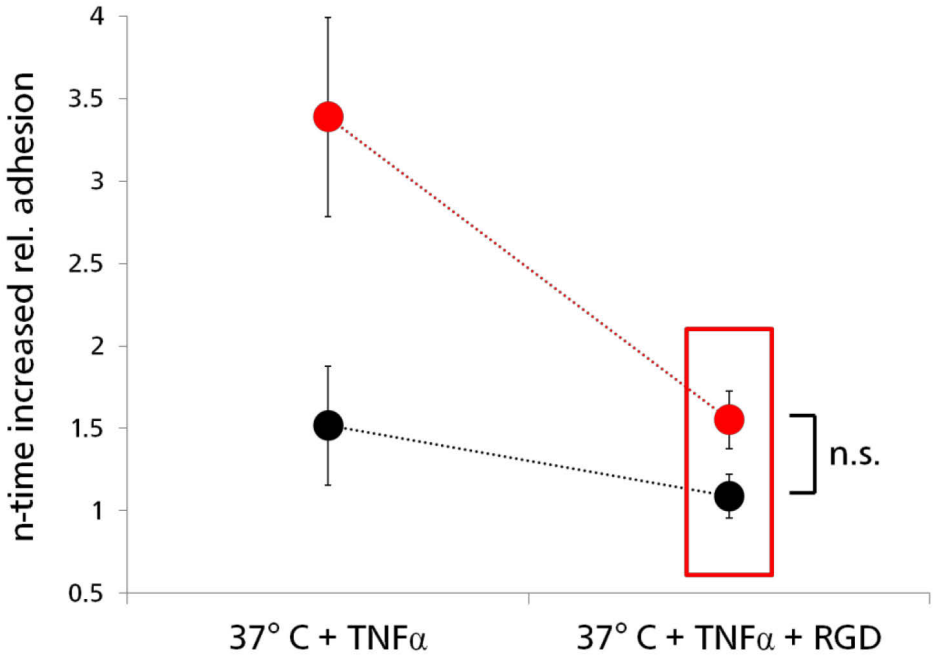

Fig. 3-10: Addition of RGD peptide is resulting in a strongly decreases adhesion of irradiated cells
Mean values ± SD for irradiated Jurkat cells (red) exhibit significantly higher relative adhesion rates than unirradiated Jurkat control cells (black) on endothelial cells at 37° C (left side of the graph). When 10 µM RGD peptide is added to the Jurkat cells prior to the assay, the adhesion rates for irradiated Jurkat cells drop down to the control level; the difference is no longer significant (n.s.).

The data show that RGD peptides have a marginal effect on the adhesion of unirradiated control cells. In contrast the same treatment greatly reduces adhesion of irradiated cells. The relative adhesion of irradiated cell drops to that of the unirradiated controls. The results of these experiments support the hypothesis that ionizing irradiation stimulates an adhesion of Jurkat cells to endothelial cells like EA.hy926 cells. This process is apparently mainly mediated by the formation of integrin clusters and involves a canonical interaction with RGD motives on partner proteins like selectins and immunoglobulins like intercellular adhesion molecules (ICAMs), endothelial-leukocyte adhesion molecules (ELAMs) and vascular cell adhesion molecules (VCAMs). This also explains the effect of low temperature (Fig. 3-9). At 4° C the integrin turnover is slowed down and cluster formation might be disturbed.

Summarized the data suggest that the adhesion rate of Jurkat cells to endothelial cells is integrin-β-1 mediated and partially controlled by the T-cell progenitors themselves. It is reasonable to assume that the concentration or clustering of integrin-β-1, which is essential for adhesion, could be affected by irradiation. This finding is of significance since integrin-β-1 is in combination with different α-integrin subtypes known as very late antigens (VLA-1-6). Integrin clustering as VLAs characterizes highly active lymphocytes (Murphy 2012). VLAs stimulate the attachment of lymphocytes to the endothelium and favors their transmigration through the endothelium to e.g. inflamed tissues.

Fig. 3-11 shows VLA-4 mediated binding (Kleen and Holmes 2008).

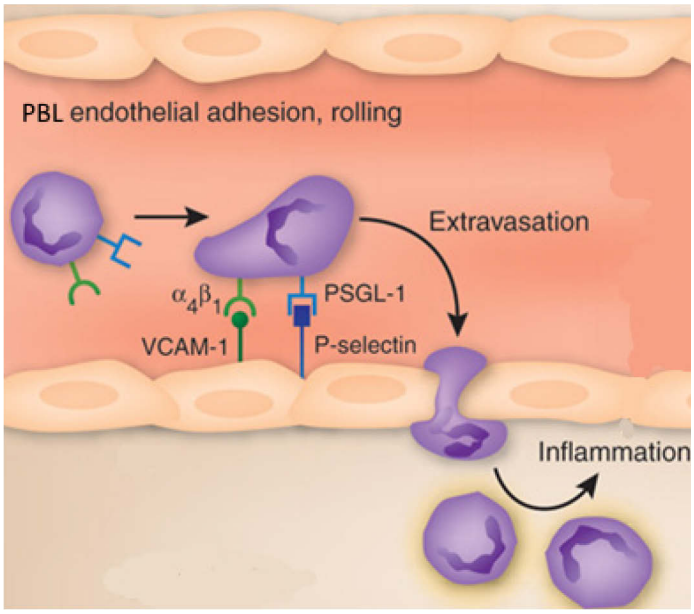

Fig. 3-11: VLA-4 expression on the surface of lymphocytes
VLA-4 is a heterodimer of integrin-α-4 and integrin-β-1 that binds VCAM-1 (vascular cell adhesion molecule-1) and mediates a tight adhesion followed by transmigration of lymphocytes through endothelial cells (modified from Kleen and Holmes 2008).

3.4.3 Single molecule microscopy of immuno stained integrin-β-1 protein

Cell adhesion is typically mediated by integrins, which form clusters in the plasma membrane of cells and facilitate cell-surface and cell-cell adhesion. To examine whether ionizing irradiation is indeed enhancing an integrin mediated adhesion of Jurkat cells by upregulating integrin-β-1, we imaged the human integrin-β-1 in fixed, unirradiated and irradiated (1.25 Gy X-ray) Jurkat cells by immune staining. The representative single molecule microscopy (SMD) images in Fig. 3-12 show that irradiation causes multiple effects: I) it elevates the number of clusters per μm^2 II) it increases the total number of integrin molecules and III) it increases the size of the clusters.

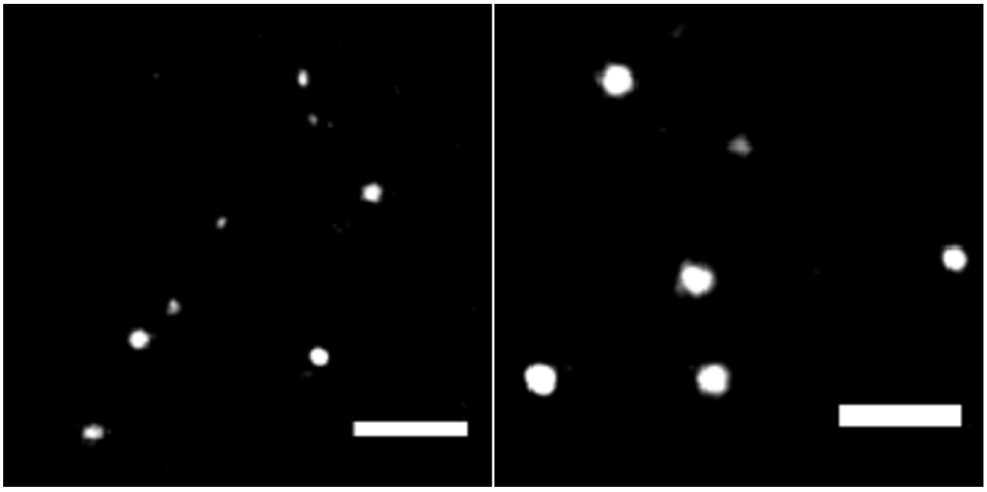

Fig. 3-12: Single molecule microscopy of immuno stained integrin-β-1 in Jurkat cells
Single molecule microscopy reveals that 1.25 Gy irradiated Jurkat cells upregulate integrin-β-1 and clustering of these integrins is enhanced (scale bar = 1 µm).

This visual impression is supported by a detailed analysis of five independent experiments. In Fig. 3-13 the number of integrin-β-1 molecules in n = 30-39 regions of interest (ROI) is shown. From the data is becomes obvious that the number of integrin-β-1 molecules per ROI is significantly increased 48 hours after irradiation with 1.25 Gy X-ray ($p < 0.0001$).

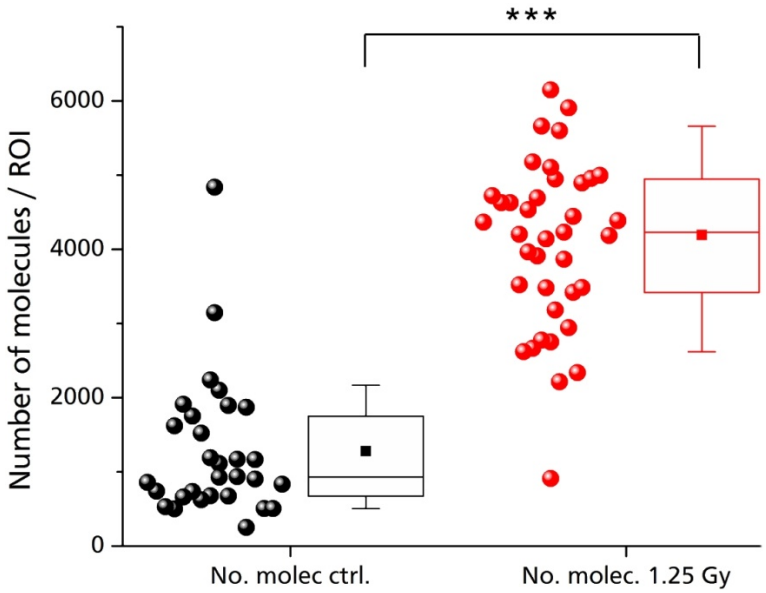

Fig. 3-13: Analysis of SMD data reveals an increased number of integrin-β-1 molecules per ROI
The mean number of molecules per regions of interest (ROI) increases clearly du to IR ($p < 0.0001$). Each circle represents data from one ROI of a single Jurkat cell imaged by SMD microscopy; box plots show mean (filled square) and median (line) as well as 25 and 75 % of the data; whiskers indicate 10 and 90 % of all cells. A high significant difference of $p \leq 0.001$ is indicated by ***.

To be biologically active, integrin molecules need to cluster. It is hence mandatory to analyze not only the number of molecules, but also the number of active integrin-β-1 clusters after irradiation. The number of integrin-β-1 clusters per analyzed area [μm^2] is shown in Fig. 3-14.

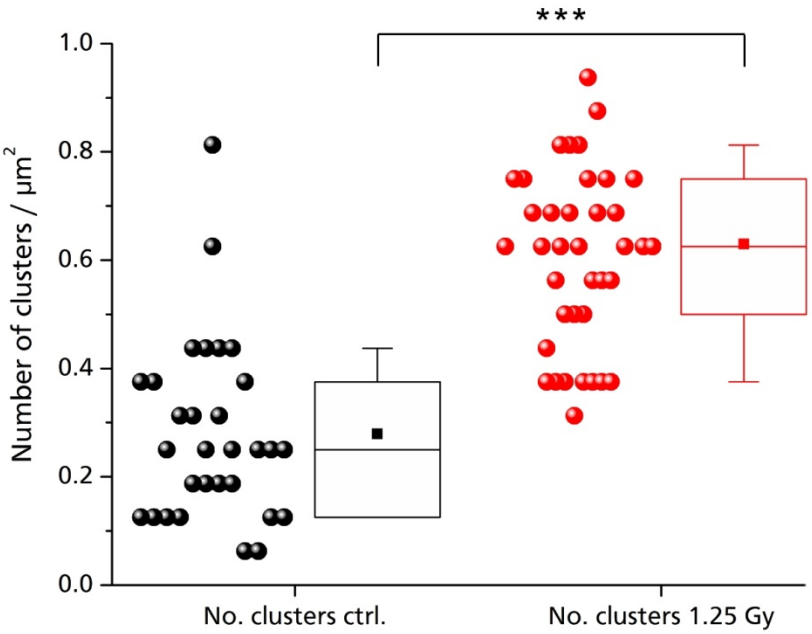

Fig. 3-14: The number of integrin-β-1 clusters per area increases significantly 48 hours after IR
The mean number of integrin-β-1 clusters per area increases clearly due to IR ($p < 0.0001$). Each circle represents data from one ROI of a single Jurkat cell imaged by SMD microscopy; box plots show mean (filled square) and median (line) as well as 25 and 75 % of the data; whiskers indicate 10 and 90 % of all cells. A high significant difference of $p \leq 0.001$ is indicated by ***.

The data confirm that irradiation causes a strong, highly significant (p = 0.0001) increase in the ratio of clustered versus unclustered molecules (Fig. 3-15).

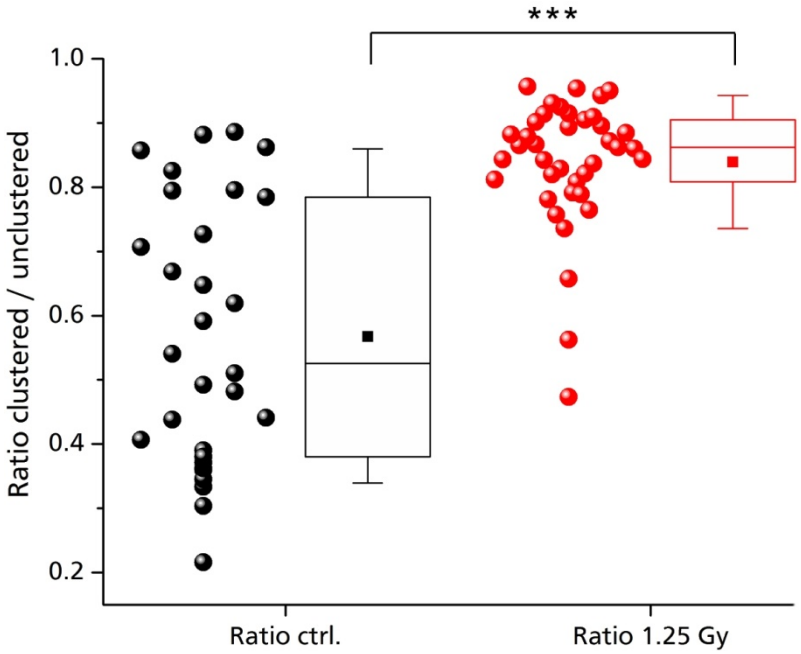

Fig. 3-15: The ratio of clustered versus unclustered molecules is clearly increased 48 hours after IR
The ratio of clustered/unclustered integrin-β-1 molecules per ROI increases clearly due to IR. Each circle represents data from one ROI of a single cell imaged by single molecule microscopy; box plots show mean (filled square) and median (line) as well as 25 and 75 % of the data; whiskers indicate 10 and 90 % of all cells. A high significant difference of p ≤ 0.001 is indicated by ***.

Both methods, namely adhesion assays and immunofluorescence staining experiments with single molecule microscopy, show that IR is able to modify integrin-β-1 regulation in Jurkat cells. It elevates the number of these adhesion molecules and augments their clustering in the plasma membrane. Collectively the data support the hypothesis that ionizing irradiation induces morphological changes and increased adhesion of Jurkat cells. These reactions resemble immune activation processes in lymphocytes and are well matching with the results for CD25 upregulation due to IR in Chapter 2.4.8.

3.5 Conclusion

Physiological adhesion assays and 3D-stacks of confocal laser scanning microscopy images shown in this chapter demonstrate that ionizing radiation triggers an increased cell-cell and cell-surface adhesion of Jurkat cells. Physiological adhesion assays under the addition of RGD peptides and single molecule microscopy analyses furthermore show that this process is mediated by an upregulation and an increased clustering of the integrin-β-1 after irradiation of Jurkat cells. This increased clustering of and the adhesion to endothelial cells is intriguingly similar to the responses of T-cells after specific immune activation.

The finding that ionizing radiation leads to enhanced expression of adhesion molecules and functional clustering of integrins in the plasma membrane leads to the hypothesis that IR presumably effects a immunomodulation or activation of these cells. This finding could be of

importance for the clinical treatment of leukemia patients. This treatment is generally a combination of chemotherapy and radiotherapy. The present data suggests that radiation radiotherapy could be associated with negative side effects like massive adhesion and transmigration of acute lymphoblastic leukemia (ALL) cells. Drugs, which suppress specific integrin-β-1 mediated adhesion might reduce such negative side effects.

3.6 References

Babel L, Grunewald M, Lehn R, et al (2017) Direct evidence for cell adhesion-mediated radioresistance (CAM-RR) on the level of individual integrin β1 clusters. Scientific Reports

Bevilacqua MP, Pober JS, Mendrick DL, et al (1987) Identification of an inducible endothelial-leukocyte adhesion molecule. Proc Natl Acad Sci USA 84:9238–42.

Butcher EC, Picker JL (1992) Physiological and moleculas mechanisms of lymphocyte homing. Annu Rev Immunol 561–591.

Cruse JM, Lewis RE (2003) Atlas of Immunology, 2., Springer Science & Business, New York, USA

Hallmann R, Jutila MA, Smith CW, et al (1991) The peripheral lymph node homing receptor, LECAM-1, is involved in CD18-independent adhesion of human neutrophils to endothelium. Biochem Biophys Res Commun 174:236–243.

Hallmann R, Zimmermann U, Sorokin LM, et al (1995) Adhesion of leukocytes to the inflammed endothelium. ScandJRheumatol 24:107–109.

Hildebrandt G, Maggiorella L, Rodel F, et al (2002) Mononuclear cell adhesion and cell adhesion molecule liberation after X-irradiation of activated endothelial cells in vitro. Int J Radiat Biol 78:315–325.

Kleen JK, Holmes GL (2008) Brain inflammation initiates seizures. Nat Med 14:1309–1310.

Kumar V, Abbas AK, Aster J (2007) Robbins Basic Pathology, 8., Elsevier, Amsterdam, Netherlands

Langhans M, Weber W, Babel L, et al (2016) The right motifs for plant cell adhesion: what makes an adhesive site? Protoplasma 1–14.

Murphy K (2012) Immuno Biology, 8., Garland Science, Taylor & Francis Group, New York USA

Ruoslahti E (1996) RGD and Other Recognition Sequences for Integrins. Annu Rev Cell Dev Biol 12:697–715.

Schindelin J, Arganda-Carreras I, Frise E, et al (2012) Fiji: an open source platform for biological image analysis. Nat Methods 9:676–682.

4 Chapter 4: IR elicits potassium channel carried currents and leads to an upregulation of KCa2.2 channels in Jurkat cells

Some of my data presented in this chapter contributed to the following publications:

Gibhardt CS, Roth B, Schroeder I, Fuck S, **Becker P,** et al (2015) X-ray irradiation activates K^+ channels via H_2O_2 signaling. Sci. Rep. 5

Roth B, Gibhardt CS, **Becker P**, et al (2015) Low-dose photon irradiation alters cell differentiation via activation of hIK channels. Pflugers Arch - Eur J Physiol 467:1835-49.

4.1 Abstract

It is well established that the ion channel composition in plasma membranes of lymphocytes resembles their immunological state and subtype. The activation of T-cells leads to a strong upregulation of calcium dependent potassium channels (KCa). In recent publications we showed with A549 cells, that KCa channels can be a target of ionizing radiation (IR) and mediate an increase in current due to an increase in the free intracellular calcium concentration after IR. Since peripheral blood lymphocytes (PBLs) do express KCa channels we wondered if we could find a similar instantaneous increase in potassium carried current in these cells. Immediately after IR we were not able to find in freshly isolated PBLs an increased current. This finding is consistent with literature data; it is well established that KCa channels are expressed in resting PBLs only at a low density. This small number of channels may not be sufficient to generate a measurable increase in conductance over the background current after irradiation. According to the literature only activated, mature T-cells or T-cell subtypes that express higher numbers of KCa channels could respond to IR with increased current. When the electrophysiological properties of the immortal Jurkat T-cell precursor cell line were analyzed before and after IR, I found that 48 hours after irradiation an upregulation of KCa channels. This IR triggered upregulation was confirmed by single molecule microscopy and is consistent with the view that IR elicits an immunological activation or immunomodulation of Jurkat cells.

4.2 Introduction

Recent publications have shown that the activity of ion channels can be modulated by ionizing radiation (IR) at doses which are typically used in cancer treatment or diagnostics (Roth et al. 2015; Gibhardt et al. 2015). The present chapter provides results, which further underscore an effect of IR on the physiology of cells via an modulation of potassium channel activity. In A549 cells, an adenocarcinoma cell line, it was found that KCa3.1 (hIK), a calcium dependent potassium channel that is likewise expressed in cells of the immune system, becomes activated within minutes after IR exposure (Roth et al. 2015). Cells that do not express KCa3.1 are not responding to IR in a similar way. By wound scratch assays and experiments with H_2O_2 it was furthermore possible to show that KCa3.1 plays a key role in the cellular response to IR. The data advocate a signaling cascade in which IR triggers a rise in H_2O_2 in cells. This causes an

elevation in the concentration of intracellular Ca^{2+}, which in turn activates KCa3.1 (Gibhardt et al. 2015). The resulting hyperpolarization could lead to radiation induced cell differentiation.

After finding that ionizing radiation in A549 cells is eliciting a signaling cascade including an elevation of cytosolic Ca^{2+}, increased KCa3.1 conductance and membrane hyperpolarization we wondered what effect IR may have on freshly isolated peripheral blood lymphocytes (PBLs). These lymphocytes are the most important cells for the acquired immune response (Fig. 4-1).

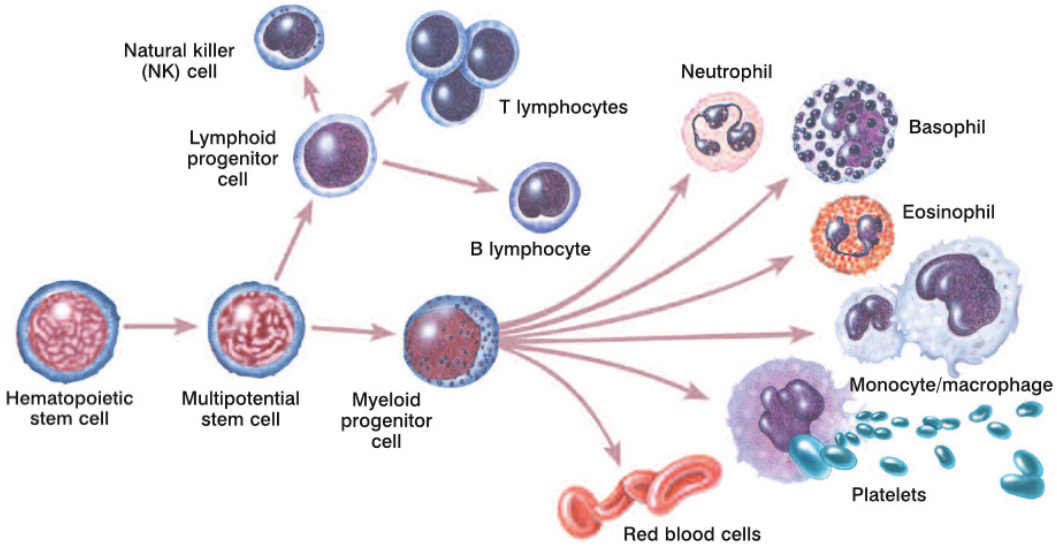

Fig. 4-1: Hematopoietic and stromal cell differentiation
Hematopoietic stem cells are able to form all cells in the hematopoietic system, which includes red blood cells, platelets, and the whole lymphatic system (i.e. T- and B-lymphocytes). Jurkat cells are so-called T-cell blast cells that exhibit most T-cell characteristics but proliferate without external stimulus, also most but not all leukemia cells still can differentiate (from Winslow et al. 2006).

According to the literature (Ghanshani et al. 2000; Beeton et al. 2001; Liebau et al. 2006) KCa3.1 is expressed in different subtypes of lymphocytes and the density of KCa3.1 channels is closely related to the immunological state of e.g. T-cells. Activation of T-cells by immune stimulation stimulate an increase in cell size (see Chapter 2) within 24-48 hours (Cuschieri and Mughal 1985; DeCoursey et al. 1987) and the number of KCa3.1 channels increases dramatically (Ghanshani et al. 2000; Cahalan et al. 2009). This upregulation and activation of KCa3.1 is of high relevance for sustaining Ca^{2+} influx and Ca^{2+} signaling for the differentiation processes (Guéguinou et al. 2014). The importance of the KCa3.1 channel in PBLs on the one hand and the effect of IR on KCa3.1 in A549 cells on the other hand raise the question on the effect of IR on K^+ channel activity in lymphocytes. An IR triggered signaling cascade as in A549 cells might be crucial for the understanding of immune responses due to ionizing irradiation.

With freshly isolated T-cells from healthy donors, where the vast majorities of T-cells are resting and not stimulated, it was not possible to find an immediate effect of IR on the conductance of whole cell currents. But when we studied the IR induced morphological changes of Jurkat cells which are leukemic T-cell progenitor cells that exhibit most T-cell characteristics and still can differentiate (Fig. 4-1), we found a clear increase of cell diameter after 24-48 hours that is dose dependent (Chapter 2.4.4). This dose dependent increase in cell diameter is similar to the increase of PBLs after immune stimulation or IR (Chapter 2.4.1).

From the literature it is known that ion channels are key players in cell swelling and growth (Lang et al. 2006). In the context of this role of ion channels we speculated that IR may stimulate the conductance of ion channels in Jurkat cells and that this may be instrumental for the increase in cell size, which was observed in response to the radiation stress. It is known that Jurkat cells are not expressing the aforementioned KCa3.1 channel (Fanger et al. 2001) but the closely related KCa2.2 (SK2) channel. Also this channel is activated by increasing cytosolic Ca^{2+} concentration and could hence serve as a target of an IR induced Ca^{2+} signaling cascade too.

4.3 Materials & Methods

4.3.1 Chemicals and antibodies

All chemicals were purchased from Sigma-Aldrich GmbH (Taufkirchen, Germany), Biochrom AG (Merck KGaA, Darmstadt, Germany), AppliChem GmbH (Darmstadt, Germany), Merck KGaA (Darmstadt, Germany), Bio-Rad Laboratories GmbH (Muinch, Germany), VWR (Darmstadt, Germany), Qiagen (Hilden, Germany) or Invitrogen (Karlsruhe, Germany) if not specified further. Antibodies were purchased from Thermo Fisher Scientific (Waltham, USA) (CD25, all secondary antibodies) and Alomone Labs (Jerusalem, Israel) (Kv1.3, KCa2.2, TRPM2). The T-cell activator "ImmunoCult™ Human CD3/CD28/CD2 T Cell Activator" was purchased from Stemcell Technologies (Vancouver, Kanada). The KCa2.2 specific ion channel blocker Tamapin was purchased from Alomone Labs (Jerusalem, Israel). All blockers and activators were dissolved in purified water or DMSO and diluted (at least 1:1000) in external solution (patch-clamp experiments) or in medium for application in cell culture.

4.3.2 Cell culture

All cells were cultivated under standard conditions with 37° C ambient temperature and 5 % CO_2. Jurkat cells are a cell line established in 1976 from the peripheral blood of a 14-year-old boy acute T-cell leukemia, a specific type of acute lymphatic leukemia (ALL). The Jurkat cell line is also called JM and grows singly or in small clumps as round, non-adherent suspension cells. The optimal split ratio is about 1:2-1:3 every 2 to 4 days at a maximum cell count of 1 x 10^6 per ml. The doubling time is 25-35 hours. For cell culture 37° C, 5 % CO_2 and RPMI 1640 medium with stable glutamine and 2.0 g/l $NaHCO_3$ + 2 mM L-glutamine, 10 % heat inactivated fetal calf serum (FCS) (Sigma-Aldrich, Germany) and 1 % mixture of penicillin/streptomycin was used. The Jurkat cell line (ACC 282) was purchased from the Leibniz-Institut DSMZ (Deutsche Sammlung von Mikroorganismen und Zellkulturen GmbH) and their immunological status is $CD2^+$, $CD3^+$, $CD5^+$, $CD6^+$, $CD7^+$, $CD8^-$, $CD13^-$, $CD19^-$, TCR α/β^+, TCR γ/δ^- ($^+$ stands for expression, $^-$ stands for no expression). A549 and Human Embryonic Kidney (HEK) 293 cells were cultivated in Dulbecco's modified minimal essential medium (DMEM) supplemented with 200 mM LGlu, 10 % FCS, and 1 % mixture of penicillin/streptomycin. The medium for A549 cells also contained 1 % non-essential amino acids (NEAA).

4.3.3 Whole cell patch clamp recordings

Membrane currents of cells were recorded in the whole cell configuration (Hamill et al. 1981) either with the portable patch clamp device (port-a-patch, Nanion, Munich, Germany) or classical patch clamp technique using an EPC-9 amplifier (HEKA Electronics, Lambrecht, Germany). For measurements of A549 or HEK-293 cells 80 % confluent cells were harvested according to standard procedure (Fertig et al. 2002). When cells were patched with the port-a-patch system, they were sealed in a solution containing (in mM) 80 NaCl, 3 KCl, 10 $MgCl_2$, 35 $CaCl_2$, 10 HEPES/NaOH, pH 7.4. For recordings a buffer with (in mM) 4 KCl, 140 NaCl, 1 $MgCl_2$, 2 $CaCl_2$, 5 D-Glucose (or sorbitol), 10 HEPES/NaOH, pH 7.4 as an external bath solution was used. The intracellular solution for port-a-patch recordings contained (in mM) 50 KCl, 10 NaCl, 60 KF, 1 EGTA, 10 HEPES/KOH, pH 7.2.

The intracellular solution used for classical patch clamp technique contained (in mM) 100 K-Asp, 40 KF, 5 KCl, 2 $MgCl_2$, 1 $CaCl_2$, 1.223 EGTA (= 1 µM free Ca^{2+}) or 2.62 EGTA (= 100 nM free Ca^{2+}) and 10 Hepes/KOH, pH 7.4. Sorbitol was used to adjust the osmolarity to 285 mOsmol/kg. The extracellular solution for classical patch clamp technique contained in standard measurements (in mM) 130 Na-Asp, 4.5 KCl, 1 $MgCl_2$, 2 $CaCl_2$ and 10 Hepes/NaOH, pH 7.4. The extracellular solution for measurements with a high external K^+ concentration ("high K^+") contained (in mM) 89.5 Na-Asp, 40.5 K-Asp, 4.5 KCl, 1 $MgCl_2$, 2 $CaCl_2$ and 10 Hepes/NaOH pH 7.4. The extracellular solution used for "high Cl^-" measurements contained (in mM) 35.5 Na-Asp, 94.5 NaCl, 4.5 KCl, 1 $MgCl_2$, 2 $CaCl_2$ and 10 Hepes/NaOH pH 7.4. Sorbitol was always used to adjust the osmolarity to 300 mOsmol/kg; the small difference in the osmolarity between the internal and external solution increased the stability of the seals.

All blockers were solved in ddH_2O and freshly prepared before each experiment by dilution in the external buffer solution. Currents were elicited with a pulse protocol consisting of voltage steps from a holding voltage at -60 mV, to 800 ms long test pulses between -100 mV and +80 mV and a 200 ms long post pulse at -80 mV. Currents were alternatively monitored with a ramp protocol. Cells were therefore clamped to an 800 ms long ramp from −120 to +100 mV. Currents were recorded with an EPC9 amplifier under the control of the Patchmaster software and data were analyzed with Fitmaster software (Heka Electronic, Lambrecht, Germany).

To limit long-lasting inactivation of Kv1.3 channels at positive voltages, we used only very short voltage pulses (100-200 ms) for channel activation. The peak currents were used for constructing I/V (current voltage relation) curves. The blocking efficiencies of different agents and the Kv-independent current portion were identified from at least 1200 ms long voltage steps from −60 to +40 mV where the peak currents were the readout according to the literature (Kuras et al. 2012). To maintain a full voltage-dependent activation of the Kv1.3 channels after each applied protocol, a cell was always kept at −60 mV for at least 1-2 min between sequential voltage clamp protocols. We found that this time was sufficient for full recovery in preceding control experiments (see also Levy and Deutsch 1996). Only cells that

exhibited a leak free current response where analyzed and in all experiments, a cell was first measured for at least 4 min under control conditions to reach a stable current response before protocols where applied which were later used for evaluation.

4.3.4 Cell irradiation

Cells were exposed in cell culture flasks to X-ray irradiation with a voltage of 90 kV and 33.7 mA using an Isovolt 160 Titan E X-ray source (GE Sensing & Inspection Technologies, Alzenau, Germany). Doses were delivered at a source to probe distance of 30 cm with cell culture flasks placed on a 2 mm aluminum sheet. The dose rates were controlled by a dosimeter (DIADOS T11003). Different doses were achieved by varying the irradiation time.

4.3.5 Single molecule measurements, image acquisition & data analysis

Single molecules measurement, image acquisition and data analysis was performed as described by Babel and co-workers (Babel et al. 2017) using a using a custom-built single molecule microscope, Fiji (Schindelin et al. 2012) and custom written software in MATLAB using the Ripley K function analysis.

4.3.6 Antibody staining

Antibody staining was performed as described by Babel and co-workers (Babel et al. 2017). In brief, a polyclonal guinea pig IgG1 antibody against the C-terminus of KCa2.2 from Alomone labs (Jerusalem, Israel) was used. To analyze single molecules in fixed cells, cells were fixed with 4 % PFA for 1 hour at 4° C and washed three times with PBS. Unspecific binding sites were blocked after fixation for 1 hour with 1 % BSA solution (AppliChem, Darmstadt, Germany) at 37° C and washed with PBS three times. The cells were afterwards incubated for 3 hour at 4° C in the desired antibody solution. Finally, cells were washed three times and imaged using STORM buffer. The STORM buffer contained like described in Babel et al. 2017: 100 mM MEA (beta-mercaptoethylamine, pH 8.5), 140 U catalase and 10 U glucose oxidase.

4.3.7 Statistical analysis

Data are expressed as means ± standard deviations (SD) of at least three different experiments, number of biological replicates (n) or independent experiments (N) are denoted. Significance was estimated by using the Student's t-test. A $p < 0.05$ was considered as significant (*), $p \leq 0.01$ is specified as ** and a high significant difference of $p \leq 0.001$ was specified as ***.

4.4 Results

4.4.1 Ionizing radiation induces increased KCa3.1 carried current in A549 cells

A previous publication (Kuo et al. 1993) has shown that potassium current in A549 cells increased after γ irradiation. Roth and co-workers as well as Gibhardt and co-workers (Roth et al. 2015; Gibhardt et al. 2015) showed that the ion channel activity of A549 cells can also increase in response to X-ray exposure as a cellular response to radiation stress. A549 cells in voltage clamp recordings reveal a current response that can be divided into a voltage independent instantaneous current (I inst.) and a slow, time dependent steady-state current (I steady). The corresponding current/voltage (I/V) relation has characteristic features (Fig. 4-2). The instantaneous current (I inst.) is quasi-ohmic; it shows no voltage dependency and contributes in A549 cells strongly to the whole cell conductance. Roth and co-workers (Roth et al. 2015) showed that the currents of A549 cells under the recording conditions are mostly carried by potassium channels. Besides KCa3.1, which is strongly expressed, also Kv1.3, hEAG and hERG were found to be expressed.

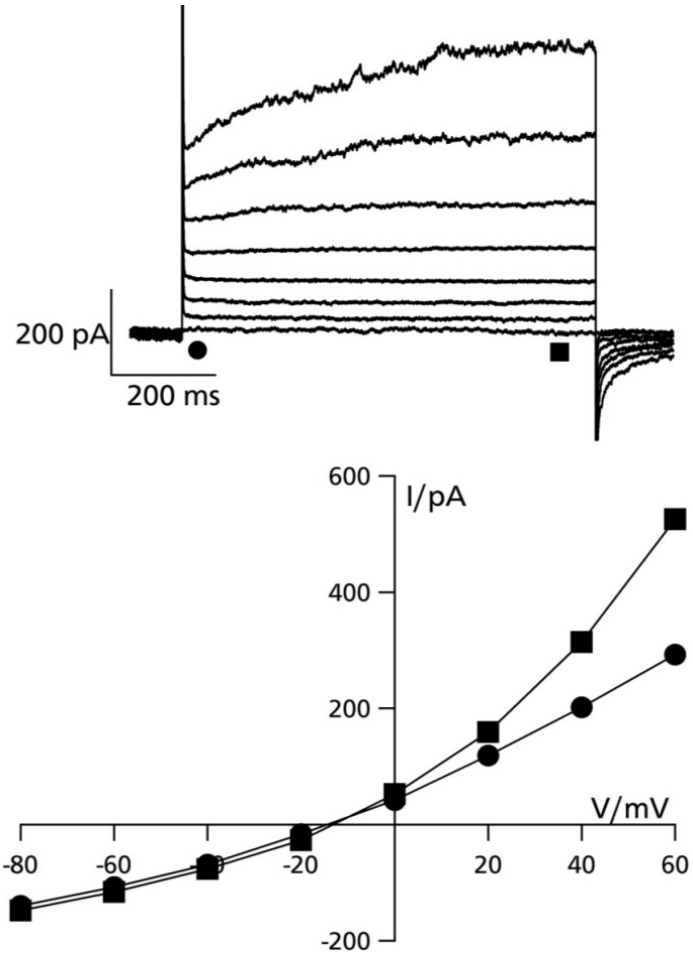

Fig. 4-2: A typical current response of an A549 cell and the corresponding I/V curve is shown
(Top) Typical current response of an A549 cell; the instantaneous current (circle) is taken after compensatory artifacts (first ~5 ms) from 5-15 ms after applying the corresponding voltage. The steady state current (square) is taken in the last 100 ms of each voltage step. The cell was clamped from a holding voltage (-60 mV) to test voltages between −80 mV and +40 mV in 20 mV steps and to a post pulse of -80 mV. (Bottom) Current/voltage (I/V) relations from the same current response (top). I inst. is indicated by circles, I steady by squares.

When A549 cells are examined with a portable patch clamp device (port-a-patch) and directly exposed to X-ray, it is possible to monitor the current response of a single A549 cell before and directly after X-ray treatment. In these measurements the instantaneous current typically increases clearly within a few minutes after IR exposure. Fig. 4-3 shows a representative A549 cell, which responded within minutes to the radiation stress of 10 Gy X-ray. The outward current is strongly increased and as a consequence the free-running membrane voltage is shifted to more negative voltages. In the case of the cell shown in Fig. 4-3 the membrane hyperpolarizes from -15 mV to -43 mV. This is consistent with the view that the current increase is carried by potassium channels and not by an increase in leak conductance.

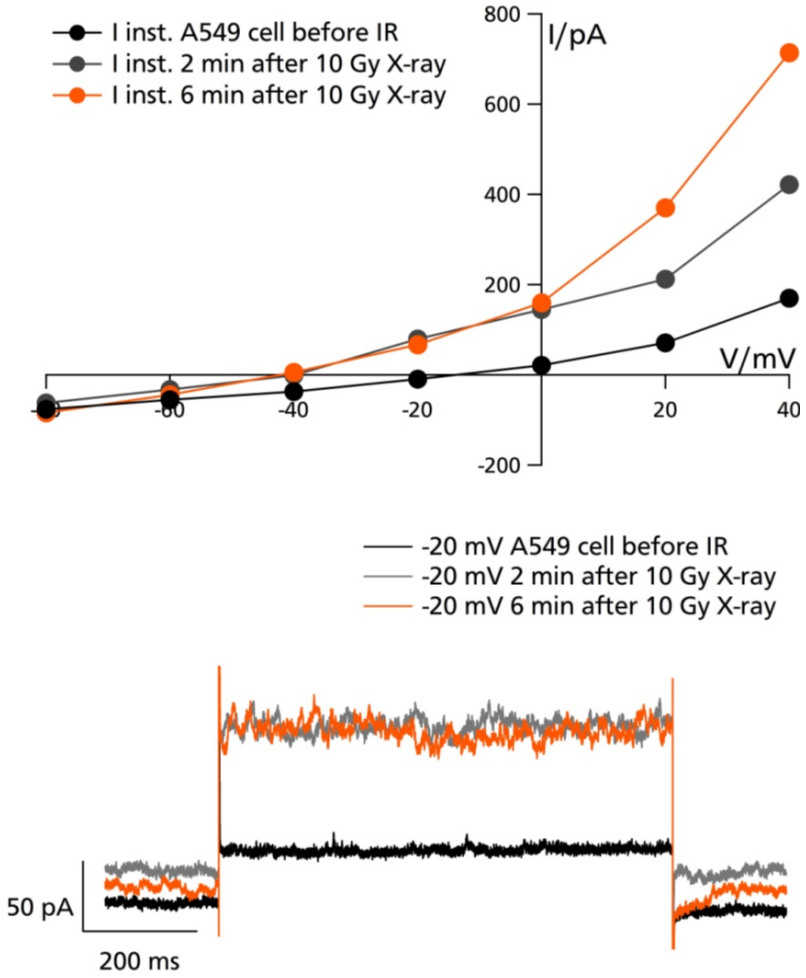

Fig. 4-3: Irradiation of A549 cells cause increase in instantaneous activating conductance
(Top) Current/voltage (I/V) relations (I inst.) from the same cell measured prior (black circles), 2 min after IR (grey) and 6 min after IR (orange). Irradiation augments a hyperpolarization. Currents were measured as in Fig. 4-2. (Bottom) Current responses to voltage pulse from -80 mV to -20 mV and back to the initial voltage. Currents were recorded 2 min before (black) and 2 or 6 min after irradiation with 10 Gy X-ray (grey & orange).

Out of 11 cells tested in this way, 8 cells responded to X-rays in the reported way with an clear increase in membrane conductance and a shifted free-running membrane voltage (Vm). The radiation-generated current increase resembles the I/V relation of KCa3.1 channels (hIK) suggesting that these channels are activated in response to IR. At a reference voltage of +40 mV, the instantaneous current increased 4 minutes after IR on average by 125 ± 120 % (± SD, N = 7).

Fig. 4-4 depicts the free running membrane voltage of individual cells before IR and at the time of maximal activation of the instantaneous conductance after IR exposure (2-8 minutes after 10 Gy X-ray). IR is resulting in a significant hyperpolarization (p = 0.03) of membrane voltage.

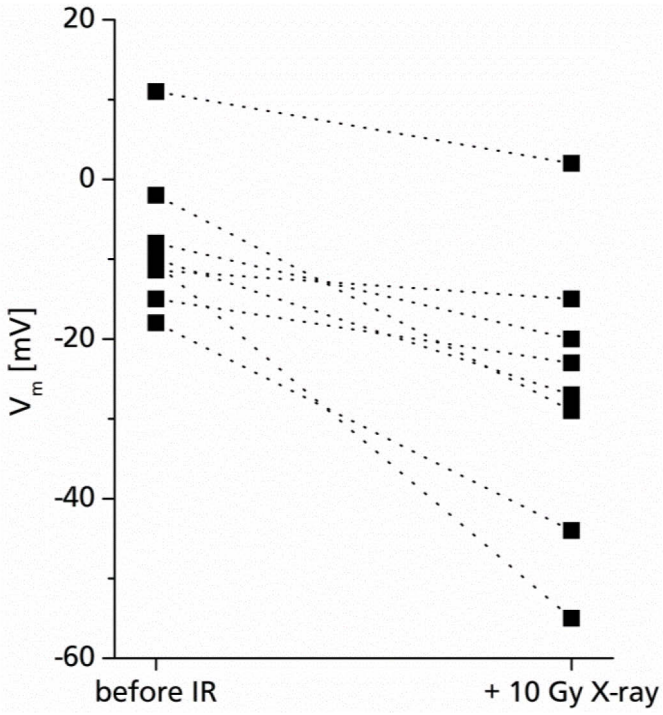

Fig. 4-4: The gain in conductance following X-ray irradiation of A549 cells causes a significant, systematic hyperpolarization in all cells tested

Black squares indicate the measured free running membrane potential of individual cells before (left) and 2-8 minutes after exposure to 10 Gy X-ray (right). All measured cells exhibit a shift of the free running membrane potential to more negative voltages (p = 0.03; N = 8).

The data translates into an average shift of the membrane voltage from -6.7 ± 9.3 mV to -23.2 ± 18.8 mV after 10 Gy X-ray treatment (N = 8). Because of the elevation of the potassium conductance the free-running membrane voltage moves closer to the theoretical Nernst voltage for K^+ (-86 mV).

4.4.1.1 Tram-34 reverts the current increase that is elicited by X-ray

Tram-34 (1-[(2-Chlorophenyl)diphenylmethyl]-1H-pyrazole) selectivity inhibits KCa3.1 currents (Wulff et al. 2001) and is discussed to be used in different therapeutic treatments like autoimmune diseases (Wulff and Castle 2010) or cancer treatment like adenocarcinoma of the pancreas in which KCa3.1 channels are upregulated (Jäger et al. 2004). Fig. 4-5 shows that the addition of this selective KCa3.1 blocker at nanomolar concentrations (300 nM) to the extracellular buffer blocks the current that was before induced by X-ray treatment. The current returns in the presence of the blocker back to the control level.

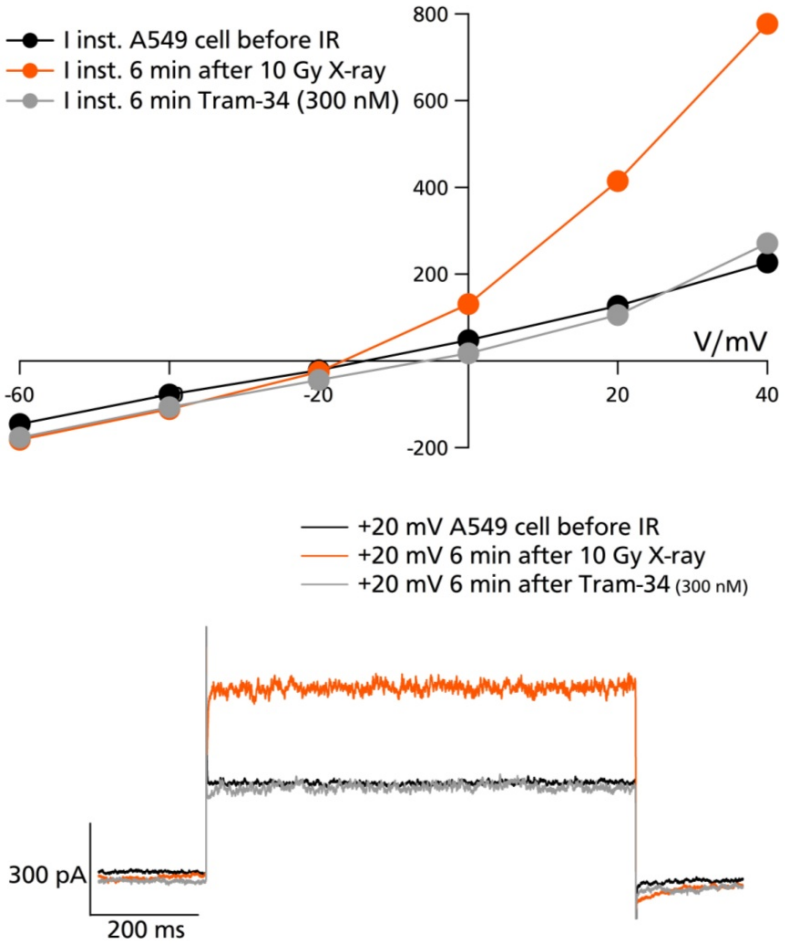

Fig. 4-5: Irradiation of A549 cells cause an increase in conductance that can be blocked by Tram-34
(Top) current/voltage (I/V) relation (I inst.) from the same cell measured prior IR (black circles), 6 min after IR (orange) and 6 min after addition of 300 nM Tram-34 (grey circles). Irradiation augments a hyperpolarization, which is reverted by the blocker. Currents were measured as in Fig. 4-2. (Bottom) current responses of the same A549 cell to voltage pulse from -80 mV to +20 mV and back to -80 mV. Currents were recorded 2 min before (black), 6 min after 10 Gy X-ray (orange) and 6 min after the addition of Tram-34 (grey).

Fig. 4-5 & Fig. 4-6 show that not only the current but also the reversal potential, which was shifted to a more negative voltage after the IR exposure, returned to more depolarized voltages in the presence of the KCa3.1 specific blocker Tram-34. Fig. 4-6 summarizes the free running membrane potential (Vm) of a population of cells before and after X-ray treatment in absence and presence of Tram-34. Irradiation of cells induces a mean hyperpolarization from -6.7 ± 9.3 mV (N = 8) to -23.2 ± 18.8 mV (N = 8). After the addition Tram-34 (300 nM) the potential drops back to -7.6 ± 14 mV (N = 5).

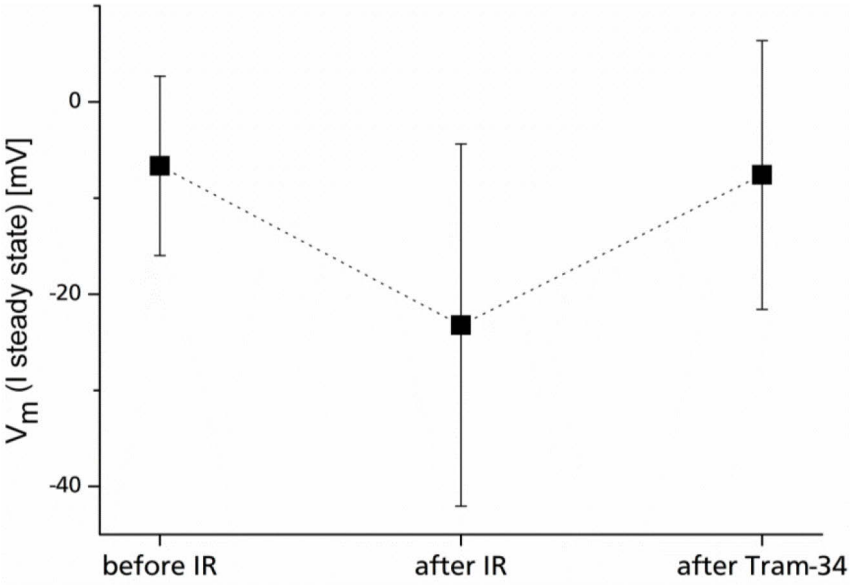

Fig. 4-6: The systematic hyperpolarization following IR can be reverted by the addition of Tram-34

Challenging A549 cells with IR leads to a hyperpolarization. Control cells exhibit a free running membrane potential of -6.7 ± 9.3 mV (N = 8), after irradiation Vm shifts to -23.2 ± 18.8 mV (N = 8). After the addition of Tram-34 Vm is shifted back to -7.6 ± 14 mV (N = 5).

The clear and compelling results of these experiments strongly suggest that KCa3.1 is responsible for the afore mentioned X-ray induced current increase.

4.4.1.2 The response is cell type specific

When 82h-6hTERT cells (Roth et al. 2015) or HEK-293 cells are exposed to X-ray no comparable increase in conductance (Fig. 4-7) or hyperpolarization (Fig. 4-8) can be observed. At +20 mV, the mean instantaneous current does not increase (+1 ± 34 %, N = 6).

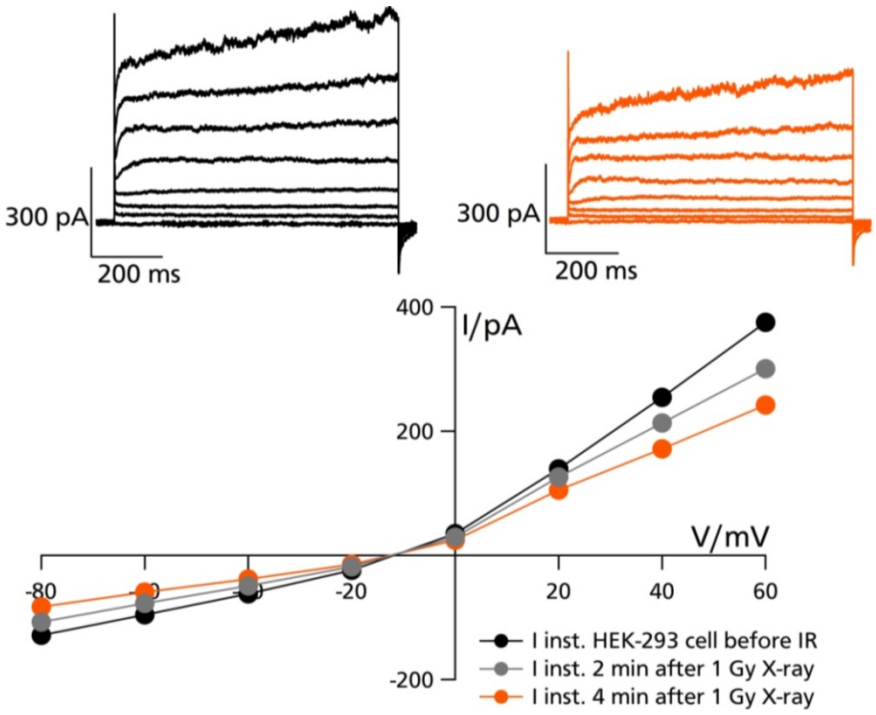

Fig. 4-7: HEK-293 cells show no increase in instantaneous current in response to IR

(Top) Typical current response of a HEK-293 cell; (bottom) I/V relations (I inst.) from the same cell measured before IR (black circles) and 2 or 4 min after IR (grey & orange). IR augments no increased conductance and no hyperpolarization. Currents were measured as in Fig. 4-2.

X-ray irradiation of these cells causes no augmented potassium carried current and no systematic change in Vm as shown in Fig. 4-8.

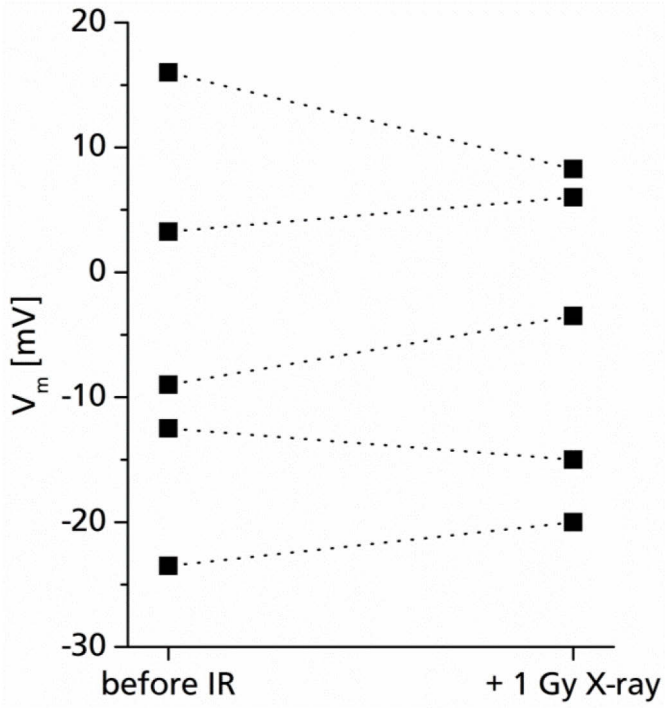

Fig. 4-8: X-ray irradiation of HEK-293 cells causes no systematic change in Vm
Challenging HEK-293 cells with IR does not lead to hyperpolarization. Vm of unirradiated cells (left) and 4 minutes after irradiation (right). Vm is not significantly changed (N = 5).

The mean voltage of membrane in HEK-293 cells (N = 5) was for control cells -5.15 ± 15.2 mV and 4 min after 1 Gy X-ray the mean V_m was not changed (-4.8 ± 12.5 mV).

The results of these experiments show that the response of A549 cells to IR is no generic response of mammalian cells to radiation. The increase of K^+ carried current is calcium dependent and cell type specific. Only cells that express calcium dependent channels like KCa3.1 can exhibit an increased K^+ channel activity in response to IR. KCa3.1 is hence a main target in the plasma membrane for ionizing irradiation.

4.4.2 Electrophysiological properties of human peripheral blood lymphocytes

From the literature it is known that five major types of ion channels are expressed in lymphocytes and that these channels play an important role in the physiology of these cells (Cahalan et al. 2009). The two predominant K^+ channels are the voltage dependent Kv1.3 and the calcium dependent KCa3.1, also known as hIK, KCNN4 or IKCa1 (Ghanshani et al. 2000; Cahalan et al. 2009). Following mitogenic stimulation or immune activation the KCa3.1 current increases. This is the result of the strong upregulation in the number of KCa3.1 channels in the plasma membrane by a factor of 10-25 (Ghanshani et al. 2000). The number of active plasma membrane KCa3.1 channels in PBLs is, according to the literature (Ghanshani et al. 2000; Beeton et al. 2001; Liebau et al. 2006; Cahalan et al. 2009), closely related to the immunological state and subtype of T-cells.

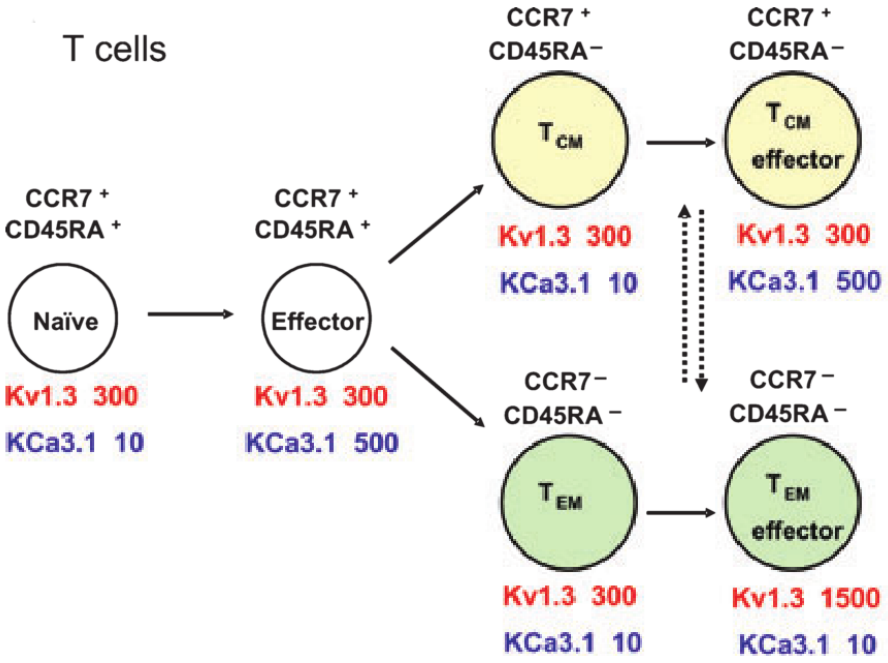

Fig. 4-9: Changes in K^+ channel expression during activation

The average number of Kv1.3 and KCa3.1 channels in different subclasses of lymphocytes is shown. Naive, central memory (T_{CM}) and effector memory (T_{EM}) cells exhibit different ratios of Kv1.3 to KCa3.1 channels reflecting their specific immunological state. Quiescent naive, T_{CM} and T_{EM} cells exhibit a K^+ channel expression pattern with ~300 Kv1.3 to ~10–20 KCa3.1 channels. Following activation T-cells upregulate KCa3.1. Only the subclass of T_{EM} upregulate Kv1.3 (modified from Cahalan et al. 2009).

This upregulation and activation of KCa3.1 is of high relevance for sustaining Ca^{2+} influx and Ca^{2+} signaling for the differentiation processes. KCa3.1 is voltage independent but Ca^{2+} dependent by a C-terminal bound Calmodulin (CaM) that senses the cytosolic Ca^{2+} level. Stimulation of PBLs via the T-cell receptor (TCR) triggers a Ca^{2+} signaling cascade, which involves an increase of the free cytosolic Ca^{2+} concentration from the resting level (< 100 nM) to micromolar (1-10 µM) concentrations. This rise in cytosolic Ca^{2+} is the result of an efflux of Ca^{2+} from internal stores like mitochondria and endosplasmatic reticulum as well as a Ca^{2+} influx via Ca^{2+} channels like the CRAC channel and the IP_3 receptor.

For a sustained, prolonged influx of extracellular Ca^{2+} through Ca^{2+} channels the cell must remain hyperpolarized; this is achieved by K^+ efflux. In this scenario the Kv1.3 channel plays a role in fine tuning. It activates when the cell is depolarized at Vm > -20 mV and inactivates again at Vm < -60 mV. The voltage independent KCa3.1 channel keeps the cell in this scenario hyperpolarized despite the entry of the divalent Ca^{2+} ions. Ca^{2+} signaling cascades trigger the activation of PBLs including altered gene expression, increase in cell diameter, production of cytokines and proliferation (Lewis and Cahalan 1995). In resting lymphocytes not only the number of KCa3.1 is low but also the activity of the channels is low due to a low cytosolic Ca^{2+} level (Cahalan et al. 2009).

In addition to the aforementioned K^+ channels, PBLs also express a ATP-dependent outwardly rectifying Cl^- channel. By the use of an ATP free internal patch clamp solution the contribution of this Cl^- current to the plasma membrane conductance, can be eliminated (Cahalan et al. 2009; Rao et al. 2010).

Fig. 4-10 shows the typical currents of a PBL. The currents are dominated by two kinetically discernible components: the large voltage and time dependent Kv1.3 channel and an instantaneous activating KCa3.1 channel.

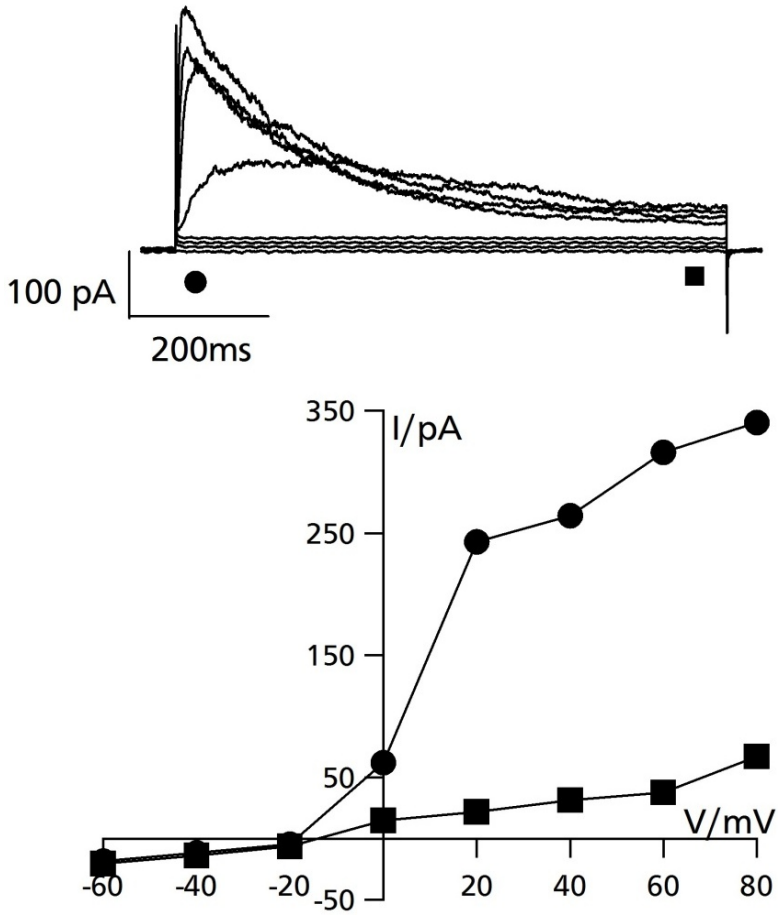

Fig. 4-10: Exemplary current response of a freshly isolated peripheral blood lymphocyte (PBL)
(Top) Typical current response of a PBL and (bottom) current/voltage (I/V) relations from the same cell. Black circles indicate where the instantaneous currents (I inst.) were taken and black squares indicate the steady state current response (I steady). The measured Vm is -19 mV for the instantaneous current response. Currents were measured as in Fig. 4-2.

The voltage dependent Kv1.3 channel conducts the majority of the outward-rectifying K^+ current at voltages more positive than approximately -20 mV. This is true for resting lymphocytes but also for Jurkat cells (Kuras et al. 2012). Kv1.3 exhibits a large outward current with a pronounced C-type inactivation. KCa3.1 in contrast is voltage independent and its current contribution can best be seen at more negative voltages than -40 mV at which the Kv1.3 is inactive. At positive voltage KCa3.1 contribution can be seen in the steady state current since Kv1.3 is at positive voltages inactivated within 400-600 ms. Fig. 4-11 shows the currents of a resting PBL in response to a voltage ramp. This protocol, in which the voltage is increasing over 800 ms from -120 to +100 mV, enables the rapid measurement of the KCa3.1 conductance (Grissmer et al. 1993).

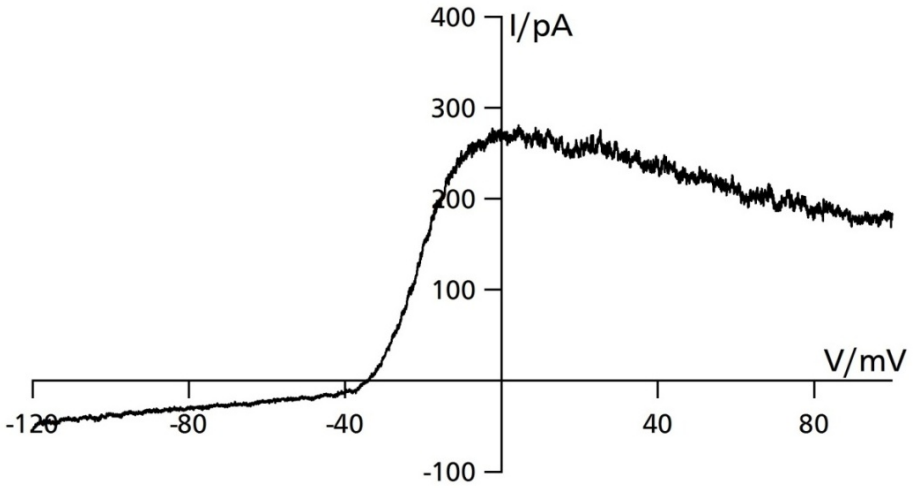

Fig. 4-11: Voltage ramp elicited current response of the same resting PBL as shown in Fig. 4-10
An 800 ms long voltage ramp protocol from -120 to +100 mV reveals the instantaneous current components of a resting PBL. At voltages more negative than -40 mV the conductance is quasi-linear but very low; this reflects the activity of voltage-independent channels. At more positive voltages, the current increases exponentially indicating the activation of the K^+ outward rectifier Kv1.3. At higher (positive) voltages the characteristic C-type inactivation of Kv1.3 can be observed.

The protocol is designed in order to differentiate the KCa3.1 current from the K^+ outward rectifier Kv1.3. In the voltage window between -120 to -40 mV the conductance is quasi linear but very low due to the low number of active KCa3.1 channels. At voltages more positive than -40 mV the current increases exponentially, reflecting the activation of Kv1.3. At higher positive voltages the characteristic C-type inactivation of Kv1.3 within the voltage ramp protocol can be observed. With the help of these characteristic properties and differences of the two main K^+ channels in Lymphocytes it is possible to quantify their relative contribution to the whole cell current without the need of channel blockers. The latter always bear the hazard of unwanted side effects (see Chapter 5).

PBLs are normally resting, so their cell cycle is arrested in the G0 cell cycle phase. They need to be stimulated by mitogens or a specific immune activation via the T-cell receptor (TCR). After such stimulation a Ca^{2+} signaling cascade is induced, that leads to a progress in cell cycle and immunological active T-cells (Khanna et al. 1999). When the electrophysiological properties of resting PBLs are compared with those of PHA-L activated PBLs, it becomes apparent that the

portion of KCa3.1 channels is significantly increased in response to the immune stimulation. Fig. 4-12 shows the current response of a PBL 48 hours after stimulation with 7.2 µg/ml PHA-L. Comparison of the whole cell currents of non-stimulated (Fig. 4-10) and stimulated cells (Fig. 4-12) reveals that after 48 hours of stimulation the whole cell current is now dominated by instantaneous activating and voltage independent current reflecting KCa3.1 and not Kv1.3 current. As a consequence the free running membrane potential is shifted to more negative voltages. Since the voltage independent and not inactivating KCa3.1 is now dominating the conductance of the cell, the instantaneous and the steady state currents at positive voltages are now nearly identical (Fig. 4-12).

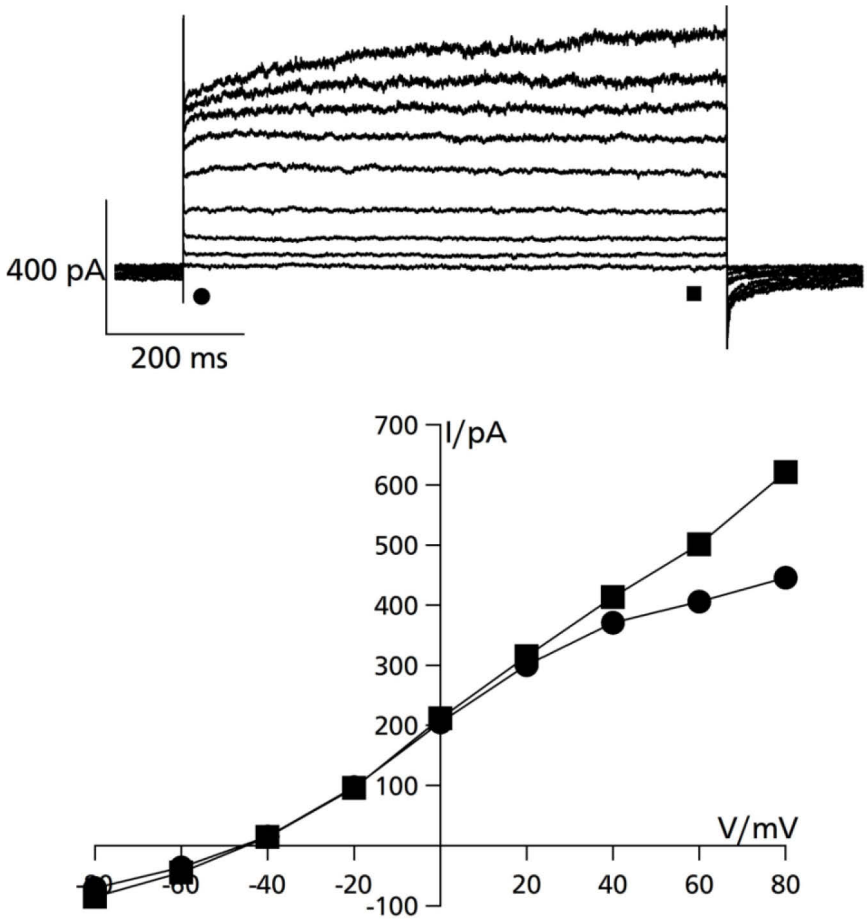

Fig. 4-12: Exemplary current response of a PHA-L stimulated PBL

(Top) Typical current response of PHA-L stimulated PBL (48 h, 7.2 µg/ml). (Bottom) current/voltage (I/V) relations from the same cell. Black circles indicate the instantaneous currents (I inst.), black squares the steady state current (I steady). Currents were measured as in Fig. 4-2.

The differences between unstimulated and stimulated cells are also evident in measurements of the currents with a ramp protocol (Fig. 4-13).

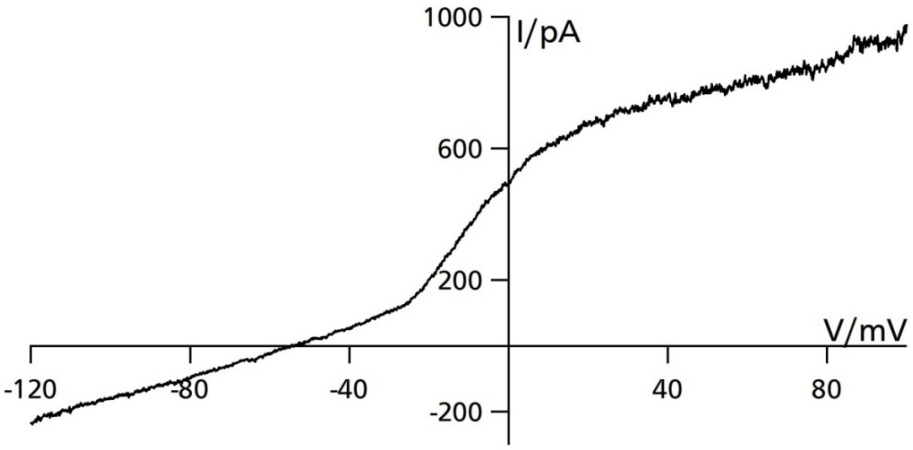

Fig. 4-13: Voltage ramp elicited current response of the same stimulated PBL as shown in Fig. 4-12
A 800 ms long voltage ramp protocol from -120 to +100 mV reveals the significantly changed instantaneous current component of stimulated PBLs compared to resting PBLs. At voltages more negative than -40 mV the conductance is quasi-linear and higher compared to resting PBLs; this reflects the increased activity of voltage independent KCa3.1 channels. At more positive voltages, the current increases exponentially indicating the activation of the K^+ outward rectifier Kv1.3. The drop of current due to an inactivation of Kv1.3 at higher positive voltages known from resting PBLs is compensated by higher activity of KCa3.1 channels.

The voltage ramp derived current response in Fig. 4-13 shows a large linear conductance increase at voltages more negative than -40 mV, which is steeper than that of resting PBLs. This reflects an increased activity of the voltage independent KCa3.1 channels. The free running membrane potential is shifted to more negative voltage, in this exemplary measurement Vm is -55 mV. At more positive voltages the current increases exponentially indicating the activation of Kv1.3. The drop of current at higher positive voltages which is characteristic for resting PBLs due to an inactivation of Kv1.3 is compensated by higher activity of KCa3.1 channels.

Fig. 4-14 shows the steady state whole cell currents of populations of resting and PHA-L activated PBLs. By the exemplary measurements in Fig. 4-12 and Fig. 4-13 it was already shown that PBL stimulation by PHA-L causes a change in the electrical properties. The KCa3.1 current, which is the predominant current at the steady state currents, is significantly increased. The mean value for N = 11 cells at +20 mV in resting PBLs is 129 ± 55 pA (N = 11) After PHA-L activation the value increases to 369 ± 166 pA (N = 7). This increase is highly significant (p = 0.0002).

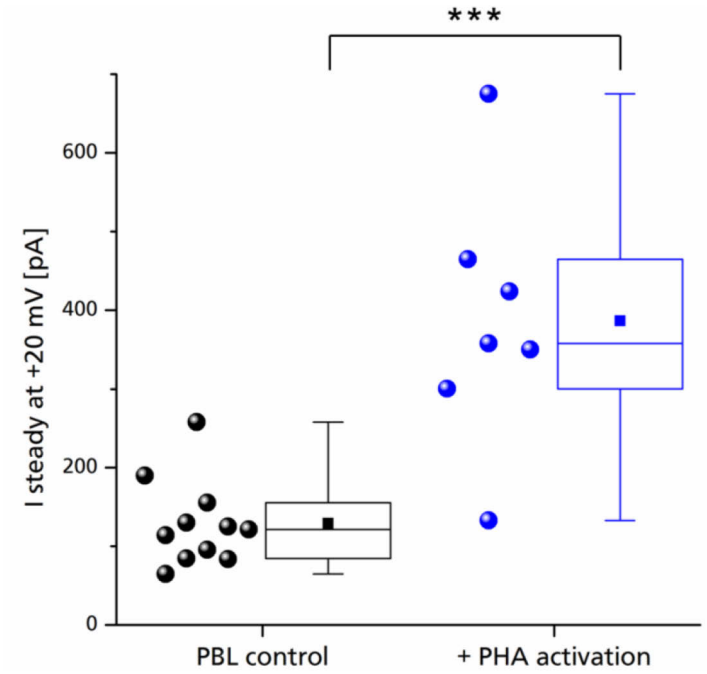

Fig. 4-14: Steady state currents of resting and PHA-L activated PBLs at +20 mV

The steady state whole cell current responses of individual resting and activated PBLs is shown; each circle represents one cell (black resting, blue activated). The box plot diagram shows the median (line), mean (square) as well as 25 and 75 % of the data. Whiskers indicate 5-95 % of the data. A high significant difference of $p \leq 0.001$ is indicated by ***.

Next, the inward current at -80 mV was analyzed. Because of the low external K^+ concentration in the standard external patch clamp solution it cannot be expected a high inward current compared to the outward current. But the inward current should be carried mostly by KCa3.1 channels under these measurement conditions. Fig. 4-15 summarizes the currents at -80 mV.

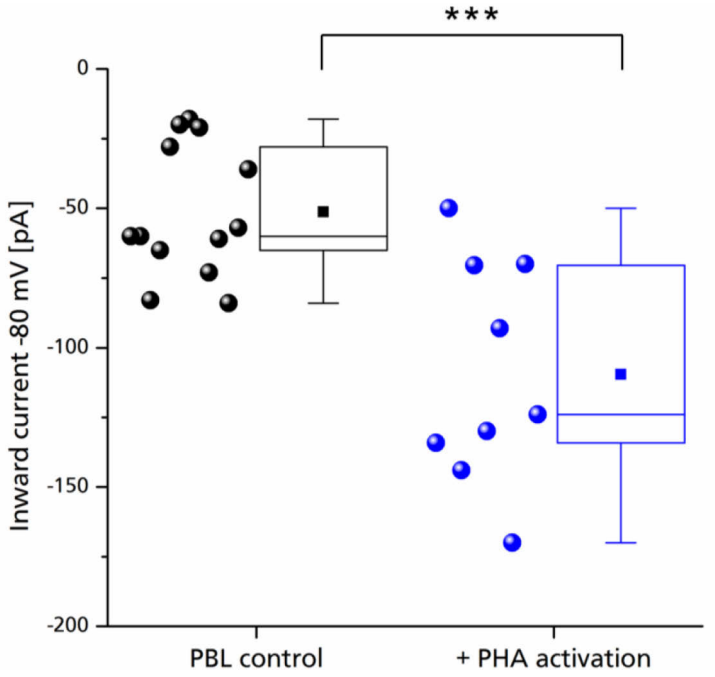

Fig. 4-15: Inward currents of resting and PHA-L activated PBLs at -80 mV

The Inward currents at -80 mV for individual resting and activated PBLs is shown; each circle represents one measured cell (black resting, blue activated). The box plot diagram shows the median (line), mean (square) as well as 25 and 75 % of the data. Whiskers indicate 5-95 % of the data. A high significant difference of $p \leq 0.001$ is indicated by ***.

As expected, the inward current increases significantly (p = 0.0004) when PBLs are stimulated by PHA-L. This increase is presumably due to the expected upregulation of KCa3.1 (Ghanshani et al. 2000; Cahalan et al. 2009). For control cells the mean inward current at -80 mV is -51 ± 24 pA whereas in activated PBLs the inward current is doubled to -110 ± 40 pA. Another parameter, which is supposed to change in response to an increase in K^+ conductance, is the free running membrane potential (Vm). Vm should shift to more negative voltages towards the theoretical Nernst potential for K^+. The data in Fig. 4-16 shows that the stimulation of PBLs is indeed causing a negative shift of Vm.

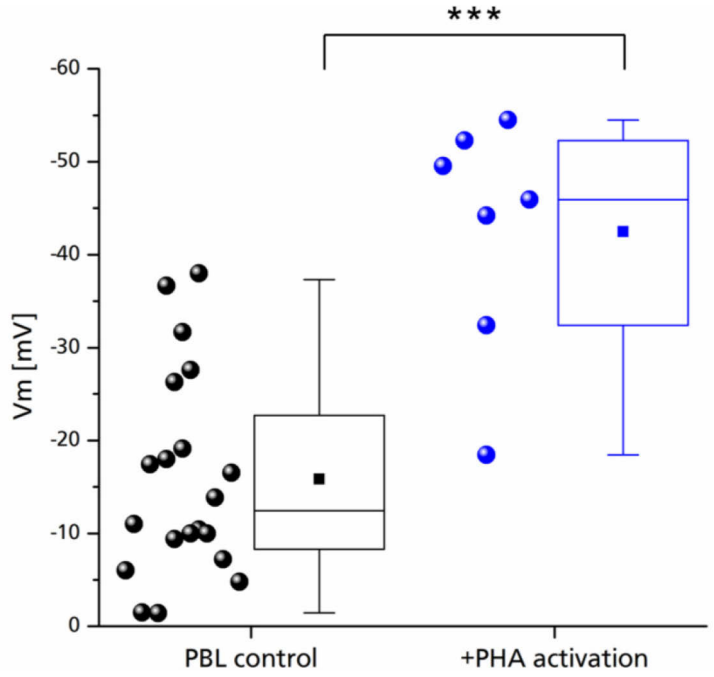

Fig. 4-16: The free running membrane potential (Vm) is more negative for stimulated PBLs
The running membrane potential (Vm) in [mV] for resting and activated PBLs is shown; each circle represents an individual measured cell (black resting, blue stimulated). The box plot diagram shows the median (line), mean (square) as well as 25 and 75 % of the data. Whiskers indicate 5-95 % of the data. A high significant difference of p ≤ 0.001 is indicated by ***.

The mean Vm value for control cells is -16 ± 11 mV; after stimulation Vm shifts to -43 ± 13 mV. This finding supports the idea that the increase in inward current after activation is at least to some extend carried by K^+ ions. The measured free running membrane voltage is not identical to the calculated theoretical Nernst potential (EK), which is -86 mV under the prevailing recording conditions. This indicates that also the conductance to other ions contributes to the free running membrane voltage. These results show that PBLs increase their number of KCa3.1 channels after PHA-L stimulation. This increase in K^+ conductance is playing an important role during cell activation (Ghanshani et al. 2000; Beeton et al. 2006; Cahalan et al. 2009).

To examine whether IR triggers an immediate increase in K^+ conductance the electrical properties of PBLs were recorded directly on a portable patch clamp device inside an X-ray tube as described in previous studies (Roth et al. 2015; Gibhardt et al. 2015) before and immediately after irradiation. Other than in experiments with A549 cells this treatment elicited no clear increase of membrane conductance in freshly isolated PBL.

A representative example is shown in Fig. 4-17. The data show that IR exposure even causes in the exemplary cell a decrease in membrane conductance.

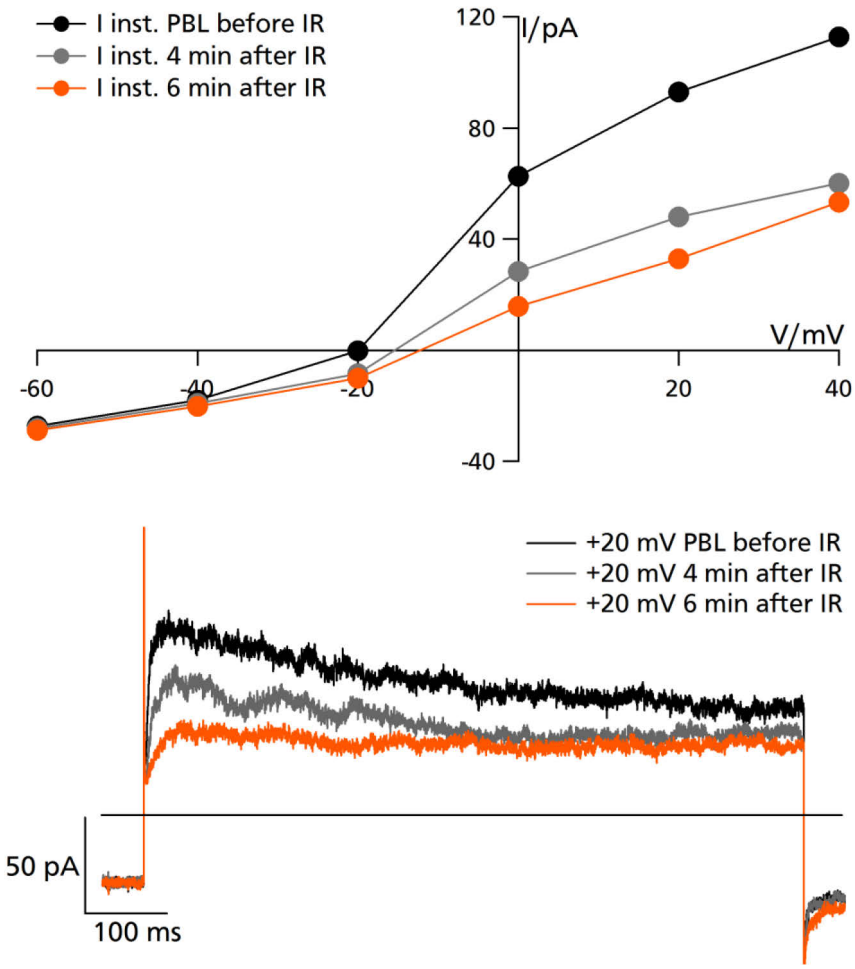

Fig. 4-17: Irradiation of freshly isolated PBLs causes no increase in instantaneous conductance
(Top) current/voltage (I/V) relations (I inst.) from the same cell measured before IR (black circles), 4 min (grey) and 6 min after 1 Gy X-ray (orange). Irradiation augments no hyperpolarization in freshly isolated resting PBLs; the reduction in current is presumable due to rundown effect. Currents were measured as in Fig. 4-2. (Bottom) Current responses to voltage pulse from -80 mV to +20 mV and back to the initial voltage. Currents were recorded 2 min before (black) as well 4 and 6 min after X-ray irradiation (grey & orange); horizontal line indicates where the current is zero.

The absence of a rapid activation of K^+ channels and membrane hyperpolarization in freshly isolated PBLs is consistent with literature data. It is well established that KCa3.1 channels are expressed in resting PBLs only at a low density (Ghanshani et al. 2000; Cahalan et al. 2009); the respective channels are only after immune stimulation upregulated. The small number of channels in resting lymphocytes may not be sufficient to generate a measurable increase in conductance over the background after irradiation. Activated PBLs like T-effector cells (Fig. 4-9) on the other hand may exhibit an IR induced response since these cells express the KCa3.1 channel at high density. It was unfortunately not possible to study the direct effects of IR on the electrical properties and KCa3.1 activation in immune activated PBLs. PBLs, which were incubated for more than 48 hours after isolating them from buffy coats, could not be sealed and maintained for the respective whole cell recordings on a port-a-patch device inside a X-ray tube. For this reason we changed the cell system to the Jurkat cell line, an immortal T-cell precursor cell line.

4.4.3 Ionizing radiation influences the ion channel composition in Jurkat cells

When we studied the morphological changes of leukemic T-cell progenitor cells (Jurkat cells) evoked by ionizing radiation (IR), we found a dose dependent increase of cell diameter after 24-48 hours (Chapter 2.4.4). This increase in cell size is similar to the increase in diameter of PBLs after immune activation (Chapter 2.4.1). After immune activation, the conductance of KCa3.1 channels is strongly upregulated and these channels play a key role in the subsequent differentiation and activation (Ghanshani et al. 2000). The positive correlation between channel activation and PBL stimulation raises the question whether the IR induced increase in the cell diameter of Jurkat cells goes along with a similar change in the membrane conductance of these cells. In order to understand whether the IR induced increase in cell diameter was related to altered transport properties in Jurkat cells I measured control and irradiated Jurkat cells. Cells were therefore irradiated with X-ray and used for patch clamp measurements 48 hours after irradiation, when the IR induced increase in cell size is at its angular point.

4.4.3.1 The electrophysiological properties of Jurkat cells

In the plasma membrane of Jurkat cells not KCa3.1 but the closely related likewise calcium dependent potassium channel KCa2.2 (SK2) is expressed (Jäger et al. 2000; Cahalan et al. 2009). KCa subtypes are distinguished on the basis of their unitary channel conductance: while KCa3.1 has a medium single channel conductance, KCa2.2 exhibits a small single channel conductance (KCa2.2). Under resting conditions and low basal cytosolic Ca^{2+} (10-100 nM) all KCa channels are closed. Activation of T-cells causes a rise in the concentration of free Ca^{2+} in the cytosol [Ca^{2+}_{cyt}] to and above 200-400 nM. This results in an activation of the channel via a C-terminal bound calmodulin (CaM) (Fanger et al. 1999). Thus a [Ca^{2+}_{cyt}] mediated signaling cascade, which can be triggered for example by TCR stimulation, opens KCa channels. This in turn keeps the plasma membrane hyperpolarized, which sustains Ca^{2+} signaling. Taken together, the current state of knowledge suggests that Ca^{2+} activated potassium channels like KCa2.2 are playing key roles in T-cell activation. It seems plausible that they are even more important than the voltage dependent Kv1.3 channel, which is the predominant outward rectifier in resting T-cells and unirradiated Jurkat cells (Fanger et al. 2001).

The outward rectifying potassium channel Kv1.3 with its characteristic voltage dependent activation and subsequent inactivation is the predominant channel in Jurkat cells (Fig. 4-18). It is reported that Kv1.3 channels conduct the majority of the outward-rectifying K^+ current in resting lymphocytes as well (Kuras et al. 2012). To confirm the presence of this channel in the Jurkat cells, cells were exposed to the Kv channel specific blocker margatoxin (MgTx), which blocks Kv1.3 with a high affinity (Kd 11.7 pM) (Bartok et al. 2014).

Fig. 4-18 shows the results of this treatment. As expected, 150 nM MgTx is able to reduce the outward rectifier current. This underscores that Kv1.3 is the main component of the outward rectifying current in control Jurkat cells.

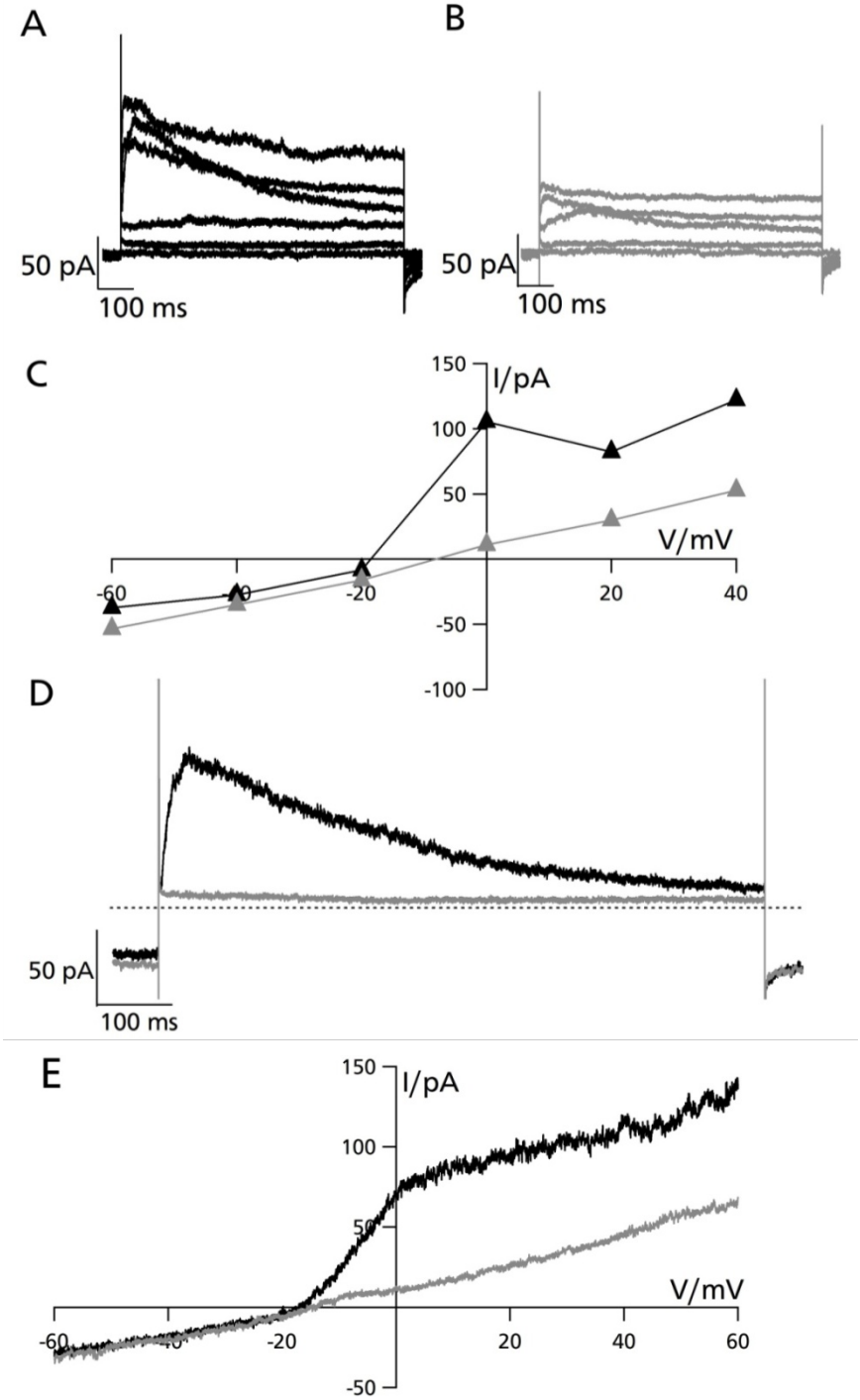

Fig. 4-18: The dominant current in Jurkat cells is carried by Kv1.3 and can be blocked by margatoxin

(A) typical current response of a Jurkat control cell before and (B) 6 min after the addition of 150 nM MgTx. (C) current/voltage (I/V) relations from the same cell. Black triangles indicate the peak current response before and grey triangles 6 min after the addition of 150 nM MgTx. Currents were measured as in Fig. 4-2. (D) A depolarizing voltage step from -60 mV to 0 mV illustrates the activating and inactivating Kv1.3 current response before (black) and 6 min after MgTx addition (grey). The typical Kv1.3 kinetic is clearly vanished. Horizontal dashed line indicates where current is zero. (E) An 800 ms long voltage ramp protocol from -60 to +60 mV reveals the different current components of Jurkat cells. At voltages more positive than -20 mV the Kv1.3 characteristic current response is visible (black) which is vanished 8 min after the addition of MgTx (grey). At voltages more negative than -20 mV the conductance is quasi-linear; this reflects the activity of voltage independent KCa2.2 channels.

Besides the two potassium channels that are expressed in T-cells and Jurkat cells, also other types of ion channels are endogenously expressed in Jurkat cells:

- Mammalian melastatin-related transient receptor potential (TRPM) channel TRPM2. It is a Ca^{2+} permeable, nonselective cation channel (Sumoza-Toledo and Penner 2011),
- TRPM7 also known as "Mg^{2+}-inhibited-Ca^{2+}-permeable current" (MIC). Its current can be neglected here, Mg^{2+} was used in the pipette solution (Prakriya and Lewis 2002),
- An ATP-dependent outwardly rectifying Cl^- channel. By using an ATP free pipette solution the contribution of the Cl^- current can be eliminated (Cahalan et al. 2009),
- KCNK18, also known as TWIK-related spinal cord potassium channel (TRESK) related K^+ channel (Pottosin et al. 2008), a two pore domain channel which is sensitive to G-protein coupled receptor agonist, pH and temperature as well as stretching and Ca^{2+}. This ion channel is discussed in the literature as a possible target for treatment for T-cell dysfunction (Pottosin et al. 2008; Han and Kang 2009),
- Na^+ currents can be ignored here since they are only expressed in 1-5 % of Jurkat cells (Cahalan et al. 1985),
- Bestrophin 1, also known as "calcium activated chloride channel" (CaCC). This Cl^- channel plays a role in cell swelling processes (Chien and Hartzell 2007)

Fig. 4-19 shows the five most important endogenous ion channel types expressed in T-cells and Jurkat cells (from Cahalan and Chandy 2009).

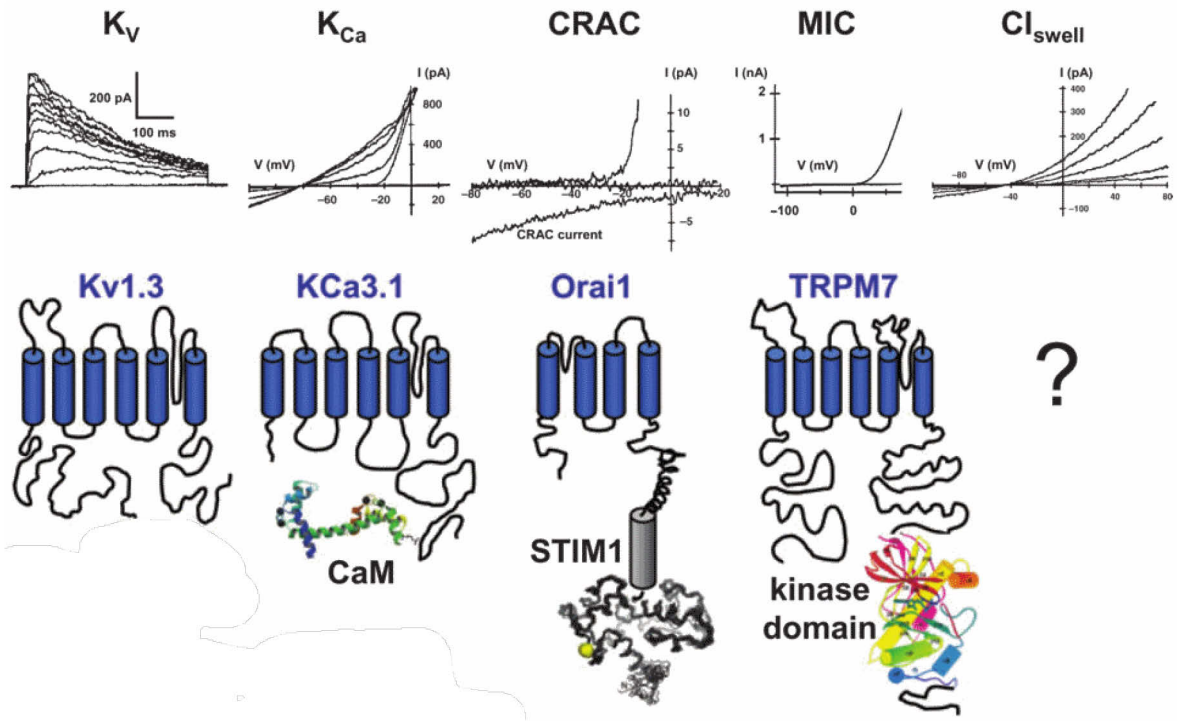

Fig. 4-19: Five important types of ion channels are expressed in T lymphocytes and Jurkat cells
Whole-cell current fingerprints, the molecular identities of membrane-spanning subunits and accessory subunits or modulating domains are shown for five channel types. From left to right: voltage dependent Kv1.3; Ca^{2+} activated K^+ channel (KCa3.1) with CaM; CRAC channel (Orai1 + STIM1) shown with structure of STIM1; MIC channel (TRPM7) with kinase domain; and Cl^-_{swell} of uncertain molecular composition (modified from Cahalan et al. 2009).

4.4.3.2 Approaches for the differentiation of endogenous ion channel type contributions to the whole-cell currents in Jurkat cells

When electrophysiological properties of individual ion channels in an ensemble of other channels are studied, three main strategies can be employed:

- *the chemical approach*: use of specific blockers. Blockers however always bear the hazard of unwanted side effects (see Chapter 5: Apamin is blocking Kv1.3 and KCa2.2);
- *the physical approach*: use of specially adapted patch clamp solutions for discriminating between e.g. sodium or potassium channels; the use of aspartate as counter-ion to Na^+ or K^+ instead of Cl^- (e.g. if Cl^- currents need to be omitted), or the addition of activating or inhibiting molecules like ATP, Mg^{2+} or Ca^{2+};
- *the biological (kinetic) approach*: use of special voltage protocols like ramps or long (respectively short) pulses to spotlight different subtypes of e.g. potassium channels due to their individual characteristics.

For generating I/V curves of Jurkat cell measurements I used only very short voltage pulses (100 ms) for channel activation to limit the long-lasting inactivation of Kv1.3 channels at positive voltages. The peak currents of each voltage were used for constructing I/V curves. To achieve a full voltage dependent activation of the Kv1.3 channels after each protocol, cells were kept at −60 mV for at least 1-2 min between sequential voltage clamp protocols; in preceding control experiments I found that this time was sufficient for full recovery (see also Levy and Deutsch 1996).

To quantify the relative contribution of Kv1.3 currents to the whole cell current, the characteristic kinetic of this channel was used. The membrane was therefore clamped from a negative holding potential (-60 mV), where Kv1.3 is in its closed but activatable state, to a relative long depolarizing voltage step, where most of Kv1.3 channels activate and show the characteristic inactivation kinetic (Kuras et al. 2012). The typical voltage protocol and resulting currents are shown in Fig. 4-20. The remaining current at the end of this long voltage step (I steady), where Kv1.3 channels no longer contribute to the apparent current, can be described as the “Kv1.3 independent current”.

The peak current minus this Kv1.3 independent current is a measure for the Kv1.3 contribution to the whole cell current (Fig. 4-20).

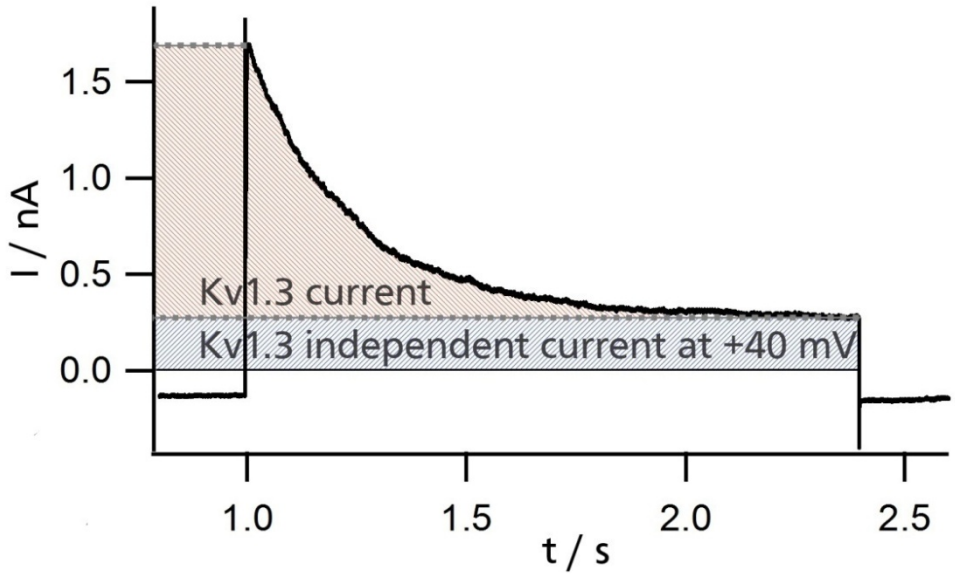

Fig. 4-20: The current response of Jurkat cells can be dissected in the Kv1.3 current and a Kv1.3 independent current

The current at the end of the long depolarizing voltage pulse (I steady) can be described as "Kv1.3 independent current" (blue) since all Kv1.3 channels are in their inactivated state and contribute no longer to the whole cell current response. The peak current minus I steady is vice versa the Kv1.3 current. Horizontal continuous line indicates where the current is zero.

Another strategy was pursued by running a train of 10 voltage ramp protocols without pauses. The first ramp elicits in this case the current of all channels and exhibits the Kv1.3 characteristic kinetic. The last ramp in contrast evokes only the Kv1.3 independent current since with every ramp protocol more Kv1.3 channels undergo the transition into the inactivated closed state. Using these experiment strategies the contribution of different channel types to the whole cell current can be separated. This provides mostly information on the Kv1.3 channel and KCa2.2 channels, since the pipette and bath solutions were composed in such a way that they suppressed most other channels. As a complementary approach also the inward current at -80 mV was analyzed as a measure for the KCa2.2 activity.

4.4.3.3 Untreated Jurkat cells exhibit homologous electrophysiological properties

In control experiments a large populations of unirradiated Jurkat cells were analyzed by whole cell recordings using the standard internal and external solution. When cells are patched in the whole cell configuration, the internal solution is replacing the cytosol within a few minutes. This circumstance was used to measure electrophysiological properties and the ion channel composition of irradiated and control cells with different defined Ca^{2+} concentrations. These defined free Ca^{2+} concentrations were achieved by using an accurate proportion of $CaCl_2$ and EGTA calculated with the "Ca^{2+}-EGTA Calculator" from Stanford University.

The low internal Ca^{2+} concentration of ~ 100 nM is reflecting a resting level; a high internal Ca^{2+} concentration of ~ 1 µM in contrast is mirroring a high Ca^{2+} level that occurs during immunological activation of T-cells.

Fig. 4-21 shows the whole cell current response of a typical Jurkat control cell patched with an internal solution containing a low free Ca^{2+} concentration.

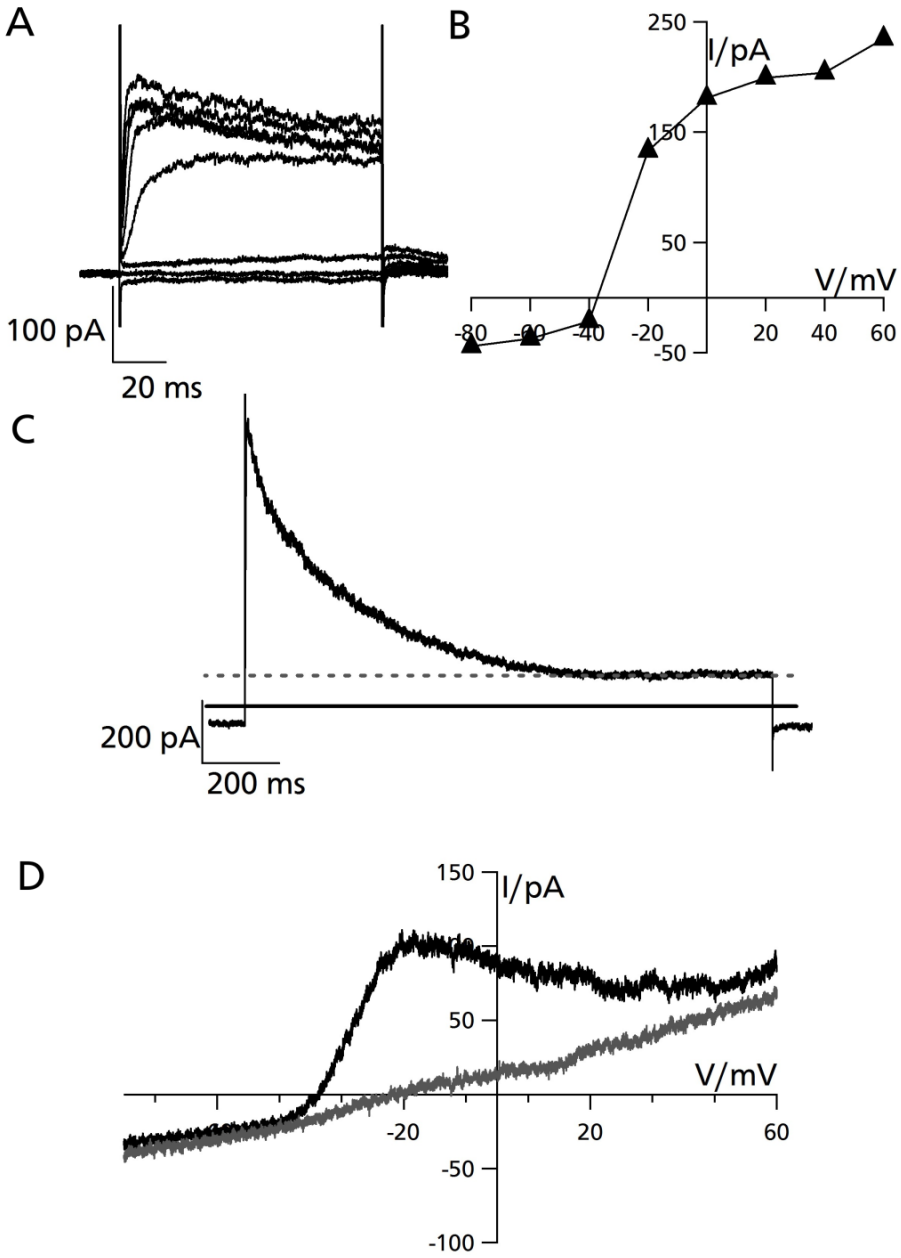

Fig. 4-21: Unirradiated Jurkat cells exhibit a homogenous current response and a very small Kv1.3 independent current portion

(A) Typical current response of a Jurkat control cell measured as in Fig. 4-2 (B) current/voltage (I/V) relations from the same cell (black triangles = peak current). (C) The depolarizing voltage step from -60 mV to +40 mV illustrates the activating/inactivating Kv1.3 current response and shows that the portion of Kv1.3 independent current is low. Horizontal dashed line indicates the Kv1.3 independent current, the continuous line indicates where the current is zero. (D) The 800 ms long voltage ramp protocol from -60 to +60 mV reveals the current components of Jurkat cells. At voltages more positive than -40 mV the Kv1.3 characteristic current response is visible (black) which is lost after 8 repetitive voltage ramps (grey). Here the Kv1.3 independent current is visible, which conductance is quasi-linear; this reflects the activity KCa2.2.

The mean Kv1.3 independent current portion of N = 8 unirradiated Jurkat cells is only 12.8 ± 6 %. The current response to a voltage step from -60 mV to +40 mV is dominated by the distinct activation/inactivation kinetics of Kv1.3. The mean inward current at -80 mV is low with only -34 ± 25 pA.

This low inward current is reflected in Fig. 4-21 D by a shallow slope at voltages < -40 mV. When the inward current is normalized to the cell surface area it is for these control cells -0.05 ± 0.04 pA/µm^2. For cell surface area estimation a picture was taken from each individual cells on the patch pipette. The cell diameter was then estimated from the image by using Fiji (ImageJ) (Schindelin et al. 2012). Control cell surfaces were estimated by assuming a spherical shape for control cells like shown in the 3D-stacks in Chapter 3.4.1. Control cells exhibit a rather uniformly current response and only minor differences in the relative contribution of the Kv1.3 independent current between individual control cells.

When control cells are patched with an internal solution containing 1 µM free Ca^{2+} the results are very similar to recordings with a low Ca^{2+} solution (Fig. 4-22). The results of these experiments suggest that Ca^{2+} has no major impact on the electrical properties of unirradiated Jurkat cells since Ca^{2+} dependent K^+ channels are only expressed in a low number. This matches with the literature for unstimulated lymphocytes (Ghanshani et al. 2000).

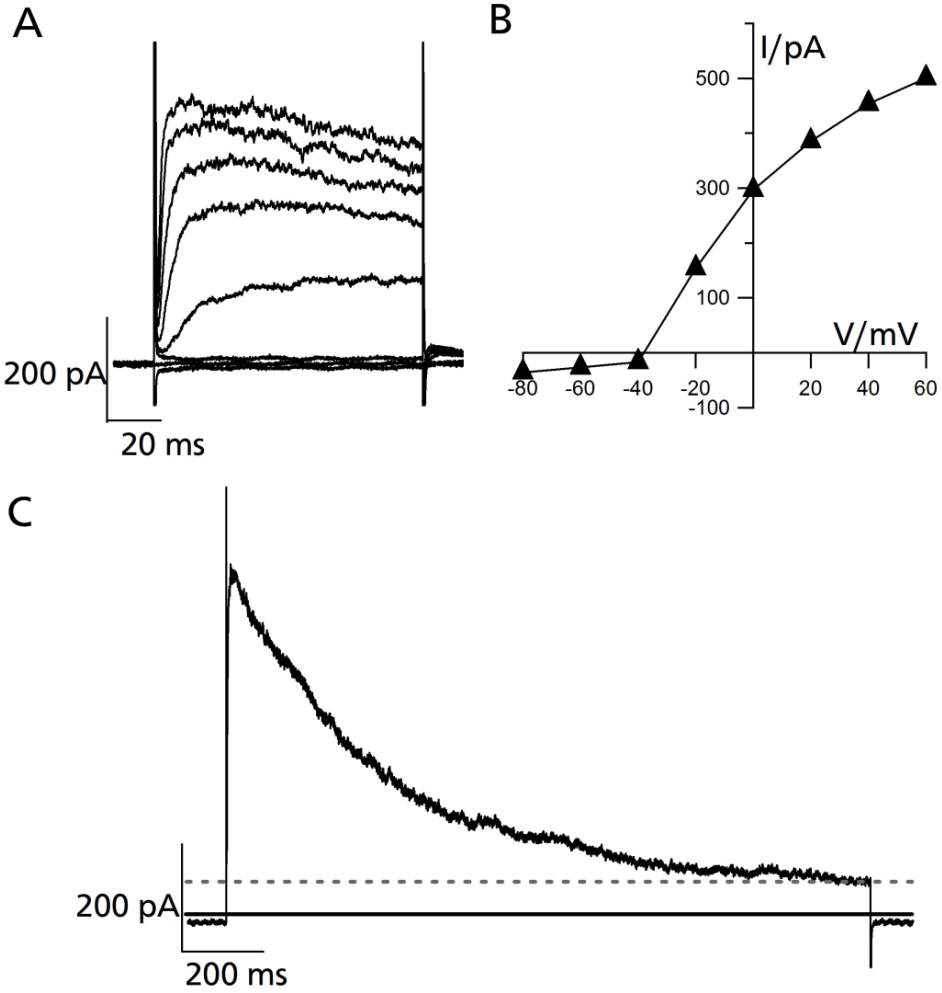

Fig. 4-22: Unirradiated Jurkat cells exhibit no increased Kv1.3 independent current with high internal free Ca^{2+} concentrations (1 µM)

(A) Typical current response of a Jurkat control cell patched with high internal Ca^{2+} concentration. Currents were measured as in Fig. 4-2. (B) current/voltage (I/V) relations from the same cell (black triangles = peak current). (C) The depolarizing voltage step from -60 mV to +40 mV illustrates the activating/inactivating Kv1.3 current response and shows that the portion of Kv1.3 independent current is low. Horizontal dashed line indicates Kv1.3 independent current, continuous line indicates where the current is zero.

The mean Kv1.3 independent current of N = 15 control Jurkat cells recorded with high internal Ca^{2+} concentration is 14.6 ± 5.2 %. This value is not significantly different from control cells patched with low Ca^{2+} solution (12.8 ± 6 %). The mean inward current at -80 mV was slightly increased with high Ca^{2+} (-49 ± 40 pA) compared to recordings with low Ca^{2+} (-34 ± 25 pA). The current density at -80 mV is -0.06 ± 0.04 pA/µm^2; a value which is not significantly different from that measured with low internal Ca^{2+}.

4.4.3.4 48 hours after irradiation the ion channel composition of Jurkat cells is changed

Jurkat cells irradiated with 1.25 Gy show an increased cell diameter and increased cell-surface adhesion. The cell surfaces of irradiated cells were hence calculated by assuming a hemispherical shape like shown in Chapter 3.4.1. When measured with a low internal Ca^{2+} concentration, most of the irradiated Jurkat cells showed a higher peak current but no significantly higher Kv1.3 independent current response compared to control cells. The typical currents of a Jurkat cell 48 hours after 1.25 Gy irradiation is shown in Fig. 4-23.

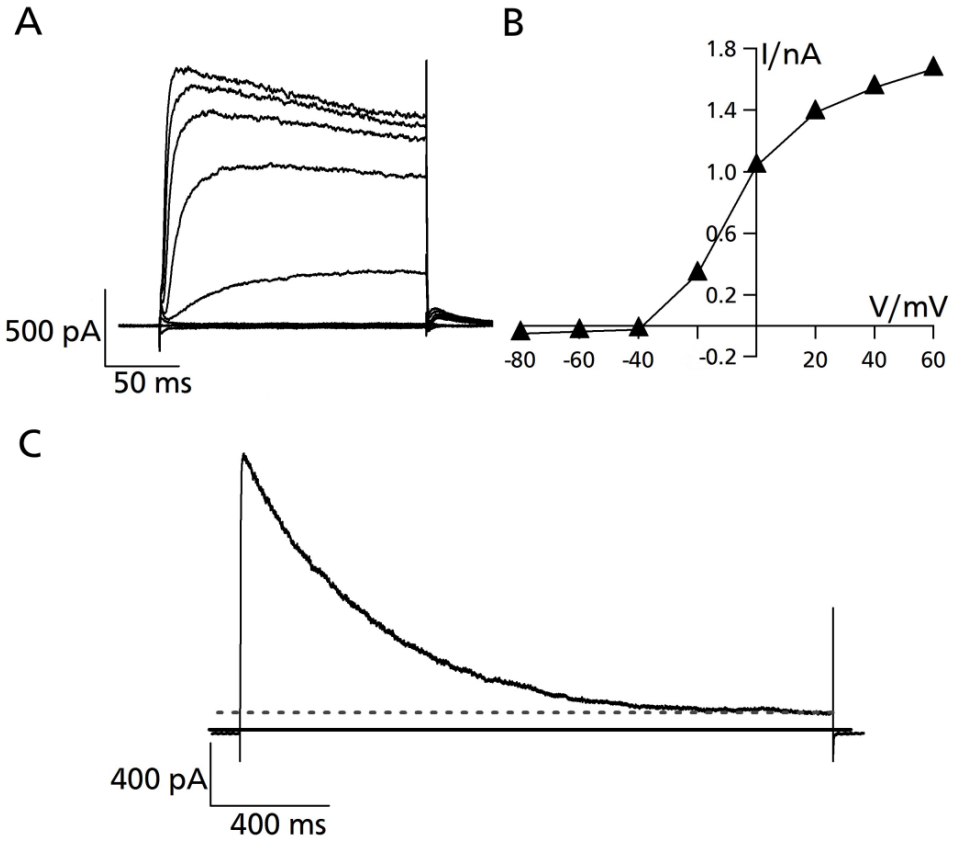

Fig. 4-23: Current response of a Jurkat cell 48 hours after irradiation and low internal Ca^{2+} concentration
(A) Typical current response of a 1.25 Gy X-ray irradiated Jurkat cell patched with low internal Ca^{2+} concentration. Currents were measured as in Fig. 4-2. (B) current/voltage (I/V) relations from the same cell (black triangles = peak current). (C) The depolarizing voltage step from -60 mV to +40 mV illustrates the activating/inactivating Kv1.3 current response and shows that the portion of Kv1.3 independent current remains low. Horizontal dashed line indicates Kv1.3 independent current, continuous line indicates where the current is zero.

The mean Kv1.3 independent current of N = 10 irradiated Jurkat cells patched with a low Ca^{2+} internal solution is 18.15 ± 7 % and hence slightly increased compared to unirradiated cells.

The Kv1.3 kinetic, that can be best observed with the help of the depolarizing voltage step to +40 mV, was very pronounced. The mean inward current at -80 mV was still low (-70 ± 30 pA) but increased compared to the control cells. When this value is divided by the cell surface area, it is -0.07 ± 0.03 pA/µm^2 and no longer significantly different from that of control cells. The same observation can be made with the Kv1.3 current (I peak – I steady). After irradiation the mean Kv1.3 current is higher (877 ± 432 pA) than in control cells (579 ± 244 pA). When the higher cell surface area of irradiated cells is considered, the mean Kv1.3 current (0.76 ± 0.4 pA/µm^2) is not significantly different from that of control cells (0.7 ± 0.3 pA/µm^2). The results of these experiments show that the absolute Kv1.3 current of irradiated Jurkat cells 48 hours after IR treatment is increased, but the current density of the Kv1.3 current remains constant.

In the next set of experiments irradiated Jurkat cells were patched with an internal solution containing a high (1 µM) free Ca^{2+} concentration. The data in Fig. 4-24 show that this condition causes a strong increase in membrane conductance of these cells. The inward current at voltages more negative than -40 mV is much more pronounced and the voltage ramp yields a steeper slope indicating a higher activity of voltage independent potassium channels. This notion of an elevated instantaneous activating current is further supported by the increase of the Kv1.3 independent current at +40 mV.

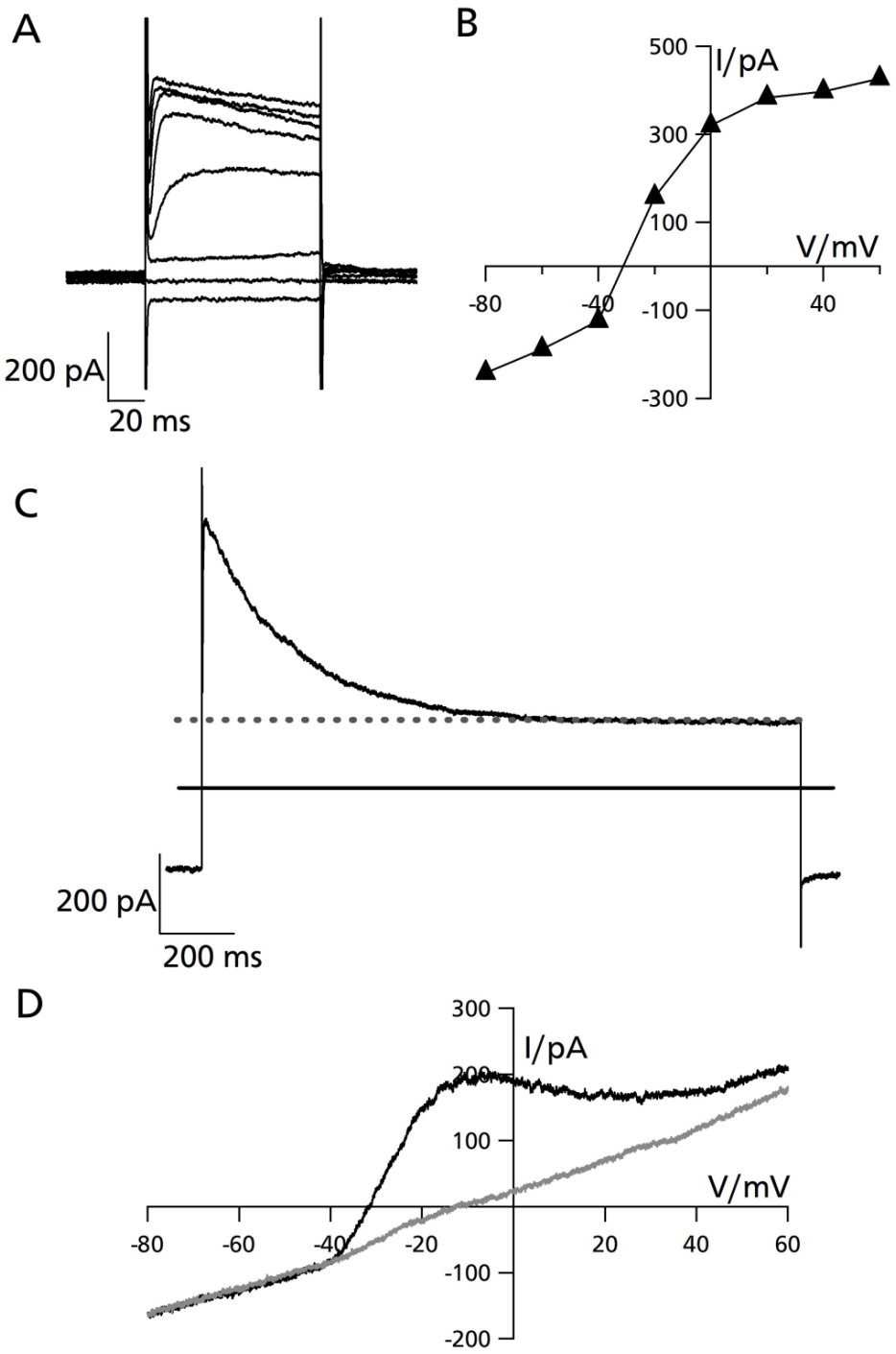

Fig. 4-24: Current response of a irradiated Jurkat cell patched with a high internal Ca^{2+} concentration

(A) Typical current response of a 1.25 Gy irradiated Jurkat cell patched with high internal Ca^{2+} concentration. Currents were measured as in Fig. 4-2. (B) current/voltage (I/V) relations from the same cell (black triangles = peak current). (C) The depolarizing voltage step from -60 mV to +40 mV illustrates the activating/inactivating Kv1.3 current response and shows that the portion of Kv1.3 independent current clearly increased (here > 30% of current). Horizontal dashed line indicates Kv1.3 independent current, continuous line indicates where the current is zero. (D) The 800 ms long voltage ramp protocol from -60 to +60 mV reveals the current components of Jurkat cells. At voltages more positive than -40 mV the Kv1.3 characteristic current response is visible (black) which is lost after several repetitive voltage ramps (grey). Here the KCa2.2 current is visible, which conductance is quasi-linear and increased compared to the control cells.

The mean Kv1.3 independent current of N = 17 cells 48 hours after irradiation with 1.25 Gy X-ray is clearly increased to 32.1 ± 11.7 %. The portion of Kv1.3 independent current is more than doubled compared to control cells.

The mean inward current at -80 mV is strongly increased to -173 ± 138 pA, which translates into a current density of -0.13 ± 0.9 pA/µm^2. Apparently, 48 hours after irradiation of these T-cell progenitor cells, a Ca^{2+} dependent potassium channel is upregulated since this instantaneous activating current is only visible when a internal solution containing a high free Ca^{2+} concentration is used.

The following figures summarize the data, which were shown in the representative whole cell measurements. Fig. 4-25 reports the Kv1.3 independent currents of 8-17 individual cells measured under different conditions.

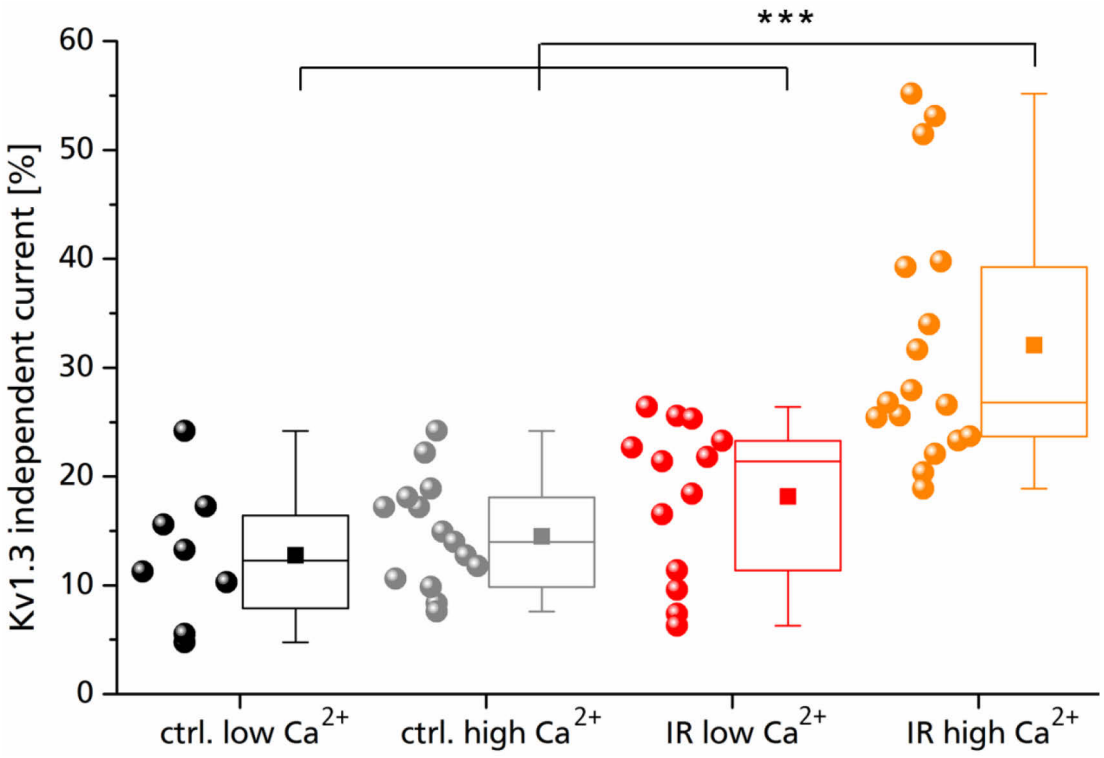

Fig. 4-25: Kv1.3 independent current is 48 hours after 1.25 Gy X-ray increased and Ca^{2+} dependent
The Kv1.3 independent current response of control and irradiated Jurkat cells is shown; each circle represents one measured individual cell (black/grey = ctrl.; red/orange = irradiated). The box plot diagram shows the median (line), mean (square) as well as 25 and 75 % of the data. Whiskers indicate 5-95 % of the data. A high significant difference of $p \leq 0.001$ is indicated by ***.

The results of this analysis show that the Kv1.3 independent current is significantly elevated 48 hours after irradiation with 1.25 Gy X-ray ($p < 0.001$). A high internal free Ca^{2+} concentration of 1 µM (high Ca^{2+}) alone, as well as IR alone is not sufficient to elicit this increase in Kv1.3 independent current. This shows that a Ca^{2+} dependent ion channel is upregulated due to IR.

Next, the inward current density at -80 mV [pA/µm^2] of 8-17 individual cells and the resulting box plot diagrams with mean and median value is shown in Fig. 4-26.

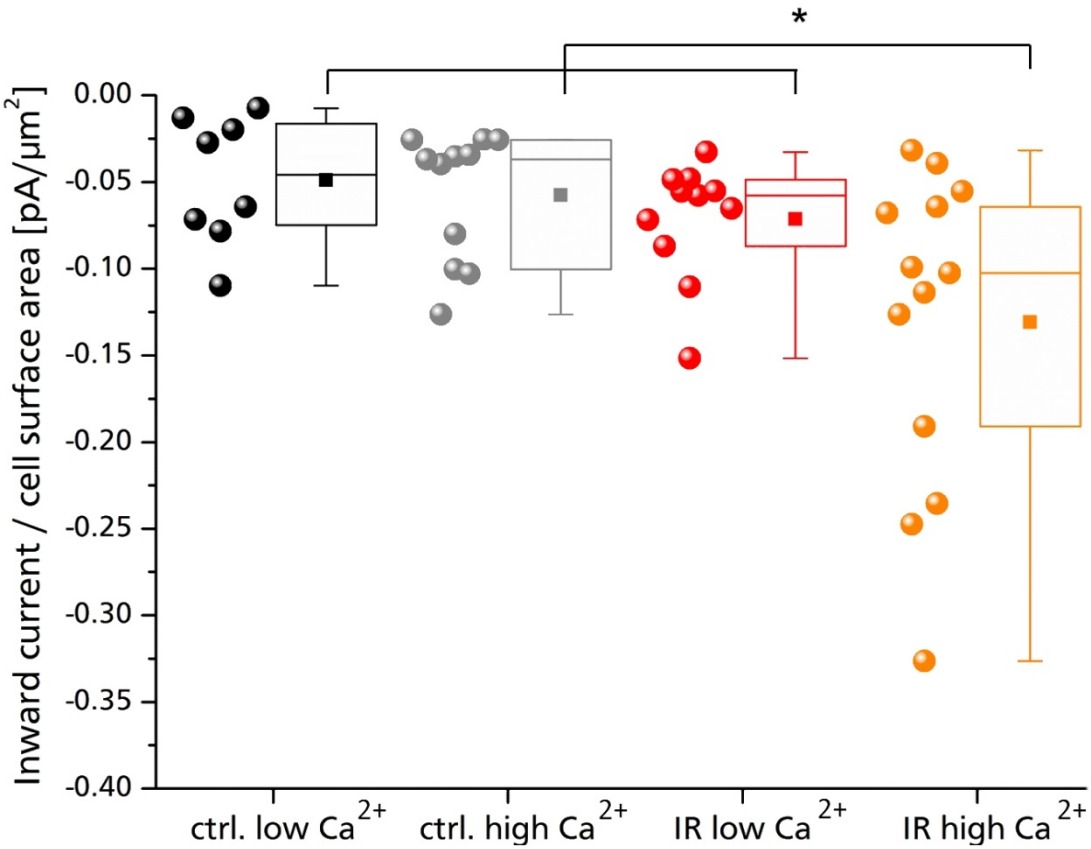

Fig. 4-26: The relative inward current per area at -80 mV is increased after IR and Ca^{2+} dependent
The inward current at -80 mV per area of control and irradiated Jurkat cells is shown; each circle represents one measured individual cell (black/grey = ctrl.; red/orange = irradiated). The box plot diagram shows the median (line), mean (square) as well as 25 and 75 % of the data. Whiskers indicate 5-95 % of the data. A moderate significant difference of $p \leq 0.05$ is indicated by *.

Like the Kv1.3 independent outward current at +40 mV, the inward current at -80 mV is increased 48 hours after 1.25 Gy X-ray in cells patched with a high Ca^{2+} concentration in the internal solution. Since a high internal free Ca^{2+} concentration of 1 µM (high Ca^{2+}) is mandatory for eliciting the elevated inward current after IR it is reasonable to assume that this current is carried by a Ca^{2+} dependent ion channel. Notably not the all irradiated Jurkat cells examined with a high internal Ca^{2+} concentration are different from the unirradiated control cells or the irradiated cells with a low internal Ca^{2+}. The mean values as well as the median values of these cells however are more negative and the measured difference is significant ($p < 0.05$).

The results indicate that a voltage independent, Ca^{2+} dependent ion channel is more active and upregulated in Jurkat cells 48 hours after irradiation with 1.25 Gy X-ray. One of the possible candidates is the Ca^{2+} dependent KCa2.2, a channel that is closely related to the KCa3.1, which is upregulated in PBLs after stimulation (see 4.4.2).

The increase in a conductance of this channel should very much like in activated PLBs cause a negative shift of the free running membrane voltage (Vm). This expected shift is however not apparent in the data (Fig. 4-28).

To further confirm that the observed increase in conductance is due to an increase in K^+ conductance in Jurkat cells after irradiation, experiments were carried out in which the external K^+ concentration was increased by a factor of 10. In the case that the increase in conductance is really related to K^+ channel activity, this elevation of K^+ should yield a higher inward current at -80 mV. The results are shown in Fig. 4-27.

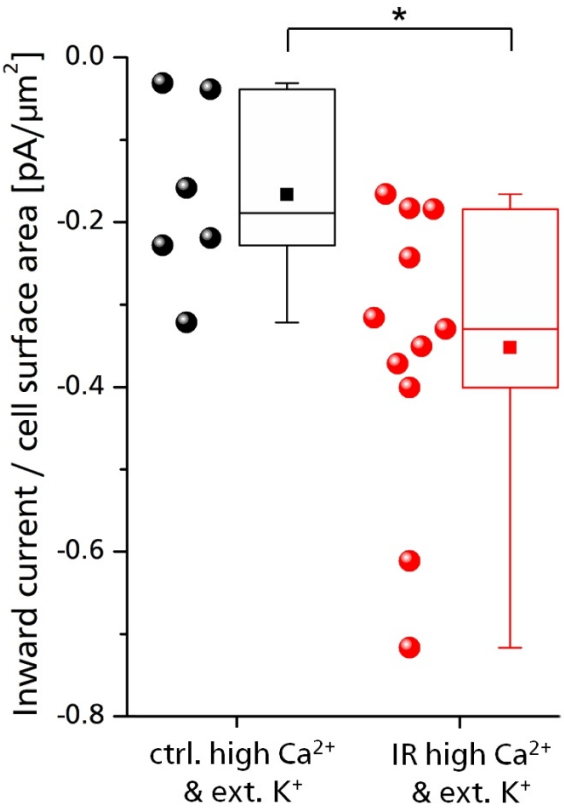

Fig. 4-27: A high external potassium concentration increases the inward current per µm² at -80 mV
The inward current under a high external K^+ concentration at -80 mV for control (black) and 1.25 Gy X-ray irradiated (red) Jurkat cells is shown; each circle represents one measured individual cell. The box plot diagram shows the median (line), mean (square) as well as 25 and 75 % of the data. Whiskers indicate 5-95 % of the data. A significant difference of $p \leq 0.05$ is indicated by *.

The inward current of irradiated cells patched with a high internal Ca^{2+} concentration is clearly increased compared to the inward current under standard external solution condition (Fig. 4-26). This supports the hypothesis that the Ca^{2+} dependent K^+ channel KCa2.2 is responsible for the observed increase in Kv1.3 independent current. When a high external potassium concentration is applied the predicted Nernst voltage for K^+ is -30 mV. The observed Vm under these conditions was for control cells -24.3 ± 3 mV and for irradiated cells -20.5 ± 5 mV. These findings support the hypothesis that a Ca^{2+} dependent potassium channel is responsible for the augmented Kv1.3 independent current.

The blocker tamapin was used for specific inhibition of KCa2.2 during these electrophysiological measurements. Tamapin is a scorpion toxin that has a remarkable selectivity for KCa2.2 and is very potent in blocking this channel (IC_{50} = 24 pM) (Pedarzani et al. 2002). My expectation was that the effect of this blocker will be only marginal on the current

response of unirradiated control cells but strong on the current response of irradiated cells patched with the high Ca^{2+} pipette solution.

Indeed, the reduction of the Kv1.3 independent current by 10 nM tamapin in control cells was only 3.3 ± 0.7 % (N = 3). The same treatment caused a 23 ± 10 % inhibition of this current in 1.25 Gy X-ray irradiated cells (N = 4). These data further support the hypothesis that KCa2.2 is upregulated due to IR.

4.4.3.5 Evaluation of the free running membrane voltage

The free running membrane voltage (Vm) is an important parameter for understanding membrane transport in cells. In the above presented experiments, the Kv1.3 independent current and the inward current at -80 mV were evaluated and discussed. In these experiments also the Vm was recorded for every measured cell. In Fig. 4-28 the mean Vm values are presented. The data show that the control cells exhibit the most negative but also most variable Vm (Nernst voltage for K^+ = -90 mV). Irradiated cells on the other hand show a slightly less hyperpolarized Vm under all measuring conditions.

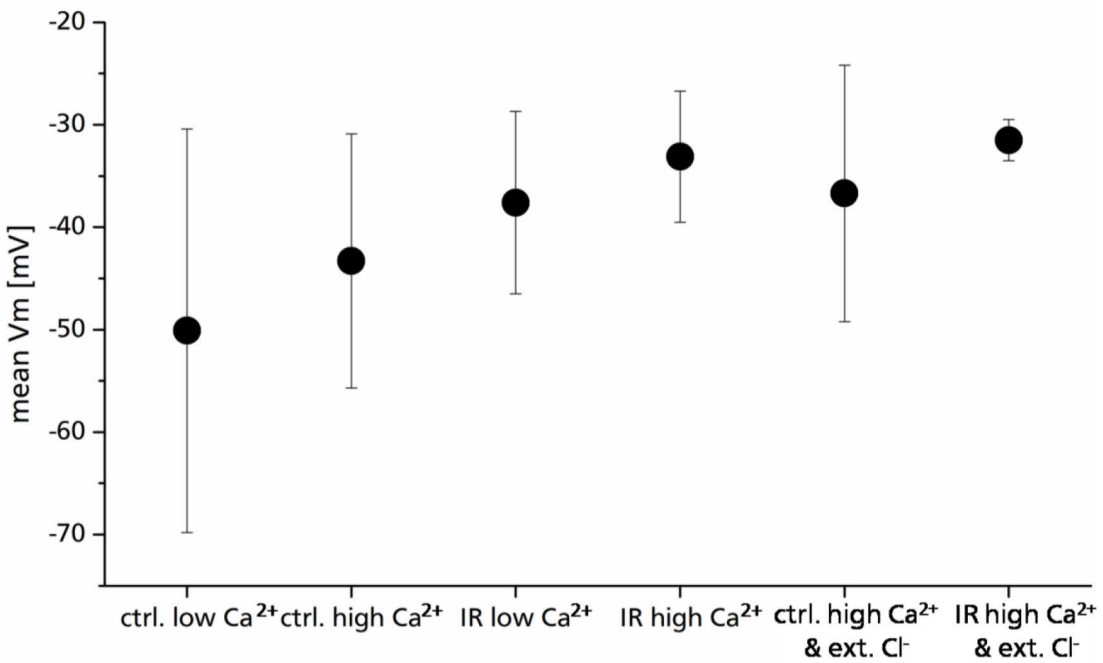

Fig. 4-28: The mean free running membrane voltage (Vm) for the different conditions
Vm was taken from the first applied ramp after cell exhibited a constant whole cell current response. Black circles represent the mean Vm, error bars indicate the standard deviation (N = 3-17).

One possible explanation for the Vm data is that other ion channels with a more positive reversal voltage, e.g. Cl^- channels, contribute to the ensemble conductance of the cells and this conductance is augmented by irradiation too. As introduced in chapter 4.4.3.2, the Cl^- concentration was kept low (external 10,5 mM / internal 11 mM) in the current experiments to omit relevant Cl^- currents. This does however not exclude a contribution of a Cl^- conductance to the Kv1.3 independent conductance and Vm in Jurkat cells. The predicted Nernst voltage for Cl^- under these conditions is -1.2 mV. An elevated activity of a Ca^{2+} dependent Cl^- channel like

Bestrophin-1 (Fig. 4-19) could be a possible explanation for the low Vm value. To test this experiments were performed using a 10 fold higher external chloride concentration. Under these conditions Vm should show a shift to more negative voltages.

The experimental results show that this is not the case (Fig. 4-28), ruling out the hypothesis of a higher Cl^- channel activity as explanation for the increased Kv1.3 independent current.

Apart from a higher Cl^- channel activity, an upregulation of TRPM2 channels could be an explanation for the low Vm value. Klumpp and co-workers (Klumpp et al. 2016) proposed a functional role of these channels in cell cycle control in Jurkat cells. However, my western blot studies exclude a higher number of TRPM2 channels as explanation for the increase in Kv independent current and the low Vm after irradiation, in N = 6 experiments the mean TRPM2 channel protein level for 1.25 Gy X ray irradiated cells was not increased compared to the TRPM2 protein level of control cells; the differences were not significant (p = 0.61). Yet CRAC and TRESK channels or sodium channel activity (Chapter 4.4.3.1) could lead to the observed depolarization of the plasma membrane of irradiated cells; this needs to be studied further.

4.4.4 Immunostaining and single molecule microscopy and analysis of KCa2.2

To examine whether ionizing irradiation is indeed causing an upregulation of KCa2.2 expression in Jurkat cells we imaged the human KCa2.2 channels in unirradiated and irradiated (1.25 Gy X-ray) Jurkat cells by immune staining. The presence of labeled channel proteins in the plasma membrane was detected a high resolution single molecule microscope. The representative images in Fig. 4-29 show that irradiation causes an elevated number of fluorescent signals in the plasma membrane of Jurkat cells. These fluorescent signals are only detected after labeling the channel with a fluorescent antibody suggesting that they report the presence of KCa2.2. channel proteins. The results of these experiments suggest that IR treatment increases the number of KCa2.2 molecules in the plasma membrane of Jurkat cells.

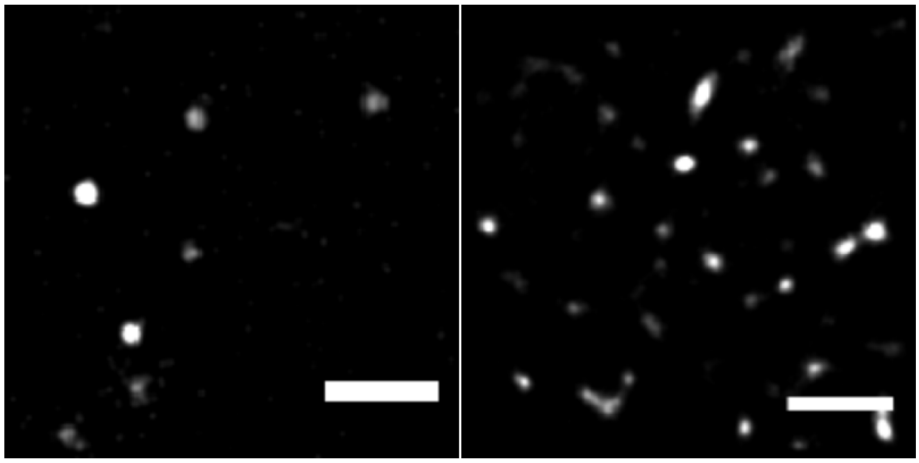

Fig. 4-29: Single molecule microscopy of immuno stained KCa2.2 in Jurkat cells
SMD microscopy confirms that 1.25 Gy irradiated Jurkat cells upregulate KCa2.2 (scale bar = 1 µm).

The visual impression from the exemplary data in Fig. 4-29 is supported by a detailed data analysis, which is shown in Fig. 4-30.

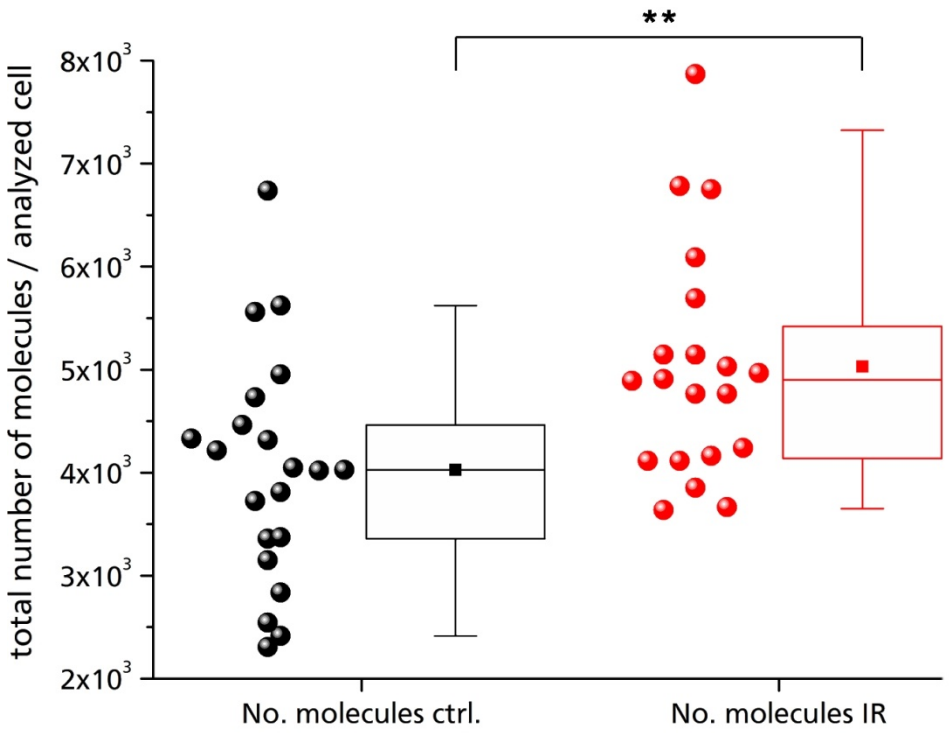

Fig. 4-30: Data analysis of single molecule microscopy reveals an increased number of KCa2.2 molecules
The mean number of KCa2.2 molecules per region of interest (ROI) increases significantly 48 hours after IR ($p < 0.0067$). Each circle represents an analyzed ROI of a single Jurkat cell; box plots show mean (filled square) and median (line) as well as 25 and 75 % of the data; whiskers indicate 10 and 90 % of all cells. A significant difference of $p \leq 0.01$ is indicated by **.

The mean number of fluorescent signals from immuno stained KCa2.2 molecules is in $n = 19$ regions of interest (ROI) higher in irradiated cells increased (48 hours after 1.25 Gy X-ray ($N = 3$)) than in control cells; the difference is significant ($p < 0.0067$).

4.5 Conclusion

In this chapter it is shown by the different techniques namely electrophysiology, immuno blotting and single molecule microscopy that the morphological changes in irradiated Jurkat cells presented in chapters 2 and 3 are associated with changes in the electrical properties including the upregulation of the calcium dependent potassium channel KCa2.2. This upregulation resembles the electrophysiological changes in T-cells during immune activation, where the upregulation of the calcium dependent potassium channel KCa3.1 is a direct marker for activation and T-cell subtype. Furthermore the mandatory volume increase after cell division or T-cell activation is initiated by an ion channel elicited osmotic swelling as the first essential step (Sarkadi and Parker 1991; Cahalan et al. 2001; Lang et al. 2006). It can be assumed that IR is able to stimulate Jurkat cells leading to an immunomodulation. Furthermore the data could be interpreted that IR is able to trigger a differentiation of immune cells. Here certainly further studies with freshly isolated T-cells of known subtype are needed to examine the by IR induced alterations.

As shown by electrophysiological measurements, both ionizing radiation and high internal Ca^{2+} concentration is needed to elicit a significant increase in the Kv1.3 independent current. This Kv1.3 independent current is carried by a calcium dependent potassium channel as shown by the use of different internal and external solutions. A high external potassium concentration leads to a higher inward current and low free calcium concentration diminishes the IR induced increase of Kv1.3 independent current. Furthermore experiments with a specific channel blocker substantiate the assumption that this Kv1.3 independent current is carried by the calcium dependent potassium channel KCa2.2. Single molecule analyses and the time that is needed to detect a higher Kv1.3 independent current furthermore shows that this increase in current is indeed the consequence of an upregulation of the number of KCa2.2 channels in the plasma membrane of Jurkat cells after IR exposure.

A close scrutiny of the data however implies that an increase in the number of KCa2.2 is not sufficient for explaining all the results. The data advocate a scenario in which also an activation of KCa2.2 channels, which are already present in unirradiated Jurkat control cells, is involved in the IR response. Control cells show in single molecule imaging more KCa2.2 channel proteins in the plasma membrane than expected from electrophysiological recordings. Under the assumption that the fluorescence intensity of the imaging data translates in a linear fashion with the number of channels in the membrane, we can assume that the channel density increases in response to IR by ~25 %. This value is much lower than the doubling of the presumed KCa2.2 current, which was measured in Jurkat cells after IR exposure. Assuming that the aforementioned assumptions e.g. the interpretation of the fluorescent signals and the identity of the KCa2.2 in the patch clamp recordings are correct, we must predict that IR also causes some kind of activation of KCa2.2 channels, which are already present in resting cells.

In recent years it was shown that KCa2.2 channels can be part of a multi-protein complex; the channel can assemble together with the casein kinase 2 (CK2) and the phosphatase PP2A indicating a direct and coupled mode of action (Bildl et al. 2004; Allen et al. 2007). In such a scenario it seems possible that a CK2 mediated CaM phosphorylation, which leads to a decreased affinity of CaM to Ca^{2+}, could play a role in the regulation of KCa2.2 activity (Allen et al. 2007; Maingret et al. 2008). This hypothesis is indirectly supported by data, which show that SRC kinases and subsequent activity of CK2 is modulated by IR (Chapter 2.4.7).

4.6 References

Allen D, Fakler B, Maylie J, et al (2007) Organization and regulation of small conductance Ca2+-activated K+ channel multiprotein complexes. J Neurosci 27:2369–2376.

Babel L, Grunewald M, Lehn R, et al (2017) Direct evidence for cell adhesion-mediated radioresistance (CAM-RR) on the level of individual integrin β1 clusters. Sci. Rep.

Bartok A, Toth A, Somodi S, et al (2014) Margatoxin is a non-selective inhibitor of human Kv1.3 K+ channels. Toxicon 87:6–16.

Beeton C, Wulff H, Barbaria J, et al (2001) Selective blockade of T lymphocyte K(+) channels ameliorates experimental autoimmune encephalomyelitis, a model for multiple sclerosis. Proc Natl Acad Sci USA 98:13942–7.

Beeton C, Wulff H, Standifer NE, et al (2006) Kv1.3 channels are a therapeutic target for T cell-mediated autoimmune diseases. Proc Natl Acad Sci USA 103:17414–9.

Bildl W, Strassmaier T, Thurm H, et al (2004) Protein kinase CK2 is coassembled with small conductance Ca(2+)-activated K+ channels and regulates channel gating. Neuron 43:847–858.

Cahalan MD, Chandy KG, DeCoursey TE, et al (1985) A voltage-gated potassium channel in human T lymphocytes. J Physiol 358:197–237.

Cahalan MD, Chandy KG, Hall I (2009) The functional network of ion channels in T lymphocytes. Immunol Rev 231:59–87.

Cahalan MD, Wulff H, Chandy KG (2001) Molecular properties and physiological roles of ion channels in the immune system. J Clin Immunol 21:235–252.

Chien L-T, Hartzell HC (2007) Drosophila bestrophin-1 chloride current is dually regulated by calcium and cell volume. J Gen Physiol 130:513–24.

Cuschieri A, Mughal S (1985) Surface morphology of mitogen-activated human lymphocytes and their derivatives in vitro. J Anat 93–104.

DeCoursey TE, Chandy KG, Gupta S, et al (1987) Two types of potassium channels in murine T lymphocytes. 89:379–404.

Fanger CM, Ghanshani S, Logsdon NJ, et al (1999) Calmodulin Mediates Calcium-dependent Activation of the Intermediate Conductance K Ca Channel, IKCa1. J Biol Chem 274:5746–5754.

Fanger CM, Rauer H, Neben L, et al (2001) Calcium-activated potassium channels sustain calcium signaling in T lymphocytes. Selective blockers and manipulated channel expression levels. J Biol Chem 276:12249–56.

Fertig N, Blick RH, Behrends JC (2002) Whole cell patch clamp recording performed on a planar glass chip. Biophys J 82:3056–62.

Ghanshani S, Wulff H, Miller MJ, et al (2000) Up-regulation of the IKCa1 potassium channel during T-cell activation. Molecular mechanism and functional consequences. J Biol Chem 275:37137–49.

Gibhardt CS, Roth B, Schroeder I, et al (2015) X-ray irradiation activates K+ channels via H2O2 signaling. Sci Rep 5:13861.

Grissmer S, Nguyen a N, Cahalan MD (1993) Calcium-activated potassium channels in resting and activated human T lymphocytes. Expression levels, calcium dependence, ion selectivity, and pharmacology. J Gen Physiol 102:601–30.

Guéguinou M, ChantÔme A, Fromont G, et al (2014) KCa and Ca2+ channels: The complex thought. Biochim Biophys Acta - Mol Cell Res 1843:2322–2333. doi: 10.1016/j.bbamcr.2014.02.019

Hamill OP, Marty A, Neher E, et al (1981) Improved Patch-Clamp Techniques for High-Resolution Current Recording from Cells and Cell-Free Membrane Patches. 85–100.

Han J, Kang D (2009) TRESK channel as a potential target to treat T-cell mediated immune dysfunction. Biochem Biophys Res Commun 390:1102–5.

Jäger H, Adelman JP, Grissmer S (2000) SK2 encodes the apamin-sensitive Ca(2+)-activated K(+) channels in the human leukemic T cell line, Jurkat. FEBS Lett 469:196–202.

Jäger H, Dreker T, Buck A, et al (2004) Blockage of intermediate-conductance Ca2+-activated K+ channels inhibit human pancreatic cancer cell growth in vitro. Mol Pharmacol 65:630–638.

Khanna R, Chang MC, Joiner WJ, et al (1999) hSK4 / hIK1 , a Calmodulin-binding K Ca Channel in. J Biol Chem 274:14838–14849.

Klumpp D, Misovic M, Szteyn K, et al (2016) Targeting TRPM2 channels impairs radiation-induced cell cycle arrest and fosters cell death of T cell leukemia cells in a Bcl-2-dependent manner. Oxid Med Cell Longev.

Kuo SS, Saad H, Koong C, et al (1993) Potassium-channel activation in response to low doses of gamma-irradiation involves reactive oxygen intermediates in nonexcitatory cells. Proc Natl Acad Sci USA 90:908–12.

Kuras Z, Kucher V, Gordon SM, et al (2012) Modulation of Kv1.3 channels by protein kinase A I in T lymphocytes is mediated by the disc large 1-tyrosine kinase Lck complex. Am J Physiol Cell Physiol 302:C1504-12.

Lang F, Shumilina E, Ritter M, et al (2006) Ion channels and cell volume in regulation of cell proliferation and apoptotic cell death. Contrib Nephrol 152:142–160.

Levy DI, Deutsch C (1996) Recovery from C-type inactivation is modulated by extracellular potassium. Biophys J 70:798–805.

Lewis RS, Cahalan MD (1995) Potassium and calcium channels in lymphocytes. Physiol 60–66.

Liebau S, Pröpper C, Böckers T, et al (2006) Selective blockage of Kv1.3 and Kv3.1 channels increases neural progenitor cell proliferation. J Neurochem 99:426–437.

Maingret F, Coste B, Hao J, et al (2008) Neurotransmitter modulation of small conductance Ca2+ -activated K+ (SK) channels by regulation of Ca2+ gating. Neuron 59:439–449.

Pedarzani P, D'Hoedt D, Doorty KB, et al (2002) Tamapin, a venom peptide from the Indian red scorpion (Mesobuthus tamulus) that targets small conductance Ca2+-activated K+ channels and afterhyperpolarization currents in central neurons. J Biol Chem 277:46101–46109.

Pottosin II, Bonales-Alatorre E, Valencia-Cruz G, et al (2008) TRESK-like potassium channels in leukemic T cells. Pflugers Arch 456:1037–48.

Prakriya M, Lewis RS (2002) Separation and characterization of currents through store-operated CRAC channels and Mg2+-inhibited cation (MIC) channels. J Gen Physiol 119:487–507.

Rao A, Hogan P, Lewis (2010) molecular basis of calcium signaling in lymphocytes: stim and orai. 491–533.

Roth B, Gibhardt CS, Becker P, et al (2015) Low-dose photon irradiation alters cell differentiation via activation of hIK channels. Pflugers Arch Eur J Physiol 467:1835–1849.

Sarkadi B, Parker JC (1991) Activation of ion transport pathways by changes in cell volume. Biochim Biophys Acta 1071:407–427.

Schindelin J, Arganda-Carreras I, Frise E, et al (2012) Fiji: an open source platform for biological image analysis. Nat Methods 9:676–682.

Sumoza-Toledo A, Penner R (2011) TRPM2: a multifunctional ion channel for calcium signalling. J Physiol 589:1515–1525.

Wulff H, Castle NA (2010) Therapeutic potential of KCa3.1 blockers: recent advances and promising trends. Expert Rev Clin Pharmacol 3:385–96.

Wulff H, Gutman G a, Cahalan MD, Chandy KG (2001) Delineation of the clotrimazole/TRAM-34 binding site on the intermediate conductance calcium-activated potassium channel, IKCa1. J Biol Chem 276:32040–5.

5 Chapter 5: The small neurotoxin apamin blocks not only small conductance Ca^{2+} activated K^+ channels (SK type) but also the voltage dependent Kv1.3 channel

The following chapter has been published in:

Voos P, Yazar M, Lautenschläger R, et al. (2017) The small neurotoxin apamin blocks not only small conductance Ca^{2+} activated K^+ channels (SK type) but also the voltage dependent Kv1.3 channel. Eur Biophys J

5.1 Abstract

Apamin is frequently used as a specific blocker of small-conductance Ca^{2+} activated (KCa / SK type) K^+ channels. Here we show that the small neurotoxin is not as specific as anticipated. It is also a high-affinity inhibitor with an IC_{50} of 13 nM of the Kv1.3 channel; it blocks the latter with potency similar to the Kv1.3 blocker PAP-1. Since SK type channels and Kv1.3 channels are frequently coexpressed in different tissues such as cells of the immune system, apamin must be used with caution as a pharmacological tool.

5.2 Introduction

The physiological relevance of a particular type of ion channel is often determined on the basis of its pharmacology. By exploiting the unique sensitivity of a channel of interest to a selective blocker, it is possible to identify the contribution of such a channel to the ensemble currents of cells or to physiological reactions.

In recent years it was found that apamin, an 18-amino acid neurotoxic peptide with two disulfide bridges from *Apis mellifera* bee venom (Habermann 1972; Kastin 2011), functions as a specific and high-affinity blocker of small-conductance Ca^{2+} activated K^+ channels (SK-channels, KCNN2, KCa2.2) (Alvarez-Fischer et al. 2013). Based on the assumption that the block of SK channels by apamin is channel specific (Hanselmann and Grissmer 1996; van der Staay et al. 1999), this drug has been frequently used in the literature for identifying the activity of the SK channel in various cells such as visceral smooth muscle, microglial cells (Khanna et al. 2001), adrenal cortex and hepatocytes (Castle et al. 1989) as well as ventricle cells (heart tissue) (Chang et al. 2013). Here we show that apamin is not as specific as thought and also effectively blocks the Kv1.3 (KCNA3) channel. Kv1.3 is a member of the Shaker family of potassium channels and broadly expressed in immune cells such as T cells, macrophages and dendritic cells. In these immune cells and other human cells such as glioma cells (Weaver et al. 2008), Kv1.3 operates in concert with calcium-dependent channels such as KCa3.1 (hiK-type, expressed in T-cells) or KCa2.2 (SK type, expressed, e.g., in Jurkat cells) for conducting K^+ efflux. The concerted activity of these channels maintains the negative membrane potential, which favors calcium entry via CRAC (Ca^{2+} release-activated calcium) channels. The resulting Ca^{2+} influx is essential for activation and stimulation of lymphocytes

and other cells of the immune system (Cahalan et al. 2001, 2009; Chandy et al. 2004). It is well established that the relative number of Kv1.3 channels differs with respect to KCa3.1/2.2 channels in cells of the immune system depending on whether they are in a resting or an activated state; the same is true for different subpopulations of lymphocytes (Ghanshani et al. 2000; Cahalan et al. 2001; Chandy et al. 2004). To understand the physiological role of individual types of channels in various types of lymphocytes and their role as target for treatment of autoimmune diseases by channel blockers (Beeton et al. 2006), it is important to discriminate different K^+ channels in the whole cell current. This can be achieved by channel blockers with a high specificity for one type of channel over others. Occasionally a blocker is not as specific as anticipated, and these data, which were obtained with such an inhibitor, need to be reconsidered (Bartok et al. 2014). Our present finding that apamin blocks not only SK channels, but also Kv1.3 underscores that this blocker cannot be used in cells, which express both types of K^+ channels, for a dissection of the SK channel from the whole cell current.

5.3 Materials & Methods

The human KCNA3 gene was cloned into a pCMV6 plasmid (OriGene Technologies, Rockville, MD) for transfection. To identify positive transfection, HEK-293 cells were co-transfected with a pEGFP-N2 plasmid containing the eGFP gene. Cells for all control experiments were transfected with the pEGFP-N2 plasmid containing the eGFP gene alone.

5.3.1 Cell culture

HEK-293 cells were cultivated under standard conditions with 37 C ambient temperature and 5 % CO_2; cells were kept in Dulbecco's modified minimal essential medium and 1:1 Ham's F-12 (DMEM Ham's F-12) medium with stable glutamine, supplemented with 10 % fetal calf serum (FCS) and 1 % penicillin/streptomycin. At about 60 % confluency cells were transiently transfected with plasmid DNA and GeneJuice (Novagen, Merck KGaA, Darmstadt, Germany) according to the manufacturer's protocol. Positive transfection of HEK-293 cells was judged from green fluorescence; the respective cells were chosen for patch clamp recordings. Jurkat cells are a cell line established in 1976 from the peripheral blood of a 14-year-old boy with acute T-cell leukemia, a specific type of acute lymphatic leukemia (ALL). The Jurkat cell line is also called JM and grows singly or in small clumps as round, non-adherent suspension cells. The optimal split ratio is about 1:2-1:3 every 2 to 4 days at a maximum cell count of 1 x 10^6 per ml. The doubling time is 25-35 hours. For cell culture 37° C, 5 % CO_2 and RPMI 1640 medium with stable glutamine and 2.0 g/l $NaHCO_3$ + 2 mM L-glutamine, 10 % heat inactivated fetal calf serum (FCS) (Sigma-Aldrich, Germany) and 1 % mixture of penicillin/streptomycin was used. The Jurkat cell line (ACC 282) was purchased from the Leibniz-Institut DSMZ (Deutsche Sammlung von Mikroorganismen und Zellkulturen GmbH); their immunological status is $CD2^+$, $CD3^+$, $CD5^+$, $CD6^+$, $CD7^+$, $CD8^-$, $CD13^-$, $CD19^-$, TCR α/β^+, TCR γ/δ^- ($^+$ stands for expression, $^-$ stands for no expression).

5.3.2 Patch clamp recordings

Membrane currents of cells were recorded with the patch clamp method in the whole-cell configuration using an EPC-9 amplifier (HEKA Electronics, Lambrecht, Germany, all other measurements) and PatchMaster software (HEKA, Lambrecht, Germany). The intracellular solution contained (in mM) 134 KCl, 1 $CaCl_2$, 2 $MgCl_2$, 1 EGTA and 10 Hepes/KOH pH 7.4. Sorbitol was used to adjust the osmolarity to 330 mOsmol/kg. The extracellular solution contained in all measurements (in mM) 150 NaCl, 5 KCl, 1 $MgCl_2$, 2.5 $CaCl_2$ and 10 Hepes/NaOH pH 7.4. Sorbitol was used to adjust the osmolarity to 340 mOsmol/kg; the small difference in the osmolarity between the internal and external solution increased the stability of the seals. PAP-1 was purchased from Sigma-Aldrich (Munich, Germany, A9459/P6124); apamin was purchased in two different batches from Sigma-Aldrich [Sigma-Aldrich Europe (Munich) and Sigma-Aldrich USA (St. Louis)] and from Tocris Bioscience (Bristol, UK). All blockers were solved in ddH_2O and freshly prepared before each experiment by dilution in the external buffer solution. The blockers were administered via a perfusion chamber (PM-1, Warner Instruments, USA). In all experiments, a cell was first measured for at least 4 min under control conditions to reach a stable current response. The effects of PAP-1 or apamin were then measured for at least 6–8 min after challenging cells with inhibitors. This time was sufficient to induce a measurable current reduction while at the same time maintaining a stable recording without changes in leak conductance. To limit long-lasting inactivation of Kv1.3 channels at positive voltages, we used only very short voltage pulses (100 ms) for channel activation. The peak currents were used for constructing I/V curves. The blocking efficiencies of different agents were identified from 1200 ms long voltage steps from −60 to +40 mV where the peak currents were the readout (Kuras et al. 2012). To achieve a full voltage-dependent activation of the Kv1.3 channels after each protocol, a cell was kept at −60 mV for at least 1–2 min between sequential voltage clamp protocols; in control experiments, we found that this time was sufficient for full recovery (see also Levy and Deutsch 1996).

5.3.3 Data analysis and statistics

All values are given as mean ± standard error of the mean (SEM) of at least three different experiments, number of biological replicates (n) or independent experiments (N) are denoted. Significance was estimated by using the Student's t-test. A $p < 0.05$ was considered as significant (*), $p \leq 0.01$ is specified as ** and a high significant difference of $p \leq 0.001$ was specified as ***. The dose-response curve was fitted by a Hill equation:

$$Inhibition = A + \frac{c^n \cdot (B - A)}{(IC_{50}{}^n + c^n)}$$

Equation 4: Hill function; A is the lower limit of inhibition (here 14 %, given by the current reduction due to current run down), B the maximal inhibition, c the apamin concentration and IC_{50} the concentration for half maximal inhibition; n is the Hill factor.

5.4 Results

5.4.1 Apamin is blocking a voltage dependent current in Jurkat cells

When we used apamin in nanomolar concentrations as a blocker of SK channels in Jurkat cells (DSMZ/ACC 282), we realized that the blocker was also inhibiting a voltage-dependent outward rectifier. Fig. 5-1 A-D show the endogenous currents of Jurkat cells before and after adding 100 nM apamin to the bath solution. In the control condition, the currents are dominated by an outward rectifying current with a voltage-dependent activation and subsequent inactivation. The latter current was strongly inhibited after addition of apamin (Fig. 5-1 B,D). Fig. 5-1 C shows the normalized current/voltage (I/V) relation (± SEM) of Jurkat cells (N = 5) before (black) and after (gray) the addition of 100 nM apamin. Since it is well established that the Kv1.3 channels conduct the majority of the outward-rectifying K^+ current in resting lymphocytes as well as in Jurkat cells (Kuras et al. 2012), we reasoned that apamin may be less specific than predicted and also serves as a potent blocker of other channels including the Kv1.3 channel.

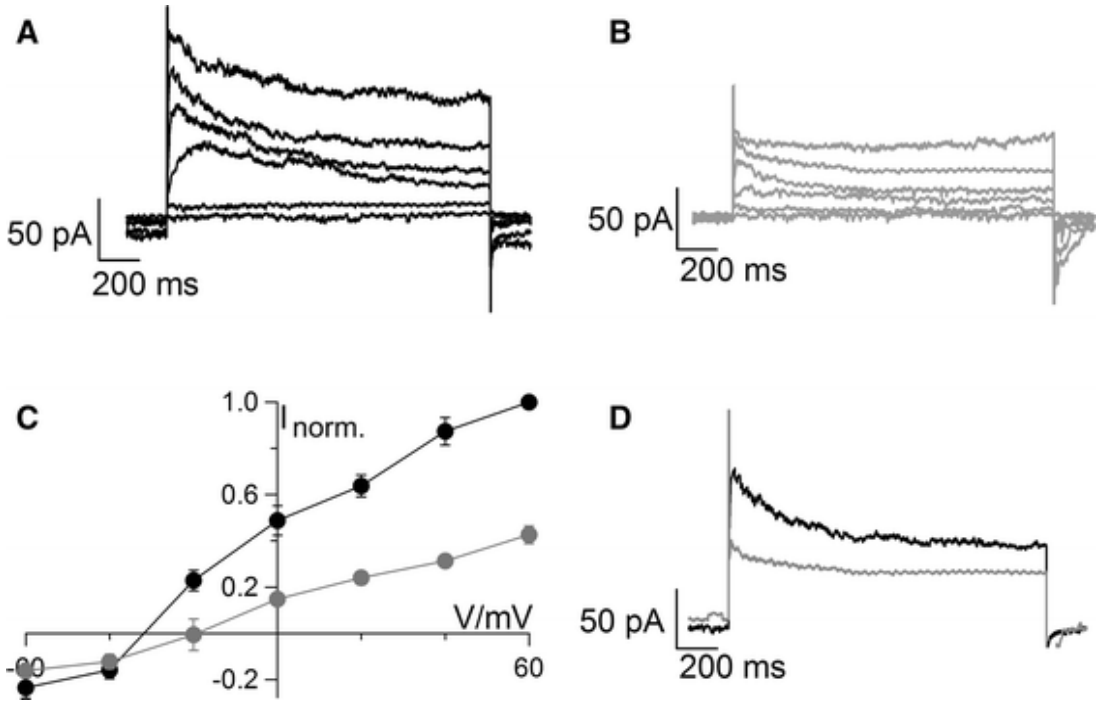

Fig. 5-1: Effect of apamin on currents in Jurkat cells.

Currents of an exemplary Jurkat cell before (A) and 8 min after adding 100 nM apamin to the bath solution (B). Mean current/voltage relations (C) of the peak current at +60 mV under control conditions for N = 5 Jurkat cells (± SEM) before (black circles) and after treatment with apamin (gray circles). (D) Current responses of the same cell to voltage step from −60 to +20 mV before (black) and after (gray) addition of 100 nM apamin. Note that apamin not only inhibits an instantaneous current, but also the time-dependent component of the outward rectifier. Currents were elicited by clamping a cell in bath medium with 4 mM K^+ from holding voltage (−60 mV) for 1400 ms to test voltages between −60 and +40 mV and to a post voltage at −60 mV.

5.4.2 Heterologous expression of Kv1.3 in HEK-293 cells and rundown effect

To test the hypothesis of off-target effects, we transiently overexpressed the Kv1.3 channel together with eGFP in HEK-293 cells and characterized the sensitivity of this channel to apamin

in whole-cell patch clamp recordings. Figure 5-2 shows typical currents of a HEK-293 cell, which was only transfected with eGFP (Fig. 5-2 A) and from a cell that was co-transfected with eGFP and Kv1.3 encoding plasmid (Fig. 5-2 E).

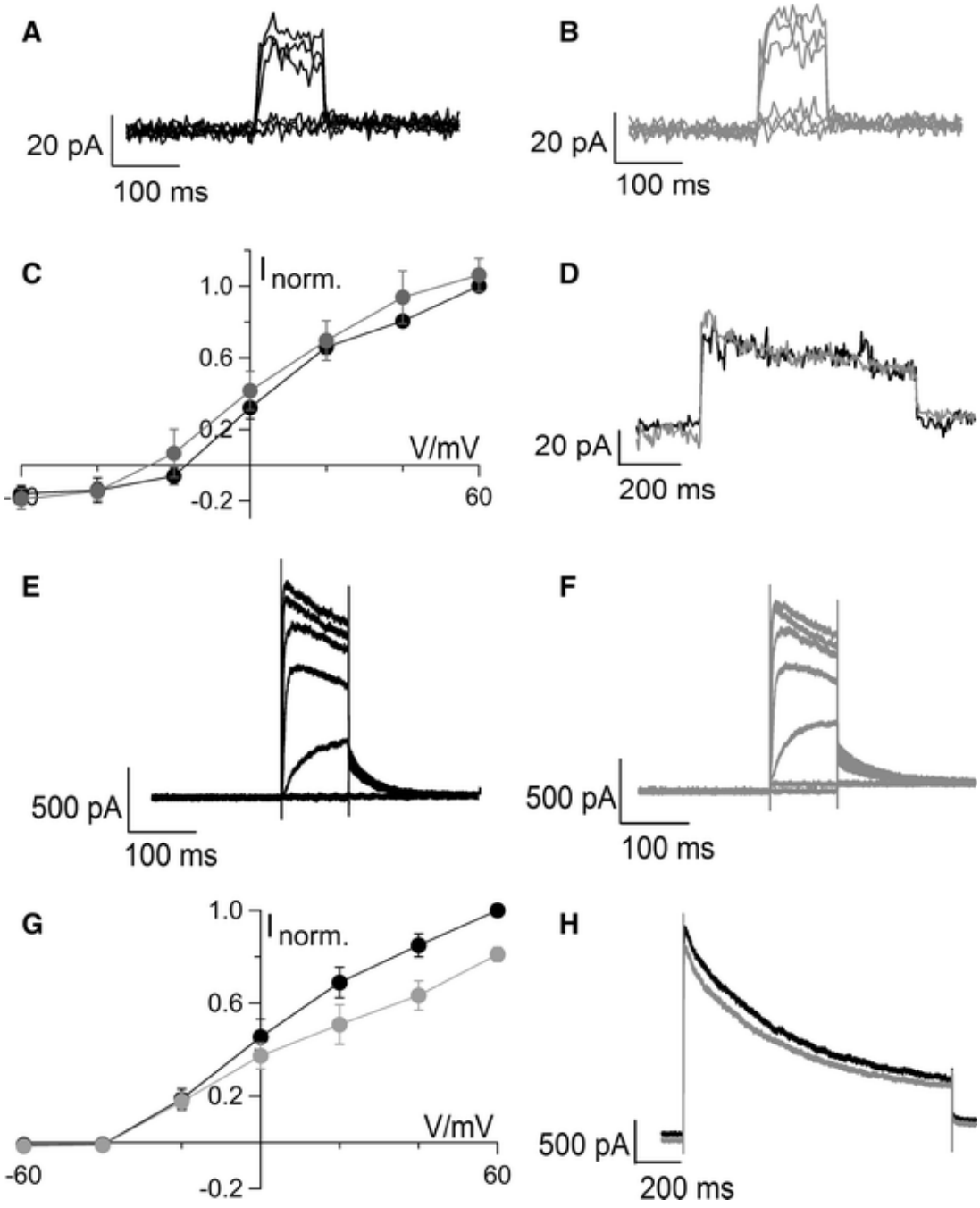

Fig. 5-2: Effect of apamin on endogenous currents and run down of Kv1.3 currents in HEK-293 cells.
Endogenous currents of an exemplary HEK-293 cell transfected with eGFP before (A) and 6 min after addition of 100 nM apamin to the bath solution (B). The currents exhibit no appreciable decrease in the presence of apamin. Mean I/V relation (N = 4 cells, ± SEM) for measurements like in (A) and (B) without (black circles) and with apamin (gray circles); data were normalized to peak current at +60 mV under control conditions (C). Current response to a voltage step from −60 to +40 mV before (black) and after (gray) addition of 100 nM apamin; the post voltage is −40 mV (D). The blocker has no perceivable effects on the endogenous currents. Currents of an exemplary HEK-293 cell coexpressing eGFP and Kv1.3 before (E) and 6 min after complete exchange of the bath medium (F). The currents exhibit the typical characteristics of Kv1.3. (G) Mean normalized I/V relation of peak currents before (black) and 8 min after continuous exchange of bath medium (gray) (± SEM) (N = 6). (H) Current responses to voltage steps from −60 to +40 mV over a 6 min period show a small run down. Currents were recorded as in Fig. 5-1.

A comparison of the currents from transfected cells and untransfected controls shows that the Kv1.3 channel is indeed active in the transfected cells (Fig. 5-2 C,G). The control currents reveal the typical small endogenous outward-rectifying current of HEK-293 cells [113 ± 33 pA (± SEM, N ≥ 7) at +40 mV] with little inactivation (Fig. 5-2 A,D). The transfected cells in contrast exhibit much larger outward currents (mean peak current 3188 ± 291 pA at +40 mV N ≥ 7) with the pronounced C-type inactivation of Kv1.3 channels (Fig. 5-2 E,H). The comparison of Fig. 5-2 A,B as well as of the normalized I/V relations (Fig. 5-2 C) shows that 100 nM apamin had no perceivable effect on the endogenous channels in Hek-293 cells. All cells were measured with a standard protocol over a period of at least 6 min before and after a complete exchange of the bath medium. The data in Fig. 5-2 E and F show that the currents of an exemplary cell, which was co-transfected with eGFP and Kv1.3, exhibited over this time a small intrinsic run down also in the absence of a blocker (Fig. 5-2 E,F,H). From similar measurements (Fig. 5-2 H, N = 6), we estimated a 14 ± 4 % (± SEM) reduction of the Kv1.3 current at +40 mV over the relevant period of recordings as a consequence of an unspecific run down.

5.4.3 Examination of PAP-1 induced blockade of Kv1.3

In the next set of experiments, we examined the response of the heterologously expressed Kv1.3 channels to 5-(4-phenoxybutoxy)psoralen (PAP-1), a specific blocker of Kv1.3 channels with an EC_{50} of 2 nM (Schmitz et al. 2005; Pereira et al. 2007). While an addition of 100 nM PAP-1 had no appreciable effect on the currents of non-transfected HEK-293 cells (Fig. 5-3 A-C), it clearly reduced the outward current of transfected cells over 6 min of monitoring (Fig. 5-3 D-G). Figure Fig. 5-3 F shows the mean normalized I/V relations (±SEM) of N = 4 cells before (black) and after (gray) the addition of 100 nM PAP-1. The effect of the blocker was time dependent, meaning that the effect of the blocker gradually increased after the addition. In a total of four cells tested in this way, we observed on average a 49 ± 11 % (N = 4) reduction of the outward current at +40 mV 6–8 min after the addition of 100 nM PAP-1 (Fig. 5-3 G). The results of these experiments confirm the expected sensitivity of the Kv1.3 channel to PAP-1. Note that the inhibition of the Kv1.3 current by 100 nM PAP-1 is not complete. To compare the inhibitory effect of PAP-1 with apamin, we used the same protocol for both blockers. In the case of PAP-1, this protocol does not guarantee full inhibition of Kv1.3 by 100 nM of this blocker. For maximal inhibition of Kv1.3, PAP-1 has to be added while the channel is in the C-type inactivated state (Schmitz et al. 2005).

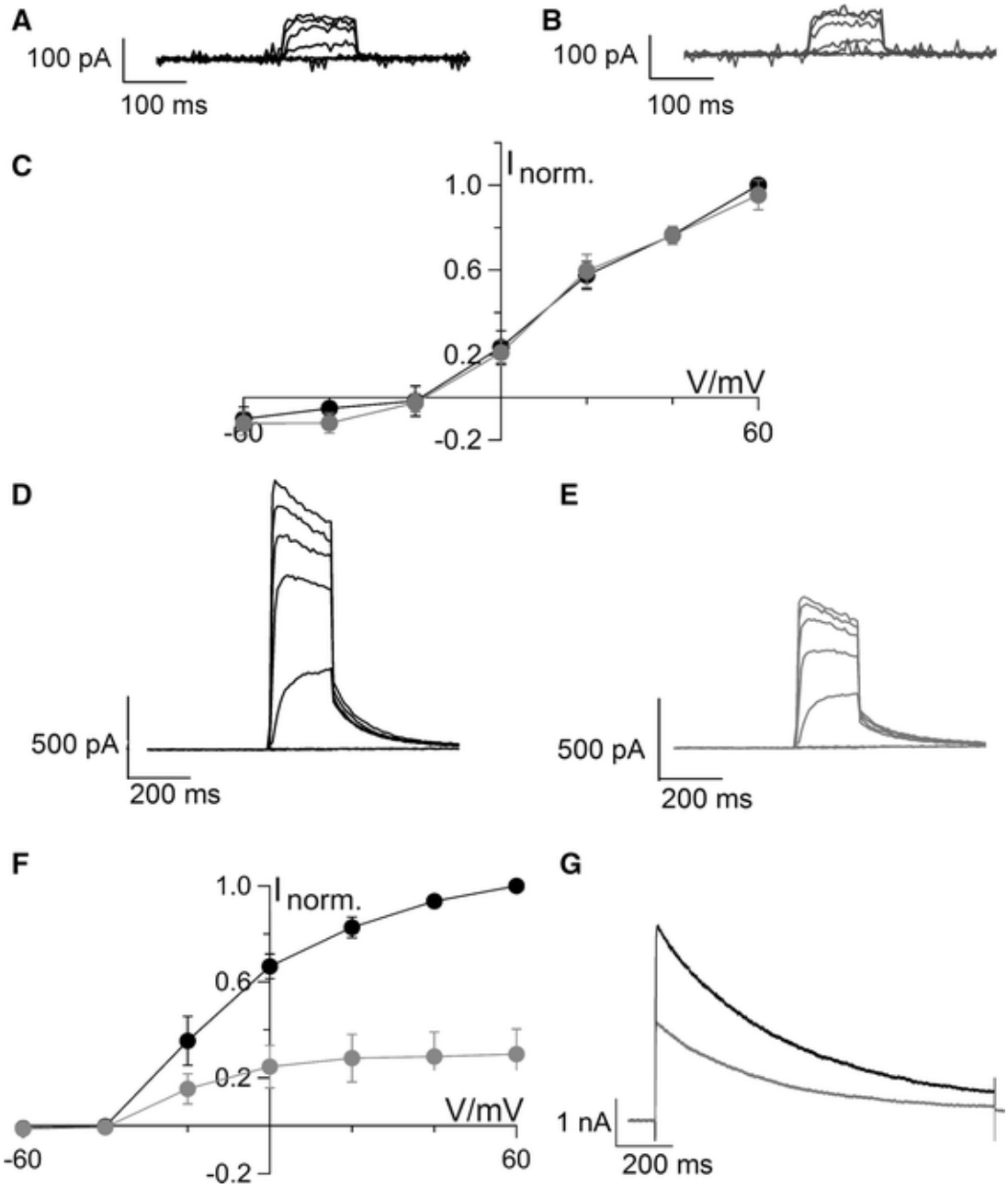

Fig. 5-3: Effect of PAP-1 on endogenous and Kv1.3 currents in HEK-293 cells.

Currents of an exemplary HEK-293 cell transfected with eGFP before (A) and 6 min after addition of 100 nM PAP-1 to the bath solution (B). This treatment has no impact on the endogenous current of HEK-293 cells. Mean normalized I/V relation (N = 3 cells, ± SEM) for currents in the absence (black) and presence of PAP-1 (gray); data were normalized to peak current at +60 mV under control conditions (C). Same treatment of HEK-293 cell coexpressing eGFP and Kv1.3 before (D) and 6 min after addition of 100 nM PAP-1 to the bath medium (E). Mean normalized I/V relation of peak currents (± SEM) obtained like in (D) and (E) before (black) and after (gray) application of blocker (N = 4) (F). Current responses of one cell to test the pulse from −60 to +40 mV before (black) and 6 min after the addition of 100 nM PAP-1 to the external solution (gray) (G). Currents were recorded as in Fig. 5-1.

5.4.4 Apamin is blocking Kv1.3 channels at low nanomolar concentrations

The current traces in Fig. 5-4 A,B show a typical example of Kv1.3 currents before and 6 min after addition of 100 nM apamin. Apamin had a strong effect on cells expressing the Kv1.3 channel; it caused a slow-progressing inhibition of the Kv1.3 current. Over the 20 min time window after the addition of apamin, the current was exponentially decreasing with a tau

value of 11 min (Fig. 5-4 D). At a reference time of 6–8 min, the Kv1.3 current was on average 47 ± 5 % (N = 8) inhibited by 100 nM apamin. Fig. 5-4 C shows the corresponding normalized current/voltage (I/V) relations of N = 8 cells in the absence and presence of apamin.

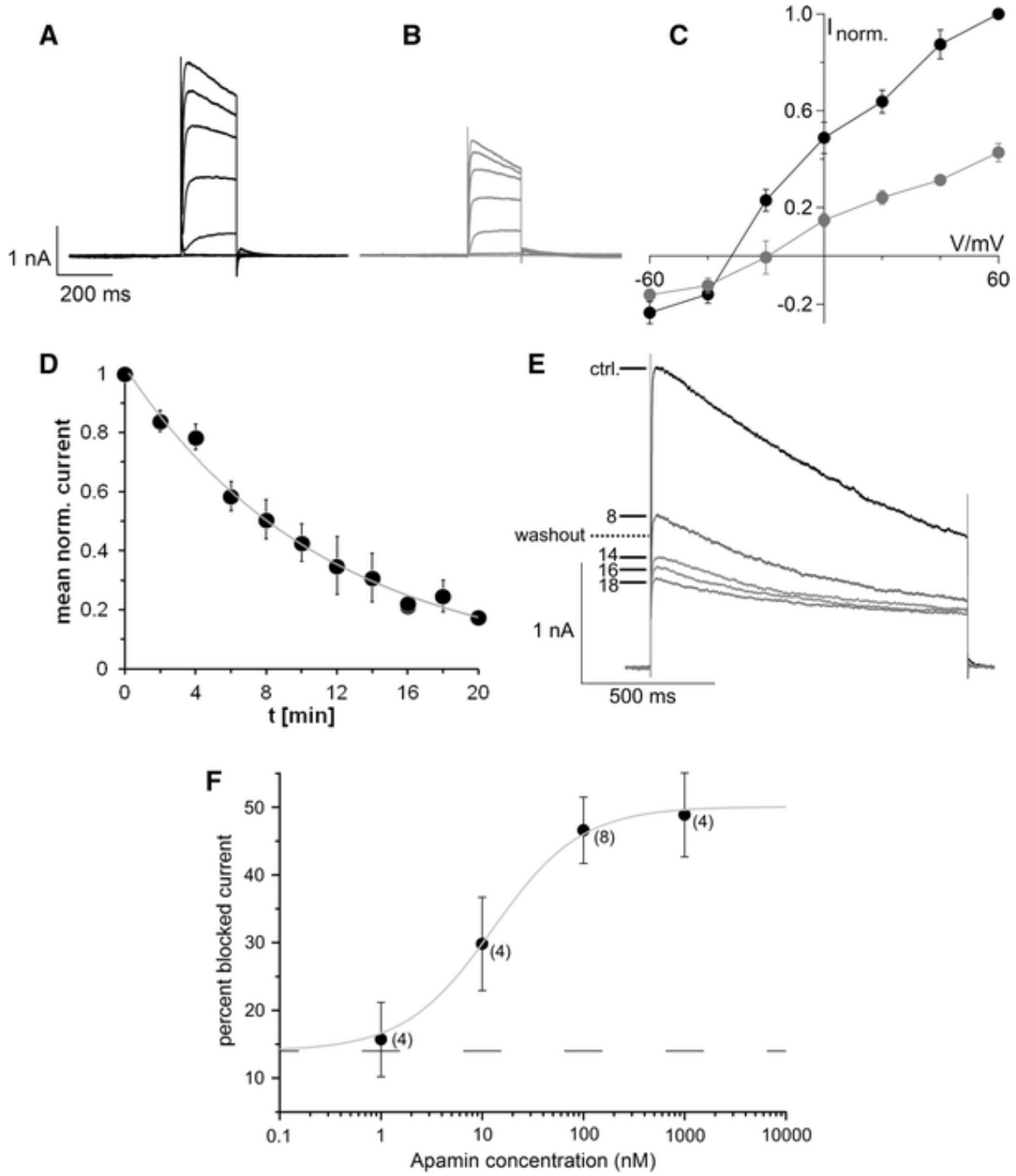

Fig. 5-4: **Effect of apamin on endogenous and Kv1.3 currents in HEK-293 cells.**

Effect of apamin on typical Kv1.3 currents in one HEK-293 cell coexpressing eGFP and Kv1.3 before (A) and 8 min after addition of 100 nM apamin to the bath medium (B). Mean I/V relation (N = 8 cells, ± SEM) for currents in the absence (black) and presence of apamin (gray); data were normalized to peak current at +60 mV under control conditions (C). Normalized Kv1.3 currents from N = 6 HEK-293 cells to clamp voltages from −60 to +40 mV before (0 min) and over a period of 20 min after the addition of 100 nM apamin to the bath medium (D). Data are fitted with a single exponential (line) yielding a time constant of 11 min for full inhibition. Inhibition of Kv1.3 as a function of apamin concentration in the bath solution (E). (F) from peak currents at a single pulse to +40 mV before and 6–8 min after the addition of apamin to the bath medium. Relative block of the peak currents (± SEM) was fitted with the Hill equation (Eq. 1); numbers in brackets report the number of independent experiments. The lower plateau was set to the value of Kv1.3 reduction

because of an intrinsic run down (14 %). Fitting yields a maximal inhibition of 50 %, an IC_{50} of 13 nM and a Hill coefficient of 1. Data were obtained as in Fig. 5-1.

We also followed the effect of apamin on Kv1.3 after washing the blocker out from the bath medium. The typical example in Fig. 5-4 E shows that the Kv1.3 channels did not recover even after washing cells with apamin-free medium for 5 min; the currents even continued to decrease in the absence of the blocker. A similar irreversibility of an apamin block of was also reported for the inhibition of K(Ca) channels in Jurkat cells (Grissmer et al. 1992). The same types of experiments as in Fig. 5-4 A-C were repeated over a concentration window between 1 nM and 1 µM apamin. The data for 100 nM were collected with synthetic apamin from two different sources (TOCRIS and Sigma); for the second also two different batches were employed. This should assure that the unexpected off-target effects of apamin on Kv1.3 are not caused by a contamination in an apamin preparation. Figure Fig. 5-4 F shows the resulting dose-response curve for the mean block efficiency (± SEM) of apamin after 6 min of application. The lowest concentration (1 nM) on average did not block the Kv1.3 conductance beyond the current reduction, which can be attributed to an unspecific run down (Fig. 5-2 E-H). The effective block of the Kv1.3 channel increases with concentrations > 1 nM approaching a maximum at 1 µM. The dose-response curve was fitted with a Hill equation (Eq. 1) using the level of current reduction by run down (14 %, dashed line) as the lower limit. The fit yields a maximal inhibition of the Kv1.3 current of 49 % after 6 min of challenging cells with apamin. The fit further provides an IC_{50} value of 13 nM with a Hill factor of 1.

5.5 Conclusion

The activity of SK channels is typically inhibited by either the scorpion venom tamapin or charybdotoxin (Pedarzani et al. 2002) or by the bee toxin apamin (Castle et al. 1989). The present data however show that apamin can no longer be considered a specific blocker of SK channels; it also blocks the Kv1.3 channel with high efficiency. It is well established that SK channels are 50 % blocked over a concentration window between 100 pM to 12 nM apamin; the latter value varies depending on the SK subtype and the expression system (Benton et al. 2013). Here we find that nanomolar concentrations of apamin are also effective in blocking Kv1.3 channels; at a concentration of some 10 nM, this peptide is already sufficient for a half maximal inhibition of these channels. In this respect, under our experimental conditions, the effect of apamin on the Kv1.3 channel is as strong as that of PAP-1, a molecule considered a specific and potent blocker of Kv1.3 channels (Schmitz et al. 2005). The lack of specificity of apamin for SK channels implies that the role of the latter in physiological processes such as diabetes or cell cycle regulation might be overestimated (e.g. Kim et al. 2015; Yi et al. 2015). Since the peptide also inhibits Kv1.3, which is frequently expressed together with SK channels in the same cells, it is possible that also the latter Kv channel contributes to the phenomena observed in response to apamin treatment. This is even more plausible considering the fact that the role of the Kv1.3 channel in diabetes and cell cycle regulation is well established (Pérez-Verdaguer et al. 2016).

SK and Kv1.3 channels share a similar architecture with six transmembrane domains (Cahalan et al. 2001). Still, their functional properties are very different. While Kv1.3 is voltage dependent with a pronounced C-type activation, the SK channel exhibits no voltage dependency, no inherent inactivation but a strong dependency on cytosolic Ca^{2+} for activation (Cahalan et al. 2009). The fact that apamin inhibits channels with such diverse functional features suggests that the mode of inhibition is based on some structural features that are shared by these different K^+ channels. This implies that also other K^+ channels apart from Kv1.3 could exhibit a profound sensitivity to apamin.

5.6 Acknowledgements

This work was supported in part by the BMBF (project 02NUK017A) and GRK 1657. Special thanks to the students Lisa Noll, Vanessa Kohl and David Schul.

5.7 References

Alvarez-Fischer D, Noelker C, Vulinović F, et al (2013) Bee Venom and Its Component Apamin as Neuroprotective Agents in a Parkinson Disease Mouse Model. PLoS One 8:2–9.

Bartok A, Toth A, Somodi S, et al (2014) Margatoxin is a non-selective inhibitor of human Kv1.3 K+ channels. Toxicon 87:6–16.

Beeton C, Wulff H, Standifer NE, et al (2006) Kv1.3 channels are a therapeutic target for T cell-mediated autoimmune diseases. Proc Natl Acad Sci USA 103:17414–9.

Benton DCH, Garbarg M, Moss GWJ (2013) The Relationship between Functional Inhibition and Binding for KCa2 Channel Blockers. PLoS One.

Cahalan MD, Chandy KG, Hall I (2009) The functional network of ion channels in T lymphocytes. Immunol Rev 231:59–87.

Cahalan MD, Wulff H, Chandy KG (2001) Molecular properties and physiological roles of ion channels in the immune system. J Clin Immunol 21:235–252.

Castle NA, Haylett DG, Jenkinson DH (1989) Toxins in the charaderization of potassium channels. Trends Neurosci 12:59–65.

Chandy KG, Wulff H, Beeton C, et al (2004) K+ channels as targets for specific immunomodulation. Trends Pharmacol Sci 25:280–9.

Chang PC, Turker I, Lopshire JC, et al (2013) Heterogeneous upregulation of apamin-sensitive potassium currents in failing human ventricles. J Am Heart Assoc 2:1–10.

Ghanshani S, Wulff H, Miller MJ, et al (2000) Up-regulation of the IKCa1 potassium channel during T-cell activation. Molecular mechanism and functional consequences. J Biol Chem 275:37137–49.

Grissmer S, Lewis RS, Cahalan MD (1992) Ca(2+)-activated K+ channels in human leukemic T cells. J Gen Physiol 99:63–84.

Habermann E (1972) Bee and wasp venoms. Science 177:314–322.

Hanselmann C, Grissmer S (1996) Characterization of apamin-sensitive Ca(2+)-activated potassium channels in human leukaemic T lymphocytes. J Physiol 3:627–37.

Kastin A (2011) Handbook of Biologically Active Peptides. Academic press, Baton Rouge, USA

Khanna R, Roy L, Zhu X, Schlichter LC (2001) K+ channels and the microglial respiratory burst. Am J Physiol Cell Physiol 280:C796–C806.

Kim JY, Kim KH, Lee WR, et al (2015) Apamin inhibits PDGF-BB-induced vascular smooth muscle cell proliferation and migration through suppressions of activated Akt and Erk signaling pathway. Vascul Pharmacol 70:8–14.

Kuras Z, Kucher V, Gordon SM, et al (2012) Modulation of Kv1.3 channels by protein kinase A I in T lymphocytes is mediated by the disc large 1-tyrosine kinase Lck complex. Am J Physiol Cell Physiol 302:C1504-12.

Levy DI, Deutsch C (1996) Recovery from C-type inactivation is modulated by extracellular potassium. Biophys J 70:798–8054

Pedarzani P, D'Hoedt D, Doorty KB, et al (2002) Tamapin, a venom peptide from the Indian red scorpion (Mesobuthus tamulus) that targets small conductance Ca2+-activated K+ channels and afterhyperpolarization currents in central neurons. J Biol Chem 277:46101-9.

Pereira LE, Villinger F, Wulff H, et al (2007) Pharmacokinetics, toxicity, and functional studies of the selective Kv1.3 channel blocker 5-(4-phenoxybutoxy)psoralen in rhesus macaques. Exp Biol Med (Maywood) 232:1338–54.

Pérez-Verdaguer M, Capera J, Serrano-Novillo C, et al (2016) The voltage-gated potassium channel Kv1.3 is a promising multitherapeutic target against human pathologies. Expert Opin Ther Targets 20:577–91.

Schmitz A, Sankaranarayanan A, Schmidt-Lasse K, et al (2005) Design of PAP-1, a selective small molecule Kv1. 3 blocker, for the suppression of effector memory T cells in autoimmune diseases. Mol Pharmacol 68:1254–1270.

van der Staay FJ, Fanelli RJ, Blokland A, et al (1999) Behavioral effects of apamin, a selective inhibitor of the SK(Ca)-channel, in mice and rats. Neurosci Biobehav Rev 23:1087–1110.

Weaver AM, Bomben VC, Sontheimer H (2008) Expression and Function of Calcium-Activated Potassium Channels in Human Glioma Cells. October 54:223–233.

Yi F, Ling TY, Lu T, et al (2015) Down-regulation of the small conductance calcium-activated potassium channels in diabetic mouse atria. J Biol Chem 290:7016–7026.

6 Chapter 6: General discussion

As a medical therapy the so-called radon balneotherapy is used to treat patients with chronic inflammatory and autoimmune diseases like Morbus-Bechterew, spondylarthrosis, osteochondrosis or eczemas with alpha particle emitting noble gas radon (^{222}Rn). The positive effects of this radon treatment are related to extra-nuclear targets of the ionizing radiation. Here elevated levels of reactive oxygen species (ROS) are good candidates for explaining therapeutic effects of Radon in cells and tissues. (Nagasawa et al. 1991; Deshpande et al. 1996; Shao et al. 2004). The same type of diseases has been already treated for decades with good success with low doses of X-ray irradiation (single dose ≤ 1 Gy, total dose ≤ 12 Gy) because this type of irradiation is known to have anti-inflammatory and analgesic effects too (Betz et al. 2010; Heyd et al. 2010). Some recent studies furthermore report a beneficial long-term effect of both types of low dose radiation treatments. These beneficial long-term effects include a reduced pain perception and reduced disease symptoms (Franke et al. 2000, 2007; Rühle et al. 2017). While the therapeutic benefits of ionizing irradiation (IR) treatments are well documented and generally accepted, the cellular and molecular mechanisms which are underlying the curative effect of radon gas therapy and low dose X-ray treatment remain still unclear (Falkenbach et al. 2005; Zdrojewicz and Strzelczyk 2006). One possible explanation for the beneficial effects of low doses of IR treatment of chronic inflammatory and autoimmune diseases is discussed in the context of an immunomodulation. It has been speculated that IR could result in a reduced number of auto-reactive lymphocytes or in an increased number of T-regulatory cells. The latter could attenuate chronic inflammatory immune reactions. This reduction of inflammatory activity may hence lead to less symptoms (Anderson et al. 1982; Betz et al. 2010). During the recent “RAD-ON01” study it was shown that radon therapy can indeed result in a modulation of peripheral blood lymphocyte (PBL) subtype numbers and that these modulations are in line with attenuation of inflammation (Rühle et al. 2017).

On the background of this hypothesis of an interplay between IR and the immune system the present thesis examined the cellular responses of immune cells after an exposure to IR. A better understanding of the cellular effects in response to IR could help to explain the mechanisms that are underlying the therapeutic benefits. The results of the present study document a so far unknown effect of low dose IR on immune cells. When the cell diameter is used as a parameter for quantification of the cellular response to IR, it can be found that X-ray treatment generates a clear increase in the cell diameter of leukemic T-cell progenitor cells (Jurkat cell line) and in a subpopulation of freshly isolated peripheral blood lymphocytes (PBL). The response of freshly isolated PBLs is variable; some exhibit also after irradiation a diameter which is in the range of the untreated controls, but with increasing doses of X-ray the mean cell diameter of PBLs increases and a widening in the distribution of cell diameters can be observed. The observed IR induced increase in cell diameter of PBLs and Jurkat cells is similar to the increase in cell diameter of PBLs after stimulation by a specific T-cell activator or the mitogen phytohemagglutinin (PHA-L).

This similarity in the response of PBLs to IR and stimulation suggests that ionizing radiation activates in these cells some kind of immune activation or modulation. Further details on this important concept, which suggest that IR can be an immune stimulus, are discussed further down.

Radiotherapy can be divided in high and low dose application and often uses the principle of fractionation where the total dose of radiation is divided into several smaller doses over a period of several days. High radiation dose therapy, which is commonly used in cancer treatment, is comprised of singles doses of 1-3 Gy and a total dose of 30-80 Gy. Low dose radiotherapy in contrast uses lower single doses ≤ 1 Gy and a total dose of 3-12 Gy (Arenas et al. 2012). When we studied the cell diameter increase elicited in Jurkat cells in response to X-ray, we used doses that are common in both radio therapeutic approaches. In the dose range from 0.5 to 5 Gy we found a clearly dose dependent cell diameter increase. These results show that doses commonly used in radiotherapy are sufficient for eliciting the immune response associated cell diameter increase in immune cells.

A detailed analysis of the IR triggered increase in cell diameter shows that it is comprised of two different components. One component is related to the impact of IR on the cell cycle. Jurkat cells respond to increasing doses of IR with increasing propensity of arresting in the G2 phase of the cell cycle. This G2 arrest is associated with a higher DNA content, a reduced condensation of DNA and thus a larger nucleus. Since the nucleus occupies a large volume portion of Jurkat cells any increase in this cellular component can cause a visible increase in the overall cell size (Rosenbluth et al. 2006). The G2 cell phase arrest associated increase in cell diameter can also be induced by the treatment with a CDK1 inhibitor whereas treatments, which interfere with immune stimulations of these cells cannot decrease the nucleus driven increase in cell diameter. The other component of the IR induced cell diameter increase in contrast is related to an immune activation of the cells similar to the increase in cell diameter of T-cells and accounts for the remaining ~ 50 % of the increase in cell diameter. Resting T-cells exhibit a defined cell diameter of ~ 7 µm. Upon immune activation via stimulation of the T-cell receptor (TCR) or after treatment with mitogens like phytohemagglutinin (PHA-L), the cell diameter increases rapidly. This increase in cell diameter is necessary because resting T-cells, which are not proliferating, have little or almost no cytoplasm; their organelles are reduced to a minimum. Upon activation T-cells increase their metabolic capacities to proliferate and secrete chemokines and cytokines which are needed for immune response (Loris et al. 1998; Iritani et al. 2002; Abbas and Lichtman 2003). Taken together the data suggest that ~ 50 % of the increase in cell size are an epiphenomenon of the IR induced arrest of the cells in the G2 phase of the cell cycle whereas the other ~ 50 % of increase in cell diameter seem to be associated with an immune activation or modulation due to IR. The interpretation of the IR triggered increase in cell size as an evidence for an immune activation of these cells is in good agreement with other data presented in this thesis.

Immuno blot experiments show that IR is able to upregulate the interleukin-2 receptor alpha chain (CD25) in Jurkat cells, a common marker for immune activation (Shatrova et al. 2015). The fact that the upregulation of this marker for immune activation occurs over the same dose of IR as the increase in cell diameter and further underscores that both cellular responses are coupled.

The stimulation of immune cells is generally associated with a significant alteration of the ion channel composition in the plasma membrane of these cells. Naive resting T-cells, which are immunological inactive and not proliferating, exhibit a K^+ channel expression pattern with 300 Kv1.3 to only 10-20 KCa3.1 channels per cell. An immunological activation and the following differentiation involves a strong upregulation in the number of the calcium dependent KCa3.1 channels in the plasma membrane by a factor of 10 to 25 in mostly all T-cell subtypes (Ghanshani et al. 2000; Cahalan et al. 2009). This highly increased number of active plasma membrane KCa3.1 channels in PBLs is, according to the literature, closely related to the immunological state of T-cells and can actually be used to determine the activity and differentiation state of T-cells (Ghanshani et al. 2000; Beeton et al. 2001; Liebau et al. 2006; Cahalan et al. 2009).

The present electrophysiological characterization of unirradiated and irradiated Jurkat cells is in good agreement with the here presented general view that irradiation triggers an immune stimulation in these cells. The data show that IR causes an effect on the level of ion channel expression and ion channel composition of the plasma membrane that is similar to that of an immune activation of PBL. IR elicits in Jurkat cells an increase in the conductance of the calcium dependent potassium channel KCa2.2. The electrophysiological data which support this increase in conductance are supported by results the imaging of immuno stained ion channels with single molecule microscopy. The latter experiments show that IR is able to trigger an upregulation of this channel protein and an increased sorting to the plasma membrane. This must be a slow process because, other than in experiments with lung cancer cells (A549 cells), IR is not causing an immediate increase in conductance (Roth et al. 2015; Gibhardt et al. 2015). Only 24-48 hours after IR treatment cells exhibit an elevated conductance of the Ca^{2+} dependent K^+ channel KCa2.2.

By studying the effect of IR on ion channels in Jurkat cells we also discovered some interesting off target effects of apamin, a molecule, which is generally used as a specific blocker of KCa2.2 (SK-channels, KCNN2) (Alvarez-Fischer et al. 2013). It occurred that apamin is less specific than anticipated in the relevant literature. It blocks not only the KCa2.2 channel but also Kv1.3, a K^+ outward rectifier which is frequently co-expressed with the KCa2.2 channel (Voos et al. 2017).

The most interesting result of the present study is related to the observation that IR accelerates a cell adhesion of Jurkat cells to glass surfaces and epithelial cells. In the context of immunological reactions adhesion is an extraordinary important process and mandatory for almost all aspects of lymphocyte function (Bevilacqua et al. 1987; Butcher and Picker 1992; Hallmann et al. 1995).

Adhesion of lymphocytes is facilitated by different cellular adhesion molecules (CAM). Especially integrins, one group of CAM, play an important role in the cell-cell and the cell-surface adhesion. Integrins are comprised of an α- and a β-chain subunit and can, together with other transmembrane and intracellular proteins, form clusters. This clustering is mandatory for biological activity of integrins. Clusters of integrin-β-1 with different α-integrin subtypes (VLA) characterize highly active lymphocytes (Cruse and Lewis 2003; Kumar et al. 2007).

Comparative morphological studies of irradiated and unirradiated Jurkat cells show that the irradiated cells exhibit an elevated adhesion and subsequent flattening to the glass surface of cover slips. This adhesion and flattening of the cell body occurs during the first 10-15 minutes after pipetting cells on the glass cover slips. Also unirradiated cells eventually adhere to the glass surface but this occurs much slower and to a lesser extent. At this point it should be mentioned that the flattening of the cells does not contribute to the aforementioned increase in cell diameter of irradiated cells. This increase in cell size was measured on suspension cells, that did not have the time to adhere to a surface. The detailed investigation of the adhesion by confocal laser scanning microscopy shows that the adhesion indeed is an active process of the Jurkat cells. This is best demonstrated by experiments, which show that a pre-coating of the cover slips with polyethylene glycol (PEG), a chemical compound that is commonly used to reduce cell-cell and cell-surface adhesion, strongly reduces the adhesion of irradiated cells.

Even more important than an enhanced adhesion of Jurkat cells to glass surfaces is the finding that the same cells also undergo an strong cell-adhesion on endothelial cells. Cell-adhesion experiments, which mimic physiological conditions, show that IR stimulates an enhanced adhesion of Jurkat cells on endothelial cells (Hallmann et al. 1995; Hildebrandt et al. 2002; Large et al. 2015). The elevated propensity for adhesion is most likely mediated by an upregulation of integrin-β-1 in irradiated Jurkat cells. Support for this interpretation comes from experiments, which show that the IR triggered adhesion of Jurkat cells can be inhibited by RGD peptides. These peptides mimic the binding motive of integrins (Ruoslahti 1996; Rossi et al. 2013; Langhans et al. 2016). When RGD peptides are added to the irradiated Jurkat cells before pipetting them on the endothelial cells during the adhesion assay, RGD peptides can outcompete the native binding partners on the endothelial cells and decrease cell adhesion. The results of the corresponding experiments are in full agreement with this assumption.

The idea of an integrin mediated cell adhesion of Jurkat cells is further supported by high resolution imaging results. The data show that IR is causing an increased surface expression of integrin-β-1 together with an increased integrin-β-1 cluster formation. Both an upregulation and a higher clustering rate, are necessary for the biological activity of integrins (Kinashi 2005; Abram and Lowell 2007; Herter and Zarbock 2013). The results of these experiments are again a strong support for the hypothesis that IR triggers an immune activation or modulation in Jurkat cells. These IR induced processes result in a spectrum of cellular responses.

One of these responses comprises an upregulation of integrins and their subsequent clustering. This upregulation and clustering finally results in an enhanced adhesion of these suspension cells to endothelial cells. The signal transduction cascade, which connects IR exposure with all the aspects of immune activation shown here is yet not fully disclosed in this study.

The data in general suggest the involvement of SRC kinases and Ca^{2+} dependent signaling steps. We showed recently that IR is able to trigger the rise of intracellular reactive oxygen species (ROS) and that these ROS elicit Ca^{2+} signaling (Roth et al. 2015; Gibhardt et al. 2015). Ca^{2+} as well as ROS in turn are universal second messengers and both are involved and crucial for the activation of lymphocytes (Delon et al. 1998; Williams and Kwon 2004; Bhakta et al. 2005; Simeoni and Bogeski 2015).

In general, Ca^{2+} signaling in lymphocytes is induced by immunoreceptor stimulation that leads to the activation of different kinases of the SRC family like Lck, Syk, Zap 70 and Fyn. These kinases amplify the signal and phosphorylate the immunoreceptor tyrosine-based activation motif (ITAM) (Cruse and Lewis 2003). The phosphorylation of ITAM in turn leads to an inositol-1,4,5-trisphosphate (IP_3) induced calcium signaling via the activation of phospholipase C (PLC) enzymes (Essen et al. 1997; Wange 2000). IP_3 binding to the IP_3 receptor finally results in a Ca^{2+} influx trough the IP_3 receptor and the calcium release from internal stores as well as NF-κB activation (Lin and Wang 2004). This influx through the IP_3 receptor and Ca^{2+} channels is mandatory because like all organelles the internal stores are in resting lymphocytes relatively small (Feske 2007; Akimzhanov and Boehning 2012). An elevation of the cytosolic Ca^{2+} concentration ($[Ca^{2+}]_{cyt}$) can result in Ca^{2+} dependent transcriptional responses and the upregulation of cytokines, chemokines and cell-adhesion molecules by transcription factors like NFAT and NF-κB that both play important roles in the immune response of lymphocytes (Cruse and Lewis 2003; Murphy 2012). Both, NFAT and NF-κB, get activated by high $[Ca^{2+}]_{cyt}$ which results in a nuclear translocation of these transcription factors (Feske et al. 2003). Interestingly, in contrast to NF-κB, NFAT needs prolonged Ca^{2+} signaling since it gets concurrently phosphorylated in the nucleus and exported again, whereas for NF-κB action a transient increase in $[Ca^{2+}]_{cyt}$ is sufficient for resulting in target gene expression (Dolmetsch et al. 1997).

Given that irradiation of the immune cells in this study was performed as a single dose of IR, the question arises if the by IR induced ROS & RNS and the subsequent increase in $[Ca^{2+}]_{cyt}$ - could be sufficient for triggering an immune response via an activation of transcription factors like NF-κB that only need a transient increase in $[Ca^{2+}]_{cyt}$. The possible activation of NF-κB needs to be studied further but would fit well to the data presented in this thesis. Recently it was even shown that NF-κB directly binds to the integrin-β-1 promoter region in response to IR resulting in an upregulation of integrin-β-1 (Ahmed et al. 2013; Nam et al. 2013). Another possibility is that IR induces a ROS & RNS production by mitochondria respectively nitric oxide synthase (NOS) due to $[Ca^{2+}]_{cyt}$ increase or as damage response due to IR.

This could result in an activation of lymphocytes by prolonged $[Ca^{2+}]_{cyt}$ signaling or by the ROS & RNS. Higher levels of ROS & RNS however could also lead to apoptosis as known from the literature (Reth 2002; Cruse and Lewis 2003). The idea behind such a T-cell stimulation directly by ROS & RNS is that reversible oxidation of cysteines could result in a similar modification like a phosphorylation of tyrosine, threonine, and serine residues. This could represent a novel global regulatory mechanism during signal transduction (Simeoni and Bogeski 2015).

Taken together the present data provide some new perspectives of the IR induced effects in immune cells. It suggests that low dose ionizing radiation can stimulate the activation or modulation of immune cells. This in turn may elicit anti-inflammatory effects in patients suffering from autoimmune diseases and chronic inflammation by changing the ratio of different immune cell subsets or directly on cellular level by modulation of the immunological state of individual lymphocyte. These conclusions are in line with some recent studies showing that the Ca^{2+} signaling in immune cells of patients with autoimmune and inflammatory diseases is abnormal and could hence lead to autoimmunity (Liossis et al. 1996). For T-cells of patients with rheumatoid diseases it could be shown that a mutation in the SRC kinase Zap-70 results in a strongly reduced TCR and Ca^{2+} signaling (Sakaguchi et al. 2003) and that these cells hereby escape the negative selection of auto reactive T-cells in the thymus. IR could influence the abnormal Ca^{2+} signaling and could in this way counteract inflammatory effects and diseases (Thangaraj et al. 2016; Rühle et al. 2017). These hypotheses are in agreement with the data presented in this study; IR is able to elicit processes that lead to an immune activation or modulation. These processes are furthermore presumably mediated by the action of SRC kinases and CK2.

Finally the finding that integrin-β-1 mediated adhesion is increased in Jurkat cells after IR could be of importance for the clinical treatment of leukemia patients. This treatment is often a combination of chemotherapy and radiotherapy. The present data suggests that radiotherapy could be associated with negative side effects like massive adhesion and transmigration of acute lymphoblastic leukemia (ALL) cells. Drugs, which suppress specific integrin-β-1 mediated adhesion might reduce such negative side effects.

Reference list general discussion

Abbas AK, Lichtman AH (2003) Cellular and Molecular Immunology. 5., Sauders, Philadelphia, USA

Abram CL, Lowell CA (2007) Convergence of immunoreceptor and integrin signaling. Immunol Rev 218:29–44.

Ahmed KM, Zhang H, Park CC (2013) NF-kB Regulates Radioresistance Mediated By ß1-Integrin in Three-Dimensional Culture of Breast Cancer Cells. Cancer Res 73:3737–3748.

Akimzhanov AM, Boehning D (2012) IP3R function in cells of the immune system. Wiley Interdiscip Rev Membr Transp Signal 1:329–339.

Alvarez-Fischer D, Noelker C, Vulinović F, et al (2013) Bee Venom and Its Component Apamin as Neuroprotective Agents in a Parkinson Disease Mouse Model. PLoS One 8:2–9.

Anderson R, Tokuda S, Williams W, Warner N (1982) Radiation-Induced Augmentation of the Response of A/J Mice to SaI Tumor Cells. 24–38.

Arenas M, Sabater S, Hernández V, et al (2012) Anti-inflammatory effects of low-dose radiotherapy. Strahlentherapie und Onkol 188:975–981.

Beeton C, Wulff H, Barbaria J, et al (2001) Selective blockade of T lymphocyte K(+) channels ameliorates experimental autoimmune encephalomyelitis, a model for multiple sclerosis. Proc Natl Acad Sci U S A 98:13942–7.

Betz N, Ott OJ, Adamietz B, et al (2010) Radiotherapy in early-stage dupuytren's contracture long-term results after 13 years. Strahlentherapie und Onkol 186:82–90.

Bevilacqua MP, Pober JS, Mendrick DL, et al (1987) Identification of an inducible endothelial-leukocyte adhesion molecule. Proc Natl Acad Sci USA 84:9238–42.

Bhakta NR, Oh DY, Lewis RS (2005) Calcium oscillations regulate thymocyte motility during positive selection in the three-dimensional thymic environment. Nat Immunol 6:143–151.

Butcher EC, Picker JL (1992) Physiological and moleculas mechanisms of lymphocyte homing. Annu Rev Immunol 561–591.

Cahalan MD, Chandy KG, Hall I (2009) The functional network of ion channels in T lymphocytes. Immunol Rev 231:59–87.

Cruse JM, Lewis RE (2003) Atlas of Immunology. 2., Springer Science & Business, New York, USA

Delon J, Bercovici N, Liblau R, et al (1998) Imaging antigen recognition by naive CD4+ T cells: Compulsory cytoskeletal alterations for the triggering of an intracellular calcium response. Eur J Immunol 28:716–729.

Deshpande A, Goodwin EH, Bailey SM, et al (1996) Alpha-particle-induced sister chromatid exchange in normal human lung fibroblasts: evidence for an extranuclear target. Radiat Res 145:260–267.

Dolmetsch R, Lewis RS, Goodnow CC,et al (1997) Differential activation of transcription factors induced by Ca2+ response amplitude and duration. Nature 336:855-858

Essen LO, Perisic O, Katan M, et al (1997) Structural mapping of the catalytic mechanism for a mammalian phosphoinositide specific phospholiase C. Biochemistry 36:1704.

Falkenbach A, Kovacs J, Franke A, et al (2005) Radon therapy for the treatment of rheumatic diseases-review and meta-analysis of controlled clinical trials. Rheumatol Int 25:205–210.

Feske S (2007) Calcium signalling in lymphocyte activation and disease. Nat Rev Immunol 7:690–702.

Feske S, Okamura H, Hogan PG, et al (2003) Ca2+/calcineurin signalling in cells of the immune system. Biochem Biophys Res Commun 311:1117–1132.

Franke A, Reiner L, Pratzel HG, et al (2000) Long-term efficacy of radon spa therapy in rheumatoid arthritis-a randomized, sham-controlled study and follow-up. Rheumatology 39:894–902.

Franke A, Reiner L, Resch KL (2007) Long-term benefit of radon spa therapy in the rehabilitation of rheumatoid arthritis: A randomised, double-blinded trial. Rheumatol Int 27:703–713.

Ghanshani S, Wulff H, Miller MJ, et al (2000) Up-regulation of the IKCa1 potassium channel during T-cell activation. Molecular mechanism and functional consequences. J Biol Chem 275:37137–49.

Gibhardt CS, Roth B, Schroeder I, et al (2015) X-ray irradiation activates K+ channels via H2O2 signaling. Sci Rep 5:13861.

Hallmann R, Zimmermann U, Sorokin LM, et al (1995) Adhesion of leukocytes to the inflammed endothelium. ScandJRheumatol 24:107–109.

Herter J, Zarbock A (2013) Integrin Regulation during Leukocyte Recruitment. J Immunol 190:4451–4457.

Heyd R, Seegenschmiedt MH, Rades D, et al (2010) Radiotherapy for Symptomatic Vertebral Hemangiomas: Results of a Multicenter Study and Literature Review. Int J Radiat Oncol Biol Phys 77:217–225.

Hildebrandt G, Maggiorella L, Rodel F, et al (2002) Mononuclear cell adhesion and cell adhesion molecule liberation after X-irradiation of activated endothelial cells in vitro. Int J Radiat Biol 78:315–325.

Iritani BM, Delrow J, Grandori C, et al (2002) Modulation of T-lymphocyte development, growth and cell size by the Myc antagonist and transcriptional repressor Mad1. EMBO J 21:4820–4830.

Kinashi T (2005) Intracellular signalling controlling integrin activation in lymphocytes. Nat Rev Immunol 5:546–559.

Kumar V, Abbas AK, Aster J (2007) Robbins Basic Pathology. 8., Elsevier, Amsterdam, Netherlands

Langhans M, Weber W, Babel L, et al (2016) The right motifs for plant cell adhesion: what makes an adhesive site? Protoplasma 1–14.

Large M, Hehlgans S, Reichert S, et al (2015) Study of the anti-inflammatory effects of low-dose radiation. Strahlentherapie und Onkol 191:742–749.

Liebau S, Pröpper C, Böckers T, et al (2006) Selective blockage of Kv1.3 and Kv3.1 channels increases neural progenitor cell proliferation. J Neurochem 99:426–437.

Lin X, Wang D (2004) The roles of CARMA1, Bcl10, and MALT1 in antigen receptor signaling. Semin Immunol 16:429–435.

Loris R, Hamelryck T, Bouckaert J, et al (1998) Legume lectin structure. Biochim Biophys Acta - Protein Struct Mol Enzymol 1383:9–36.

Murphy K (2012) Immuno Biology. 8., Garland Science, Taylor & Francis Group, New York, USA

Nagasawa H, Little JB, Inkret WC, et al (1991) Response of X-Ray-Sensitive CHO Mutant Cells (xrs-6c) to Radiation: II. Relationship between Cell Survival and the Induction of Chromosomal Damage with Low Doses of αParticles. Radiation Research 126:280–288.

Nam J-M, Ahmed KM, Costes S, et al (2013) β1-Integrin via NF-κB signaling is essential for acquisition of invasiveness in a model of radiation treated in situ breast cancer. Breast Cancer Res 15:R60.

Reth M (2002) Hydrogen peroxide as second messenger in lymphocyte activation. Nat Immunol 3:1129–1134.

Rosenbluth MJ, Lam WA, Fletcher DA (2006) Force microscopy of nonadherent cells: a comparison of leukemia cell deformability. Biophys J 90:2994–3003.

Rossi E, Sanz-Rodriguez F, Eleno N, et al (2013) Endothelial endoglin is involved in inflammation: Role in leukocyte adhesion and transmigration. Blood 121:403–415.

Roth B, Gibhardt CS, Becker P, et al (2015) Low-dose photon irradiation alters cell differentiation via activation of hIK channels. Pflugers Arch Eur J Physiol 467:1835–1849.

Rühle PF, Wunderlich R, Deloch L, et al (2017) Modulation of the peripheral immune system after low-dose radon spa therapy: Detailed longitudinal immune monitoring of patients within the RAD-ON01 study. Autoimmunity 0:1–8.

Ruoslahti E (1996) RGD and Other Recognition Sequences for Integrins. Annu Rev Cell Dev Biol 12:697–715.

Shao C, Folkard M, Michael BD, Prise KM (2004) Targeted cytoplasmic irradiation induces bystander responses. Proc Natl Acad Sci USA 101:13495–13500.

Shatrova AN, Mityushova E V., Aksenov NA, Marakhova II (2015) CD25 expression on the surface of Jurkat cells. Cell tissue biol 9:364–370.

Simeoni L, Bogeski I (2015) Redox regulation of T-cell receptor signaling. Biol Chem 396:555–568.

Thangaraj G, Manakov V, Cucu A, et al (2016) Inflammatory effects of TNFα are counteracted by X-ray irradiation and AChE inhibition in mouse micromass cultures. Chem Biol Interact 259:313–318.

Voos P, Yazar M, Lautenschläger R, et al (2017) The small neurotoxin apamin blocks not only small conductance Ca2+ activated K+ channels (SK type) but also the voltage dependent Kv1.3 channel. Eur Biophys J.

Wange R (2000) LAT, the Linker for Activation of T Cells: A Bridge Between T Cell-Specific and General Signaling Pathways. Sci STKE 63

Williams MS, Kwon J (2004) T cell receptor stimulation, reactive oxygen species, and cell signaling. Free Radic Biol Med 37:1144–1151.

Zdrojewicz Z, Strzelczyk J (2006) Radon Treatment Controversy. Dose-Response 4(2):106-118.

IV Appendix

IV.1 List of figures

IV.2 List of abbreviations

$[Ca^{2+}]_{cyt}$	Cytosolic calcium concentration
µg	Microgram
µl	Microliter
µM	Micromolar
µm	Micrometer
A549	Adenocarcinomic human alveolar basal epithelial cell line
ALL	Acute lymphatic leukemia
APS	Ammonium persulfate
ATP	Adenosine triphosphate
BCIP	5-Bromo-4-chloro-3-indolyl phosphate
BMBF	Bundesministerium für Bildung und Forschung
BSA	Bovine serum albumin
C	Compton effect
Ca^{2+}	Calcium
CaCC	Calcium activated chloride channel
CAM	Cell adhesion molecules
CaM	Calmodulin
CD	Cluster of differentiation
CDK1	Cyclin-dependent kinase 1
CK2	Casein kinase 2
CLSM	Confocal laser scanning microscope
CRAC	Calcium release-activated calcium channel
DMEM	Dulbecco´s modified minimal essential medium
DMSO	Dimethyl sulfoxide
DNA	Deoxyribonucleic acid
DSMZ	Deutsche Sammlung von Mikroorganismen und Zellkulturen GmbH
EBIO	1-Ethyl-2-benzimidazolinone
EDTA	Ethylenediaminetetraacetic acid

eGFP	Enhanced green fluorescent protein
EGTA	Ethylene glycol-bis(β-aminoethylether)-N,N,N',N'-tetraacetic acid); chelator
ELAM	Endothelial-leukocyte adhesion molecule (E-selectin)
EPC-9	Amplifier from HEKA Elektronik
ER	Endoplasmic reticulum
FACS	Fluorescence-activated cell sorting
FAK	Focal adhesion kinase
FCS	Fetal calve serum
G1-phase	Gap1-phase; cell cycle
G2-phase	Gap2-phase; cell cycle
Gy	Gray; SI unit of absorbed radiation
h	Hour
H_2O_2	Hydrogen peroxide
HEK293	Human embryonic kidney cell line
HEPES	4-(2-hydroxyethyl)-1-piperazineethanesulfonic acid; organic buffering agent
HEPES	4-(2-hydroxyethyl)-1-piperazineethanesulfonic acid
hERG	Human ether-à-go-go-related gene codes for Kv11.1
Hoechst	2'-(4-hydroxyphenyl)-5-(4-methyl-1-piperazinyl)-2,5'-bi-1H-benzimidazole trihydrochloride hydrate; DNA dye
I	Current
I/V	Current / voltage relation
ICAM	Intercellular adhesion molecule (CD54)
Iinst	Instantaneous current
IP	Immunoprecipitation
IR	Ionizing radiation
ITAM	Immunoreceptor tyrosine-based activation motif
Itd	Time dependent current
JM	Another abbreviation for Jurkat cell line
KCa	calcium-activated potassium-channel
KCa2.2	Human small-conductance Ca2+-activated K+-channel 2; KCNN2, SK2

KCa3.1	Human intermediate-conductance Ca2+-activated K+-channel; KCNN4, hIK
KCNA3	Kv1.3; voltage dependent potassium channel
KCNK18	TRESK, TWIK-related potassium channel
kDa	Kilo Dalton; atomic mass unit
keV	Kilo electron volt
KOH	Potassium hydroxide
Kv1.3	Voltage-gated potassium channel; shaker rel. subfamily, member 3 KCNC1
LET	Linear-energy transfer (LET; keV/µm)
LGlu	L-Glutamin
MCF-7	Breast cancer cell line (Michigan Cancer Foundation-7)
MeV	Mega electron volt
MgTx	Margatoxin
MHC	Major histocompatibility complex
MIC	Mg^{2+} - inhibited Ca^{2+} - permeable current
min	Minutes
ml	Milliliter
mM	Millimolar
M-phase	Mitosis phase; cell cycle
MW	Molecular weight
MΩ	Megaohm
NBT	Nitro blue tetrazolium
NDPK-B	Nucleoside-diphosphate kinases
NEAA	Non-essential amino acids
NFAT	Nuclear factor of activated T-cells
nM	Nanomolar
nm	Nanometer
NO	Nitric oxide
NOS	Nitric oxide synthase
Orai	Calcium release-activated calcium channel protein

pA	Picoampere
PAP-1	5-(4-phenoxybutoxy)psoralen; specific Kv1.3 blocker
PBL	Peripheral blood lymphocytes (human)
PBMC	Peripheral blood monocytes (human)
PBS	Phosphate buffered saline
pCMV6	Mammalian vector (plasmid)
PE	Photoelectric effect
PEG	poly-ethylene-glycol
pEGFP-N2	Mammalian vector containing eGFP gene
PFA	Paraformaldehyde; used for cell fixation
pH	Potential of hydrogen
PHA-L	Phytohaemagglutinin-L
PI	Propidium iodide
PM	Plasma membrane
PP2A	Protein phosphatase 2
pS	Picosiemens
PVDF	Polyvinylidene difluoride
RBC	Red blood cells
RBE	Relative biological effectiveness
RGD	Tripeptide Arg-Gly-Asp
RNAse	Ribonuclease; a type of nuclease that catalyzes the degradation of RNA
RNS	Reactive nitrogen species
RO3306	(5Z)-5-(6-Quinolinylmethylene)-2-[(2-thienylmethyl)amino)-4(5H)-thiazolone
ROI	Region of interest
ROS	Reactive oxygen species
Rpm	Rounds per minute
RPMI	Roswell Park Memorial Institute medium
RT	Room temperature
s	Second
SD	Standard deviation

SDS	Sodium dodecyl sulfate
SEM	Standard error of the mean
SK	Small conductance potassium channel
SMD	Single molecule microscope
SOCE	Store-operated calcium entry
SOD	Superoxide-dismutase enzyme
S-phase	Synthesis-phase; cell cycle
SRC	Non-receptor tyrosine kinases
STIM1	Ca2+ sensor protein stromal interaction molecule
STORM	Stochastic optical reconstruction microscopy buffer
TBB	Tetrabromobenzotriazole
TCR	T-cell receptor
TEMED	Tetramethylethylenediamine
TNF	Tumor necrosis factor
TRAM-34	1-[(2-Chlorophenyl)diphenylmethyl]-1H-pyrazole; hIK channel blocker
Treg	Regulatory T-cells
TRESK	TWIK-related potassium channel
Tris	Tris(hydroxymethyl)aminomethane
TRPM	Transient receptor potential ion channels
VCAM	Vascular cell adhesion molecule (CD106)
VLA	Very late antigen
Vm	Membrane potential
X-ray	Roentgen radiation

IV.3 Own work

Experiments, data analysis and writing were exclusively done by myself, with exception of:

-The single molecule microscopy and analysis of the acquired data was performed with the help of Laura Babel, M.Sc..

-The evaluation of the H_2O_2 induced cell diameter increase presented in Chapter 2 was done by Sebastian Fuck, M.Sc..

-The cell culture of EA.hy926 cell line was performed by Fabian Weipert, M.Sc. who helped me with the execution of the physiological adhesion experiments too.

-The majority of electrophysiological measurements of HEK-293 cells heterogeneously expressing Kv1.3 shown in Chapter 5 were performed by René Lautenschläger (Bachelor-Student) and Mehtap Yazar (Bachelor-Student) under my supervision. Two measurements with Apamin were performed in a practical course by the students Lisa Noll, Vanessa Kohl and David Schul.

-Propidium iodide staining of alpha particle irradiated cells was performed by internship student Dominik Seipel under my supervision.

-Western blot experiments were performed with the help of Silvia Haase (technical employee).

IV.4 Acknowledgments / Danksagung

An dieser Stelle möchte ich mich bei allen Personen bedanken, die zum Gelingen dieser Arbeit beigetragen haben!

Vor allem bedanken möchte ich mich bei:

Herrn Prof. Gerhard Thiel für die Chance in seiner tollen Arbeitsgruppe diese Doktorarbeit erarbeiten zu dürfen, sein immer offenes Ohr und die vielen Anregungen. Nicht zuletzt aber auch für die Freiheiten das Thema selbständig in neue Richtungen entwickeln zu dürfen.

Herrn Prof. Bodo Laube für die Übernahme des Koreferats.

Herrn Prof. Franz Rödel und Fabian Weipert, M.Sc. für die Möglichkeit meine Adhäsionsversuche am Universitätsklinikum Frankfurt durchzuführen sowie die Unterstützung und tolle Atmosphäre während der Arbeit und in Kaffepausen.

GRK1657, GREWIS und DFG für die finanzielle und inhaltliche Unterstützung dieser Arbeit.

Frau Laura Babel, M.Sc. für die gemeinsamen spannenden Projekte am Single Molecule Device sowie die Hilfe bei der Auswertung der Daten.

PD Tobias Meckel und Dr. Markus Langhans für Tipps und Tricks zu allen Fragen rund um die Mikroskopie und Antikörperfärbung.

Frau Dr. Bianca Bertulat und Herrn Dr. Alexander Rapp für die Bereitstellung und das Einarbeiten in das Operetta-System der AG Cardoso.

Herrn Karl Schuller und der Werkstatt für allerlei tolle “hausgemachte” Gerätschaften.

Und natürlich Frau Dr. Brigitte Hertel und Frau PD Indra Schröder für die jederzeit offene Tür zu eurem Büro und offene Ohren für Probleme, Fragen und Anliegen.

Der gesamten AG Thiel für die tolle Arbeitsatmosphäre, das Grillen, Frühstücken, Kegeln, Fußballspielen, Kickern und die “Bierdonnerstage”.
Und natürlich der “alten und neuen” Besetzung im Kinderzimmer.

Ganz besonders erwähnen möchte ich hier Vera Bandmann, Lucia Carillo, Basti Roth, Chris Braun & Oliver Rauh für eine ganz besonders tolle Zeit und eure Freundschaft!
Die außergewöhnlichen Kneipenabende und Partys inklusive der zahlreichen unmöglichen Ereignisse und Begebenheiten werden mir immer in Erinnerung bleiben. Ich bin dankbar den “Sprung” in die AG geschafft zu haben um euch noch als meine AG kennengelernt zu haben!

Den immer hilfsbereiten und sachkundigen TAs Silvia Haase, Silvia Lenz und Mirja Manthey.

Barbara Reinhards für ihre unerschöpfliche Geduld mit uns chaotischen Doktoranden.

Aber auch meinem lieben Unikollegen und einem meiner besten Freunde Johannes Gantner danke ich für die tolle Zeit während des Studiums und der Diplomarbeitszeit! Man kann wohl zurecht behaupten, dass ich ohne dich nicht bei der AG Thiel gelandet ware.

Meiner ganzen Familie, vor allem meiner Mutter Brigitte - danke für die Unterstützung während des Studiums und Deinen Glauben an mich! Meinem Bruder Alexander möchte ich herzlich für die Ermutigung & Unterstützung vor allem während meines Auslandsaufenthaltes in Norwegen danken. Meinem Schwiegervater Hans-Peter danke ich für das aufmerksame Korrekturlesen dieses “Schmökers”.

Zu guter Letzt danke ich meiner lieben Anne - für Deine Geduld, Ermutigung, Unterstützung und Liebe während der gesamten Doktorandenzeit. Meiner kleinen Tochter Linnea danke ich einfach dafür, dass sie da ist - Du bist ein riesiges Geschenk, das ich bis heute nicht begreife!

IV.5 Declaration - Ehrenwörtliche Erklärung

Ehrenwörtliche Erklärung:

Ich erkläre hiermit ehrenwörtlich, dass ich die vorliegende Arbeit entsprechend den Regeln guter wissenschaftlicher Praxis selbstständig und ohne unzulässige Hilfe Dritter angefertigt habe.

Sämtliche aus fremden Quellen direkt oder indirekt übernommenen Gedanken sowie sämtliche von Anderen direkt oder indirekt übernommenen Daten, Techniken und Materialien sind als solche kenntlich gemacht. Die Arbeit wurde bisher bei keiner anderen Hochschule zu Prüfungszwecken eingereicht.

Darmstadt, den _____

_____

Patrick Voos (geb. Becker)

IV.6 Curriculum vitae and publications

Personal information

Name	Voos, née Becker
Surname	Patrick
Date of birth	08/18/1986, Karlsruhe
Nationality	German

Education and working experience

07/2017	Doctoral degree graduate
2013 - 2017	Doctoral degree candidate at the Technische Universität Darmstadt "Low dose ionizing radiation induces morphological and immunological modulation of immune cells" Doctoral advisor: Prof. Dr. G. Thiel
2008 - 2013	Study of biology at the Technische Universität Darmstadt Major study fields: Biochemistry; Plant physiology; Systematic botany Diploma thesis: „Characterization of the cesium blockade of the viral potassium channels Kcv_{NTS} and their filter mutant $Kcv_{NTS\ T45/46S}$" Diploma grade 1.0 with distinction Advisor: Prof. Dr. G. Thiel
2011	Internship at the Department of Cell and Molecular Biology of Prof. Atle M Bones at the Norwegian University of Science and Technology (NTNU) in Trondheim, Norway (6 weeks)
2010 - 2011	Erasmus exchange student at NTNU Trondheim, Norway
2009 - 2011	Research assistant at the Technische Universität Darmstadt
2006	Abitur at the Ludwig-Marum Gymnasium Pfinztal, Berghausen

Publications

01/2017	**Voos P**, Yazar M, Lautenschläger R, et al. The small neurotoxin apamin blocks not only small conductance Ca^{2+} activated K^+ channels (SK type) but also the voltage dependent Kv1.3 channel. Eur Biophys J
08/2015	Roth B, Gibhardt CS, **Becker P**, et al. Low-dose photon irradiation alters cell differentiation via activation of hIK channels. Eur J Physiol 467:1835-49.
12/2014	Gibhardt CS, Roth B, Schroeder I, Fuck S, **Becker P,** et al. X-ray irradiation activates K^+ channels via H_2O_2 signaling. Sci. Rep. 5
04/2014	Braun CJ, Lachnit C, **Becker P**, et al. Viral potassium channels as a robust model system for studies of membrane–protein interaction. BBA – Biomembranes 1838:1096–1103

Je mehr man schon weiß, desto mehr hat man noch zu lernen. Mit dem Wissen nimmt das Nichtwissen in gleichem Grade zu oder vielmehr das Wissen des Nichtwissens.

Friedrich Schlegel deutscher Schriftsteller (1772 - 1829)